ROS Generation in Human Aldehyde Oxidase And the Effects of ROS and Reactive Sulfhydryl on the Activity of the Enzyme

Mariam Esmaeeli Moghaddam

Dissertation
zur Erlangung des akademischen Grades
"doctor rerum naturalium"
(Dr. rer. nat.)
in der Wissenschaftsdisziplin "Biochemie"

August 2021

eingereicht an der
Mathematisch-Naturwissenschaftlichen Fakultät
Institut für Biochemie und Biologie
der Universität Potsdam

Published online on the
Publication Server of the University of Potsdam:
https://doi.org/10.25932/publishup-53460
https://nbn-resolving.org/urn:nbn:de:kobv:517-opus4-534600

Declaration of the Academic Honesty:

I, Mariam Esmaeeli Moghaddam Tabalvandani, hereby confirm that this dissertation is exclusively my own work, that I have only submitted it to the University of Potsdam, Germany, that I have prepared it independently without any unauthorized aids, sources or resources, and that any aids, sources or resources used have been fully cited and acknowledged.

Potsdam, 23.08.2021 Mariam Esmaeeli Moghaddam Tabalvandani

Acknowledgement

I express my deepest gratitude to all those who made my PhD work possible. To my supervisor Prof. Silke Leimkuehler, for her scientific and personal support and all the vivid intriguing discussions we had. Our long weekly meetings are the most I will miss and the most I will remember. To Prof. Maria Joao Romao who welcomed me in the friendly environment of her lab in Lisbon. And to Prof. Lloyd Ruddock for the time he generously spent and patiently answered my a million and one questions.

I thank Dr. Cristiano Mota and Dr. Teresa Santos-Silva for the insightful discussions on the structural aspects of my project and for their friendly support during my stays in Lisbon. I also thank Dr. Alessandro Foti, as a senior PhD at first, and as a good friend later who always kept being an enthusiastic scientist with new ideas and endless curiosity.

I am genuinely grateful to the lab members, Moses, Abrar, Arek, Alka, Hament, Moritz, Sebastian, Ben, Kim, Tugba, Akanksha and others who provided a smooth atmosphere to focus on research. My special thanks go to Frau Lehmann, meine liebe Angelika, who practically showed that science can flow despite the language barrier.

At the end, I would like to mention my family and friends and all those without whom I would have never been able to finish this thesis.

List of Publications:

1. Interrogating the Inhibition Mechanisms of Human Aldehyde Oxidase by X-ray Crystallography and NMR Spectroscopy: The Raloxifene Case
   Cristiano Mota, Ana Diniz, Catarina Coelho, Teresa Santos-Silva, **Mariam Esmaeeli**, Silke Leimkühler, Eurico J. Cabrita, Filipa Marcelo, and Maria João Romão, *J. Med. Chem. 2021, XXXX, XXX, XXX-XXX, August 20, 2021*, https://doi.org/10.1021/acs.jmedchem.1c01125

2. Involvement of aldehyde oxidase in the metabolism of aromatic and aliphatic aldehyde-odorants in the mouse olfactory epithelium
   Naoki Takaoka, Seigo Sanoh, Shigeru Ohta, **Mariam Esmaeeli**, Silke Leimkühler, Mami Kurosaki, Mineko Terao, Enrico Garattini, and Yaichiro Kotake, *manuscript under revision*

3. Human aldehyde oxidase (hAOX1): structure determination of the Moco-free form of the natural variant G1269R and biophysical studies of single nucleotide polymorphisms
   Cristiano Mota, **Mariam Esmaeeli**, Catarina Coelho, Teresa Santos-Silva, Martin Wolff, Alessandro Foti, Silke Leimkühler, and Maria João Romão. *FEBS Open Bio. 2019 May; 9(5): 925–934., doi: 10.1002/2211-5463.12617*

Contribution to Conferences:

1. Human Aldehyde Oxidase (hAOX1): Characterisation of a Cysteine-containing Loop
   Molybdenum and Tungsten Enzymes Conference (MoTEC), Potsdam, Germany, July 2019, Poster presentation

2. Aldehyde Oxidase and Dithiothreitol: Unordinary Effect of an Ordinary Stabilizing Agent
   Bioanalysis workshop for PhD students, Luckenwalde, Germany, November 2018, Oral presentation

3. Human Aldehyde Oxidase: Structure-function studies on a cysteine-rich loop
   Bioanalysis workshop for PhD students, Luckenwalde, Germany, November 2017, Oral presentation

Table of Contents

Abbreviations

Å	Ångström: 10^{-10} m
°C	degree Celsius: x + 273.15 k
λ	wavelength
µ	micro: 10^{-6}
A_{xxx}	absorbance with indicated wavelength
AMP	adenosine 5'-monophosphate, [(2R,3S,4R,5R)-5-(6-amino-9H-purin-9-yl)-3,4-dihydroxyoxolan-2-yl] methyl phosphate
Amp	ampicillin
AOX	aldehyde oxidase gene
AOX / AOXs	aldehyde oxidase(s)
APS	ammonium persulfate
bp	base pair(s)
CD	circular dichroism
CMP	cytidine 5'-monophosphate
cPMP	cyclic pyranopterin-monophosphate
CV	column volume(s)
Da	Dalton: 1 g/mol
DCPIP	2,6-dichlorophenolindophenol
DMSO	dimethyl sulfoxide, methanesulfinylmethane
DNA	deoxyribonucleic acid
DPI	diphenyleneiodonium
DTT	1,4-dithio-D-threitol, 1,4-disulfanylbutane-2,3-diol
e.g.	exempli gratia, for example
EDTA	ethylenediaminatetraacetate, 2-((2-[bis(carboxylatomethyl)amino]ethyl((carboxylatomethyl) amino) acetate
EPR	electron paramagnetic resonance
ESI-MS	electrospray ionization-mass spectroscopy
EtBr	ethidium bromide, 3,8-diamino-5-ethyl-6-phenylphenanthridin-5-ium bromide
EtOH	ethanol
EXAFS	extended x-ray absorption fine structure
FAD / $FADH^{\cdot}$ / $FADH_2$	flavin-adenine-dinucleotide (oxidized, semiquinone and reduced form)
FeS	iron-sulfur cluster
g	acceleration of gravity: 9.80665 m/s^2
GmbH	gesellschaft mit beschränkter hafting (company with limited liability)
GMP	guanosine 5'-phosphate
GTP	guanosine 5'-triphosphate
h	hour
HPLC	high pressure liquid chromatography
i.e.	id est, that is
ICP-OES	inductively coupled plasma-optical emission spectroscopy

IDP	intrinsically disordered protein
IPTG	isopropyl-β-d-thiogalactopyranoside
IMAC	immobilized-metal affinity chromatography
k	kilo: 10^3
LB	lysogenic broth
LU	light units
m	meter, milli: 10^{-3}
MCS	multiple cloning site
MeOH	methanol
MES	4-morpholineethanesulfonate, 2-(morpholin-4-yl) ethane-1-sulfonate
min	minute: 60 s
Moco	Molybdenum cofactor
MPT	molybdopterin
MS	mass spectroscopy
n	nano: 10^{-9}
NAD+ / NADH	nicotinamide dinucleotide (oxidized, reduced form)
NTA	nitriloacetate, 2-[bis(carboxylatomethyl)amino]acetate
O/N	over-night
PAGE	polyacrylamide-gel electrophoresis
PCR	polymerase chain reaction
PDB	protein data bank
pH	decimal cologarithm of proton concentration
pK_a	decimal cologarithm of acid dissociation constant
RNA	ribonucleic acid
ROS	reactive oxygen species
rpm	revolutions per minute
RT	room temperature
SEC	size exclusion chromatography
SDS	sodium dodecyl sulfate
SNP	single nucleotide polymorphism
T	temperature
TEMED	tetramethylethylenediamine, [2-(dimethylamino) ethyl] dimethylamine
Tris	tris-(hydroxymethyl) aminomethane, 2-amino-2-(hydroxymethyl) propane-1,3-diol
U	enzyme activity unit: 1 µmol/min
UV-Vis	ultraviolet-visible
V	volt: 1 $kg.m^2/a.s^3$
XDH(s)	xanthine dehydrogenase(s)
XO(s)	xanthine oxidase(s)
XOR(s)	xanthine oxidoreductase(s)

Summary

Aldehyde oxidases (AOXs) (E.C. 1.2.3.1) are molybdoflavo-enzymes belonging to the xanthine oxidase (XO) family. AOXs in mammals contain one molybdenum cofactor (Moco), one flavin adenine dinucleotide (FAD) and two [2Fe-2S] clusters, the presence of which is essential for the activity of the enzyme. Human aldehyde oxidase (hAOX1) is a cytosolic enzyme mainly expressed in the liver. hAOX1is involved in the metabolism of xenobiotics. It oxidizes aldehydes to their corresponding carboxylic acids and hydroxylates N-heterocyclic compounds. Since these functional groups are widely present in therapeutics, understanding the behaviour of hAOX1 has important implications in medicine. During the catalytic cycle of hAOX1, the substrate is oxidized at Moco and electrons are internally transferred to FAD via the FeS clusters. An electron acceptor juxtaposed to the FAD receives the electrons and re-oxidizes the enzyme for the next catalytic cycle. Molecular oxygen is the endogenous electron acceptor of hAOX1 and in doing so it is reduced and produces reactive oxygen species (ROS) including hydrogen peroxide (H_2O_2) and superoxide ($O_2^{\cdot-}$). The production of ROS has patho-physiological importance, as ROS can have a wide range of effects on cell components including the enzyme itself.

In this thesis, we have shown that hAOX1 loses its activity over multiple cycles of catalysis due to endogenous ROS production and have identified a cysteine rich motif that protects hAOX1 from the ROS damaging effects. We have also shown that a sulfido ligand, which is bound at Moco and is essential for the catalytic activity of the enzyme, is vulnerable during turnover. The ROS produced during the course of the reaction are also able to remove this sulfido ligand from Moco. ROS, in addition, oxidize particular cysteine residues. The combined effects of ROS on the sulfido ligand and on specific cysteine residues in the enzyme result in its inactivation. Furthermore, we report that small reducing agents containing reactive sulfhydryl groups, in a selective manner, inactivate some of the mammalian AOXs by modifying the sulfido ligand at Moco. The mechanism of ROS production by hAOX1 is another scope that has been investigated as part of the work in this thesis. We have shown that the ratio of type of ROS, i.e. hydrogen peroxide (H_2O_2) and superoxide ($O_2^{\cdot-}$), produced by hAOX1 is determined by a particular position on a flexible loop that locates in close proximity of FAD. The size of the cavity at the ROS producing site, i.e. the N5 position of the FAD isoalloxazine ring, kinetically affects the amount of each type of ROS generated by hAOX1. Taken together, hAOX1 is an enzyme with emerging importance in pharmacological and medical studies, not only due to its involvement in drug metabolism, but also due to ROS production which has physiological and pathological implications.

Zusammenfassung

Aldehyd-Oxidasen (AOXs) (E.C. 1.2.3.1) sind Molybdo-Flavo-Enzyme aus der Familie der Xanthin-Oxidasen (XO). AOXs in Säugetieren enthalten einen Molybdän-Cofaktor (Moco), ein Flavin-Adenosin-Dinukleotid (FAD) und zwei [2Fe-2S]-Cluster, deren Anwesenheit für die Aktivität des Enzyms essentiell ist. Die Humane Aldehyd-Oxidase (hAOX1) ist ein zytosolisches Enzym, das hauptsächlich in der Leber exprimiert wird und am Stoffwechsel von Xenobiotika beteiligt ist. hAOX1 oxidiert Aldehyde zu ihren entsprechenden Carbonsäuren und hydroxyliert N-heterocyclische Verbindungen. Da diese funktionellen Gruppen in Therapeutika weit verbreitet sind, hat das Verständnis des Verhaltens von hAOX1 wichtige Auswirkungen auf medizinische Studien. Während des Katalysezyklus von hAOX1 wird das Substrat an Moco oxidiert und die Elektronen werden über die FeS-Cluster intern auf FAD übertragen. Ein Elektronenakzeptor am FAD nimmt die Elektronen auf und re-oxidiert das Enzym für den nächsten Katalysezyklus. Molekularer Sauerstoff ist der endogene Elektronenakzeptor von hAOX1, der reduziert wird und reaktive Sauerstoffspezies (ROS) einschließlich Wasserstoffperoxid (H_2O_2) und Superoxid ($O_2^{\cdot-}$) produziert. Die Produktion von ROS hat pathophysiologische Bedeutung mit weitreichenden Auswirkungen auf die Zellbestandteile und das Enzym selbst.

In der vorliegenden Arbeit haben wir gezeigt, dass hAOX1 aufgrund der endogenen ROS-Produktion seine Aktivität über mehrere Katalysezyklen verliert und haben ein Cystein-reiches Motiv identifiziert, das hAOX1 vor den ROS-schädigenden Wirkungen schützt. Wir haben auch gezeigt, dass ein an Moco gebundener und für die katalytische Aktivität des Enzyms essentieller Sulfidoligand unter reduzierenden Bedingungen anfällig ist. Die im Verlauf der Reaktion entstehenden ROS sind in der Lage, diesen Sulfidoliganden aus dem Moco zu entfernen. ROS oxidieren auch bestimmte Cysteinreste. Die kombinierten Effekte von ROS auf den Sulfidoliganden und Cysteine führen zu einer Inaktivierung des Enzyms. Darüber hinaus berichten wir, dass Reduktionsmittel, die eine reaktive Sulfhydrylgruppe enthalten, selektiv einige der Säuger-AOX inaktivieren, indem sie den Sulfidoliganden beim Moco modifizieren. Der Mechanismus der ROS-Produktion durch hAOX1 ist ein weiterer Bereich, der im Rahmen dieser Arbeit untersucht wurde. Wir haben gezeigt, dass die Art von ROS, d. h. Wasserstoffperoxid (H_2O_2) und Superoxid ($O_2^{\cdot-}$), die von hAOX1 produziert wird, durch eine bestimmte Position auf einem flexiblen Loop bestimmt wird, die sich in der Nähe von FAD befindet. Es scheint, dass die Größe der Kavität an der ROS-produzierenden Stelle, d. h. die N5-Position des FAD-Isoalloxazin-Rings, die Menge jedes ROS-Typs, der von hAOX1 erzeugt wird, kinetisch beeinflusst. Zusammenfassend ist hAOX1 ein Enzym mit zunehmender Bedeutung in pharmakologischen und medizinischen Studien, nicht nur aufgrund

seiner Beteiligung am Arzneimittelstoffwechsel, sondern auch aufgrund der ROS-Produktion, die physiologische und pathologische Auswirkungen hat.

1. Introduction

1.1. Aldehyde Oxidases: A Historical Overview

Aldehyde oxidase (AOX) is a complex enzyme. The first mention of an unknown enzyme with an ability to oxidize aldehydes was in the report of xanthine oxidase (XO) extraction from pig liver (Corran, et al. 1939). One year later in 1940 Gordon, Green and Subrahmanyan isolated this enzyme through multiple steps of ammonium sulfate precipitation using heat to denature the XO impurities (Gordon, et al. 1940). The Gordon aldehyde oxidase was described as a flavo-enzyme that contained flavin adenine dinucleotide (FAD) and some unknown prosthetic groups with overlapping absorbance at 450 nm. The catalytic cycle was explained as the reduction of a flavin group by an aldehyde substrate (acetaldehyde in this work) and the re-oxidation of the reduced FAD by molecular oxygen. Knox and Grossman in 1948 proposed that the enzyme called aldehyde oxidase from rabbit liver was a quinone oxidase which was able to metabolize N-methylnicotinamide (Knox and Grossman 1948). Following a modified procedure of Gordon in 1954, a sample of AOX with higher purity was obtained from pig liver and the presence of molybdenum was confirmed (Mahler, et al. 1954). In this study, which was an extension to a similar approach used to characterize XO (Mackler, et al. 1954), the authors reported 0.5 mg of Mo per molecule of FAD in the protein, but commented that Mo could be split from the enzyme over the course of purification. However, since Mo is silent in the UV-Vis spectroscopy, they suggested that another chromophoric group, likely a heme-associated substance, should be present in the enzyme. Additionally, they observed the inhibitory effect of the compounds known as sulfhydryl inhibitors including iodoacetate and arsenite on AOX similar to XO. In the 1960s Igo and co-workers proposed that AOX from pig liver was a form of XO and that the heme component of the enzyme was not part of the catalytic cycle (Igo and Mackler 1960). As an attempt to explain the physiological role of AOXs, they later developed their hypothesis and suggested that AOX was the solubilized fragment of the terminal electron transport system in the liver mitochondria (Mackler, et al. 1961). In 1962 the rabbit liver AOX was thoroughly investigated in a research led by Handler (Rajagopalan, et al. 1962). In this study the presence of an iron-containing prosthetic group was described in more detail and remarkable different substrate specificity in comparison with XO was pointed out. This study also suggested that a quinone, likely in the form of coenzyme Q, was a possible integral part of the rabbit liver to play a role as an internal electron transfer system in the enzyme.

The investigations until early 60s did not decipher whether the Mo center present in the enzyme is directly bound to the protein or it is part of an unknown prosthetic group. In 1964 and in a separate line of research Pateman and colleagues reported a series of mutations in *Aspergillus niger* that carried inactive forms of xanthine dehydrogenase (XDH) and nitrate reductase (NR) (Pateman, et al. 1964). They proposed that the mutations were related to the biosynthesis pathway of an unknown cofactor common for NR and XDH, which they abbreviated as CNX. In 1968 Rajagopalan showed that the rabbit liver AOX upon reduction with N-methylnicotinamide (as substrate) or dithionite (as a reducing agent) exhibited three types of signals detectable by electron paramagnetic resonance (EPR) spectroscopy (Rajagopalan, et al. 1968). The signals were associated with flavin semiquinone, Mo (V) and a non-heme iron complex. Rapid titrations indicated an intramolecular electron transfer with the migration of reducing equivalents from the molybdenum center towards the flavin through the non-heme iron complexes. The identity of the non-heme iron complexes and a possible ligand bound to Mo, however, remained unidentified. Branzoli and Massey in 1974 identified a mixture of the active and inactive forms of the enzyme in the freshly purified samples (Branzoli and Massey 1974). They provided evidences that the active form of the enzyme contained a cyanolysable persulfide residue at its active site This finding explained the inhibitory effect of the sulfhydryl inhibitors previously described (Mahler, et al. 1954).

Eventually, in the 1980s the mysteries of the cofactor carrying molybdenum and the iron complexes were solved with the noble works of Rajagopalan. The ligand bound to the Mo center in XO, NR and sulfite oxidase (SOX) was isolated from the purified enzymes as an inactive fluorescent adduct in 1980 (Johnson, et al. 1980). The chemical structure of the ligand was fully explained a few years later as a bidentate dithiolene pterin ring (Kramer, et al. 1987). In 1982 Barbar and colleagues were able to apply EPR spectroscopy to characterize the non-heme iron complexes in the rabbit liver AOX as two spectroscopically distinguishable [2Fe-2S] clusters (Barber, et al. 1982a) using a similar approach that had been used for the chicken liver XDH a few years earlier (Barber, et al. 1980).

Today AOXs (E.C.1.2.3.1) are classified as members of the xanthine oxidase family of molybdoenzymes with the ability to oxidize a wide range of substrates containing aldehyde functional groups and N-heterocyclic bonds, with molecular oxygen as their exclusive physiological electron acceptor. However, the endogenous substrate and thus the physiological role of AOXs have mainly remained unclear to date. In this literature review, the focus will be on the human aldehyde oxidase (hAOX1), however, AOXs from other species will be briefly mentioned when emphasis on their differences or similarities in comparison with hAOX1 sets a base for a better understanding.

1.2. Molybdenum and Molybdoenzymes

About one third of all proteins require a metal center for their proper functionality or maintenance of their structure (Waldron, et al. 2009). Molybdenum (Mo) is the only metal in the second row of the transition elements which is essential in trace amounts for most living organisms (Hille, et al. 2014; Waldron, et al. 2009). In non-biological systems molybdenum can switch between various oxidation states from -2 in carbonyl anions to +6 in molybdenum (VI) oxide (Ellis 2003). Higher oxidation states, i.e. +3, +4, +5 and +6, are more stable and associated to the molybdenum occurrence in Earth crust and to its biological roles. Bioavailability of molybdenum is owed to the solubility of molybdenum (VI) oxide in alkaline water. Molybdenum (VI) oxide forms molybdate (MoO_4^{2-}) which can be up taken by living organisms. Molybdenum has been identified in only less than 1% of proteins (Waldron, et al. 2009), but its versatile redox chemistry has made it essential for the function of a range of dehydrogenases and oxidoreductases in oxidation / reduction catalysis (Hille 2002).

Metal centers can coordinate to the amido and carbonyl groups on the backbone of proteins as well as to the side chains of aspartate, glutamate, serine and tyrosine through oxygen, to glutamine, asparagine, histidine, and arginine through nitrogen, and to cysteine and less commonly to methionine through sulfur (Harding, et al. 2010). However, Mo in proteins is not directly bound to the peptide backbone and it forms two other organizations: iron-sulfur-cluster-based molybdenum cofactor (FeMoco) and pterin-based molybdenum cofactor (Moco) (see **Figure 1.1.** for the structural details of the variety of the molybdenum cofactors). FeMoco with an overall composition of [7Fe-9S-Mo-C-homocitrate] is present in the active site of nitrogenases and is anchored to the protein backbone by a cysteine residue to the terminal Fe and a histidine residue to Mo (**Figure 1.1., A**) (Lancaster, et al. 2011; Spatzal, et al. 2011). Mo in FeMoco adopts an octahedral geometry with three sulfide groups bridged to three irons, one bidentate homocitrate and one imidazole group of a histidine residue. The catalytic activity of nitrogenases is crucial for the existence of life. Nitrogenases are responsible for nitrogen fixation, a process in which the highly stable bond in dinitrogen molecule (N_2) is reduced to ammonia (NH_3), which in return provides a usable nitrogen source for nucleic acids and protein biosynthesis (Burén, et al. 2020).

In the pterin-based Moco, Mo is coordinated to one or two pyranopterin ligands through the enedithiolate side chain that provides the basis of the complex, as shown in **Figure 1.1.** and reviewed in various articles (Hille, et al. 2014; Schwarz, et al. 2009; Terao, et al. 2016). Mo can

possess a five- or six-coordinate geometry in the active sites of the molybdoenzymes depending on the number of coordinating pterin ligands. When Mo is bound to two enedithiolate side chain pterin ligands, a trigonal prismatic geometry with six coordination sites is formed. This arrangement is present in the DMSO reductase family of molybdoenzymes (**Figure 1.1., B**). The ligands occupying the remaining two positions diversely vary in the members of the family: one position is bound to oxo or sulfido ligand while the other is coordinated to a cysteine, seleno-cysteine, serine, aspartate or a hydroxyl ligand depending on the enzyme.

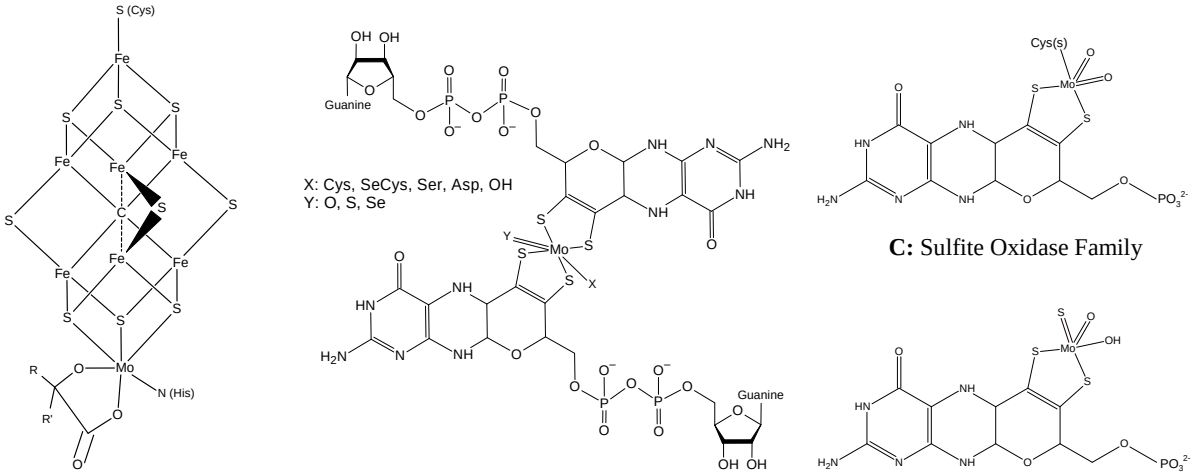

A: Nitrogenase **B:** DMSO Reductase Family **C:** Sulfite Oxidase Family **D:** Xanthine Oxidase Family

Figure 1.1.: Structures of the molybdenum containing cofactors: A: FeMoco: The iron-sulfur-based molybdenum cofactor found in nitrogenases. The Mo center is coordinated to three sulfide bridges, one bidentate homocitrate and the imidazole group of a histidine. **B:** Moco in the DMSO reductase family: two pterin ligands are bound to the Mo center. The two other coordination sites are occupied by a cysteine, seleno-cysteine, aspartate, serine or a hydroxyl ligand and an oxo or sulfido at the positions X and Y, respectively. **C:** Moco in the sulfite oxidase family: the Mo center is coordinated to one pterin ligand, two oxo and one cysteine ligand. **D:** Moco in the xanthine oxidase family: Mo adopts a similar coordination sphere as in sulfite oxidases, except that a hydroxyl and a sulfido group replaced the oxo and cysteine ligands

When Mo is coordinated to one pterin, the overall geometry of the complex is a five-coordinate square pyramid. This geometry of Moco is found in the xanthine oxidase (XO) and sulfite oxidase (SOX) families. In the sulfite oxidase family the bidentate enedithiolate side chain occupies two equatorial positions; while in the other two equatorial positions Mo is coordinated to one oxo ligand and one sulfur group from a cysteine in the protein backbone. The axial site is occupied by another oxo ligand (**Figure 1.1., C**). A similar arrangement is observed in the structure of Moco in the xanthine oxidase family, except that a sulfido ligand replaces the cysteine residue and the equatorial oxo ligand is exchanged with a catalytically labile hydroxyl group (**Figure 1.1., D**).

Aldehyde oxidase (AOX) is a member of the xanthine oxidase family. This family, in addition to CO-dehydrogenase, nicotinate dehydrogenase and 4-hydroxybenzoyl-CoA reductase, includes xanthine oxidoreductases (XOR), whose nomenclature refers to the interconvertibility of xanthine dehydrogenase (XDH) and xanthine oxidase (XO) forms of the same gene product in mammals. Throughout this text XDH, XO and XOR will be used interchangeably when referring to the mammalian enzymes.

1.3. Molybdenum Cofactor Biosynthesis

Molybdenum containing enzymes are vastly found across the kingdoms of life. The Moco biosynthesis pathway is highly conserved in archaea, bacteria and eukaryotes and the proteins involved are homologues at the domain or subunit level (Leimkühler 2017). In *E. coli*, the organism in which the Moco biosynthesis is the best understood, nine proteins encoded by the operons moaABCD, mobAB, mocA, moeAB, and mogA are specifically involved in the pathway (Rajagopalan 1996; Shanmugam, et al. 1992). In addition, two proteins which participate in general sulfur trafficking in the cell, i.e. IscS, a house-keeping L-cysteine desulfurase, and TusA, a sulfur carrier protein (Leimkühler, et al. 2017), play roles in the Moco biosynthesis. In humans the proteins encoded by MOCS (molybdenum cofactor synthesis) genes including MOCS1A, MOCS1B, MOCS2A, MOCS2B and MOSC3 (Reiss and Johnson 2003) together with gephyrin, a moonlighting protein with additional roles in neuronal cells (Tyagarajan and Fritschy 2014), HMCS, the human Moco sulfurase (Peretz, et al. 2007) and NFS1, the L-cysteine desulfurase (Marelja, et al. 2013) mediate the biosynthesis of Moco.

Biosynthesis of the core of Moco occurs through three main steps: **1)** formation of cyclic pyranopterin monophosphate (cPMP) through cyclization of a guanine triphosphate (GTP) (Wuebbens and Rajagopalan 1993) **2)** formation of the mature pyranopterin (MPT) through sulfuration of cPMP (Pitterle, et al. 1993) and **3)** coordination of Mo center to the enedithiolate group of MPT (Joshi, et al. 1996). The intermediate formed in each step is stable and can be isolated. In humans MOCS1A and MOCS1B are responsible for the cyclization of a GTP through a radical SAM (S-adenosyl methionine) mechanism to form cPMP (Leimkühler 2017). The conversion of cPMP to MPT by insertion of two sulfur atoms into cPMP is catalyzed by an MPT synthase composed of MOCS2A and MOCS2B (Stallmeyer, et al. 1999). The insertion of molybdate into MPT is a two-step process mediated by the two-domain protein gephyrin that first activates MPT in an ATP-dependent reaction followed by the ligation of molybdate to the MPT-

AMP. The activity of gephyrin is ATP and Mg^{2+} dependent for the adenylation of MPT and the eventual formation of Mo-MPT (Belaidi and Schwarz 2013).

The Moco maturation is completed by a final step of sulfuration depending on the type of Moco. The prokaryotic sulfuration systems identified to date consist of the L-cysteine desulfurase IscS and a protein-specific molecular chaperon, for instance PaoD for the *E. coli* periplasmic aldehyde oxidase PaoABC (Otrelo-Cardoso, et al. 2014b). A persulfide sulfur is transferred from IscS to the Moco site via a cysteine on the molecular chaperon (Neumann, et al. 2007). This sulfur group replaces an oxo ligand at Moco and forms a sulfido ligand (Mo=S). In humans, the sulfuration system has evolved into one protein and formed the human Moco sulfurase (HMCS) (Peretz, et al. 2007). HMCS contains an N-terminal L-cysteine desulfurase domain that binds a pyridoxal-phosphate (PLP) and a C-terminal domain providing a binding site for Mo-MPT. The sulfur transfer mechanism is not intensively investigated for HMCS, but better understood for the plant orthologue Moco sulfurase ABA3. In ABA3 an L-cysteine is desulfurated at the N-terminal domain in a PLP-dependent manner and the released sulfur forms a persulfide with a highly conserved cysteine on the enzyme (Heidenreich, et al. 2005). Binding of Mo-MPT to the C-terminus triggers a relay for the persulfide to be transferred from the N-terminus to the Moco site.

Divergent sulfuration systems in prokaryotes and eukaryotes limit the heterologous expression of eukaryotic Moco containing enzymes. But fortunately, the sulfido ligand can be chemically reconstituted to obtain active enzymes, a strategy that has been successfully used for the production of hAOX1 in *E. coli* expression system (Foti, et al. 2016).

1.4. Evolution and Gene Organization of Aldehyde Oxidases

Aldehyde oxidases (AOXs, E.C 1.2.3.1) and xanthine dehydrogenases (XDHs, E.C 1.17.1.4) are closely related enzymes (Gordon, et al. 1940). The evolutionary relations of AOXs and XDHs was first shown by Terao and colleagues (TERAO, et al. 1998). XDHs are highly conserved and ubiquitous enzymes from bacteria to plants and mammals, while prokaryotic aldehyde oxidases are not vastly reported. Reconstitution of genome sequencing data showed that *AOX* genes are the result of multiple events of *XDH* gene duplication, deletion and neofunctionalization (Garattini, et al. 2003; Rodriguez-Trelles, et al. 2003). A phylogenetic study in 2013 (Kurosaki, et al. 2013) revealed two distinct lineage of evolution for AOXs from XDHs (**Figure 1.2.**). It is suggested that an initial bacterial *XDH* gene duplication gave rise to the development of the set of *AOX* genes today found in bacteria, protists, algae, insects and plants, while a second *XDH* gene duplication event, likely in a fish ancestor, is the origin of the *AOX* genes present in vertebrates.

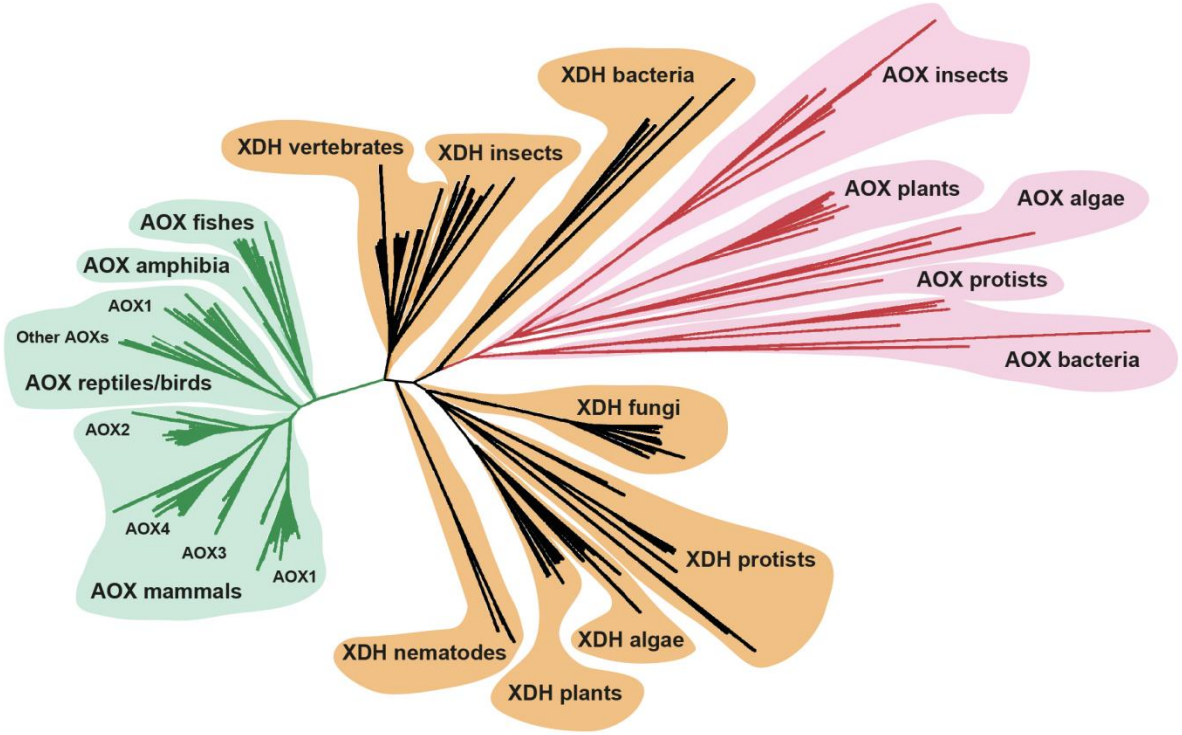

Figure 1.2.: Unrooted phylogenetic tree of AOXs and XDHs: The comparison of some of the available genes encoding for AOXs and XDHs in the kingdom of life suggests that AOXs are the result of at least two events of gene duplication and neofunctionalization of XDHs. These events give rise to the prokaryote/plant/insect and vertebrate branches of AOXs. The tree is reprinted with a generous direct permission from Prof. Enrico Garattini, Istituto di Ricerche Farmacologiche, Mario Negri, Milan, Italy.

Protein sequence analyses indicate higher similarities between prokaryotic XDHs and AOXs or between eukaryotic XDHs and AOXs than between prokaryotic and eukaryotic AOXs (Rodriguez-Trelles, et al. 2003). The sites under positive selection are those with major amino acid differences in AOXs compared with XDHs. These sites are accumulated around the FAD domain and near the substrate binding site in the Moco domain. Interestingly, the regions around the FeS clusters, which do not show major different functions in XDHs and AOXs, are more strictly conserved. The diversity around the Moco active site results in substrate specificity. XDHs can oxidize xanthine and hypoxanthine as the physiological substrate and a group of N-heterocyclic compounds as exogenous substrates. In AOXs a broad range of aldehydes and N-heterocyclic compounds can bind and be oxidized at Moco. The amino acid arrangements in the FAD domain changes the endogenous electron acceptor, i.e. nicotinamide dinucleotide (NAD^+) in XDHs has been replaced with oxygen as an obligate terminal electron acceptor in AOXs. In mammals the FAD active site has further undergone variations so that the interconversion of the dehydrogenase to oxidase form does not occur in AOXs (Nishino, et al. 2008; Stirpe and Della Corte 1969). An example of such positive selection is observed in the Gln423-Lys433 loop together with the Cys992 and Cys535 in bovine XDH (bXDH) where the cysteines are replaced with tyrosines in hAOX1 and the loop

Gln430-Lys440 adopts a conformational change that closes the NAD^+ binding pocket. These aspects and the consequences of the conformational change will be discussed in more details later.

Gene duplication and deletion or pseudogenization is the source of multiple isoenzymes of AOXs found in vertebrates and possibly in plants today (Garattini, et al. 2003; Kurosaki, et al. 2013). Among plants four aldehyde oxidases i.e. AO1-AO4, are found in barley (*Hordeum vulgare L.*) (Omarov, et al. 1999) and in *A. thaliana* (*Arabidopsis thaliana*) (Seo, et al. 2000a), while three functional aldehyde oxidases genes, i.e. *TAO1-TAO3*, along with two pseudogenes, i.e. *TAO4* and *TAO5*, were detected in tomato (*Solanum licopersicum*) (Min, et al. 2000). In vertebrates it is thought that an ancestral fish *AOX* gene has contributed to multiple gene duplication events and led to the generation of two separate loci on the same chromosome in reptiles and avians. The duplication events were further evolved in mammals and initially resulted in a four-loci cluster of four *AOX* genes (*AOX1*, *AOX3*, *AOX4* and *AOX2*) on the same chromosome (see **Figure 1.3.** for the comparison of the *AOX* gene cluster in human, chimpanzee, rhesus monkey, cat and mouse). Subsequently and in a species dependent manner, either all four genes remained functional as detected in mice, or some were inactivated through pseudogenization. This condition is observed in cats (*Felis catus)* with only *AOX2* remaining functional and rhesus monkies *(Macaca mulatta*) with *AOX3* and *AOX4* being pseudogenized. Complete gene deletion along with pseudogenization resulted in the only *AOX1* functional gene present in primates, e.g. in human (*Homo sapiens*) and

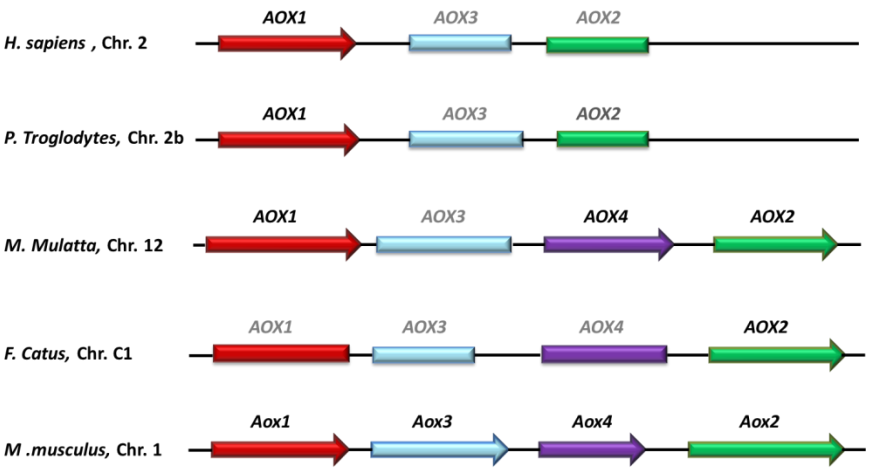

Figure 1.3.: *AOX* gene organization in human in comparison with chimpanzee, rhesus monkey, cat and mouse: Different number of *AOX* functional genes (shown in arrows) and pseudogenes (shown in boxes) are present in human (*Homo sapiens*), chimpanzee (*Pan troglodytes*), rhesus monkey (*Macaca mulatta*), cat (*Felis catus*) and mouse (*Mus mucullus*). Rodents carry the highest number of functional *Aox* genes, while primates have only saved *AOX1* functional. The pseudogenization has occurred on any of the copies, e.g. in cats only *AOX2* and in monkies only *AOX1* and *AOX2* remained functional.

chimpanzee (*Pan troglodytes)*. These species are devoid of the *AOX4* loci, but they present pseudogenes of *AOX3* and *AOX2* (Kurosaki, et al. 2013; Mota, et al. 2018).

1.5. Tissue Specificity and Biological Roles of Aldehyde Oxidases

Studies on aldehyde oxidases are more dedicated to the eukaryotic and in particular to the mammalian enzymes. These enzymes are best known as drug metabolizers. A broad range of therapeutics that contain aldehyde functional group or aromatic N-heterocycles are reported to be inactivated through oxidation and/or hydroxylation by mammalian AOXs (Mota, et al. 2018). In plants the physiological roles of aldehyde oxidases have been deciphered with more details (Seo, et al. 2000a; Yergaliyev, et al. 2016), however, the endogenous substrates for the majority of mammalian enzymes remain unknown to date.

The tissue-specific expression profiles, known mostly for plants, mouse and human enzymes, can give insights into the biological roles of aldehyde oxidases. In the plant model organism *A. thaliana* AAO1 is expressed in seedlings, roots and seeds, while AAO2 is found in seedlings and roots (Akaba, et al. 1999). AAO1 and AAO2 catalyze the oxidation of indole-3-acetaldehyde and 1-naphthaldehyde to their corresponding carboxylic acids. AAO3, the most studied isoenzyme of *A. thaliana*, is mainly expressed in the leaves (Koiwai, et al. 2004; Seo, et al. 2000b). AAO3 catalyzes the last step of biogenesis of abscisic acid, a plant hormone important under normal and stress conditions (Seo, et al. 2000a). AAO4 has been detected in siliques (Seo, et al. 2000b). AAO4 detoxifies a range of aldehyde containing substrates through which delays the silique senescence (Srivastava, et al. 2017). In tomatos, TAO2 and TAO3 are found in leaves and their abundance increases upon viral infection. It has been suggested that TAO2 and TAO3 are important in playing roles in defence mechanisms by enhancing the level of hydrogen peroxide and superoxide (Yergaliyev, et al. 2016).

In mammals the most studied enzyme *in vivo* are mouse AOXs. The $Aox^{4-/-}$ knockout animals were generated in 2009 by Terao and co-workers (Terao, et al. 2009). The *mAox4* transcript is detectable in the fertilized ovum, inner ear, tongue and epidermal layer of skin, with the highest amount of *mAox4* present in the Harderian gland (Terao, et al. 2009; Terao, et al. 2016). $Aox^{4-/-}$ mice show perturbation in the expression of the genes related to the circadian rhythms, and a phenotypic lowered locomotor activity in parallel with resistance to diet-induced obesity. Metabolomic analyses in the Harderian gland indicated altered metabolites of serotonin/melatonin biosynthesis, in particular tryptophan and 5-hydroxyindolacetic acid. Given the relation between the serotonin/melatonin pathway, circadian rhythm and fat deposition, it seems that mAOX4 is

involved in the serotonin/melatonin biosynthesis and 5-hydroxyindolacetic acid is its potential physiological substrate. *mAox2* mRNA is restrictedly transcribed in the nasal cavity and is highly abundant in the Bowman's gland of the submucosal layer. It has been suggested that mAOX2 plays a role in olfactory processes (Naoki Takaoka and colleagues, manuscript under publication). The tissue specificity of other mouse AOXs, i.e. mAOX1 and mAOX3, are not clearly tied to their suggested functions to date. *mAox1* transcripts are present in the inner ear, seminal vesicles, central nervous system, liver and lung while *mAox3* genes are found in significant amounts in the liver, lung, oviduct and testis. mAOX1 and mAOX3 are co-expressed in the liver, a biological significance that makes mice poor model organisms for *in vivo* studies of hAOX1. Despite there are studies suggesting roles for mAOX1 in the amyotrophic lateral sclerosis (ALS) (Bendotti, et al. 1997), the functionality of mAOX1 and mAOX3 are not fully deciphered yet.

In humans, hAOX1 mRNA transcriptome is estimated based on expressed sequence tag (EST) data (UniGene Hs.406238) (Terao, et al. 2020). It was observed that a high level of *AOX1* transcript is present in the liver, adrenal glands, and adipose tissue, followed by lower levels in kidney, trachea, glandular epithelium of prostate, bone and connective tissue. Studies on knock-out HepG2 cells suggest a potential role of hAOX1 in interacting with the ATP binding cassette transporter 1 (ABA1). ABA1 transporter participates in the phospholipid transfer to apolipoproteins. This study indicates that upon generation of reactive oxygen species (ROS), hAOX1 modulates the activity of ABAC1 (Sigruener, et al. 2007). This line of study emphasizes on the catalytic activity of hAOX1 towards acetaldehyde produced during ethanol metabolism and retinal as endogenous substrates (Graessler and Fischer 2007). In both studies the main effect is explained as a response to reactive oxygen species (ROS) which are generated by hAOX1. Involvement of AOXs in the retinoic acid biosynthesis is suggested by earlier reports too (Huang, et al. 1999). The human Moco sulfurase (HMCS) is essential to acquire active forms of both XDH and AOX. Deleterious mutations in HMCS cause xanthinuria type II while the systemic biosynthesis of retinoic acid is not impaired (Ichida, et al. 2001; Yamamoto, et al. 2003). These studies show that human individuals with a genetic lesion in HMCS present minor clinical symptoms and no significant abnormalities. Overall, it seems that *XDH* and *AOX1* are not essential genes, but the physiological role of hAOX1 is not clear to date.

1.6. Domain Architecture and Cofactor Arrangement

All known eukaryotic AOXs are homodimer of a monomer that contains three main domains: a 20 kDa iron-sulfur cluster domain at the N-terminus that accommodates two [2Fe-2S] clusters, a 40-45

kDa central domain with a flavin adenine dinucleotide (FAD) molecule that provides the electron acceptor binding site, and a large domain of 80-85 kDa at the C-terminus that envelopes Moco where the oxidation of the reducing substrate occurs (**Figure 1.4.**) (Hille, et al. 2014). The iron-sulfur cluster domain consists of two fused ferredoxin-like sub-domains carrying FeSII in a β-sheet-based structure and FeSI in a principally α-helical secondary structure. FeSII is the N-terminal cluster that in the tertiary structure folds closer to the FAD site. The Moco domain also consists of two fused sub-domains at the interface of which Moco is located.

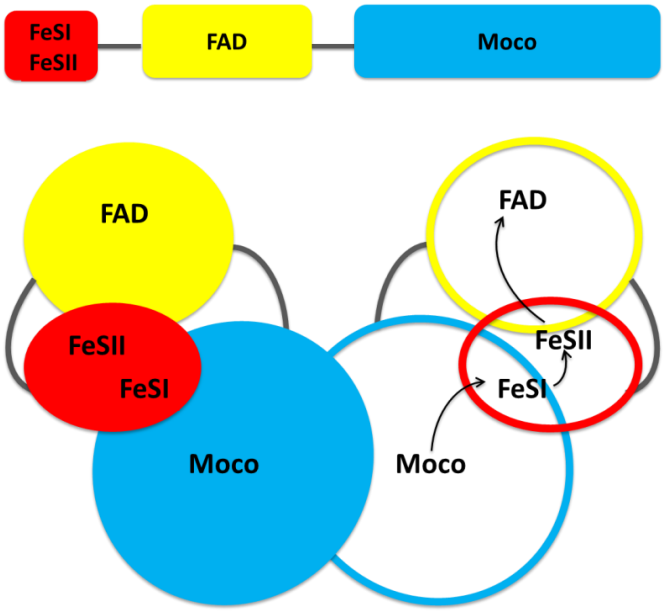

Figure 1.4.: The general domain architecture of aldehyde oxidases: In the primary structure of eukaryotic AOXs (top) three main domains are distinguished: An N-terminal FeS cluster (red), a central FAD (yellow) and a C-terminal Moco domain (blue). In the quaternary structure (bottom) the FeS cluster domain folds in between the Moco and FAD domains to provide an electron path (shown in arrows) from the oxidation site (Moco) to the reduction site (FAD). Linkers that connect the domains are shown in grey lines.

The prokaryotic AOXs are organized in subunits with similar architecture; however, some enzymes carry additional non-protein ligands or lack some of the domains. For instance, *E. coli* aldehyde oxidase, PaoABC, is organized in two subunits: the A subunit carries the two [2Fe-2S] clusters and FAD, while the B subunit is the counterpart of the Moco domain in eukaryotic AOXs with high degrees of sequence and structure similarities (Otrelo-Cardoso, et al. 2014). In addition, a spectroscopically silent [4Fe-4S] cluster is located in the B subunit of PaoABC. In the aldehyde oxidase from *Desulfovibrio gigas*, MOP, the FAD domain is completely absent and the enzyme only contains the FeS and Moco subunits (Romão, et al. 1995).

1.7. Human Aldehyde Oxidase: X-ray Crystal Structure and Cofactor Properties

The X-ray crystal structure of hAOX1 was solved in 2015 to 2.6 Å resolution (Coelho, et al. 2015). The homodimer structure of hAOX1, presented in **Figure 1.5.** with each domain carrying the redox-active centers colour coded, shows an overall butterfly shape similar to the other members of the

XO family. Each monomer consists of three main domains: a 20 kDa N-terminal FeS domain that contains two spectroscopically distinct [2Fe-2S] clusters, a 40 kDa central domain that harbours an FAD and a large 80 kDa C-terminal Moco binding domain. The N-terminal FeS domain in the tertiary structure folds in between the FAD and Moco domains through the linker I, residues 166-231. The FAD and Moco domain connection is facilitated by the linker II, residues 516-555. The dimer interface is at the Moco domain with Mo centers being about 50 Å apart resulting in an overall 150 Å x 90 Å x 65 Å size dimer.

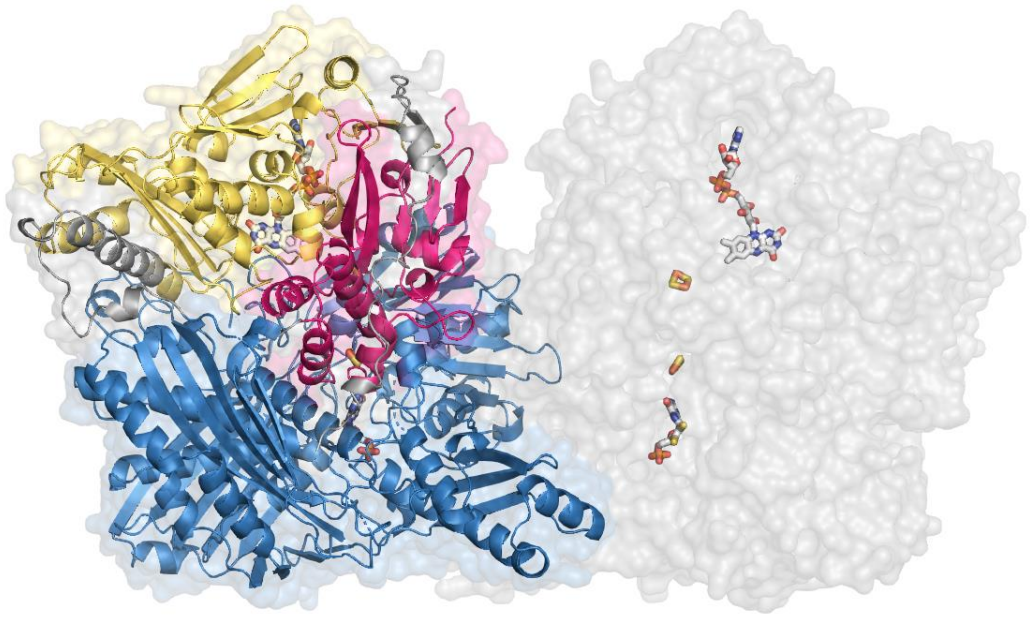

Figure 1.5.: The ribbon representative of the X-ray crystal structure of human aldehyde oxidase (hAOX1) and the cofactor arrangement: The structure of hAOX1 (PDB: 4UHW) is a butterfly dimer similar to the rest of the XO family enzymes consisting of the three domains and four cofactors: The monomer on the left shows the 20 kDa N-terminal domain (coloured in red) that carries two [2Fe-2S] clusters, the 40 kDa central domain (shown in yellow) that harbours an FAD molecule and the 80 kDa C-terminal domain (depicted in blue) that buries a molybdenum cofactor (Moco). Two linkers (coloured in grey) at the C-terminus of the FeS and FAD domains connect the domains to each other. The monomer on the right represents the cofactor arrangement with Moco in about 6 Å from FeSI, and FAD being 7 Å apart from FeSII. The two FeS clusters are about 12 Å apart. The distance between the two molybdenum centers is about 40 Å and the dimer interface locates at the Moco domain.

The N-terminal FeS domain is the shortest domain with two strictly conserved binding sites for the two [2Fe-2S] clusters which are 11.6 Å apart. FeSII is bound to Cys 44, 49, 52 and 74 and locates closer to the FAD site at a 7.1 Å distance. FeSI binds to Cys 114, 117, 149 and 151 and is closer to Moco with only 6.1 Å distance. The two iron-sulfur clusters are not distinguishable by their UV-Vis absorbance, but they show distinct EPR signals (Hartmann, et al. 2012). FeSI gives slightly rhombic *g* tensor that develops at relatively higher temperatures (80 K) similar to those observed for

ferredoxin type [2Fe-2S] clusters in many other proteins (Hille 1996; Hille, et al. 2014). FeSII presents an unusual EPR signal with a more rhombic *g* tensor that can only be detected at lower temperatures (~ 30 K). The strong rhombic *g* value and broad lines which are unusual for [2Fe-2S] clusters appear probably due to the uncommon solvent accessibility of FeSII. The line widths and *g* values observed for the two [2Fe-2S] clusters in hAOX1 are similar to those reported for mAOX1 (Schumann, et al. 2009) and mAOX3 (Mahro, et al. 2011). The redox potentials of the [2Fe-2S] clusters have been reported for hAOX1 (Dr. Martin Mahro PhD thesis, 2013), mAOX3 (Mahro, et al. 2013) and rabbit liver AOX (Barber, et al. 1982a). It was observed that in AOXs the redox potential of FeSI is more positive than FeSII, which is a reverse order to what is measured in XOR enzymes (FeSI: -310 mV and FeSII: -255 mV in cow milk XO (Barber and Siegel 1982) compared to FeSI: -279 mV and FeSII: -329 mV in hAOX1 (Dr. Martin Mahro PhD thesis, 2013), FeSI: -206 mV and FeSII: -286 mV in mAOX3 (Mahro, et al. 2013) and FeSI: 207 mV and FeSII: -310 mV in rabbit liver AOX (Barber, et al. 1982a)). Given the lowest redox potential assigned to Mo IV/V and Mo V/VI in both XOR enzymes and AOXs, the lower redox potentials for FeSII than FeSI in AOXs suggest that electrons which are received by FeSI from Moco are less readily accepted by FeSII**.** The importance of this feature will be discussed more in relation to the ROS generation in AOXs.

The central 40 kDa domain harbours an FAD cofactor which provides a binding site for the terminal electron acceptor. Two loops, the FAD variable loop 1 (residues ^{430}QAQRQENALAI^{440}) and FAD variable loop 2 (residues ^{1230}TRGPDQ^{1235}) are involved in FAD binding and orientation (Coelho, et al. 2012). The isoalloxazine ring of FAD is stacked between the leucine residues 344 and 438, the latter being a part of the FAD variable loop 1. The counterpart region in mammalian XOR enzymes (residues ^{423}QASRREDDIAK^{433} in bovine XOR) undergoes a conformational change upon the formation of a disulfide bridge between Cys992 and Cys535 (bXOR numbering) (Nishino, et al. 2008; Stirpe and Della Corte 1969). The loop consequently flips and blocks the NAD^+ accessibility and only allows the molecular oxygen to enter the FAD site. These events eventually lead to the interconversion of the dehydrogenase to the oxidase form of bXOR. An equivalent conformational change has not been observed in AOXs (Turner, et al. 1995) and they are locked in the oxidase form. Recent studies suggest that the FAD variable loop 1 and particularly Leu438 have roles in determining the type of reactive oxygen species (ROS) produced by hAOX1 (Foti, et al. 2017).

The catalytic C-terminal domain which is connected to the FAD domain through the linker II (residues 516-555) carries Moco where the oxidation of a substrate takes place (Coelho, et al. 2015). The Moco binding site is conserved among the family, but the diversity in the substrate

binding funnels determines the substrate specificity. The residues Gln1203, and conserved Phe807 and Arg921 surround Moco and stabilize the pterin geometry through hydrogen bonding and hydrophobic interactions. The overall amino acid arrangement around Moco, i.e. the residues Met889, Ile1018, and conserved Ala919 which are involved in substrate recognition and orientation, provides a more spacious active site pocket than that in bovine XOR. The substrate gate 1 in hAOX1, residues ^{652}SFCFFTEAEK^{662}, is less negatively charged with bulkier hydrophobic residues than in bXOR (^{645}ETGLFNDET^{653}). On the contrary, the substrate gate 2 in hAOX1, residues ^{880}LDESLF^{885}, carries more negatively charged residues than in bXOR (^{871}RDLSHS^{876}). These differences lead to different substrate specificity for hAOX1 from bXOR. Despite the main active site glutamate (Glu1270 in hAOX1, Glu1261 in bXO) is highly conserved among AOXs and XDHs, residue His884 in bXOR, which is proposed to be involved in the reaction mechanism, is replaced by a lysine (K893 in hAOX1) in aldehyde oxidases. Interestingly, in the crystal structure of hAOX1 published by Coelho and co-workers (Coelho, et al. 2015) the essential sulfido ligand at Moco has been refined with only 0.6 occupancy. This was primarily explained due to the low resolutions that do not allow a better visualization of this group. However, the sensitivity of the sulfido ligand in hAOX1 under the conditions that the crystallization experiments have been performed might be a potential reason for the low sulfido saturation.

1.8. Proposed Reaction Mechanism and ROS Production

AOXs hydroxylate N-hetero aromatic cycles and oxidase aldehyde groups. These reactions take place at Moco. The electrons produced are internally via FeS clusters transferred to the FAD site, where an oxidizing substrate receives the electrons. The reaction mechanism for aldehyde oxidases was primarily proposed based on the studies on XOR enzymes (Xia, et al. 1999), however, investigations on aldehyde oxidases revealed the AOX-specific features of the mechanism (Coelho, et al. 2012; Foti, et al. 2016; Mahro, et al. 2011; Schumann, et al. 2009) (see **Figure 1.6.**). The reaction is initiated by a base-assisted proton abstraction from the equatorial Mo-OH. This is mediated by a strictly conserved glutamate (Glu1270 in hAOX1) locating at the Moco active site. The oxygen of the hydroxyl group of Mo-OH nucleophilically attacks the partially positively charged carbon center on the substrate. Simultaneously, the hydride formed on the substrate carbon atom is transferred to the Mo=S group to form Mo-SH. The transition state (TS) is a tetrahedral with a C-O bond on the product partially formed and a C-H bond on the substrate partially broken (not shown in **Figure 1.6.**). The TS breaks down to form an intermediate in which the Mo(IV) center is bound to the product through an oxygen. A hydroxide from a water molecule displaces the product from the Mo coordination sphere, while Moco is two-electron reduced. The Mo-SH is

deprotonated to return back to the Mo=S and the electrons flux to the other redox active centers of the enzyme. The last step is the re-oxidation of the enzyme that occurs through the oxidizing substrate, i.e. the electron acceptor, once the electrons are received. This prepares the enzyme for the next catalytic cycle.

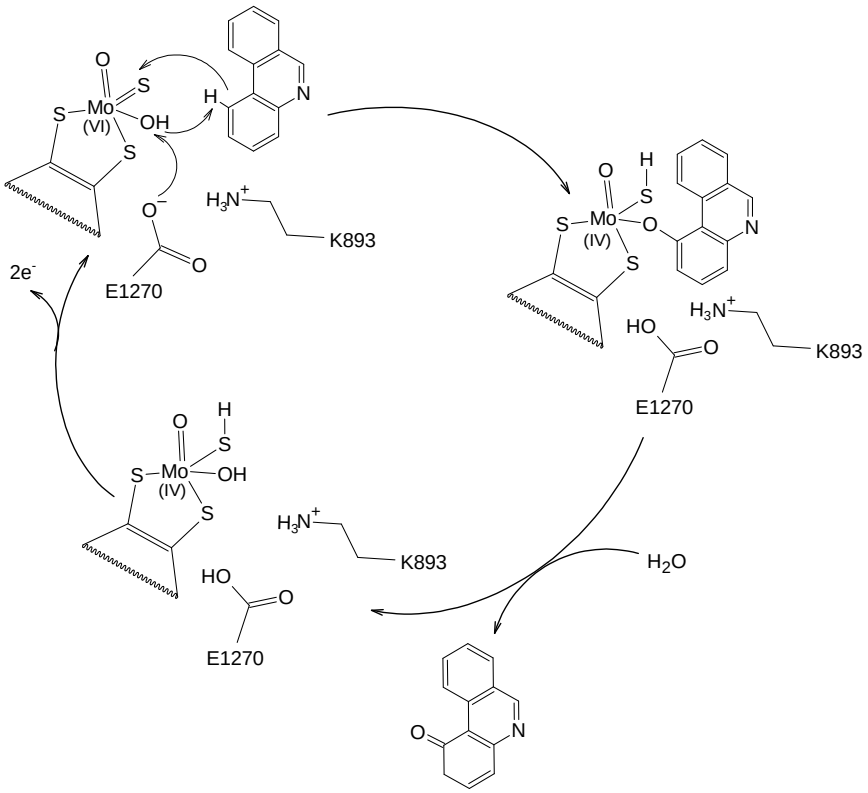

Figure 1.6.: Base-assisted reaction mechanism proposed for AOXs: E1270, when deprotonated, abstracts proton from catalytically labile Mo-OH which in return nucleophilically attacks the partially positive carbon center on the substrate. Simultaneously, the hydride from the substrate is transferred to Mo=S and forms Mo-S-H. A water molecule displaces the product from the Mo coordination sphere and Mo-S-H gets deprotonated to generate Mo=S. The electrons are transferred to the other redox centers and Mo(IV) is re-oxidized to Mo(VI).

The highly conserved active site glutamate (Glu1270 in hAOX1) is essential for the base activation of the Mo-OH to form a strong nucleophile (Mo-O^-) that initiates the nucleophilic attack. The other active site residues, including the highly conserved Lys893 (shown in **Figure 1.6.**) together with Met889 and Val811 stabilize the transition state through hydrogen bonding and hydrophobic interactions (Coelho, et al. 2012). Molecular dynamics simulations of aldehyde and N-heterocycle substrates docking to the active site of mAOX3 suggest that the salt bridge formed between the glutamate and lysine (Glu1270 and K893, hAOX1 numbering) and π-π stacking and dipole-ion interactions established at the active site orient the substrate towards Moco. The reaction mechanism shown in **Figure 1.6.** is supported by experimental evidences including site-directed

mutagenesis which studied the active site amino acid residue roles (Coelho, et al. 2012; Schumann, et al. 2009) and by density-functional theory (DFT) calculations (Alfaro and Jones 2008).

The second product of the catalytic activity of AOXs includes an electron acceptor which is reduced at the FAD site. The intramolecular electron transfer is initiated with the production of reducing equivalents in the reductive half-reaction at Moco. Subsequently, the electrons are transferred via the FeS clusters to the FAD active site, where the oxidative half-reaction takes place. FAD is a cofactor capable to switch between three oxidation states, the oxidized form known as quinone (FAD), the one-electron reduced form semiquinone radical ($FADH^{\cdot}$), and the two-electron reduced form hydroquinone ($FADH_2$) (**Figure 1.7.**). Formation of $FADH^{\cdot}$ or $FADH_2$ depends on the number of the electrons transferred from the FeS clusters. When oxygen is used as the oxidizing substrate, the reactive oxygen species (ROS) including hydrogen peroxide and superoxide are produced, while the enzyme gets re-oxidized and prepared to start a new catalytic cycle.

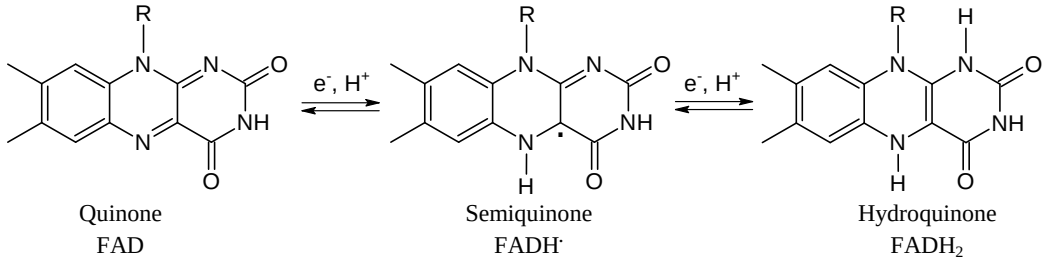

Figure 1.7.: Different redox states of the flavin adenine dinucleotide (FAD): The isoalloxazine ring of FAD switches between three oxidation states upon receiving electrons: the oxidized form quinone (FAD), the one-electron reduced form semiquinone radical ($FADH^{\cdot}$), and the two-electron reduced form hydroquinone ($FADH_2$).

Investigating the internal electron transfer and formation of ROS in AOXs are of particular interest, especially after reporting hAOX1-L38V, a natural variant of hAOX1 that unlike the WT predominantly generates superoxide over hydrogen peroxide (Foti, et al. 2017). The ROS production mechanism in the mammalian XOR enzymes, which are able to switch between the oxidase and dehydrogenase forms, has been extensively investigated. While only the dehydrogenase form of XORs, i.e. XDH, is capable of utilizing NAD^+ as the oxidizing substrate, both XDH and XO forms of XORs can utilize oxygen as electron acceptor to produce ROS.

Nishino and colleagues in several studies (Nishino, et al. 2008; Nishino and Okamoto 2000) have shown that the electron transfer depends upon the thermodynamically favoured state of FAD in XOR enzymes. The redox potential of the $FADH^{\cdot}/FADH_2$ couple in the XDH form is more negative than that of $FAD/FADH^{\cdot}$ implying that the semiquinone ($FADH^{\cdot}$) in XDHs is more thermodynamically favoured. In the oxidase form of XOR enzymes, i.e. in XOs, the redox potential

of the $FADH^{\cdot}/FADH_2$ couple is less negative than that of $FAD/FADH^{\cdot}$ That indicates a more thermodynamically stabilized hydroquinone ($FADH_2$) over semiquinone ($FADH^{\cdot}$). The semiquinone radical ($FADH^{\cdot}$) can transfer one electron to the molecular oxygen to produce superoxide radical ($O_2^{-\cdot}$), while $FADH_2$ is capable of transferring two electrons to oxygen to form hydrogen peroxide. XDHs use NAD^+ as their preferred electron acceptor; however, oxygen can bind at the FAD site of both XOs and XDHs. The stabilization of the semiquinone ($FADH^{\cdot}$) in XDHs results in the predominant production of superoxide over hydrogen peroxide in the absence of NAD^+ as the oxidizing substrate (Nishino and Okamoto 2000).

The reducing equivalents are distributed on the redox active centers of the enzyme based on their redox potentials. However, the reaction of oxygen with semiquinone ($FADH^{\cdot}$) in comparison with the hydroquinone ($FADH_2$) is also kinetically controlled (Hille and Massey 1986; Hille, et al. 2014). In XOs, in the partially (i.e. two or four electron) reduced enzyme in comparison with the fully (six electron) reduced enzyme the electron transfer from FeSII to FAD is the rate limiting step. This results in the formation of a mix of hydrogen peroxide and superoxide the proportion of which is determined by the rate of the electron transfer from FeSII to FAD. The validity of this model has yet to be investigated for AOXs including hAOX1, however, given the more negative redox potential of FeSII than FeSI in AOXs, the electron accumulation on FeSI might have an effect on the kinetics of the electron transfer from FeSII to FAD.

1.9. Importance of Human Aldehyde Oxidase

hAOX1 is a cytosolic enzyme largely expressed in the liver, but its endogenous substrate has not been identified to date (Terao, et al. 2020). hAOX1 exhibits a wide substrate specificity allowing it, together with cytochrome P450 and XO, to metabolize a diverse range of xenobiotics with therapeutic applications during the phase I drug metabolism (Mota, et al. 2018). In phase I drug metabolism a reactive or polar group, often through hydroxylation, oxidation, reduction, cyclization or decyclization, is introduced into the drug substrate. Being a bi-substrate enzyme, hAOX1 is able to oxidize a broad range of compounds containing aldehyde or N-heterocycle groups at the Moco site, and to reduce substances carrying nitro, N-oxide, S-oxide, isothiazol and amides at the FAD site. Therapeutics such as famciclovir, zaleplon, zoniporide, methotrexate and carbazeram that contain an N-heterocycle group, citalopram and retinal carrying an aldehyde group and nitrazepam, sulindac, imipramine and nicotinamide which are able to accept electrons through their N-oxide, S-oxide, isothiazol and amides groups are among the drugs being metabolized by hAOX1.

hAOX1, in addition, may get involved in the drug metabolism through inhibitory mechanisms (Mota, et al. 2018). In general, an increase in the rate of metabolism of a given therapeutic or a pharmacologically active metabolite leads to a decrease of the duration and/or the intensity of the drug action. Inhibition of the enzymes involved in drug metabolism has an opposite effect. The drugs that have been reported to have inhibitory effects on hAOX1 include estrogenic compounds, phenothiazines, dibenzapines, flavonoids, purines and pyrimidines. Despite the contradictory information available for the inhibitors of hOAX1, the inhibitory effects can be categorized based on the inhibitor binding site, i.e. the oxidation (Moco) or reduction (FAD) sites, which lead to competitive inhibition, or specific binding sites that result in uncompetitive or none-competitive inhibition. Raloxifene, estradiol and quercetin have been reported as Moco inhibitors of hAOX1, while maprotiline and amitriptyline are among the FAD inhibitors. Prephenazine, chlorpromazine and thioridazine are the drugs with inhibitory effects on hAOX1 by binding on the sites other than the two active sites (Mota, et al. 2018).

In recent years and with extensive studies on the physio-pathological effects of ROS on living organisms, the ROS producing enzymes have attained emerging importance. Together with XORs, AOXs are a source of ROS in cells. Further investigation of AOXs, including hAOX1, would shed light on the potential new aspects of their involvement in cellular pathways.

2. Aims of the Project

In this project we aim to investigate the role(s) of six conserved cysteine residues located on a flexible region of hAOX1 and their reactivity towards reactive oxygen species (ROS). We will also focus on the nature of hAOX1 inactivation over the course of its catalytic cycle or in the presence of small sulfhydryl containing agents. Finally, the mechanism of ROS production at the flavin adenine dinucleotide (FAD) site of the enzyme will be investigated. The main approach for these studies will be applying *in vitro* biochemical and biophysical methods. Site directed mutagenesis and heterologous protein expression will be used to produce variants of hAOX1 and the quality of the protein produced will be assessed with their UV-Vis spectra (Foti, et al. 2016). The molybdenum and iron contents will be determined using induced coupled plasma-optical emission spectroscopy (ICP-OES) (Neumann and Leimkühler 2008) and Moco load will be in parallel assessed by measuring the amount of Form A, the fluorescent adduct of Moco (Johnson, et al. 1984). The enzymatic reaction will be measured using different electron acceptors, i.e. molecular oxygen and 2,6-dichlorophenolindophenol (DCPIP) (Foti, et al. 2016). In addition, the amount of different types of ROS that hAOX1 variants are able to generate will be determined using a cytochrome C reduction assay (McCord and Fridovich 1969). The thermal stability of the variants will be compared using thermoFAD, a method recently optimized for hAOX1 (Mota, et al. 2019). Circular dichroism (CD) and electrospray ionization-mass spectroscopy (ESI-MS) will be used to compare the modifications introduced to the enzyme under different conditions. The study will in parallel apply X-ray crystallography and structural methods for better understanding the aspects of hAOX1. The outcome of this project is expected to enable us to better understand the behaviour of hAOX1 during turnover and broaden our knowledge of the role of hAOX1 in metabolizing various drugs.

3. Materials and Methods

3.1. Materials

3.1.1. Bacterial Strains

Table 3.1.: The bacterial strains used in this study

Strain	Description	Reference
DH5α	F$^-$, *supE44*, *ΔlacU169*, [Ø80*lacZ*ΔM15]*hsdR17*, *recA1*, *endA1*, *gyrA96*, *thi-1*, *relA1*, (res$^-$, *mod*$^+$), *deoR*	(Hanahan 1983)
TP1000	F$^-$, *ΔlacU169*, *araD139*, *rpsL150*, *relA1*, *ptsF*, *rbsR*, *flbB*, *Δ(mobAB)*	(Palmer, et al. 1996)

3.1.2. Plasmids

Table 3.2.: Expression vectors used in this thesis

Plasmid[1]		Protein encoded	Shortened for
WT	pAF00	human AOX1- codon optimized	WT
Cysteine Variants	pME52	human AOX1-C161A/C165A/C170A/C171A/C179A/C180A	6A
	pME53	human AOX1-C161D/C165D/C170D/C171D, C179D/C180D	6D
	pME51	human AOX1-C170A/C171A/C179A/C180A	4A
	pME50	human AOX1-C170A/C171A/C179A	3A
	pME49	human AOX1-C179A/C180A	2A-2
	pME48	human AOX1-C170A/C171A	2A-1
	pME46	human AOX1-C161A	C161A
	pME47	human AOX1-C165A	C165A
Natural Variants	pME54	human AOX1-N176Y	N176Y
	pME55	human AOX1-G177E	G177E
	pME56	human AOX1-V178F	V178F
	pAF11	human AOX1-L438V	L438V
FAD Variants	pAF20	human AOX1-L438A	L438A
	pAF21	human AOX1- L438F	L438F
	pAF22	human AOX1- L438K	L438K
	pAF16	human AOX1- N436D/A437D	N436D/A437D
	pAF17	human AOX1- N436D/A437D/L438I	N436D/A437D/L438I
Chimeric Variants	pME57	human AOX1 cysteine loop (K162-V235) replaced by *D. melanogaster* AOX1 loop (K161-Q206)	dAOX1-Chim.
	pME58	human AOX1 cysteine loop (K162-V235) replaced *G. gallus* XDH loop (R164-C254)	gXDH-Chim.
	pME59	human AOX1 cysteine loop (K162-V235) replaced by *R.*	*Rc* XDH-Chim.

		capsulatos XDH loop (E147-G172)	
	pME60[2]	human AOX1 FAD variable loop 1 (Q430-I440) replaced by bovine XO/XDH loop (Q432-K433)	bXO-FAD-Chim.
Mouse Enzymes	pmAOX1-co	mouse AOX1- codon optimized	mAOX1
	pmAOX2-co	mouse AOX2- codon optimized	mAOX2
	pMMA1	mouse AOX3- codon optimized	mAOX3
	pmAOX4	mouse AOX4- codon optimized	mAOX4

1: Plasmid names are based on the name of the person who constructed them. Plasmids made for this thesis start with pME. AF and MMA refer to Alessandro Foti and Martin Mahro, respectively.

2: This plasmid was made by step-by-step site directed mutagenesis to exchange the whole loop amino acids one-by-one. The primers to generate this construct were previously reported (Dr. Alessandro Foti PhD thesis, 2017) and the last step was completed by ME.

3.1.3. Primers

Table 3.3.: Primers used in this thesis for site-directed mutagenesis: The mutated sites are bold underlined.

Protein encoded	Primer (5'-3')	T_m (°C)[1]
human AOX1-C161A	Forward: CCGATTATTGATGCA**GC**TAAAACCTTTTG	66.9
	Reverse: CAAAAGGTTTTA**GC**TGCATCAATAATCGG	
human AOX1-C165A	Forward: CATGTAAAACCTTT**GC**TAAAACCAGCGGTTG	66.0
	Reverse: CAACCGCTGGTTTTA**GC**AAAGGTTTTACATG	
human AOX1-C170A/C171A	Forward: GTAAAACCAGCGGT**GC**T**GC**CCAGAGCAAAGAAAATG	72.1
	Reverse: CATTTTCTTTGCTCTGG**GC**A**GC**ACCGCTGGTTTTAC	
human AOX1-C170A/C171A/C179A	Forward: GAAAATGGTGTT**GC**TTGTCTGGATC	64.5
	Reverse: GATCCAGACAA**GC**AACACCATTTTC	
human AOX1-N176Y	Forward: GCCAGAGCAAAGAA**T**ATGGTGTTTGTTGTC	73.3
	Reverse: GACAACAAACACCAT**A**TTCTTTGCTCTGGC	
human AOX1-G177E	Forward: CAGAGCAAAG**AA**AATGAAGTTTGTTGTCTGGATC	71.3
	Reverse: GATCCAGACAACAAACTTCATTTTC**TT**TGCTCTG	
human AOX1-V178F	Forward: CAGAGCAAAGAAAATGGTTT**TT**GTTGTCTGGATC	71.3
	Reverse: GATCCAGACAAC**AA**AAACCATTTTCTTTGCTCTG	

1: For the procedure to calculate T_m see section 3.2.1.5.

3.1.4. Buffers and Media

Table 3.4.: Buffers used in this study

Buffer	Composition
Mini-prep A1 buffer	50 mM Tris x HCl, 1 mM EDTA, 1:100 RNase mixed before use, pH 8.0, 4 °C
Mini-prep A2 buffer	200 mM NaOH, 1.25% w/v SDS
Mini-prep lysis buffer	300 mM NaCl, 50 mM NaH_2PO_4
Agarose gel running (TE) buffer	40 mM Tris-acetate, 1 mM EDTA, pH 8.0
Agarose gel buffer	1% w/v agarose in 40 mM Tris-acetate, 1 mM EDTA, pH 8.0, 0.4% v/v ethidium bromide
SDS-PAGE running buffer	192 mM glycine, 25 mM TrisHCl, 0.1 % w/v SDS, pH 8.2
SDS-PAGE loading sample buffer (4x)	0.5 M TrisHCl, 40% v/v glycine, 2.5% SDS, 5% 2-mercaptoethanol, 0.005% Bromophenol Blue
SDS-PAGE staining solution	50% v/v methanol, 10% v/v acetic acid, 0.1% Coomassie Brilliant Blue
SDS-PAGE destaining solution	20% v/v methanol, 7% v/v acetic acid
SDS-PAGE resolving buffer (4x)	1.5 M TrisHCl, pH 8.8
SDS-PAGE stacking buffer (4x)	1.5 M TrisHCl, pH 6.8
Resuspension buffer	50 mM sodium phosphate, 300 mM NaCl, pH 8.0
Wash buffer 1	50 mM sodium phosphate, 300 mM NaCl, 10 mM imidazole, pH 8.0 at 4 °C
Wash buffer 2	50 mM sodium phosphate, 300 mM NaCl, 20 mM imidazole, pH 8.0 at 4 °C
Elution buffer	50 mM sodium phosphate, 300 mM NaCl, 250 mM imidazole, pH 8.0 at 4 °C
Sulfuration buffer	50 mM KH_2PO_4, 0.1 mM EDTA, pH 7.4
Size exclusion chromatography buffer	50 mM TrisHCl, 200 mM NaCl, 1 mM EDTA, pH 8.0
Activity buffer	50 mM TrisHCl, 200 mM NaCl, 1 mM EDTA, pH 8.0
K-MES	500 mM KOH x 2-(N-morpholino)-ethanosulfonic acid, pH 6.3
MES-buffer	12% w/v glycerol, 50 mM $CaCl_2$, 45 mM $MnCl_2$, 2% v/v K-MES, pH 6.8

Table 3.5.: Media used in this study

Media	Composition
Lysogeny Broth	5 g Yeast extract, 10 g NaCl, 10 g Peptone
LB	5 g Yeast extract, 10 g NaCl, 10 g Trypton
LB Agar	2% w/v Agar, 5 g Yeast extract, 10 g NaCl, 10 g Trypton

3.1.5. Enzymes

Table 3.6.: Enzymes purchased in this study

Enzyme	Company
Endonuclease EcoRI	New England BioLabs or Thermo Fisher Scientific
Endonuclease NdeI	New England BioLabs or Thermo Fisher Scientific
Endonuclease DpnI	Thermo Fisher Scientific
DNA polymerase (Herculase II)	Agilent
T4 DNA Ligase	Thermo Fisher Scientific
DNase	Sigma
Alkaline phosphatase	Thermo Fisher Scientific
Xanthine Oxidase	Roche

3.2. Methods

3.2.1. Molecular Biology

3.2.1.1. Competent Cell Preparation

Cells can up take plasmids if they are treated with metal ions to facilitate the passage of DNA molecules through the cell membranes. To do this one method is as follows. One colony from the previously prepared or purchased cells was grown in 100 mL Lysogeny Broth (LB)-media (Bertani 1951) supplemented with 20 mM sterile $MgSO_4$ at 37 °C and 200 rpm until OD at 550 nm reached 0.9. Cells were gently stirred on ice water for 2 minutes and incubated on ice water for 28 minutes. Cells were centrifuged at 2500 rpm and 0 °C for 12 minutes and pellet was resuspended in 16 mL MES buffer. The resuspended cells were incubated for another 10 minutes on ice water and centrifuged again at 2500 rpm and 0 °C for 12 minutes. Cells were gently resuspended with 4 mL MES buffer, aliquoted in cold tubes to 50-100 µL, flash frozen in liquid nitrogen and stored at -80 °C for further uses.

3.2.1.2. Heat Shock Transformation Adopted from a Method Introduced by Hanahan (Hanahan 1983)

Transformation is a process in which plasmids are up-taken by competent cells. Competent cells were thawed for 5-10 minutes on ice and 0.5 to 1 µL of the plasmid was added and mixed by gently pipetting up and down and incubated on ice for 30 minutes. Cells were then incubated for 45 seconds at 42 °C and immediately transferred to ice for 3-5 minutes. 700 µL LB media was added to the transformants and grown at 37 °C for 1 hour. Transformants were then plated on LB-agar (LB containing 2% w/v agar) supplemented with appropriate antibiotic and grown over/night at 37 °C. Selected single colonies were grown in 3 mL LB media supplemented with for appropriate antibiotic 16-18 hours at 37 °C and 200 rpm and plasmids were isolated using NucleoSpin plasmid kit (MACHEREY-NAGEL) (see section 3.2.1.7.).

3.2.1.3. Agarose Gel Electrophoresis

DNA fragments are charged species that can migrate if exposed to an electric field. The rate of their migration depends on their size and shape, and hence, it is possible to separate DNA fragments in an electric field. This can be done on a network of agarose gels which provide pores with similar size range of the DNA samples. In this study 1% w/v agarose gels in 40 mM Tris-acetate, 1 mM EDTA, pH 8.0 was used to separate or visualize the DNA fragments in an electric field (70 to 110 V). The gel was supplemented with 0.4% ethidium bromide (EtBr) that binds to DNA and absorbs in the UV range so that the DNA bands are visible on the gel under a UV light. Size of the DNA fragments was estimated using a 1 kb DNA ladder (Fermentas).

3.2.1.4. Extraction of DNA Fragments from Agarose Gels

When needed, DNA fragments were extracted from agarose gels using NucleoSpin Extract II Kit (Macherey-Nagel). The agarose gel pieces containing the DNA of interest was dissolved in NT buffer (200 µL buffer per 100 mg gel) at 50 °C for 10-15 minutes. The solution was loaded in a column equipped with a silica membrane where the DNA fragments bind. Column was centrifuged at 11000 g for 1 min and the flow through was discarded. 700 µL of an ethanolic buffer was used to wash the membrane using another step of centrifugation. DNA was eluted using 40-50 µL sterile water preheated to 70 °C followed by a step of centrifugation. DNA samples were stored at -20 °C until further use.

3.2.1.5. Site Directed Mutagenesis after the Technique Used by Zheng (Zheng, et al. 2004)

In site directed mutagenesis (SDM) technique it is possible to mutate only one or two specific base pairs in a plasmid (Zheng, et al. 2004). This results in an exchange of a single amino acid at an aimed position. To do this, one pair of primers with the mutation site around the middle is designed and in a PCR process the whole plasmid is replicated to multiple copies. Using this technique, the plasmid containing human aldehyde oxidase gene with an N-terminal hexa-histidine tag generated previously (Foti, et al. 2016) was used as template in the next steps. A single nucleotide exchange was applied through site directed mutagenesis to obtain natural and cysteine variants listed in **Table 3.3.** For each variant a primer with 20 to 30 base pair length was designed with one or two nucleotides around the middle of the

oligonucleotide exchanged to result in the mutation. Melting temperatures (T_m) of the oligonucleotides were calculated using the following formula (Rychlik, et al. 1990):

$$T_m = 81.5 + 0.41 * GC\% - 675/n - mismatch\%$$

in which n is the number of the base pairs and $GC\%$ is the guanine and cytosine content. Optimum T_m was considered between 65 to 75 °C and oligonucleotides were synthesized by Eurofins (see **Table 3.3.** for the list of primers). Polymerase chain reaction (PCR) was performed using Herculase II Fusion DNA polymerase (Agilent) and PCR reactions and programs were set up according to the manufacturer's instruction. Following is an example of the PCR reaction mixture and program:

PCR reaction mix

Template DNA	50-100 ng
Forward primer	25 pmol
Reverse primer	25 pmol
Nucleotide mixture (dNTPs)	15 µmol
5x Herculase II buffer	10 µL
Herculase II DNA polymerase	1 µL
Total volume	**50 µL**

PCR reaction program

Initial denaturation	5 minutes at 95 °C
Denaturation*	30 seconds at 95 °C
Annealing	1 minute at 65 °C
Extension*	5 minutes at 68 °C
Final extension	7 minutes at 68 °C

***:** Denaturation to extension steps were repeated for 18 cycles

PCR products were digested using 10 U of DpnI (Thermo Fisher Scientific) to remove the methylated DNA and 5 µL of the resulting DNA mix was loaded on an agarose gel to confirm the production of the plasmid DNA. 20-30 µL of the PCR products was then transformed into DH5α cells as described before.

3.2.1.6. Plasmid Construction

Other plasmids (listed in **Table 3.2.**) were constructed using synthetic gene fragments purchased from Thermo Fisher Scientific that contained the desired mutations and the internal cutting sites of NdeI and EcoRI. The synthetic fragments were *E. coli* codon-optimized and replaced the corresponding fragment in the template. The plasmid containing human aldehyde oxidase gene with an N-terminal hexa-histidine tag generated previously (Foti, et al. 2016) was used as the template. NdeI and EcoRI (New England BioLabs or Thermo Fisher Scientific) and T4 DNA ligase (Thermo Fisher Scientific) were used to insert the gene piece into the template following the digestion/ligation protocols provided by the manufacturers. Ligation products were transformed into DH5α competent cells as described above.

3.2.1.7. Plasmid Isolation

Plasmids were isolated using NucleoSpin plasmid kit (MACHEREY-NAGEL) based on a SDS/alkaline lysis. 3-mL culture was centrifuged at 11000 g for 1 minutes and the pellet was resuspended in A1 buffer supplemented with 1:1000 RNase. A2 lysis buffer containing SDS was used to lyse the cells and A3 neutralizing buffer was added to facilitate the binding of plasmid DNA to the silica membrane. Lysate was cleared with centrifugation at 11000 g at RT for 10 minutes. Plasmid DNA present in the supernatant was bound to the silica membrane through a centrifugation step at 11000 for 1 minute and washed twice using an ethanolic washing buffer. Plasmid DNA was eluted using 40-50 µL

sterile water preheated to 70 °C followed by a step of centrifugation. Plasmid samples were stored at -20 °C until further use. Correctness of the mutations was confirmed by sequencing the plasmids at Eurofins.

3.2.2. Protein Production

3.2.2.1. Expression of hAOX1 after the Method Established by Hartman et al (Hartmann, et al. 2012)

Expression vectors were transformed into TP1000 competent cells (Palmer, et al. 1996) using a heat shock procedure as described above and the transformants were grown on LB-agar media (LB containing 2% w/v agar) for 16-18 hours at 37 °C. A few single colonies were picked and grown in a liquid LB media supplemented with 150 mg/mL ampicillin, 1 mM sodium molybdate and 20 mM isopropyl-β-D-1-thiogalactopyranoside (IPTG) for16-18 hours at 37 °C with no shaking to avoid oxygenation. The pre-culture was then used to inoculate 1 L of LB media containing peptone as carbon source enriched with 1 mM sodium molybdate, 20 mM IPTG and 150 mg/mL ampicillin in a 1:500 ratio. The cultivation was performed in 2 L flasks to minimize oxygenation and continued for 24 hours at 30 °C and 130 rpm. Cells were harvested by centrifugation at 4 °C and 8000 g for 5 minutes, resuspended in 10 mL of resuspension buffer (50 mM sodium phosphate, 300 mM NaCl, pH 8.0) per 1 L of culture and frozen at -20 °C until further use.

3.2.2.2. Immobilized Metal Affinity Chromatography Using Nickel-nitriloacetic Acid

Cells were slowly thawed at RT, carefully homogenized by vortexing after addition of 1 µg/mL DNase and applied to a cell cracker (Beijer Electronics, TS Benchtop Series) set at 1.35 kbar and 12 °C. Flow through was applied to the cell cracker one more time and the second flow through was cleared from cell debris by centrifuging at 21000 g and 4 °C for 60 minutes. Clear lysate was applied on a self-packed Nickel-nitriloacetic acid (Ni-NTA) column containing 0.5 mL matrix per liter of culture. Ni-NTA matrix was pre-washed with dH_2O and equilibrated with wash buffer 1 (50 mM sodium phosphate, 300 mM NaCl, 10 mM imidazole, pH 8.0 at 4 °C). Flow through was loaded twice to the column for better batch binding and the unspecifically bound proteins were washed off with 20 column volume (CV) of wash buffer 1 and wash buffer 2 (50 mM sodium phosphate, 300 mM NaCl, 20 mM imidazole, pH 8.0 at 4 °C). hAOX1 was eluted with 15-20 mL of the elution buffer (50 mM sodium phosphate, 300 mM NaCl, 250 mM imidazole, pH 8.0 at 4 °C) and the buffer was exchanged to the sulfuration buffer (50 mM KH_2PO_4, 0.1 mM EDTA, pH 7.4) using PD-10 columns (GE, Superdex G25 M). Eluted protein was concentrated using centrifugal concentrator (Sartorius or Amicon) with 100 kDa cut-off membrane to about 7 mL, aliquoted in 1 mL fractions and incubated overnight (16-18 hours) in an anaerobic chamber (Coy Laboratory Products) under 2% H_2 and 98% N_2 atmosphere.

In anaerobic purification the above steps were carried out in an anaerobic chamber except for the cell lysis and lysate clearing which were carried out outside the chamber using sealed centrifuge tubes to minimize the oxygen contact.

3.2.2.3. Chemical Sulfuration Adopted from Wahl et al and Foti et al (Foti, et al. 2016; Wahl, et al. 1982)

A chemical reconstitution of the sulfido ligand at Moco was carried out based on an original method developed by Wahl and co-workers in 1982 which was later modified for aldehyde oxidase by Foti et al (Foti, et al. 2016; Wahl, et al. 1982). Enzyme purified through IMAC-NiNTA was subjected to buffer exchange to the sulfuration buffer (50 mM KH_2PO_4, 0.1 mM EDTA, pH 7.4) and incubated under anaerobic chamber (2% H_2 and 98% N_2) at 4 °C for 16-18 hours. Anaerobic sample was subsequently treated with 2 mM of sodium sulfide, 500 µM of sodium dithionite and 25 µM methylviologen. The pH of the stock solutions was initially adjusted to 7.4. The mixture was incubated at room RT for 30 minutes under anaerobic chamber and the reaction was stopped by exchanging buffer to the SEC buffer (50 mM TrisHCl, 200 mM NaCl, 1 mM EDTA, pH 8.0) using PD-10 columns under aerobic condition at RT.

3.2.2.4. Size Exclusion Chromatography

Protein obtained from the previous step was concentrated to 2 mL using spinning concentrators (Sartorius or Amicon) with 100 kDa cut-off membrane and injected to a Superdex 200 pg 16/600 (GE Healthcare) column. The protein was eluted using SEC buffer (50 mM TrisHCl, 200 mM NaCl, 1 mM EDTA, pH 8.0) at 4 °C and elution was monitored in parallel at 280, 450 and 550 nm. Fractions were analyzed on 10% SDS-PAGE and the specific activity of the fractions corresponding to the symmetrical dimer peak were measured before the samples were combined and stored at -20 °C for further analysis.

3.2.3. Enzyme Characterization

3.2.3.1. Sodium Dodecyl Sulfate-Polyacrylamide Gel Electrophoresis after the Method Established by Laemmli (Laemmli 1970)

Similar to DNA fragments, proteins can be separated when exposed to an electric field on a polymer gel. However, the charge of proteins varies depending on the protein and is often not high enough to result in a detectable migration on the gel. Sodium dodecyl sulfate (SDS) is a surfactant that is able to bind proteins and confers negative charge to them. Proteins are further denatured by heat and hence, they are linearized and able to migrate depending on their size on a network of a polymer when exposed to an electric field. This method was developed by Laemmli in 1970 (Laemmli 1970). In our studies, after each step of purification, protein samples were resolved on Coomassie (Coomassie Brilliant Blue R250) stained 10% sodium dodecyl sulfate-polyacrylamide gels (SDS-PAGE) under reducing conditions. 1 mM 2-mercaptoethanol was used as reducing agent in the SDS-sample buffer and samples were denatured at 95 °C for 5 minutes prior to loading on the gel. 5-10 µg of protein were loaded on each well and the gel was subjected to an electric field (40 mA per gel). When appropriate, free thiols on cysteine residues were protected by 10x molar ratio excess of N-ethylmaleimide (NEM) or iodoacetamide (IAM).

3.2.3.2. UV-Vis Absorption

A Shimadzu UV-2401PC spectrophotometer was used to record the light absorbance of the protein samples (stored in 50 mM TrisHCl, 200 mM NaCl, 1 mM EDTA, pH 8.0) in the range of ultraviolet (UV) to visible wavelength from 250 to 800 nm. Quartz cuvettes (Hellma, Germany) were used to record the spectra and protein concentration was calculated using the absorbance at 450 nm considering 21100 $M^{-1}cm^{-1}$ extinction coefficient and 150 kDa molecular weight (MW) for hAOX1 variants.

3.2.3.3. Metal Content Determination Adopted from a Method Established by Neumann and Leimkuehler (Neumann and Leimkühler 2008)

Inductively coupled plasma optical emission spectroscopy (ICP-OES) was applied to determine the metal content in the wet-ashed enzyme samples. Samples were prepared in triplicates by adding 1:1 volume ratio of 65% nitric acid to 5-10 µM enzyme in parallel with buffer (50 mM Tris HCl, 200 mM NaCl, and1 mM EDTA, pH 8.0) in duplicates as control. Samples were then wet-ashed at 100 °C for 16-18 hours and diluted 4 times by adding distilled water after cooling down to RT. Measurements were performed using Optima 2100 DV (PerkinElmer Life and Analytical Sciences) and a multi element solution (Solution XVI, Merk) as standard at wavelengths 202, 203, and 204 nm for molybdenum, 238, 239 and 259 nm for iron and 206.2 and 213 nm for zinc. The resulting concentrations were related to the amount of protein

assuming four iron, one molybdenum, and one zinc (when applicable) centers in each monomer and reported as percentage.

3.2.3.4. Moco Determination According to a Method Developed by Johnson and Colleagues (Johnson, et al. 1984)

Form A, a fluorescent adduct of Moco, was extracted from protein samples under oxidative acidic condition and detected by high performance liquid chromatography (HPLC) in a method originally developed by Johnson and co-workers (Johnson, et al. 1984). 200 µL of about 1 µM protein was denatured with 25 µL of 1% I_2/2% KI in 1 M HCl and incubated overnight at room temperature. The denatured protein was removed by centrifugation for 10 minutes at 12,000 rpm and the supernatant was added to 50 µl of freshly prepared 1% ascorbic acid. The pH was adjusted to 8.3 by addition of 100 µL 1 M unbuffered TrisHCl. The phosphate monoester of Form A was cleaved by addition of one unit of alkaline phosphatase (1 µL) (Thermo Fisher Scientific) and 15 µL of 1 M $MgCl_2$. The mixture was incubated for 45 minutes at room temperature in dark and reaction was stopped by adding 10 µL of 50% acetic acid. Dephospho Form A was identified by HPLC (Agilent 1100 Series) using a C-18 reversed phase HPLC column (Thermo Scientific), equilibrated with 5 mM ammonium acetate with 15% methanol. Fluorescence was measured with excitation at 383 nm and emission at 450 nm using a FLD detector (Agilent 1100 Series).

3.2.3.5. ThermoFAD Stability Measurements According to a Method Adjusted for hAOX1 by Mota et al (Mota, et al. 2019)

The ThermoFAD assays were performed by Dr. Cristiano Mota in the Universidade Nova de Lisboa using a StepOnePlus system (Applied Biosystems) with a 470 nm extinction wavelength and SYBR Green fluorescence emission filter at 520 nm as optimized before (Mota, et al. 2019). The optimal protein concentration was 5 µM in 20 µL samples in 50 mM TrisHCl, 200 mM NaCl, 1 mM EDTA, pH 8.0 buffer. The unfolding process was followed in a temperature gradient from 25 to 90 ^{o}C and the fluorescence signal was collected for 46 minutes. All experiments were performed in triplicates and the melting temperature (T_m) values were obtained from the maxima in the plot of the first derivative of the fluorescence against temperature. The data analysis was performed by ME using Origin (version 2018b).

3.2.4. Enzyme Assays

3.2.4.1. Specific Activity Measurements

All the measurements were performed at room temperature and the values reported are the average of at least three independent measurements with standard deviation shown as ±SD. Activity of hAOX1 variants and mouse AOXs (mAOX1, mAOX2, mAOX3 and mAOX4) were measured in the presence of 40 µM phenanthridine in 500 µL reaction and air-saturated activity buffer (50 mM TrisHCl, 200 mM NaCl, 1 mM EDTA, pH 8.0) when molecular oxygen was used as final electron acceptor. Formation of phenanthridinone (extinction coefficient 6400 $M^{-1}cm^{-1}$) was followed at 321 nm for 30 seconds using a Shimadzu UV-2401PC spectrometer. Enzyme concentration was kept at 150-200 nM. 100 µM DCPIP with molar extinction coefficient of 16100 $M^{-1}cm^{-1}$ was used as an alternative electron acceptor when mentioned and reaction was tracked at 600 nm for 60 seconds.

PaoABC was produced and generously provided by Muhammad Abrar Hasnat with 20% Mo load. 500 µM benzaldehyde and 0.7 µM enzyme (ε_{450}: 23686 $M^{-1}cm^{-1}$, MW: 136 kDa) were used in a 500 µL reaction and appearing

of product with the molar extinction coefficient of 1321 $M^{-1}cm^{-1}$ at 295 nm was recorded in air-saturated PaoABC activity buffer (50 mM TrisHCl, 200 mM NaCl, 1 mM EDTA, pH 6.0).

Rc XDH was produced and kindly provided by Jasmin Kurtzke with 80% saturation of Mo. 10 nM of the enzyme with ε_{450} of 31600 $M^{-1}cm^{-1}$ and MW of 135 kDa was used in a 500 µL reaction in the activity buffer (50 mM TrisHCl, 200 mM NaCl, 1 mM EDTA, pH 6.0) with 1 mM xanthine and 1 mM nicotinamide adenine dinucleotide (NAD^+) and the formation of NADH with molar extinction coefficient of 6220 $M^{-1}cm^{-1}$ at 340 nm was followed.

bXO was purchased from Roche with ε_{450} of 35800 $M^{-1}cm^{-1}$ and MW of 150 kDa. The Mo and Fe saturation was assumed 100%. The enzymatic reaction was monitored in an air-saturated activity buffer (50 mM TrisHCl, 200 mM NaCl, 1 mM EDTA, pH 8.0) at 295 nm using 1 mM xanthine as substrate with ε_{295} of 8400 $M^{-1}cm^{-1}$ in the presence of 10 nM of enzyme.

The specific activity was calculated according to:

$$\frac{(mAbs/\min) * \varepsilon_{reactant}(M^{-1}.cm^{-1}) * 1\ cm * Reaction\ volume\ (mL)}{mg\ of\ enzyme}$$

where $mg\ of\ enzyme$ is obtained from

$$\left(Absorbance\ 450\ nm/\varepsilon^{450}_{enzyme}\ (M^{-1}.cm^{-1}) * 1\ cm\right) * MW\ (g.mol^{-1}) * Enzyme\ Volume\ (mL)$$

The final specific activities were normalized to the Mo% of each enzyme to obtain comparable values and reported as U/mg or mU/mg depending on the enzyme.

3.2.4.2. Steady State Kinetic Measurements

Steady state kinetic measurements were performed for hAOX1 variants (stored in 50 mM TrisHCl, 200 mM NaCl, 1 mM EDTA, pH 8.0) in reaction set-ups as explained for the specific activity except that a range of 2 -100 µM of phenanthridine was used unless mentioned otherwise. The enzyme concentration was kept at 150-200 nM. The kinetic parameters were obtained by fitting the data to the Michaelis-Menten equation. The Michaelis-Menten behaviour was confirmed by fitting the data in parallel to the Hill model. Origin (versions 2018b, 9.55 and 2016, 9.3) was used for data analysis.

3.2.4.3. Enzyme Inactivation Assay

Inactivation assay was established in a 500 µL reaction mix containing 160 µM (about 5 times K_m) phenanthridine and 150-180 nM enzyme in an air-saturated buffer (50 mM TrisHCl, 200 mM NaCl, 1 mM EDTA, pH 8.0). Formation of phenanthridinone (molar extinction coefficient 6400 $M^{-1}cm^{-1}$) was followed at 321 nm for 1800 seconds. A linear fit of the first 30 seconds of the reaction progress curve gave the V_{max} at 160 µM of phenanthridine and the turnover was calculated according to:

$$Turnover(s^{-1}) = \frac{V_{max}(Absorbance/s) * Reaction\ Volume(\mu L) * \varepsilon^{321}_{phenanthridinone}}{\mu mol\ Enzyme * Fe\%}$$

The first derivative of the progress curve against time was obtained and the behaviour was fitted into exponential decay equation using Origin (versions 2018b, 9.55 and 2016, 9.3) according to

$$y = A_1 * e^{(-x/t1)} + y_0$$

where the equation is equivalent to enzyme inactivation description as in

$$A = (A_0 - A_{min})e^{k_D t} + A_{min}$$

where y is the activity at time t, A_0 is the activity at time zero, A_{min} is the minimum activity recorded for the enzyme, t is time and k_D is the first-order activity decay constant (Householder and Gomori 1943). The enzyme inactivation follows a first-order decay pattern over time, which allows calculating the enzyme half-life ($t_{1/2}$) by

$$t_{1/2} = 0.693/k_D$$

3.2.4.4. Reactive Oxygen Species (ROS) Assay Adopted from a Method Developed by McCord and Fridovich (McCord and Fridovich 1969)

The amount of superoxide ($O_2^{\cdot-}$) was directly obtained from the reduction of bovine cytochrome C (ε_{550}: 28000 $M^{-1}cm^{-1}$, MW: 12.3 kDa) in a reaction mix containing 40 µM phenanthridine, 40 µM cytochrome C and 150-200 nM of hAOX1 variants in air-saturated activity buffer (50 mM TrisHCl, 200 mM NaCl, 1 mM EDTA, pH 8.0) following the increase in the absorbance at 550 nm for 30 seconds. The control reactions performed in parallel contained a similar composition in addition to 100 U/mL of catalase or 20 µM superoxide dismutase (SOD). The extra signal in the presence of SOD was subtracted from the main reaction when observed. The total ROS was obtained from the reaction of 40 µM of phenanthridine and 150-200 nM of hAOX1 variants. The reported percentage of superoxide was calculated from the ratio of superoxide to total ROS for each variant.

The inhibition in the reduction of cytochrome C was assessed in the presence of 5 µM diphenyleneiodonium (DPI), a specific inhibitor of FAD (Reis, et al. 2020) in a similar reaction as explained above and the uninhibited and inhibited reduction of cytochrome C were reported as specific activity, mU/mg (nmol/min.mg).

3.2.5. Structural Studies

3.2.5.1. Crystallization

hAOX1 crystallization was set up based on previous reports in collaboration with the research group of Pro. Maria Joao Romao and with the help of Dr. Cristiano Mota in Universidade Nova de Lisboa (Coelho, et al. 2015). Different variants were incubated with 30 mM dithiothreitol (DTT) for 10 minutes prior to crystallization. Screening was performed through a hanging-drop vapour diffusion method using 4 µL of 5-10 mg/mL enzyme depending on the variant and 0.1 and 0.2 M sodium malonate (pH 5.0 and 6.0) and 12-22% polyethylene glycol (PEG) 3350 as precipitant solution. Crystals appeared at 293 K a few hours after crystallization was set up and grew maximally to about 0.1 mm length after 24 hours. Crystals of good morphology were transferred to the cryo-protectant solution provided by the mother liquor supplemented with 15% (v/v) glycerol and flash frozen in liquid nitrogen.

In soaking experiments the cryo-solution was supplemented with 10 mM of Ca^{2+}, Fe^{3+}, Zn^{+2}, as chloride salts and As^{+3} as $NaAsO_2$ for 10 minutes prior to flash freezing. In co-crystallization trials the enzyme was incubated with 1-2 mM of Fe^{3+}, Zn^{+2}, As^{+3} for 1 hour on ice and was taken for screening as explained above.

hAOX1-L438V crystals were obtained in a condition containing 0.2 M sodium malonate (pH 5.0), 20% polyethylene glycol (PEG) 3350, 1mM of raloxifene and 1% DMSO. The crystallization experiments were performed by Dr. Cristiano Mota.

3.2.5.2. Data Collection and Structure Solution

hAOX1 different variants diffracted up to 3.0 Å resolution at beamlines ID30B from the European Synchrotron Radiation Facility (ESRF) in Grenoble, France at wavelength of 0.978. Crystals of hAOX1-L438V diffracted up to 2.7

Å at beamline XALOC from ALBA (Barcelona) at wavelength of 0.979 Å. Data sets were processed using XDS package (Kabsch 2010) and Aimless (Evans and Murshudov 2013). Data collection statistics for hAOX1-L438V are presented in **Table 3.7.**

The structure of hAOX1-L438V was solved by Dr. Cristiano Mota from the Universidade Nova de Lisboa using molecular replacement method and Phaser (McCoy, et al. 2007). The structure of hAOX1-WT (PDB entry: 4UHW) was used as the search model. The protein model was built manually using Coot (Emsley, et al. 2010) and phenix.refine (Afonine, et al. 2012) and the quality of the model was evaluated by MolProbity (Davis, et al. 2007).

Table 3.7.: Crystallographic data processing and refinement statistics

Co-Crystal	hAOX1-L438V-Raloxifene
PDB ID	-
Diffraction data	
Wavelength (Å)	0.979
Beamline (ALBA)	XALOC
No. Crystals	1
Space group	$P4_32_12$
Cell dimensions (Å)	a= b =149.37, c=268.82
Resolution range of data (Å) (last shell)	48.15 – 2.60 (2.64 – 2.60)
Completeness (%) (last shell)	99.9 (99.6)
R_{merge} (last shell)	0.114 (1.502)
R_{meas} (last shell)	0.123 (1.629)
I/σ(I) (last shell)	11.9 (1.3)
CC1/2 (last shell)	0.999 (0.608)
Redundancy (last shell)	7.4 (6.7)
Refinement	
Reflections used in refinement (work (free))	93642 (4593)
R_{work} (last shell)	0.2124 (0.3503)
R_{free} (last shell)	0.2431 (0.3763)
Nº of non-hydrogen atoms	20651
Protein	20125
Ligands	339
Solvent	187
Geometry and B-factors	
RMSD bond lengths (Å)	0.002
RMSD bond angles (º)	0.597
Average B-factor ALL ($Å^{2)}$	60.41
Protein ($Å^2$)	60.39
Solvent ($Å^2$)	49.96
Ramachandran favored (%)	96.43
Ramachandran outliers (%)	0.43
Molprobity score	1.56
Clashscore	5.87

3.2.6. Electrospray Ionization Mass Spectroscopy (ESI)

For electrospray ionization mass spectroscopy analysis hAOX1 was incubated with 100x molar ratio IAM or NEM for 30 minutes at room temperature and ran on a reducing or non-reducing SDS-PAGE depending on the condition required. Bands were cut and dried using a SpeedVac (Christ RVC 2-18) and sent for the analysis to the proteomics lab. The MS measurements were performed by Dr. Manfred Nimtz from the proteomic lab of Prof. Dr. Lothar Jänsch in Helmholtz Centre for Infection Research, Braunschweig, Germany. Bands were incubated with DTT and subsequently with a second label methyl methanethiosulfate (MMTS) and IAM, respectively for the IAM and NEM treated samples) to ensure the exposed free thiols were protected. Tryptic digestion was performed thereafter at 37 °C overnight. Peptides were then extracted from the gel, desalted, separated by HPLC (Evosep, Odense) and measured on an ESI-TIMSTOF mass spectrometer (Bruker, Bremen) (More technical details will be provided in the manuscript). Analysis of the peptides was performed with the help of Prof. Lloyd Ruddock from the University of Oulu, Finland. Percentage of each modification was calculated in a semi-quantitative method (similar to the method applied by Shetty and colleagues

(Shetty, et al. 2007)) considering the intensity of the peptides carrying the modification against all the peptides containing a residue of interest.

3.2.7. Near UV Circular Dichroism (CD) Spectroscopy

Near UV CD measurements were performed using a JASCO 815 CD spectropolarimeter calibrated with 1S-(+)-10-camphorsulphonic acid (Kelly, et al. 2005) and equipped with a Peltier PTC-423S device to maintain the temperature at 22 ± 0.1 °C. Samples contained 400 µL of 8-10 µM protein (concentration based on the absorption at 450 nm) in a buffer consisting of 50 mM TrisHCl, 200 mM NaCl, 1 mM EDTA, pH 8.0. CD spectra were recorded in a quartz cuvette of 1 mm path length (Hellma, Germany) in a wavelength range from 350 to 600 nm in three accumulations. Baseline was corrected with the buffer and ellipticities were converted to mean residue ellipticities Θ_{MRW} considering the protein concentration based on the absorbance at 280 nm or 450 nm. All measurements were performed in triplicates and the final spectra were reported as the average of the three measurements.

4. Results

4.1. Mysteries of a Flexible Region Containing Conserved Cysteines

4.1.1. A Flexible Region Carrying Cysteines of Unknown Function

In the primary structure of most XO family enzymes in higher eukaryotes a sequence of about 40-70 amino acid residues has evolved at the C-terminus of the FeS domain that carries conserved cysteines (**Figure 4.1.**). A similar unstructured region is present in prokaryotic XDHs and AOXs and in a few plant family members, but it is shorter and lacks the cysteine residues. The cysteines in the eukaryotic family members are organized in highly conserved vicinal pairs in a $CC(X)_{7\text{-}8}CC$ motif in both AOXs and XDHs and in a less conserved $C(X)_3C$ motif which exclusively appears in AOXs. A comprehensive alignment, partially shown in **Figure 4.1.,** reveals that the number of amino acids in the region increases from prokaryotes to plants, invertebrates and finally to vertebrates. One pair of vicinal cysteines is present in *D. melanogaster* XDH and in *X. laevis* AOX1, further developed to two pairs in *C. elegans* and in several fish AOXs, e.g. *S. salar, D. rerio* and *X. maculatus*. The motif has evolved to $C(X)_3C(X)_4CC(X)_7CC$ in AOXs in amphibians, reptiles, birds and mammals, however, the cysteines on the $C(X)_3C$ motif are less conserved than the vicinal cysteine pairs. In XDHs the $C(X)_3C$ motif is not present while avian XDHs carry four pairs of vicinal cysteines. The orientation of the thiol side chains on cysteines and the position of the loop in the region around the cysteines (the region shown in the alignment in **Figure 4.1.**) cannot be seen in any of the X-ray crystal structures available for eukaryotic XDHs and AOXs, probably due to high flexibility and consequent low electron density of the region. The appearance of these cysteines in eukaryotes and their conservation suggest a function for the loop and cysteines shared within the family.

The cysteine-containing flexible region in hAOX1 starts at Cys161 only 10 residues after the FeSI cluster binding site. K162-V236 is a fragment annotated as an extension to the FeS domain (InterPro IPR014313) (see the schematic in **Figure 4.2.**). The region around the cysteines from 167 to 199 is highly flexible and only partially visualized in the crystal structure (PDB entry: 4UHW) (Coelho, et al. 2015). The first cysteine pair, Cys170 and Cys171, is separated from the second pair, Cys179 and Cys180, by seven residues including glutamate, serine, glutamine, lysine and glycine which are among the residues generally found in intrinsically disordered proteins (IDP) (Uversky 2013). Three natural variants N176Y, G177E and V178F have been reported as the results of single

```
H.sapiensAOX1          159  DACKTFCK-T----------------------SGCCQSKEN-GVCCLDQGINGLPEFEEG 194
B.taurusAOX1           159  NACKTFCK-T----------------------SGCCQSKEN-GVCCLDQGMNGLPEFEEG 194
M.musculusAOX1         158  DACKTFCK-A----------------------SACCQSKEN-GVCCLDQEINGLAESQEE 193
M.musculusAOX2         162  ESGRTFCM-E----------------------PDGCPQKGT-GQCCLDQKESDS--SGSK 196
M.musculusAOX3         163  ESAKSFCP-S----------------------STCCQMNGE-GKCCLDEEKNE---PERK 194
M.musculusAOX4         162  ESGKTFSQ-K----------------------STVCQMKGS-GKCCMDPDEK--CLESRE 195
R.norvegicusAOX1       158  DACKTFCR-A----------------------SGCCESKEN-GVCCLDQGINGSAEFQEG 193
R.norvegicusAOX2       159  ESGRTFCM-E----------------------SDGCLQKGT-GQCCLDQKEGDS--SGSK 196
R.norvegicusAOX4       156  ESGKTFSP-E----------------------SSVCQMKGS-GKCCMDLDEG--CSESTK 193
C.porcellusAOX1        156  DAGKTFCK-T----------------------SGCCQSKEN-GVCCLDQGVNGVQEA-EG 192
C.porcellusAOX4        162  ESGKTFCA-N----------------------PTVCQVKRP-GRCCLEQEEEEAGSVHTR 197
O.cuniculusAOX1        159  EAYKTFCK-T----------------------SDCCQNKEN-GFCCLDQGINGLPEVEEE 194
O.cuniculusAOX4        158  ESGKTFCV-E----------------------STICQVKGT-GKCCMDQEEK—SSLGSQ  195
E.cabullusAOX1         159  DACKTFCK-T----------------------SGCCQSKEN-GVCCLDQGINELPEFEEG 194
E.cabullusAOX4         158  ESGKTFCV-E----------------------STVCQVKGS-GRCYMEQDER--PFVTRQ 195
C.l.familiarisAOX2     158  ESGKTFCR-E----------------------STVCGMKSS-GKCCMDQEER--SFVNRQ 195
C.l.familiarisAOX3     162  ASGRTFCV-E----------------------SNGCQQRGT-GKCCLDPGGNDSSSVGRE 197
C.l.familiarisAOX4     154  ESGKTFCR-E----------------------STVCGMKSS-GKCCMDQEER--SFVNRQ 187
P.capensisAOX1         163  DACKTFSK-S----------------------TGCCQSKEN-GVCCLNGEINGLSEVDEG 198
E.europaesAOX          172  DACKTFCK-T----------------------SGCCQSKEN-GTCCLDQGINESQEPEEE 207
N.visonAOX             159  DACKTFCK-T----------------------SGCCQSKEN-GVCCLDQGINELTEFEEG 194
D.ordiiAOX             159  EAGKTFCK-T----------------------SGCCQSKEN-GVCCLDQGVNGLPELEED 194
S.scrofaAOX1           160  DACKTFCK-T----------------------SGCCQGKEN-EVCCLDQGINGLPEFEEG 195
S.scrofaAOX2           163  ESGKTFCS-E----------------------SNGCQQKGT-GKCCLDQGENDSASLDRK 198
B.mutusAOX             159  NACKTFCK-T----------------------SGCCQSKEN-GVCCLDQGINGLPEFEEG 194
I.tridecemlineatusAOX1 159  DTCKTFSK-T----------------------FGCCQGKEN-GTCCLDQGINGLPELEEG 194
T.syrichtaAOX1         134  DACRTLCK-D----------------------SACCQGKEN-GVCCLDQGINELLEFEEG 169
M.lucifugusAOX1        159  DACKTFCN-T----------------------SGCCQSKEN-GVCCLNQGINGFPELEEG 194
L.africanoAOX1         163  DACKSFCK-T----------------------TDCCQSKEN-GVCCLDEEINELPGFEEG 198
M.fascicularisAOX1     159  DACKTFCE-T----------------------SGCCQSKEN-GVCCLDQRINGLPEFEEG 194
M.fascicularisAOX2     163  ESGRTFCM-E----------------------SNSCQQKGT-GKCCLDWGENDSSRLGKK 198
P.paniscusAOX1         145  DACKTFCK-T----------------------SGCCQSKEN-GVCCLDQGINGLPEFEEG 181
G.g.gorillaAOX1        159  DACKTFCK-T----------------------SGCCQSKEN-GVCSLDQGINGLPEFGEG 194
A.melanoleucaAOX3      162  ASGRTFCV-E----------------------SNGCQQKGT-GKCCLDPRGNDSSSLLRE 197
H.sapiensXDH           158  QGFRTFARD-----------------------GGCCGGDGNNPNCCMNQKK------DHS 188
B.taurusXDH            158  QGFRTFAKN-----------------------GGCCGGNGNNPNCCMNQKK------DHT 188
R.norvegicusXDH        157  QGFRTFAKD-----------------------GGCCGGSGNNPNCCMNQTK------DQT 187
M.musculusXDH          160  QGFRTFAKD-----------------------GGCCGGSGNNPNCCMSQTK------DQT 190
F.catusXDH             158  QGFRTFARD-----------------------GGCCGGSGNDLNCCMNQKT------DHK 188
M.lucifugusXDH         161  QGFRTFARD-----------------------GGCCGGNVDNPNCCMNQKK------DDT 191
M.gallopavoAOX1        164  DACKTFCK-D----------------------SVCCQSKAN-GRCCLDQEEDL---SGRE 196
S.c.australisAOX       164  DACKTFCE-E----------------------SICCQSKAN-GKCCLDQKDDL---FDNG 196
A.platyrhynchosAOX      90  DACKTFCK-E----------------------SVCCQSRAS-GKCCLDHEEDL---FDKE 124
G.gallusAOX1           164  DACKTFCK-D----------------------SVCCQSKAN-GRCCLDQEEDL---FDRE 196
G.gallusAOX2           163  DSYASFAK-E----------------------QTCCQLRGT-GQCCLDQEELGCSSS-AG 197
G.gallusXDH            162  EGYRTFAVDSNCCGKAANGTGCCHSKGENSMNGGCCGGKANGPGCCMNEKE------N-V 214
M.gallopavoXDH         162  EGYRTFAVDSNCSGSIANGTGCCRSKGENSVNGGCCGGKANGPGCCMNEKE------N-M 214
T.guttataXDH           161  EGYRTFAKDMNGCGRAANGTGCCRSGKENAMNGGCCGGKANGPGCCMNGKED-----N-V 213
F.albicollisXDH        162  EGYRTFAKDMNCCGRIANGTGCCHSGRENTMNGGCCGGKANGPGCCMNGKEG-----SMK 216
A.sinensisXDH          177  EGYKTFTVE-----------------------GGCCGGRGQKNGCCMSNVNGAQNGSEEQ 213
A.sinensisAOXlike      174  ESCKTFCK-E----------------------SVCCQVSSNKGNNCLDEEKVTSF---PE 202
A.sinensisAOX4         164  DACKTFCK-D----------------------LDCCKIREN-ENCCLDLKENLLL-SGKG 198
A.carolinensisAOX1     178  DGFKTFCK-E----------------------SVCCQNKEN-GVCCLDQEDQLSLLPNKE 202
P.sinensisXDH          159  QGYRTFAKTG---------------------KSEGCCGGKASGQGCCMNEKE------DNA 192
P.sinensisAOX2         162  DTYKSFAG-E----------------------AACCQLRGT-GQCCLDKEEDVCSSSDKG 197
X.laevisAOX1           162  DGCRTFCN-K----------------------TDCCQVKEN-GM-------EKISTPDTV 190
D.rerioAOX6            162  DGYRTFCE-S----------------------ENCCLLNGSTC-NVLNGNG-------SA 190
X.maculatusAOXbeta     162  DGCRTFCQ-E----------------------GNCCQANGGA-NCCLNGEGNA---NESE 194
O.latipesAOXbeta       161  DGCRTFCQQE----------------------ANCCQVNGGG-NCCLNGEKIT---NEDS 195
L.oculatusAOXbeta      162  DGYKTFCG-A----------------------SNCCQTNSNGD-CCLNEELLG---QD-- 192
S.salarAOX1like        162  DGCKTFSP-E----------------------SNCCQANGNGAGCCLNGESSP---ERSE 195
D.rerioXDH             177  EGYKTFTVE-----------------------GGCCGGRGQKNGCCMSNVNGAQNGSEEQ 213
C.elegansAOXGad3       157  EALYSFSSES----------------------GGCCGGNKTGGGCCKDKSSS-----DED 189
D.melanogasterXDH      162  EGYKTFTKEFACG-------------------------MGDKCCKVNGKGCGGGDDTQ 194
D.melanogasterAOX1     158  DAMKSFAVDSNIQ-------------------------VPAECIDIEDLSTKKCPKT 189
O.sativaAOX1           175  DACKSFAADVDL---------------------------------------EDLGLNSFWK- 196
A.thalianaAAO3         160  DACKSFASDVDI---------------------------------------EDLGLNSFWK- 181
G.maxAOX2              175  DACKSFAADFDI---------------------------------------EDLGLNSFWR- 196
R.communisAOX          105  DVCKSFAADVDM---------------------------------------EDLGLNSFWK- 126
S.lycopersicumABA      174  DACKTFAADVDI---------------------------------------EDLGFNSFWK- 195
E. coliPaoABC          218  AAIEDAAGEIKS---------------------------------------------- 229
R.capsulatusXDH        144  RAAEAAAGEP-P---------------------------------------------- 154
T.vaginalisXDH         174  EAMREFSTDNKP---------------------------N----------------DS- 188
```

Figure 4.1.: Amino acid sequence alignment around a flexible region at the C-terminus of the FeS domain in XDHs and AOXs from prokaryotes to mammals: The region in prokaryotes is shorter and does not contain any cysteines, while it is longer in plants, with only a single cysteine which is not conserved. Cysteine pairs start to appear in higher organisms from one pair in *D. melanogaster* XDH to two pairs in *C. elegans* AOX and to fish, reptiles, birds and mammals. Birds XDH contain four pairs of vicinal cysteines. Two less conserved single cysteines in a $C(X)_3C$ motif, exclusively found in AOXs but not in XDHs, appear in the higher organisms. The organisms are abbreviated as following: *Homo sapiens: H. sapiens, Bos taurus: B. Taurus, Mus musculus: M. musculus, Rattus norvegicus: R. norvegicus, Cavia porcellus: C. porcellus, Oryctolagus cuniculus: O. cuniculus, Equus caballus: E. caballus, Canis lupus familiaris: C. l. familiaris, Procavia capensis: P. capensis, Erinaceus europaes: E. europaes, Neovison vison: N. vison, Dipodomys ordii, Sus scrofa: S. scrofa,Bos mutus: B. mutus, Ictidomys tridecemlineatus: I. tridecemlineatus, Tarsius syrichta: T. syrichta, Myotis lucifugus: M. lucifugus, Loxodonta africano: L. africano, Macaca fascicularis: M. fascicularis, Pan paniscus:P. paniscus, Gorilla gorilla gorilla: G. g. gorilla, Ailuropoda melanoleuca: A. melanoleuca, Anolis carolinensis: A. carolinensis, Felis catus: F. catus, Meleagris gallopavo: M. gallopavo, Struthio camelus australis: S. c. australis, Anas platyrhynchos: A. platyrhynchos, Gallus gallus: G. gallus, Taeniopygia guttata: T. guttata, Ficedula albicollis: F. albicollis, Alligator sinensis: A. sinensis, Pelodiscus sinensis: P. sinensis, Xenopus laevis: X. laevis, Danio rerio: D. rerio, Xiphophorus maculatus: X. maculatus, Oryzias latipes: O. latipes, Lepisosteus oculatus: L. oculatus, Salmo salar: S. salar, Caenorhabditis elegans: C. elegans, Drosophila melanogaster: D. melanogaster, Oryza sativa: O. sativa, Arabidopsis thaliana: A. thaliana, Glycine max: G. max, Ricinus communis: R. communis, Solanum lycopersicum: S. lycopersicum, Escherichia coli: E. coli, Rhodobacter capsulatus: R. capsulatus, Trichomonas vaginalis: T. vaginalis.*

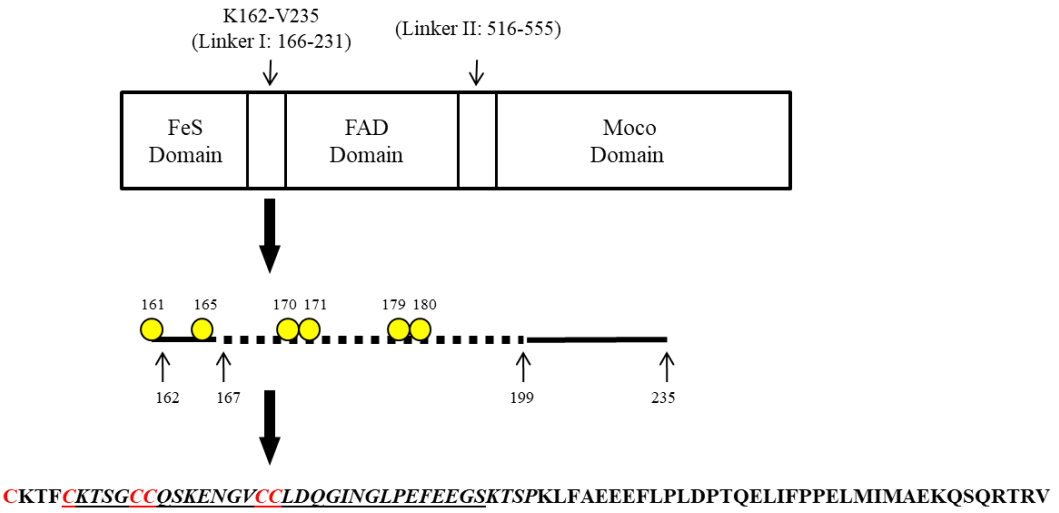

Figure 4.2.: Schematic of the flexible region carrying cysteines in hAOX1: The overall domain architecture of hAOX1 is shown on top with the K162-V236 fragment which is annotated as an extended region added to the C-terminus of the FeS domain (InterPro accession code: IPR014313). The middle scheme shows the region that starts after a partially conserved single cysteine (Cys161) and includes another partially conserved single cysteine (Cys165) and two vicinal cysteine pairs Cys170, Cys171 and Cys179, Cys180. Cysteines are shown in yellow circles and the parts which are not visible in the crystal structure are indicated as a dashed line. The full sequence of the region is shown below the schematic with the fragment which is not visible in the crystal structure in underlined *italics*.

nucleotide polymorphisms (SNP) in proximity to the cysteines in the region. Despite extensive studies on the XO family of molybdoenzymes and hAOX1 in particular, there has been no mention of these cysteines in the literature. To investigate possible roles for the region and cysteines we focused on hAOX1, an enzyme with well-established methods to produce and study *in vitro* (Foti, et al. 2016).

4.1.2. Production and Characterization of hAOX1 Variants with Different Composition of the Flexible Region

4.1.2.1. Enzyme Production

Three groups of constructs listed in **Table 4.1.** (see also **Table 3.2.** in section 3.1.2., Materials and Methods) were generated to study the role of cysteines present in the flexible region: cysteine variants, natural variants and chimeric variants. The cysteine variants were produced with the cysteines exchanged to alanines either in the $^{161}C(X)_3C^{165}$ motif as single cysteines or in the $^{170}CC(X)_7CC^{180}$ motif where two, three or four cysteines were replaced. Additionally, two plasmids, 6A and 6D, which lacked the entire six cysteines in the region, were constructed. The cysteines were replaced with aspartates in 6D to mimic any potential negative charges that might develop from the formation of $-SO_2^-$ or $-SO_3^-$ species on the cysteines induced by ROS which are generated during the catalytic cycle.

Table 4.1.: The hAOX1 variants made for studying the flexible region containing cysteines

	Protein	Shortened for
Cysteine Variants	DACKTFCKTSGCCQSKENGVCCLDQGINGLPEFEEG	WT
	DAAKTFAKTSGAAQSKENGVAALDQGINGLPEFEEG	6A[1]
	DADKTFDKTSGDDQSKENGVDDLDQGINGLPEFEEG	6D[1]
	DACKTFCKTSGAAQSKENGVAALDQGINGLPEFEEG	4A[1]
	DACKTFCKTSGAAQSKENGVACLDQGINGLPEFEEG	3A[2]
	DACKTFCKTSGCCQSKENGVAALDQGINGLPEFEEG	2A-2[1]
	DACKTFCKTSGAAQSKENGVCCLDQGINGLPEFEEG	2A-1[2]
	DAAKTFCKTSGCCQSKENGVCCLDQGINGLPEFEEG	C161A[2]
	DACKTFAKTSGCCQSKENGVCCLDQGINGLPEFEEG	C165A[2]
Natural Variants	DACKTFCKTSGCCQSKEYGVCCLDQGINGLPEFEEG	N176Y[2]
	DACKTFCKTSGCCQSKENEVCCLDQGINGLPEFEEG	G177E[2]
	DACKTFCKTSGCCQSKENGFCCLDQGINGLPEFEEG	V178F[2]
Chimeric Variants	human AOX1 cysteine loop (K162-V235) replaced by *D. melanogaster* AOX1 loop (K161-Q206)	gXDH-Chimera[1]
	human AOX1 cysteine loop (K162-V235) replaced *G. gallus* XDH loop (R164-C254)	dAOX1-Chimera[1]
	human AOX1 cysteine loop (K162-V235) replaced by *R. capsulatos* XDH loop (E147-G172)	*Rc* XDH-Chimera[1]

1: Constructed using synthetic gene fragment
2: Constructed using site directed mutagenesis method (see Table 3.3. in Materials and Methods for the list plasmids)

Three natural variants, i.e. N176Y, G177E and V178F, with an exchanged amino acid which locates near the cysteines in the flexible region, have been reported in the SNP database (Sherry, et al.

2001). The plasmids carrying genes for these variants were generated and studied in parallel with WT and the cysteine variants.

In addition, the region around the cysteines in hAOX1 from Lys162 to Val235 was exchanged to its counterparts in *R. capsulatus* XDH (*Rc* XDH) (E147-G172), *D. melanogaster* AOX1 (dAOX1) (K161-Q206) and *G. gallus* XDH (gXDH) (R164-C254). The region in these enzymes are noticeably different in length varying from 26 amino acid residues in *Rc* XDH to 46, 74 and 89 in dAOX1, hAOX1 and gXDH, respectively. The region in hAOX1, gXDH and *Rc* XDH is overall negatively charged, while dAOX1 contains more positively charged residues and the overall charge is positive. The number of cysteines present in the region differs, from no cysteine in *Rc* XDH to two single ones in dAOX1, and four pairs of vicinal cysteines in gXDH.

Plasmids were aerobically overexpressed in *E. coli* TP1000 cells (*ΔmobAB*) (Palmer, et al. 1996) and proteins were purified as described elsewhere (Foti, et al. 2016) in two consequent steps of an immobilized metal affinity chromatography (IMAC) using a nickel nitrilotriacetic acid (Ni-NTA) column followed by a size exclusion chromatography (SEC). The elution profiles of the variants produced for this study (**Figure 4.3.)** showed distinct separation of tetramer, dimer and monomer peaks eluted at 55, 62 and 70 mL, respectively, except for the hAOX1-*Rc* XDH-chimera that did not result in any soluble protein being expressed. Exchanging cysteines in the flexible region with alanines in 6A, 4A, 3A, 2A-1, and 2A-2 did not change the SEC elution trace of the enzyme in comparison with WT, but replacing the cysteines with aspartates in 6D lowered the aggregation and tetramer peaks. The single cysteine variants, C161A and C165A, and the natural variants, N176Y, G177E and V178F, showed similar patterns of SEC profile to that of WT.

The average yield of the production was about 1 mg/L with the highest amount of 1.5 mg/L for C165A and 1.4 mg/L for 6D, 4A and 3A, and lowest yield of 0.5 mg/L for N176Y and 6A (see **Table 4.2.**). The chimeric variants, hAOX1-gXDH-chimera and hAOX1-dAOX1-chimera, resulted in slightly higher aggregation peaks than WT and more pronounced impurity peaks around 90 mL elution. The yield for the both chimeric variants was about 0.2 mg/L which was significantly less than the average production yield suggesting a lower stability. The hAOX1-*Rc* XDH-chimera did not result in soluble protein. Overall, the production of these variants, except hAOX1-*Rc* XDH-chimera, suggests a similarly shared tertiary structure and folding process.

The SEC fractions were resolved on reducing Coomassie stained SDS-PAGE gels and the dimer peak fractions were combined for further use. The final protein samples, ran in parallel on a

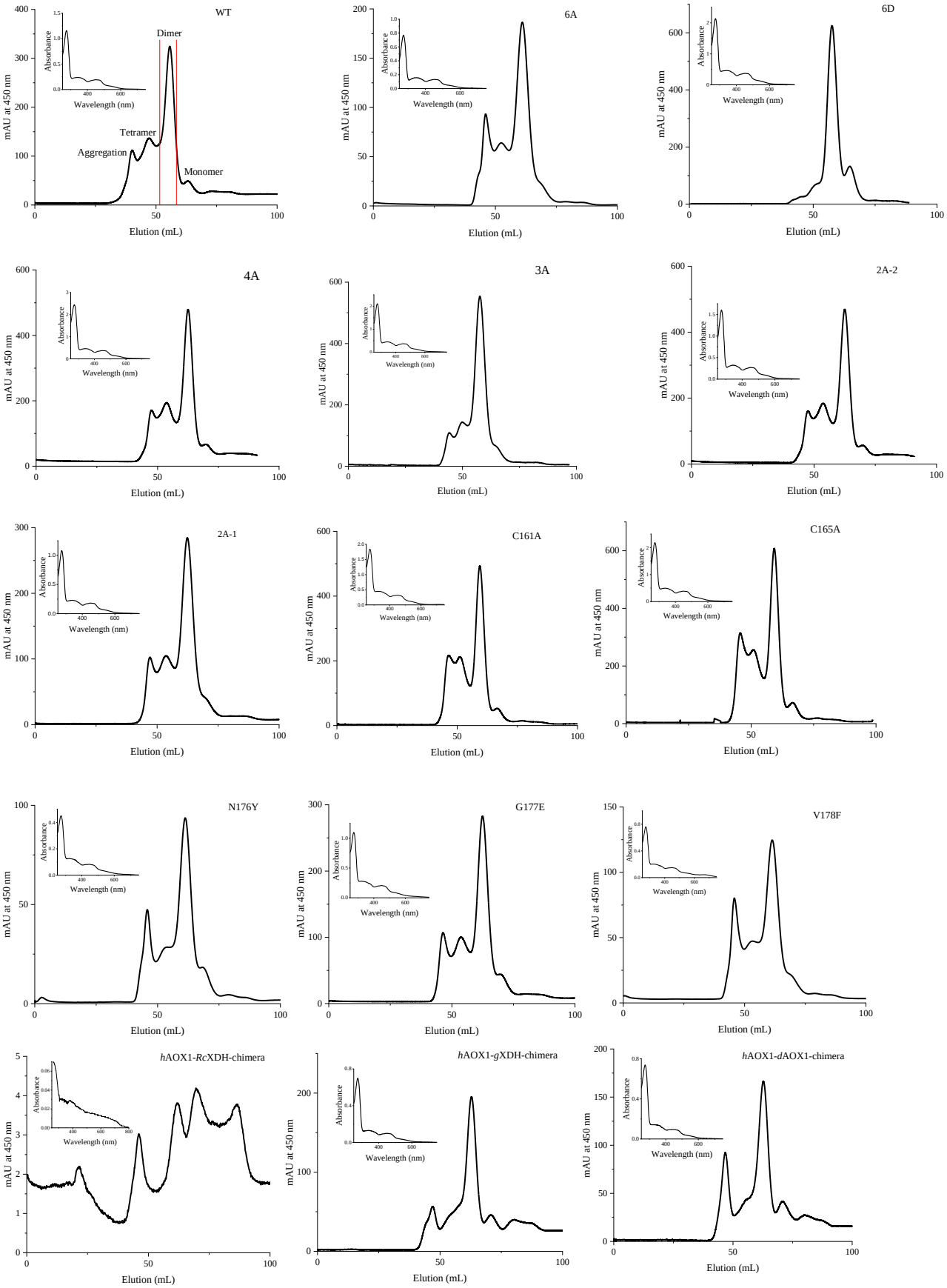
WT
Dimer
Tetramer
Aggregation
Monomer
6A
6D
4A
3A
2A-2
2A-1
C161A
C165A
N176Y
G177E
V178F
hAOX1-RcXDH-chimera
hAOX1-gXDH-chimera
hAOX1-dAOX1-chimera
mAU at 450 nm
Elution (mL)
Absorbance
Wavelength (nm)

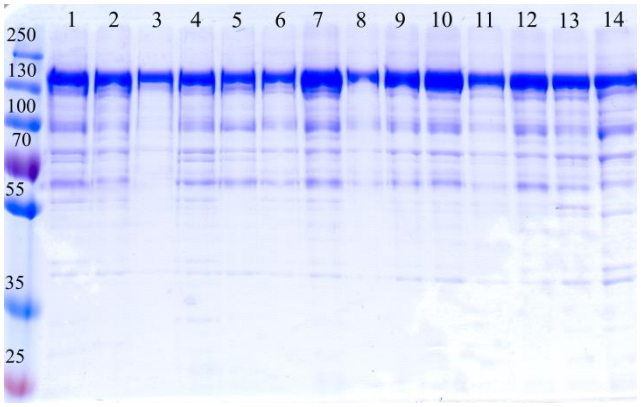

Figure 4.3.: SEC traces, UV-Vis spectra (insets) and Coomassie stained reducing SDS-PAGE of the variants produced in this study: Typical feature of tetramer, dimer and monomer elution peaks, respectively, around 55, 62 and 70 mL (indicated for WT) was obtained for all the variants using a Superdex 200 pg 16/600 column and 50 mM TrisHCl, 200 mM NaCl, 1 mM EDTA, pH 8.0 as elution buffer, except for *Rc* XDH-chimera. The first peak around 48 mL is corresponding to the aggregates elution. Insets show the UV-Vis spectra of the variants and feature maximum absorbance for the FeS clusters, FAD and protein backbone at 550, 450 and 280 nm, respectively. Except for the *Rc* XDH-chimera that does not contain any detectable aldehyde oxidase activity, no significant difference was observed in the overall UV-Vis spectra of other variants in comparison with WT. Note that the Y axis scale has been amended to maximize the resolution for each variant. Coomassie stained reducing SDS-PAGE 10% gel of the variants produced in this study with the lanes labelled from 1 to 14, respectively, corresponding to WT, 6A, 6D, 4A, 3A, 2A-2, 2A-1, C165A, C161A, N176Y, G177E, V178F, hAOX1-gXDH-chimera and hAOX1-dAOX1chimera, shows consistent degradation pattern.

reducing Coomassie stained SDS-PAGE gel for better comparison (**Figure 4.3.**), showed a consistent degradation pattern as described before for WT (Hartmann, et al. 2012).

4.1.2.2. Determination of the Active Portion of the Variants

hAOX1 is a homodimeric enzyme with four cofactors, one Moco, two [2Fe-2S] clusters and one FAD, in each monomer. Heterologous expression systems can potentially result in partially active enzymes mainly due to inefficient cofactor insertion. Therefore, the UV-Vis absorption and metal content of the variants were measured for initial characterization and comparison. The UV-Vis absorption of the purified proteins were recorded from 800 to 250 nm and characteristic peaks at 550, 450 and 280 nm corresponding, respectively, to the maximum absorbance of FeS clusters, FAD and protein backbone were determined (**Figure 4.3.,** insets). Except for the hAOX1-*Rc* XDH-chimera which did not show any cofactors absorbance, the other variants featured typical spectra similar to what was observed for WT. A_{280}/A_{450} and A_{450}/A_{550} are experimental ratios reported for XO and XDH as indices of purification quality when they are, respectively, close to 5 and 3 (Leimkuhler, et al. 2003). The values of A_{280}/A_{450}, summarized in **Table 4.2.**, for the cysteine and natural variants showed overall high purification quality with most of the variants exhibiting

A_{280}/A_{450} about 5 and A_{450}/A_{550} close to 3. 4A with A_{280}/A_{450} of 5.9 and V178F with A_{280}/A_{450} of 4.0 exhibited the highest and lowest ratios, respectively. V178F had the lowest value of 2.0 for A_{450}/A_{550} too, which indicated lower FAD content for this enzyme. Other variants showed narrow variations of A_{450}/A_{550} around 3.0 (see **Table 4.2.**). The two chimeric variants, hAOX1-gXDH- and hAOX1-dAOX1-chimera, presented the highest values of 6.6 and 7.2 for A_{280}/A_{450} with A_{450}/A_{550} being 3.0, which seemed to be the result of both relatively higher levels of degradation products and overall lower cofactors loads. Absorbance at 450 nm was used to determine the concentration of each sample considering the calculated molar extinction coefficient of 21100 $M^{-1}cm^{-1}$ and molecular weight of 150 kDa. Note that absorbance at 450 nm shows the FAD containing species of the enzyme and hence, the inactive species lacking the FAD cofactor were excluded in the concentration.

Table 4.2.: Yield, metal saturation and UV-Vis spectra features of the enzymes produced in this study

Enzyme		**Yield (mg/L)**	**Fe (%)[1]**	**Mo (%)[1]**	**A_{280}/A_{450}[2]**	**A_{450}/A_{550}[2]**
WT		0.8	47.6 ± 11.1	34.9 ± 4.1	5.5	3.1
Cysteine Variants	6A	0.5	68.0 ± 3.3	> 100	5.4	3.1
	6D	1.4	72.5 ± 1.3	> 100	5.3	3.0
	4A	1.4	64.3 ± 9.3	> 100	5.9	3.0
	3A	1.4	80.0 ± 0.7	> 100	5.1	2.8
	2A-2	0.7	58.3 ± 1.2	66.4 ± 3.1	5.6	3.4
	2A-1	1.0	44.4 ± 1.4	42.7 ± 2.3	5.4	3.0
	C161A	1.2	67.3 ± 2.7	43.0 ± 7.8	4.6	2.3
	C165A	1.5	76.7 ± 1.6	55.6 ± 4.2	4.9	2.6
Natural Variants	N176Y	0.5	47.8 ± 1.3	52.2 ± 8.9	5.1	2.8
	G177E	0.8	47.0 ± 4.8	29.8 ± 5.4	4.3	2.1
	V178F	0.6	49.4 ± 5.5	37.1 ± 6.3	4.0	2.0
	L438V	1.0	54.5 ± 4.8	47.0 ± 4.2	5.6	2.9
Chimeric Variants	gXDH-Chim	0.2	65.6 ± 1.4	78.5 ± 8.1	6.6	3.0
	dAOX1-Chim	0.2	63.2 ± 2.0	> 100	7.2	3.0

1: Fe and Mo contents were obtained from ICP-OES measurements in 5-10 µM protein wet-ashed samples and related to the maximum number of one Mo and 4 Fe per monomer of the enzyme.

2: A_{280}/A_{450} and A_{450}/A_{550} were calculated from the values obtained from the UV-Vis spectra.

The metal content of each variant was determined in wet-ashed (65% HNO_3, 100 °C, O/N) samples using inductively coupled plasma - optical emission spectrometry (ICP-OES) (see **Figure 4.4., A** and **Table 4.2.** for the values and comparison) (Neumann and Leimkühler 2008). WT showed 35 percent of Mo and 47 percent of Fe which were similar to the values measured for the natural variants, i.e. about 30-50 percent Mo and about 50 percent Fe. The cysteine and chimeric variants contained 70-80 percent Fe which was about 20-30 percent more than WT. However, the molybdenum saturation in the majority of enzymes with altered cysteines, i.e. in 6A, 6D, 4A, 3A and dAOX1-chim., was more than 100 percent. This might be due to unspecifically bound molybdenum, which was triggered by altering the environment on the surface of the protein or it might imply higher or 100 percent Moco load. Hence, Moco was comparatively monitored in WT and selected cysteine variants, i.e. in 6A, 6D and 3A with a method in which Form A, a fluorescent adduct of Moco, was extracted under oxidative acidic conditions and detected by HPLC (Johnson, et al. 1984) (see **Figure 4.4., B**). It was observed that the Moco levels were about 15-20 percent higher in these cysteine variants than in WT. Since a similar pattern was observed for the iron saturation, Fe percent calculated from the ICP-OES measurements was used to determine the relative active portion of each variant when normalization was needed.

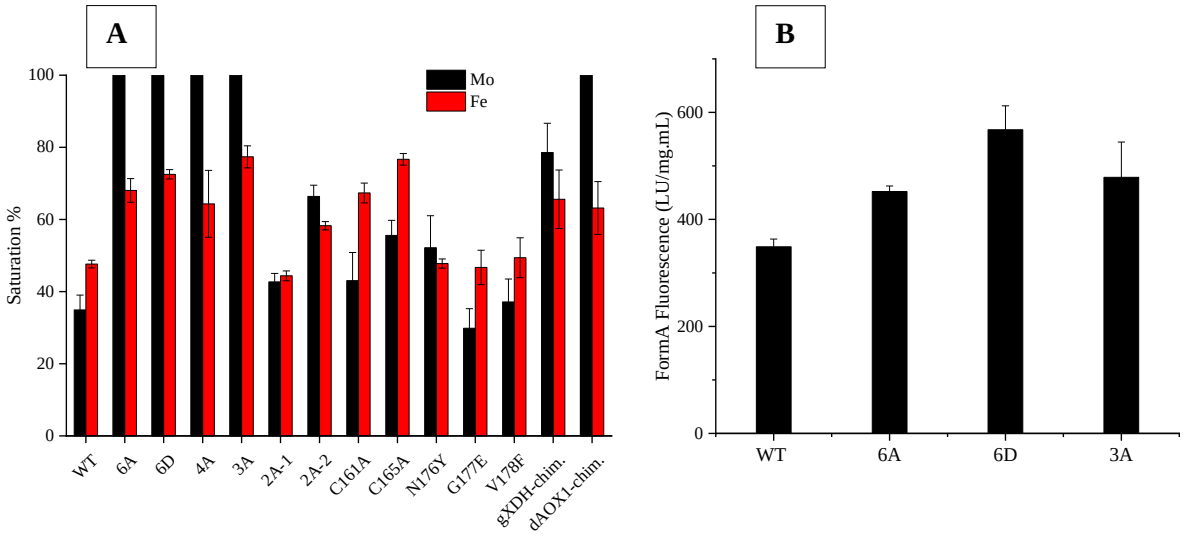

Figure 4.4.: A: Metal saturation of the variants produced for this study determined by ICP-OES: Fe and Mo contents were obtained from ICP-OES measurements in 5-10 µM protein wet-ashed samples and related to the maximum number of one Mo and 4 Fe per monomer of the enzyme. WT is loaded with 35% and 47% of Mo and Fe, respectively. 6A, 6D, 4A, 3A and dAOX1-chim. show a molybdenum level of higher than 100% which implies unspecifically bound metal. The other cysteine variants, gXDH-chim. and the natural variants contain comparable level of Mo and Fe as WT. **B: Comparison of Moco content of 6A, 6D and 3A with WT:** Form A content was measured in 200 µL of about 1 µM samples of selected variants. 6A, 6D and 3A contain about 15-20% higher Moco than WT. This pattern is consistent with the Fe% saturation, thus, Fe% was used to determine the active portion of each variant when needed.

4.1.2.3. Steady State Kinetics and ROS Production

The steady state kinetic parameters were obtained by following the formation of phenanthridinone, the oxidized product of phenanthridine, at 321 nm in the concentration range from 2 to 80 µM of phenanthridine. A slight substrate inhibition was observed in concentrations above 80 µM. Enzyme concentration was kept at 150-200 nM and molecular oxygen was used as the second substrate in excess as in air-saturated activity buffer (50 mM TrisHCl HCl, 200 mM NaCl, 1 mM EDTA, pH 8.0). The increase in the absorbance was linear during the first 30 seconds of the reaction. This was then used to calculate the rate of product formation at each concentration. Rate against substrate concentration resulted in a Michaelis-Menten behaviour from which the V_{max} and K_m for each variant were obtained. The Hill coefficient was around 1.1 ± 0.1 when data in parallel was fitted in Hill equation (see **Figure A1** and **Table A5** in the Appendix of this thesis for the details of the MM and Hill fits). The k_{cat} values calculated from V_{max} were normalized to the iron saturation level for each enzyme to obtain comparable values summarized in **Table 4.3.** and presented in **Figure 4.5**. The values reported are the average of at least three independent measurements with standard deviation shown as ±SD.

The steady state kinetic parameters determined for WT were about 500 min^{-1} k_{cat} and 27 µM K_m which resulted in the catalytic efficiency, k_{cat}/K_m, of about 19 $\mu M^{-1}.min^{-1}$. The cysteine variants showed k_{cat} values around 300 to 400 min^{-1} which were slightly lower than the k_{cat} of WT. 6D and 2A-1 with turnovers of about 150 min^{-1} and 680 min^{-1}, respectively, were the exceptions to this pattern, as 6D was significantly slower and 2A-1 slightly faster than WT. The K_m values for 6A, 6D and the two single cysteine variants, C161A and C165A, were relatively close to that of WT, while 4A, 3A, 2A-1 and 2A-2 showed lower affinity for phenanthridine than WT with the values, respectively, 41, 39, 47 and 52 µM. As a result of the decreased k_{cat} and increased K_m, the catalytic efficiency, k_{cat}/K_m, of the cysteine variants were about 7 to 13 $\mu M^{-1}.min^{-1}$ which were about 40-50 percent less than WT.

Among the natural variants, G177E behaved similar to WT, while both V178F and N176Y were slower enzymes with, respectively, up to half and one third of the k_{cat} observed for WT. The K_m values for both V178F and N176Y were slightly less than that of WT with the values, respectively, 19 and 15 µM, which consequently led to lowered catalytic efficiency about 13 and 10 $min^{-1}.\mu M^{-1}$. L438V, a superoxide producing natural variant reported previously (Foti, et al. 2017), was as fast as WT in oxidizing phenanthridine but with about half the affinity of WT for this substrate. Consequently, the k_{cat}/K_m of L438V was decreased to as low as that of N176Y.

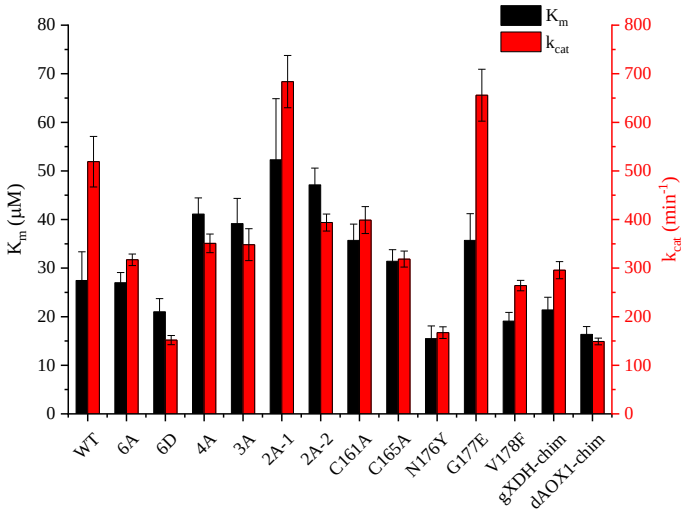

Figure 4.5.: Steady state kinetics parameters of the variants produced in this study: K_m and k_{cat} were obtained by following the product formation at 321 nm using 2-80 µM phenanthridine and 150-200 nM enzyme in air-saturated buffer (50 mM TrisHCl, 200 mM NaCl, 1 mM EDTA, pH 8.0). Cysteine variants, except 2A-1, are overall less efficient enzymes with less turnovers than WT and slightly lower affinity for phenanthridine. dAOX1-chim. and 6D present the least turnovers among the cysteine and chimeric variants. G177E among the natural variants behaves closely similar to WT, while N176Y and V178F are less efficient enzymes with lowered k_{cat} and increased K_m compared to WT. Turnover numbers are normalized to 100% iron saturation for each variant to obtain comparable values.

The chimeric variants, hAOX1-gXDH-chim. and hAOX1-dAOX1-chim., showed, respectively, 295 and 149 min^{-1} k_{cat} which were approximately 40 and 70 percent less than the k_{cat} measured for WT. They showed higher affinities than WT for phenanthridine with the values of 21 and 16 µM. Therefore, despite the significantly lower turnovers, the chimeric variants had catalytic efficiencies in the range of those of the cysteine variants.

hAOX1 generates reactive oxygen species (ROS) including hydrogen peroxide and superoxide in every catalytic cycle when oxygen is reduced as the terminal electron acceptor. It has been previously published that different variants of hAOX1 produce a different ratio of peroxide to superoxide (Foti, et al. 2017). The amount of superoxide was directly obtained from the reduction of cytochrome C by superoxide at 550 nm (McCord and Fridovich 1969) while the total ROS (H_2O_2 and $O_2^{-}\cdot$) was determined from the oxidation of phenanthridine at 321 nm. The final ratio of superoxide to the total ROS was reported as the percentage of superoxide generated in the reaction. To examine whether altering the flexible region composition either in the cysteine positions or the surroundings affects the superoxide to peroxide ratio, the amount of superoxide was quantified for the variants produced in this study. The cysteine and chimeric variants together with N176Y, G177E and V178F produced about 20 percent superoxide similar to WT, while L438V generated significantly higher amounts of superoxide to about 70 percent as reported previously (see **Table 4.3.** for the detailed values).

Overall the differences observed for the cysteine, chimeric and natural variants in the folding and tertiary structure, cofactor insertion and loading and steady state kinetic parameters were not significant. When observed, the slight differences cannot be explained through direct effects on any of the active sites or cofactors involved in the catalytic cycle. These differences also do not potentially suggest a role for the cysteines present in the flexible region. Therefore, we hypothesised that the cysteines might be involved in metal binding sites, structure stabilization or responding to the enzyme own ROS production.

Table 4.3.: The steady state kinetic parameters and superoxide to peroxide ratio of WT in comparison with the variants made to investigate the flexible region containing cysteines

Enzyme		k_{cat} (min^{-1})[1]	K_m (µM)[1]	K_{cat}/K_m ($min^{-1}.µM^{-1}$)	Superoxide (%)[2]
WT		519.0 ± 51.9	27.5 ± 5.9	18.9 ± 4.5	23.0 ± 2.1
Cysteine Variants	6A	317.1 ± 11.8	27.0 ± 2.1	11.7 ± 1.0	22.8 ± 1.3
	6D	151.7 ± 9.5	21.0 ± 2.7	7.2 ± 1.0	21.9 ± 1.7
	4A	351.0 ± 19.1	41.1 ± 3.3	8.5 ± 0.8	17.6 ± 1.4
	3A	348.2 ± 32.8	39.2 ± 5.2	8.9 ± 1.4	20.0 ± 1.9
	2A-2	393.8 ± 17.6	47.1 ± 3.5	8.4 ± 0.7	17.2 ± 0.6
	2A-1	683.8 ± 53.8	52.3 ± 12.6	13.1 ± 3.3	19.4 ± 1.1
	C161A	398.8 ± 27.7	35.7 ± 3.4	11.2 ± 1.3	21.5 ± 3.1
	C165A	318.5 ± 16.5	31.4 ± 2.4	10.1 ± 0.9	22.0 ± 1.6
Natural Variants	N176Y	167.2 ± 11.9	15.5 ± 2.6	10.8 ± 2.0	16.2 ± 3.2
	G177E	655.8 ± 53.4	35.7 ± 5.5	18.8 ± 3.2	23.5 ± 0.9
	V178F	264.1 ± 10.8	19.4 ± 1.8	13.8 ± 1.4	21.6 ± 5.0
	L438V	644.6 ± 96.8	59.7 ± 12.9	10.8 ± 2.8	75.9 ± 3.7
Chimeric Variants	gXDH-Chim	295.7 ± 17.7	21.4 ± 2.6	13.8 ± 1.9	23.0 ± 2.4
	dAOX1-Chim	149.1 ± 6.8	16.4 ± 1.6	9.1 ± 1.0	24.3 ± 2.6

1: The kinetic measurements were performed in air-saturated buffer (50 mM TrisHCl, 200 mM NaCl, 1 mM EDTA, pH 8.0) in the range of 2 to 80 µM of phenanthridine. The enzyme concentration was kept at 150-200 nM depending on the variant. k_{cat} values were normalized to 100% iron content as a full complement of two [2Fe-2S] clusters.

2: Superoxide measurements were done in air-saturated buffer as mentioned above in the presence of 150-200 nM of enzyme with addition of 40 µM of cytochrome C in the main reaction, and 100 U/mL of catalase and 20 µM superoxide dismutase in the control reactions. Phenanthridine was kept at 40 µM.

4.1.3. Cysteines as Potential Metal Binding Sites

Cysteines are among the amino acid residues abundantly found in metal binding sites in proteins (Pace and Weerapana 2014). For instance, in the *E. coli* aldehyde oxidase, PaoABC, an additional [4Fe-4S] has been identified to be coordinated via cysteines at a loop located at the C-terminus of the B subunit (Otrelo-Cardoso, et al. 2014). This [4Fe-4S] cluster is spectroscopically silent and the presence of higher iron content was the initial hint of its existence. Given the heterologous expression system used for hAOX1, chances would be high that a hypothetical [4Fe-4S] cluster bound to the cysteines in this region was lost. To examine this, hAOX1-WT and the 2A-1 variant were expressed as described before, for each enzyme the cells were split into two batches and were in parallel purified aerobically and anaerobically in a one-step IMAC, Ni-NTA. The metal saturation was determined for each sample with ICP-EOS and compared with each other (see **Table 4.4.**). The molybdenum levels were near or more than 100 percent saturation for both WT and 2A-1 purified under anaerobic or aerobic conditions which indicated possible unspecifically bound Mo to the protein. The amount of iron was about 15 percent less in the anaerobically produced enzymes for both WT and 2A-1 than the enzymes purified aerobically. If a hypothetical [4Fe-4S] cluster was lost during the aerobic purification, we would expect higher iron level in the sample purified anaerobically. However, the iron contents did not imply loss of metal during IMAC purification.

In addition, 3A and WT were produced as explained earlier and since zinc is the most abundant structural metal bound to cysteines (Pace and Weerapana 2014), the amount of zinc was determined in parallel with molybdenum and iron (see **Table 4.4.**). The amount of molybdenum and iron were consistent with the values obtained before (see section 4.1.2.2. and **Table 4.2.**), but the magnitude of the errors associated with the measured amount of zinc in the samples, i.e. 13.8 ± 10.5% and 6.5 ± 5.5% in WT and 3A, respectively, suggested that the level of zinc present in the enzymes was probably negligible (**Table 4.4.**).

WT, 2A-1, 2A-2, 3A, 6A and 6D were crystallized in collaboration with the lab of Prof. Maria Joao Romao and with the help of Dr. Cristiano Mota in the Universidade Nova de Lisboa. Crystals of WT and 2A-1 were natively grown under the conditions described elsewhere (Coelho, et al. 2015) and soaked in cryo-solution supplemented with 10 mM of Fe^{3+}, Zn^{+2}, As^{+3} as chloride salts and $NaAsO_2$ for 10 minutes before flash freezing in liquid nitrogen. WT and 2A-1 were also tried to be co-crystalized with 1 to 2 mM of Fe^{3+}, Zn^{+2}, As^{+3} from which only conditions containing As^{+3} resulted in crystals. 6A, 6D, 3A, 2A-2 and 2A-1 were in addition natively grown and taken for data collection, however, the electron density detected around residues 167 to 199 was not improved and

these residues could not be modelled. Furthermore, no extra metal binding sites were detected in the structures analysed (data not shown).

Table 4.4.: Molybdenum and iron content compared in aerobic vs anaerobic purification and zinc content in WT vs 3A

Enzyme	Mo (%)[1]	Fe (%)[1]	Zn (%)[1, 3]
WT + O_2 [2]	114.9 ± 16.0	80.7 ± 11.4	
WT – O_2 [2]	106.7 ± 18.3	65.8 ± 6.9	
2A-1 + O_2 [2]	103,2 ± 20.6	70.1 ± 9.2	
2A-1 – O_2 [2]	99.5 ± 6.9	54.1 ± 2.3	
WT	74.1 ± 8.7	53.9 ± 2.6	13.8 ± 10.5
3A	111.1 ± 3.7	77.4 ± 3.1	6.5 ± 5.5

1: Metal contents were estimated from 5-10 µM wet-ashed protein samples using ICP-OES and related to the maximum number of one Mo as in Moco and 4 Fe as in 2x[2Fe-2S] clusters per monomer of the enzyme.
2: Produced through only a one-step IMAC, Ni-NTA purification
3: Zinc was only measured for WT vs 3A for comparison assuming one Zn per monomer of the enzyme.

Taken together these experiments did not provide any evidence that the cysteines present in the flexible region contribute a functional or structural metal binding site. This may suggest another function for these cysteines.

4.1.4. Impact of Altering the Flexible Region Composition on the Enzyme Thermal Stability

hAOX1 is a cytosolic enzyme, therefore the cysteines in the flexible region are unlikely to form structural disulfide bonds. The thermal stability of the cysteine variants was compared to that of WT using thermoFAD to investigate whether the stability of the enzyme was impaired when the cysteines were not present. ThermoFAD is a modified thermal shift assay that relies on the changes of intrinsic fluorescence of FAD when protein undergoes a thermal denaturation (Forneris, et al. 2009). The method is widely applied to estimate the stability of flavoproteins and has been previously successfully used for hAOX1 (Mota, et al. 2019). In collaboration with Dr. Cristiano Mota from the Universidade Nova de Lisboa thermoFAD was used to compare the unfolding of the variants in which the flexible region with the cysteines clustered was manipulated. Samples of 1 µM protein were heated from 25 to 90 °C and increases in the intrinsic fluorescence were recorded.

In the plot of normalized fluorescence versus temperature (**Figure 4.6.** panels **A** to **C**) two unfolding events were distinguished for all the enzymes, except for the hAOX1-dAOX1 chimeric variant. The melting temperature (T_m) of each unfolding state was obtained from the maxima in the plot of the first derivative of normalized fluorescence against temperature (see the T_ms compared in **Figure 4.6.**, panel **D** and listed in **Table 4.5.**).

WT was initially partially unfolded around 66 °C before it was fully denatured at 75 °C. The first melting temperature showed a narrow variation of 0.6 °C around the average value of 65.7 °C. This

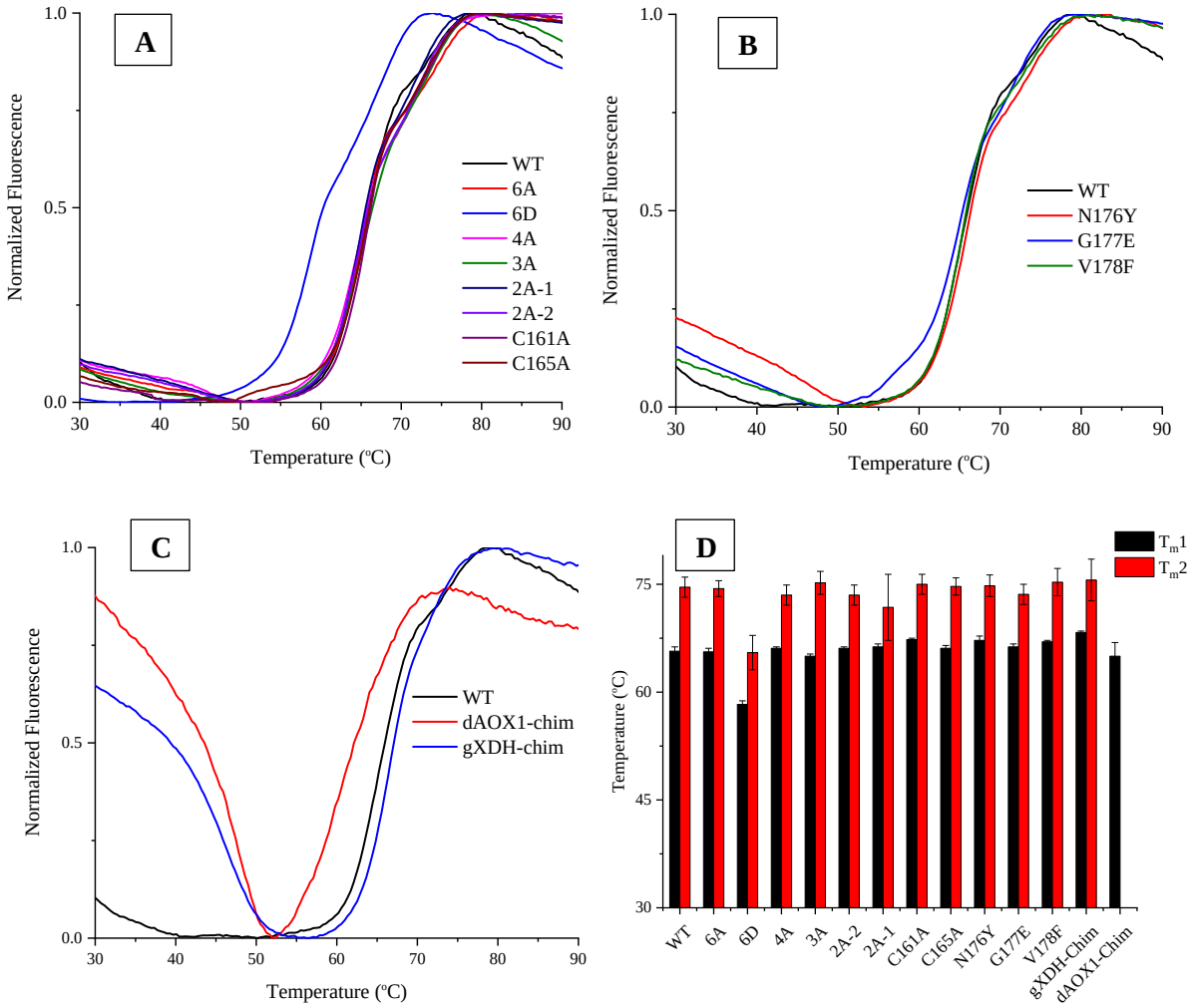

Figure 4.6.: Thermal stability of WT in comparison with the cysteine variants (A), natural variants (B) and chimeric variants (C) and their melting temperatures (D): The denaturation of 1 µM enzyme samples in 50 mM TrisHCl, 200 mM NaCl, 1 mM EDTA, pH 8.0 was followed by the change in the intrinsic fluorescence of FAD while the temperature was increased from 25 to 90 °C (shown from 30 to 90 °C in the graphs). The denaturation shows two unfolding steps for all the variants around 65 and 75 °C except for dAOX1-chim. and 6D which are significantly less stable than WT and other variants. 6D unfolds in two steps with melting temperatures about 10 degrees less than those of WT at 58 and 65 °C while the denaturation of dAOX1-chim. occurs in one step at 65 °C.

indicated a sharper transition than the second unfolding step at 74.6 °C with bigger magnitude of error of 1.4 °C. This pattern was consistently observed for the natural variants N176Y, G177E and V178F. The initial fluorescence of N176Y was higher than WT suggesting precipitation or soluble aggregation that partially exposed FAD, but it did not result in less global thermal stability. The cysteine variants, except 6D, presented close melting temperatures (T_m) to those of WT and similar two-step denaturation pattern, suggesting that the replacement of cysteines with alanines did not induce thermal global instability in the enzyme. However, introducing six negatively charged

Table 4.5.: Thermal stability of WT in comparison with the variants made to investigate the flexible region containing cysteines

Enzyme		**T_m 1 (°C)**	**T_m 2 (°C)**
	WT	65.7 ± 0.6	74.6 ± 1.4
Cysteine Variants	6A	65.6 ± 0.5	74.4 ± 1.1
	6D	58.3 ± 0.5	65.5 ± 2.4
	4A	66.1 ± 0.2	73.5 ± 1.4
	3A	65.0 ± 0.3	75.2 ± 1.6
	2A-2	66.1 ± 0.2	73.5 ± 1.4
	2A-1	66.3 ± 0.4	71.8 ± 4.6
	C161A	67.3 ± 0.2	75.0 ± 1.4
	C165A	66.1 ± 0.4	74.7 ± 1.2
Natural Variants[1]	N176Y	67.2 ± 0.6	74.8 ± 1.5
	G177E	66.3 ± 0.4	73.6 ± 1.4
	V178F	67.0 ± 0.2	75.3 ± 1.9
Chimeric Variants	gXDH-Chim.	68.3 ± 0.2	75.6 ± 2.9
	dAOX1-Chim.	65.0 ± 1.9	-

1: L438V stability, studied and reported before (Mota, et al. 2019), did not show significant difference with WT.

aspartates at the cysteine positions decreased the thermal stability by about 8 to 10 °C for each T_m compared to WT. Exchanging the entire flexible region in hAOX1 to that of dAOX1, however, changed the unfolding process and hAOX1-dAOX1-chimeric variant underwent one slow step of unfolding with a T_m around 65 °C. The hAOX1-gXDH-chimeric variant behaved similar to WT, but

both chimeric variants had elevated initial fluorescence, possibly due to the presence of soluble aggregation at lower temperatures.

4.1.5. Enzyme Inactivation Studies

4.1.5.1. Inactivation of hAOX1-WT

Our investigation in search of a role for the cysteines present in the flexible region suggested that these residues do not participate in stabilizing the structure by providing a metal binding site. Another potential role for the cysteines is responding to the generation of ROS by the enzyme. The response could be a late event that affects the activity and half-life of the enzyme over a longer reaction course, as previously observed by Abbasi and colleagues (Abbasi, et al. 2019). To test this hypothesis, the enzyme reaction of WT was followed for 1800 seconds to allow enzyme inactivation to be reached. The enzyme concentration was narrowly kept at 150-180 nM and excess amounts of the both substrates, phenanthridine of about $5K_m$ (160 µM) and oxygen in air-saturated buffer (about 200 µM), were used to ensure that substrates depletion would not occur. Panel **A** of **Figure 4.7.** shows the progress curve of phenanthridinone formation as an increase in the absorption at 321 nm over 1800 seconds for WT. It was observed that after about 300 seconds the increase in the absorbance declined and then tended to level off. Up to this absorbance roughly about 50 µM of substrates was used up. To further confirm that the observed behaviour was not due to substrate depletion, two control assays were performed: the same reaction was set up and the absorbance against time was recorded for 1800 seconds as shown in **Figure 4.7.**, panel **B** in black curve. Then, in the first control assay another 160 µM of phenanthridine was added to the same reaction mix. The absorbance at 321 nm showed no increase after addition of fresh phenanthridine (red line in **Figure 4.7., B**). Subsequently and in the second control assay another 170 nM of hAOX1-WT was added to the same cuvette and the absorbance was recorded for 1800 seconds (blue curve in **Figure 4.7., B**). Interestingly, the rise in the absorbance was comparable to the initial reaction and a similar pattern of changing the rate of product formation over time was observed. This suggests that the decreasing trend of the activity is not due to neither of the substrates depletion or product inhibition.

A linear fit of the first 30 seconds of the reaction yielded the V_{max} (Absorbance/s) at 160 µM concentration of phenanthridine (the inset in **Figure 4.7., A**) and turnover (s^{-1}) was calculated according to

$$Turnover(s^{-1}) = \frac{V_{max}(Absorbance/s) * Reaction\ Volume(\mu L) * \varepsilon^{321}_{phenanthridinone}}{\mu mol\ Enzyme * Fe\%}$$

where the reaction volume and extinction coefficient of phenanthridinone at 321 nm were 500 µL and 6400 $M^{-1}cm^{-1}$, respectively.

The first derivative of absorbance against time gave the activity of enzyme at each time point, plotting of which versus time presented a declining trend (**Figure 4.7.**, **C**). This behaviour was fitted into exponential decay equation using Origin according to

$$y = A_1 * e^{(-x/t1)} + y_0$$

where the equation is equivalent to the enzyme inactivation description as in

$$A = (A_0 - A_{min})e^{k_D t} + A_{min}$$

where y is activity at time t, A_0 is activity at time zero, A_{min} is the minimum activity recorded for the enzyme, t is time and k_D is the first-order activity decay constant (Householder and Gomori 1943). The enzyme inactivation follows a first-order decay pattern over time, which allows calculating the enzyme half-life ($t_{1/2}$) by

$$t_{1/2} = 0.693/k_D$$

where k_D is the inactivation rate constant obtained from the exponential decay fit in the previous step. Half-life is the time required for the initial activity to decrease by half. These analyses were applied for at least five independent measurements and the average values for turnover and half-life are presented in **Table 4.6.** (see also **Table A1** in the Appendix of this thesis for the details of measurements and steps of analysis). $Turnover * t_{1/2}$ is a useful measure that shows the number of turnovers that the enzyme is able to perform by the time it reaches to half of its initial activity.

hAOX1-WT presented a turnover of 5.4 per second at 160 µM of phenanthridine and a half-life of 58 seconds. Hence, WT could perform about 300 turnovers by the time when 50 percent of its inactivation was reached.

In the next step the inactivation of 6A was compared with WT and the effect of ROS scavengers, glutathione and exogenous ROS on these enzymes were investigated.

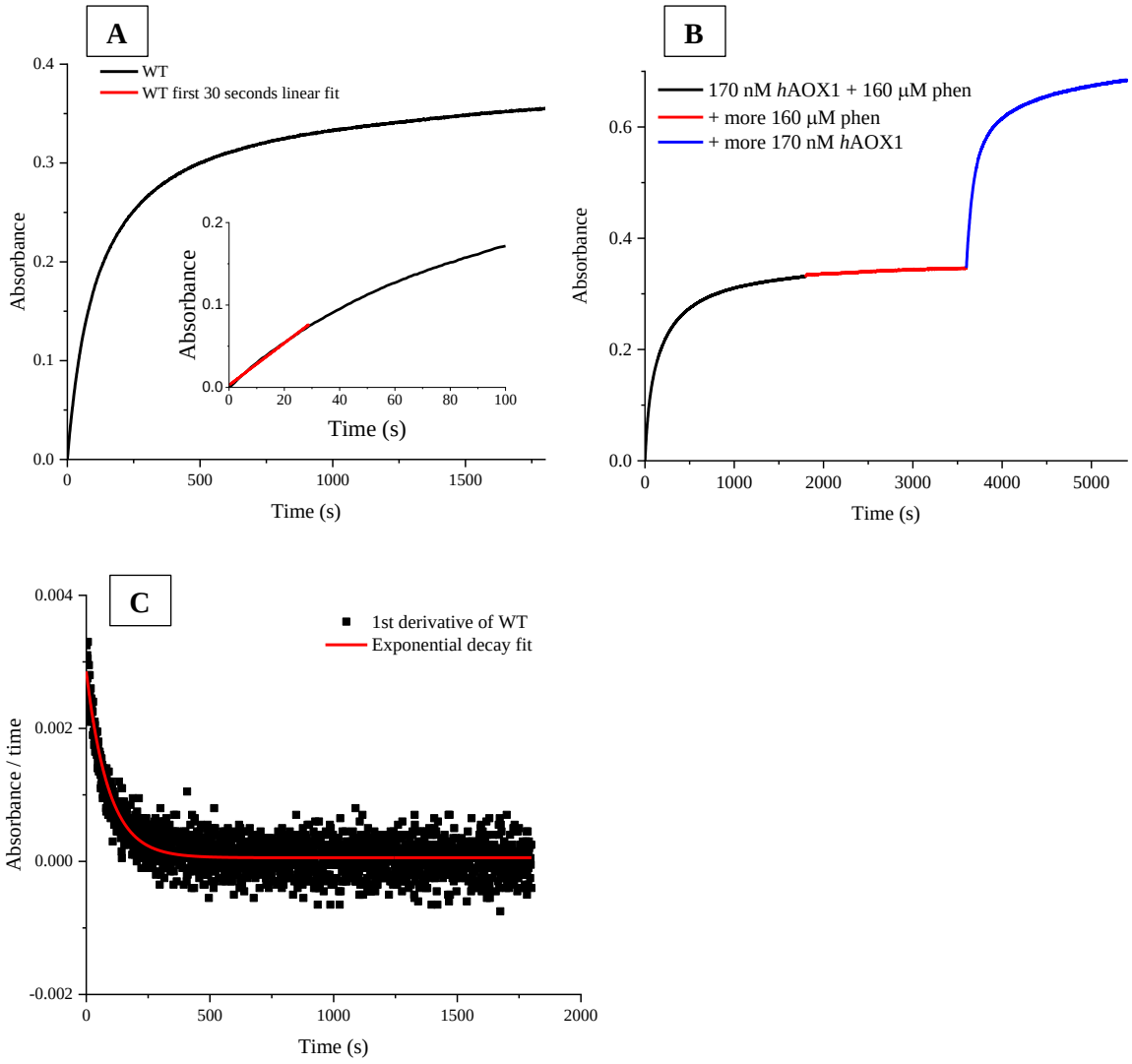

Figure 4.7.: **Inactivation studies of hAOX1-WT: A:** The progress curve (aborbance vs time) over 1800 seconds: The enzyme reaction was followed for 1800 seconds and absorbance was recorded at 321 nm in a reaction mix containing 160 µM (~ $5K_m$) phenanthridine and 170 nM WT in air-saturated buffer (50 mM TrisHCl, 200 mM NaCl, 1 mM EDTA, pH 8.0). The slope of a linear fit of the first 30 seconds of the reaction (**inset**) yields the V_{max} (Absorbance/s) at this concentration of substrate, from which turnover is calculated. **B:** Addition of 160 µM more phenanthridine (shown in red) after enzyme inactivation is achieved (shown in black) does not restart the reaction, which indicates substrate deplition is not the reason for the declining behaviour. Addition of 170 nM more WT enzyme (shown in blue) howerever, recovers the reaction that continues until inactivation of the new batch of the enzyme occurs. **C:** First derivative of the absorbance against time plotted versus time (s) (dots in black) gives the change of activity for the enzyme at each time point. With an exponential decay fit of the activity (red curve) the half-life of the enzyme can be determined. Inactivation event was reported as number of turnovers during the half-life of enzyme in bar charts (see **Figure 4.8., B** and **Figure 4.9.**). The average values for turnover, half-life and the number of turnover during half-life are reported in **Table 4.6.** Details of the measurements together with the T-test results are shown in **Table A1** and **A2** in the Appendix.

4.1.5.2. Comparison of WT and 6A Inactivation under Different Conditions

6A, the variant in which the entire six cysteines in the flexible region are replaced with alanines, was similarly assessed for its inactivation behaviour (see **Figure 4.8.** for the comparison of WT and 6A inactivation). The half-life and the number of the turnover during the half-life of the enzyme

were obtained from the progress curve (absorbance against time) and the exponential decay fit (shown as inset) (see **Figure 4.9.** for the 6A curves together with the other variants in this study and **Table 4.6.** for the values). 6A showed 65 seconds of half-life which was slightly longer than 58 seconds half-life of WT, but with only 1.6 per second turnover versus 5.6 per second turnover of WT (see **Figure 4.8.** and **Table 4.6.**). The number of turnovers that 6A was able to perform before half of it was inactivated was circa 100, which was one third of that of WT. This implies that at least one cysteine in the region plays a role which allows the enzyme to perform more turnovers by the time it reaches its half-life point.

The enzymatic reaction was performed in the presence of ROS scavengers (100 U/mL catalase and 20 µM superoxide dismutase) or glutathione (10 mM GSH) in separate experiments to investigate whether the ROS scavengers or glutathione would delay the inactivation of WT or 6A. The progress curve (the plot of absorbance against time) for the representative measurements (**Figure 4.8., A**) showed separately clustered curves for WT and 6A native, ROS scavenger or GSH supplemented reactions. The turnovers for WT and 6A in the presence of the ROS scavengers or glutathione were 5.2 and 1.7 per second, respectively, which were not significantly different from their native conditions. A similar behaviour was observed for the half-lives of 63 and 62 seconds for WT, and 63 and 68 seconds for 6A in the presence of catalase/SOD and GSH, respectively (see **Table 4.6.**

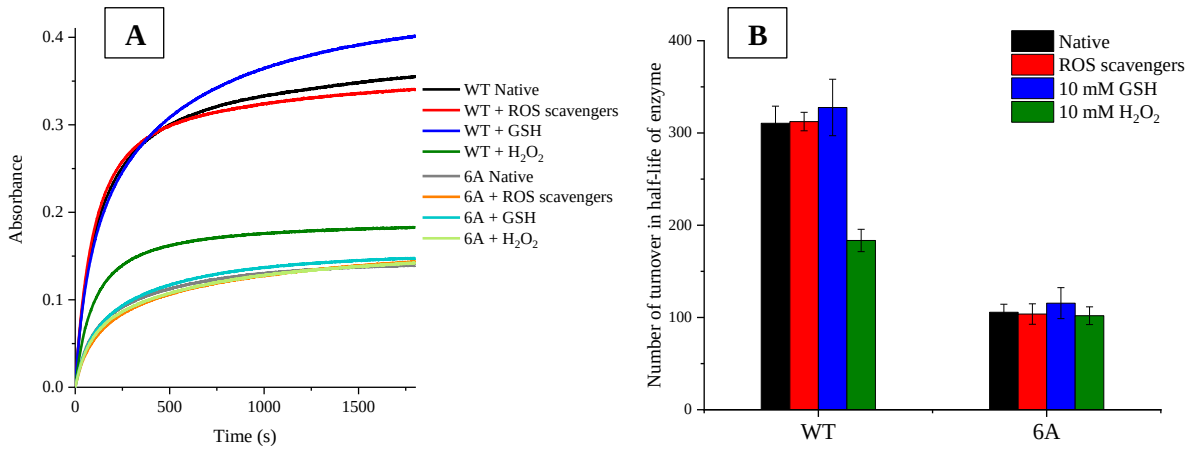

Figure 4.8.: The effect of adding ROS scavengers, glutathione and exogenous ROS on WT and 6A inactivation: A: The progress (absorbance against time) curves for WT and 6A in the presence of ROS scavengers (100 U/mL catalase and 20 µM SOD) or 10 mM glutathione are closlely clustered to their native conditon curve, while pre-incubated WT with 10 mM H_2O_2 has fall down near to the 6A cluster. **B:** The number of turnovers during the half-life of WT in camparison with 6A in the presence of ROS scavengers, glutathine or in the samples treated with H_2O_2: The number of turnover that 6A performed by the time half of the enzyme gets inactivated is about one third of that of WT. Adding ROS acavengers or glutathione to the reaction did not significantly affect the inactivation of WT or 6A, however, pre-treatment of the enzymes with 10 mM H_2O_2 as a source of exogenous ROS resulted in significantly greater damage to WT.

for the values). The number of turnovers that WT or 6A were able to perform by the time they reached to their 50 percent inactivation were 312 and 327 for WT and 103 and 115 for 6A, respectively, in the presence of catalase/SOD and glutathione, which were close to 310 and 105 for WT and 6A, respectively, in their native conditions (**Figure 4.8., B** and **Table 4.6.**). These observations suggested that the ROS scavengers and glutathione were not able to prevent enzyme inactivation. The detailed values and T-test results are presented in **Table A1 and A2** in the Appendix of this thesis.

4.1.5.3. The Effect of Exogenous ROS on the Inactivation of WT and 6A

The inability of the ROS scavengers or glutathione to recover WT or 6A raises the question whether the enzyme's own ROS are involved in the earlier inactivation of 6A in comparison with WT. If so, the addition of hydrogen peroxide (H_2O_2) as a source of exogenous ROS may affect WT and 6A differently. To test this, the enzyme was incubated with 10 mM of H_2O_2 for 30 minutes at room temperature, H_2O_2 was subsequently removed and the inactivation was similarly assessed. The curve of absorbance over time for the H_2O_2 treated 6A clustered with the other measurements for this enzyme, however, the hydrogen peroxide treated WT dropped down close to the 6A cluster (**Figure 4.8., A**). The turnovers and half-lives for these samples showed that H_2O_2 significantly lowered the number of turnovers down to 3 per seconds for WT, while the half-life remained unchanged around 60 seconds (**Table 4.6.**). This resulted in about 180 turnovers that WT was able to perform before half of the enzyme was inactivated (**Figure 4.8.**, **B)**. Interestingly, H_2O_2 did not affect the 6A turnover or half-life and this variant performed 1.6 turnovers per second and had a half-life of 65 seconds similar to the native condition where the enzyme was not treated with hydrogen peroxide. This experiment demonstrated that ROS could damage the WT enzyme. In addition, it implied that 6A was unprotected against the endogenous ROS so that the maximal damage had already been exerted and exogenous ROS did not affect the enzyme beyond that.

4.1.5.4. The Effect of the Flexible Region Composition on the Enzyme Inactivation

6A, the variant lacking all cysteine residues in the flexible region, showed significantly less number of turnovers during its half-life. This suggests that at least one cysteine in this region facilitated keeping the enzyme in turnover for a longer time. To dissect out which cysteine was most likely involved in the process, the inactivation studies were repeated for other cysteine variants as well as the natural and chimeric variants. **Figure 4.9.** shows representatives of the progress curves (absorbance vs time) and the first derivative versus time curves (as insets) for the enzymes in this study. It was observed that these enzymes followed a similar pattern of inactivation with random

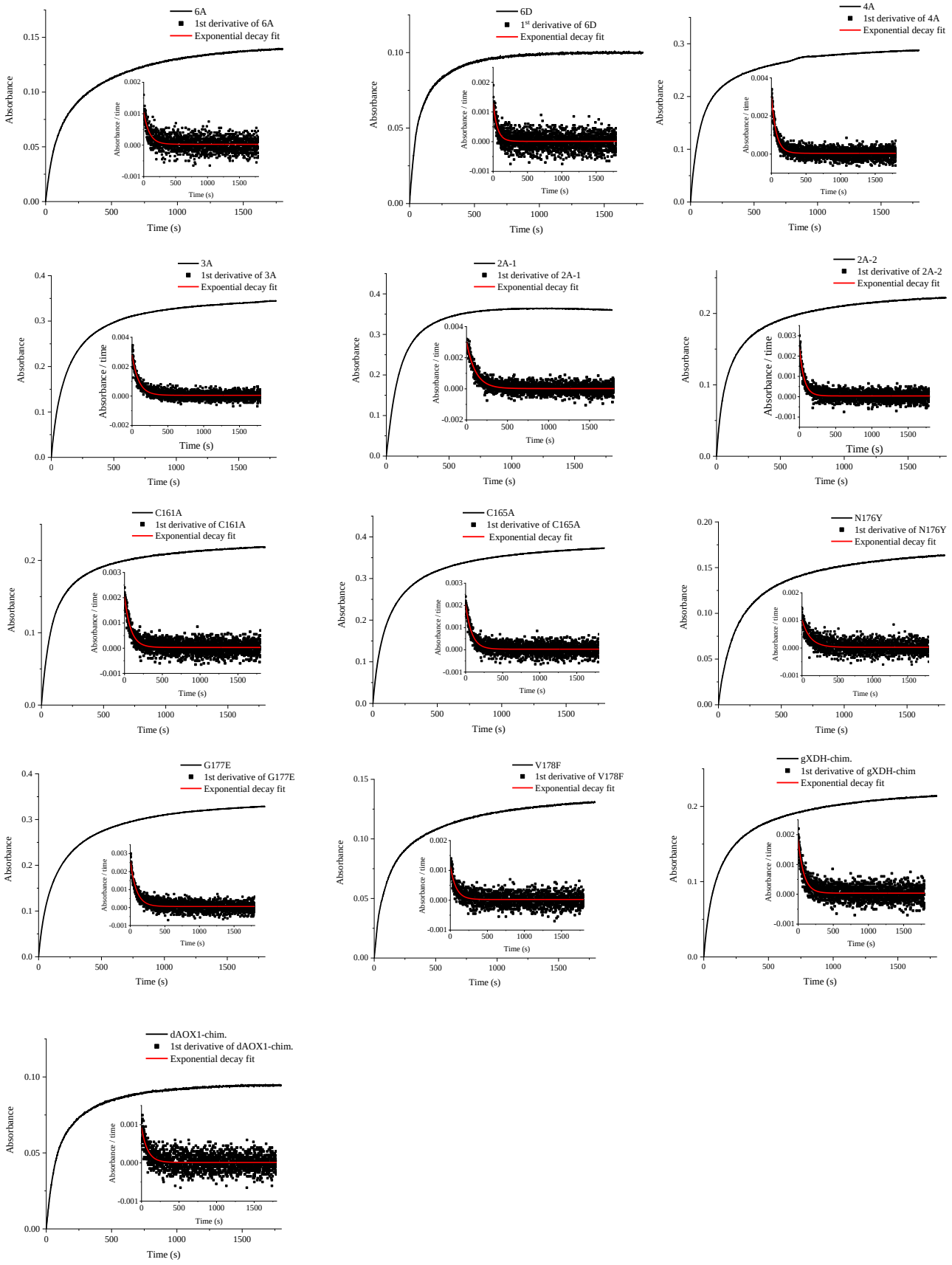

Figure 4.9.: Inactivation studies on the cysteine, natural and chimeric variants: Progress curves: Formation of product was recorded for 1800 seconds at 321 nm in a reaction containing 160 µM (~ 5K_m) phenanthridine and 160-180 nM enzyme in air-saturated buffer (50 mM TrisHCl, 200 mM NaCl, 1 mM EDTA, pH 8.0). The absorbance decreases

over time and indicates the enzyme inactivation. Insets: The first derivative of absorbance againt time yields the activity at each time point, which is plotted versus time (black dots). The declining behaviour of the activty over time is fitted to the exponential decay function (red curves in the inset graphs) from which half-lives obtained for each enzyme. The variants in this study followed a similar pattern of inactivation. Note that the Y axis scale is ammended to maximize the resolution.

error residuals. The turnovers and half-lives were obtained through a similar procedure of analysis as explained in the previous sections after at least three independent measurements. The average values of turnover, half-life and the number turnover during the half-life of the enzyme ($Turnover * t_{1/2}$) are listed in **Table 4.6.** and the number of turnover that each enzyme could perform by the time it reached to its half-life are compared as bar charts presented in **Figure 4.10.** (see also **Table A1** and **A2** in the Appendix for details of the measurements, steps of analyses and T-test results).

The single cysteine variants, C161A and C165A, together with 2A-2, 3A and 4A presented about 2.8 to 3.4 turnovers per seconds which were significantly less than WT with 5.4 turnovers per seconds (**Table 4.6.**). With half-lives around 50 to 60 seconds, these variants performed about 170-180 turnovers during their half-lives, significantly less than WT with 310 turnovers (**Figure 4.10.**). This behaviour was more pronounced, as previously mentioned, for 6A in which all six cysteines were replaced with alanines. When negatively charged aspartates were introduced to replace cysteines, the effect was even more enhanced, due to the dual effect of shortened half-life to 40 seconds and lowered turnover to 1.2 per seconds. Interestingly, 2A-1, in which Cys170 and Cys171 were exchanged with alanines, behaved similar to WT with a slightly higher half-life of about 68 seconds. This resulted in performing 359 turnovers before it reached its 50 percent activity which was slightly higher than that of WT. Overall, it seems that Cys161 and Cys165 present in the $C(X)_3C$ motif, which is exclusively found in aldehyde oxidases, and Cys179 and Cys180 present in the $CC(X)_7CC$ motif, may be important to protect the enzyme from its own ROS products.

G177E among the natural variants showed a similar inactivation pattern as WT with 4.8 per second turnover and 57 seconds of half-life. N176Y showed a half-life of 78 seconds with only 2.3 turnovers per second while V178F had a half-life similar to WT with 3 turnovers per second. This resulted in more vulnerable enzymes than WT with about 175-180 turnovers during their half-lives. L438V, the superoxide producing natural variant (Foti, et al. 2017), behaved similar to N176Y with 2.3 turnovers per seconds and 76 seconds of half-life. This variant appeared to be significantly less protected than WT despite it having been undisturbed around the cysteine-containing region. This

hints on a more damaging effect that superoxide might exert compared to peroxide during the turnover.

The chimeric variants, gXDH-chim. and dAOX1-chim., showed, respectively, 3.6 and 1.4 turnovers per second with 45 and 60 seconds of half-life. The number of turnover that they were able to perform during their half-lives were significantly less than WT, with overall greater effect for dAOX1-chim., in which the entire flexible region was replaced with a shorter sequence that lacked the cysteines.

The inactivation studies on the natural and chimeric variants suggest that the exact composition of the flexible region is needed for the cysteines to exert their full protection role.

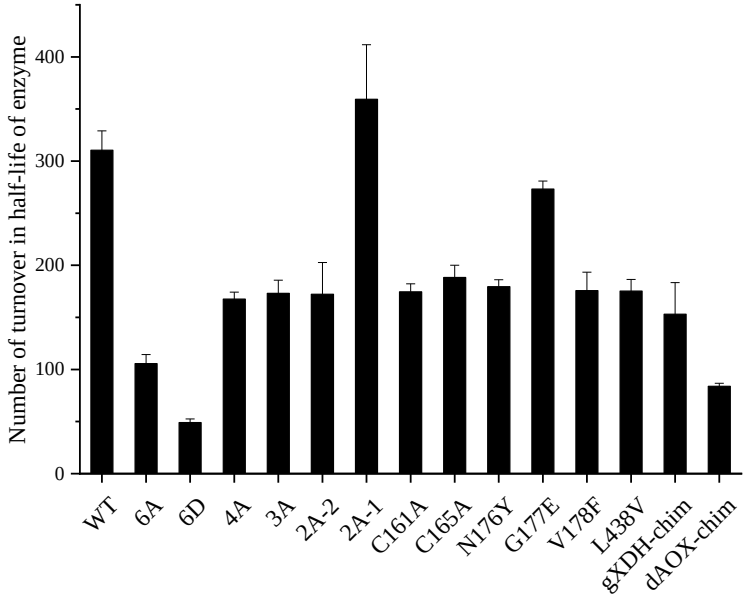

Figure 4.10.: The effect of the flexible region composition on the inactivation of hAOX1: The number of turnover in half-life of enzyme was obtained from the values listed in **Table 4.6** and from $Turnover * t_{1/2}$. The cysteine and chimeric variants show significantly less turnovers during their half-lives than WT, except for 2A-1 that shows values similar to WT. G177E among the natural variants behaves as WT, but N176Y and V178F are more vulnerable than WT. L438V is a superoxide generating natural variant that gets inactivated significantly faster than WT.

Table 4.6.: Average values of turnover, half-life and number of turnover in half-life of enzyme for the the cysteine, natural and chimeric varinats.

Enzyme		Condition	Turnover (s^{-1})[1]	$t_{1/2}$ (s)[1]	Turnover x $t_{1/2}$
WT		Native	5.4 ± 0.7	58.0 ± 4.1	310.5 ± 18.5
		cat/SOD[2]	5.2 ± 0.1	60.0 ± 0.9	312.3 ± 10.0
		GSH[3]	5.2 ± 0.3	63.3 ± 2.7	327.7 ± 30.6
		H_2O_2[4]	3.0 ± 0.1	62.0 ± 6.0	183.5 ± 12.1
Cysteine Variants	6A	Native	1.6 ± 0.1	65.7 ± 9.6	105.6 ± 8.7
		cat/SOD[2]	1.7 ± 0.3	63.3 ± 6.9	103.8 ± 11.1
		GSH[3]	1.7 ± 0.1	68.1 ± 8.2	115.5 ± 16.8
		H_2O_2[4]	1.6 ± 0.1	65.5 ± 6.0	101.9 ± 9.6
	6D	Native	1.2 ± 0.2	40.0 ± 6.8	49.0 ± 3.5
	4A	Native	3.4 ± 0.1	49.0 ± 0.5	167.6 ± 6.6
	3A	Native	2.8 ± 0.1	61.6 ± 2.9	173.0 ± 12.6
	2A-2	Native	3.8 ± 0.9	46.1 ± 3.5	172.2 ± 30.4
	2A-1	Native	5.2 ± 0.3	68.7 ± 8.5	359.4 ± 52.4
	C161A	Native	3.1 ± 0.1	55.7 ± 4.3	174.5 ± 7.7
	C165A	Native	3.0 ± 0.3	62.5 ± 2.9	188.3 ± 11.7
Natural Variants	N176Y	Native	2.3 ± 0.2	78.8 ± 5.2	179.5 ± 6.5
	G177E	Native	4.8 ± 0.3	56.9 ± 4.5	273.2 ± 7.6
	V178F	Native	3.0 ± 0.3	58.4 ± 4.4	175.6 ± 17.8
	L438V	Native	2.3 ± 0.1	76.8 ± 3.9	175.2 ± 11.3
Chimeric Variants	*g*XDH-Chim.	Native	3.6 ± 1.0	45.2 ± 17.0	153.0 ± 30.3
	*d*AOX1-Chim.	Native	1.4 ± 0.1	60.0 ± 7.2	83.8 ± 3.0

1: Values were obtained from at least three independent measurements.

2 : 100 U/mL catalase (cat) and 20 µM superoxide dismutase (SOD) were added to the reaction.

3 : The reaction mix was supplemented with 10 mM GSH freshly prepared in the activity buffer.

4 : Enzyme was incubated with 10 mM H_2O_2 for 30 minutes at room temperature. H_2O_2 was removed before the enzyme reaction started.

4.2. The Nature of the Damage to hAOX1 During the Course of Turnover

4.2.1. Reconstitution of the Sulfido Ligand in ROS Damaged Samples

Previous studies on XOR enzymes suggest that the sulfido ligand bound at Moco is vulnerable when the enzyme is turning over (Lynch and Fridovich 1979), an effect that has been suggested to be due to the production of ROS by XORs. To investigate whether hAOX1 behaves similarly, 3 samples of 150 nM hAOX1-WT were in parallel incubated with 10 mM H_2O_2 aerobically ($+O_2$) and anaerobically ($-O_2$) and with 160 µM phenanthridine for 30 minutes at room temperature. H_2O_2 and phenanthridine were subsequently removed and the activity was measured aerobically. It was observed that the specific activities of the samples treated with H_2O_2 anaerobically and with phenanthridine were nearly totally lost while the sample treated with H_2O_2 aerobically showed only a slight decrease in the activity (see **Figure 4.11.** and **Table 4.7.** for the comparison and the details of the values). The sulfido ligand was then anaerobically reconstituted using 2 mM sodium sulfide in the presence of 500 µM sodium dithionite in the samples where loss of activity was observed. The activity of the phenanthridine treated sample was recovered to 475 nmol/min.mg, which was about 45 percent of its initial value in the native condition. The anaerobically H_2O_2 treated sample

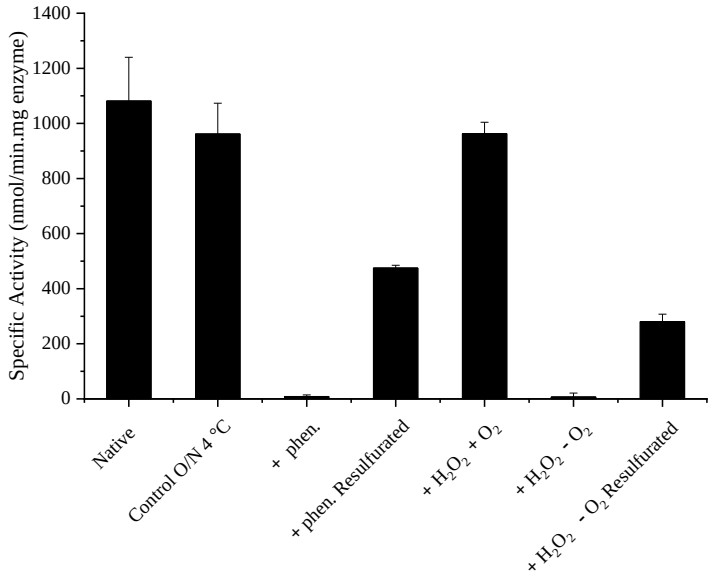

Figure 4.11.: The effect of exogenous and endogenous ROS on the sulfido ligand: Samples of 150 nM hAOX1-WT were pre-incubated with 160 µM of phenanthridine and 10 mM hydrogen peroxide and the sulfido ligand was chemically reconstituted using 2 mM of sodium sulfide in the presence of 500 µM sodium dithionite and 25 µM of methylviologen under anaerobic condition (98% N_2, 2% H_2) in 50 mM KH_2PO_4, 0.1 mM EDTA, pH 7.4. The specific activities were measured in an air-saturated buffer (50mM TrisHCl, 200 mM NaCl, 1 mM EDTA, pH 8.0) using 40 µM of phenanthridine and 150 nM of enzyme. Resulfuration of the sample treated with substrate leads to about 30 to 50 percent regain of the activity.

regained activity to about 280 nmol/min.mg which was nearly 30 percent of its initial activity after the re-sulfuration. Note that the sample incubated overnight under the anaerobic chamber at 4 °C with 962 nmol/min.mg activity represented the initial activity for the anaerobically H_2O_2 treated enzyme.

The loss of activity of hAOX1 after incubation with substrate or with hydrogen peroxide under anaerobic, but not aerobic, conditions suggest that the reduced form of the enzyme, and not the oxidized form, is vulnerable to ROS. However, the partial regain of the activity after the reconstitution of the sulfido ligand can be due to combined effects induced by ROS.

Table 4.7.: Average values of specific activity for the samples treated with phenanthridine and hydrogen peroxide in the presence and absence of oxygen and before and after the reconstitution of the sulfido ligand

Condition	Specific Activity (nmol/min.mg)[1]
Native	1081.3 ± 158.2
Native, 4 °C O/N, - O_2 [2]	962.0 ± 111.2
+ Phenanthridine[3]	8.6 ± 5.7
+ Phenanthridine, Resulfurated	475.1 ± 9.8
+ H_2O_2, + O_2[4]	962.9 ± 41.2
+ H_2O_2, - O_2[4]	7.3 ± 13.6
+ H_2O_2, - O_2, Resulfurated	280.6 ± 27.0

1: Specific actvity was measured in a 500 µL reaction containing 40 µM phenanthridine and 150 nM enzyme at 321 nm for 30 seconds in an air-saturated buffer (50 mM TrisHCl, 200 mM NaCl, 1 mM EDTA, pH 8.0).
2: The control for the anneorobically H_2O_2 treated sample in paralell incubated under anaeorobic condition at 4 °C O/N.
3 and **4** : 150 nM of enzyme was incubated with 160 µM phenanthridine or 10 mM H_2O_2, in the presence or absence of oxygen, prior to the reactions for 30 minutes at room temperature and phenanthridine or H_2O_2 were removed before the enzyme reaction started.

4.2.2. Electrospray Ionization Mass Spectroscopic Studies on ROS Damaged Samples

ROS are able to oxidize vulnerable amino acid residues, i.e. methionines, cysteines, and to a lesser extent tyrosines, tryptophans and histidines. These events can disrupt protein structure and function (Davies 2016). To investigate whether endogenous and exogenous ROS caused different pattern of oxidation in cysteine and methionine residues of hAOX1, samples exposed to endogenous and exogenous ROS were analyzed with mass spectroscopy. Samples of 150 nM hAOX1 were treated with 10 mM H_2O_2 or 160 µM phenanthridine and after subsequent removal of H_2O_2 and

phenanthridine were incubated with a 10x molar ratio of N-ethylmaleimide (NEM) and together with a control native sample resolved on a 10 percent SDS-PAGE. The protein bands were digested with trypsin in the presence of dithiothreitol (DTT) and iodoacetamide (IAM) as a second alkylating agent to protect the free thiols. Desalted peptides were detected using electrospray ionization mass spectroscopy (ESI-MS) and the identified peptides were sorted based on the mass shifts considering NEM, sulfinate ($-SO_2^-$) and sulfonate ($-SO_3^-$) adducts of cysteines and sulfoxide (-O) adduct of methionine. The percentage of each modification was calculated in a semi-quantitative method (similar to the method for instance applied by Shetty and colleagues (Shetty, et al. 2007)) considering the intensity of the peptides carrying the modification against all the peptides containing each cysteine or methionine residue (see **Table 4.8.** for the cysteine oxidation and NEM modification and **Table A4** in the Appendix for the detailed values of methionine oxidation). The MS measurements were performed by Dr. Manfred Nimtz from the proteomic lab of Prof. Dr. Lothar Jänsch in Helmholtz Centre for Infection Research, Braunschweig, Germany and the analysis was performed with the help of Prof. Lloyd Ruddock from the University of Oulu, Finland.

4.2.2.1. Cysteine Surface Exposure in Comparison with Cysteine Oxidation

40 out of total 42 cysteines of hAOX1 were detected by ESI-MS, all 40 of which showed some levels of modification by NEM. 27 cysteines were found to be oxidized in at least one condition (see **Table 4.8.** for the values). 2 cysteines, Cys562 and Cys1193, were not found in any of the peptides detected. Also, Cys980 was an exception in which the oxidation level decreased in the presence of ROS sources, possibly due to the altered charges and loss of the peptides to be detected.

The overall oxidation of cysteines was about 1%, 15% and 7%, respectively, in the native condition, and in the H_2O_2 and phenanthridine treated samples. Different domains showed different levels of oxidation. In the native condition, and in the H_2O_2 and phenanthridine treated samples the levels were 0.5%, 5% and 2% for the FeS domain; 1%, 23% and 9% for the FAD domain; and 2%, 25% and 10% for the Moco domain (**Figure 4.12.**, panel **A**). Cysteine oxidation was higher in the samples treated with 10 mM H_2O_2, and the FAD and Moco domains showed higher oxidation than the FeS domain.

Reactivity of free thiols towards alkylating agents such as NEM is commonly used as a measure for the solvent accessibility of each cysteine. The percentage of the NEM modification against the oxidation for each cysteine were plotted to investigate whether a linear correlation between the exposure of the free thiols and their oxidation would exist (see **Figure 4.12.**, panels **B**, **C** and **D** for the correlation plots and **Table 4.8.** for the details of the values). In the correlation plots, obtained

separately for each condition, each spot represented one cysteine where the percentage of its NEM alkylation and oxidation were shown, respectively, on the Y and X axes.

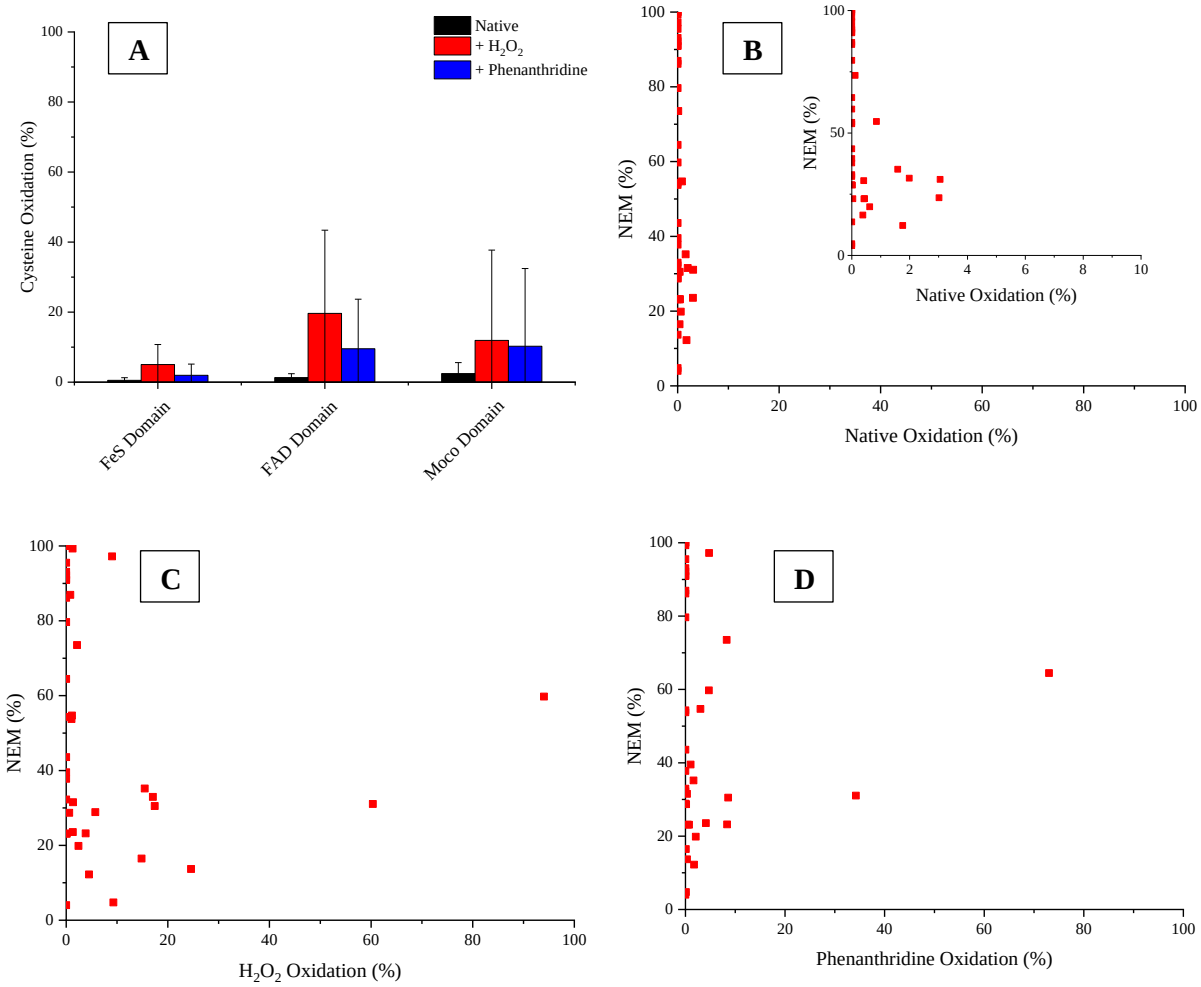

Figure 4.12.: The domain oxidation (A) and the correlation of cysteine exposure to their oxidation in different conditions (B-D): A: The overall percentage of oxidation for each domain was obtained from the sum of the oxidation of the cysteines in the native condition and in the 150 nM hAOX1 samples treated with 10 mM H_2O_2 or with 160 µM phenanthridine. **B-D:** The correlation between the solvent accessibility of the cysteines and their oxidation is presented as the percentage of the NEM modification (NEM (%)) plotted against the percentage of the oxidation in each condition (Oxidation (%)). Each spot represents one cysteine. The values are listed in **Table 4.8. Inset** in **B** is a zoom-out of the values under 10 percent for a better resolution.

Overall, the exposure (as determined by NEM reactivity) against oxidation plots (**Figure 4.12.**, panels **B**, **C** and **D**) did not show a global linear behaviour, i.e. a higher oxidation did not occur on the cysteines with higher NEM accessibility. About one third of the cysteines in the 3 conditions, i.e. in the native condition, and in the samples treated with H_2O_2 or phenanthridine, were accumulated along the NEM axis that included 13 cysteines with about 30 to 100 percent NEM

modification. This implies that 13 cysteines with partially or fully exposed free thiols were not oxidized in any of the conditions. In the native condition, 9 cysteines, i.e. Cys79, 151, 161, 460, 472, 494, 834, 935 and 1103, were about 20 to 90 percent reactive towards NEM, but they were only less than 1 percent oxidized. In the samples treated with H_2O_2 the amount of oxidation was higher, but the majority of the most accessible thiols did not show a high oxidation level. The most highly oxidized cysteines in the presence of H_2O_2 were Cys654 and Cys400 with, respectively, 94 and 60 percent of oxidation. These cysteines showed, respectively, 60 and 30 percent alkylation modification by NEM. In the phenanthridine treated sample, 3 cysteines, i.e. Cys151, 460 and 834, showed about 8 percent oxidation with about 20, 30 and 70 percent NEM modification. Cys654 with only less than 5 percent oxidation and Cys600 with 75 percent oxidation were both up to 60 percent reactive towards NEM. Overall, the oxidation of cysteines did not linearly increase with thiol accessibility in the 3 conditions.

4.2.2.2. Oxidation of Cysteines Induced by Exogenous and Endogenous ROS

The resulfuration experiments (section 4.2.1.) suggested that endogenous and exogenous ROS might affect hAOX1 differently. Therefore, the oxidation in the native condition was considered as the basal level of oxidation that occurred during protein production and sample preparation. The oxidation of cysteines in the samples treated with H_2O_2 and phenanthridine were compared with the basal oxidation in the native condition (see **Figure 4.13.**, panels **A** and **B**). Note that when the oxidation in the native condition was zero, a minimum value of 0.04 which was the minimum oxidation detected, was assigned to the native condition to avoid infinite values for the ratios. These ratios showed clearly that site specific oxidation differed between exogenous ROS and endogenous ROS generated during the catalytic cycle.

The ratio of the H_2O_2 to native oxidation (**Figure 4.13.**, panel **A**) represents the oxidation induced by H_2O_2. Cys654, locating on the surface at the substrate gate I, was about 2400 fold more oxidized in the presence of H_2O_2 than in the native condition, while Cys1242 and Cys910 were about 500 fold and Cys179 and Cys180 about 200 fold more oxidized when treated with exogenous ROS. The ratio of the phenanthridine to native oxidation (**Figure 4.13.**, panel **B**) showed that Cys600 had the largest fold difference (1800 fold) upon substrate turnover. Hence, this cysteine, located on a short alpha helix in the Moco domain and 20 Å distant from the Mo center, got immensely more oxidized in the presence of endogenous ROS. Cys654, 798 and 834 were up to 100 fold more oxidized in the phenanthridine treated enzyme than in the native condition. The different pattern of cysteine

oxidation in the presence of phenanthridine in comparison with hydrogen peroxide suggests that the endogenous and exogenous ROS affect hAOX1 differently.

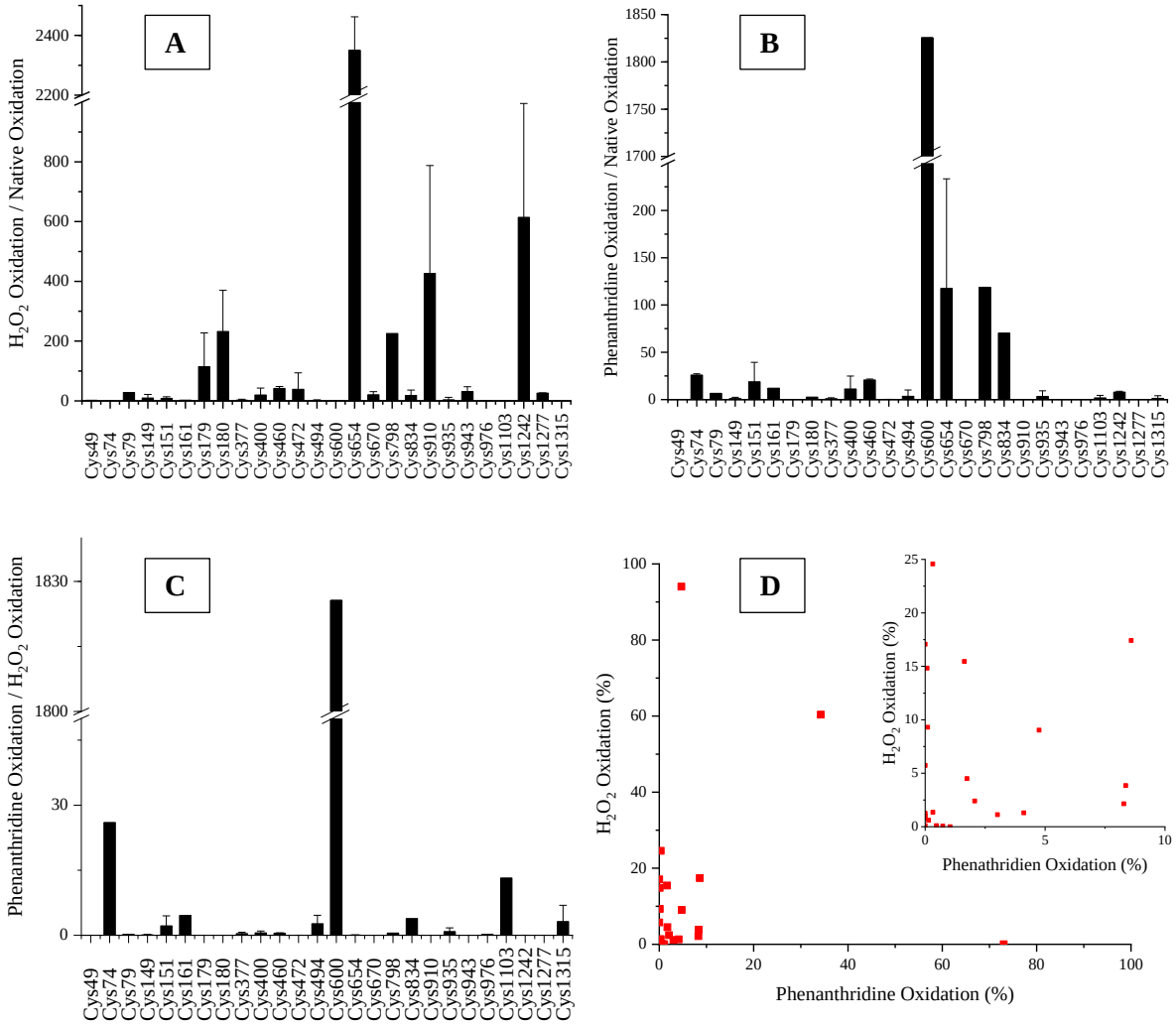

Figure 4.13.: Comparison of the cysteine oxidation in different conditions: A and **B:** The ratios of cysteine oxidation in the samples treated with exogenous ROS (**A**) and endogenous ROS (**B**) to the oxidation in the native condition as basal oxidation. **C:** The ratio of cysteine oxidation in the phenanthridine to H_2O_2 treated samples as an indicator of specific oxidation induced by endogenous ROS. When an oxidation value in the denominator was zero, a minimum value of 0.04 was assigned to avoid infinite values. **D:** The correlation plot of the oxidation in the presence of the exogenous ROS against the endogenous ROS. Each spot represents one cysteine with its corresponding phenanthridine and H_2O_2 oxidation shown, respectively, on the X and Y axes. **Inset** shows a zoom-out of the values under 10 percent for a better resolution (see **Table 4.8.** for the details of the values).

The ratio of phenanthridine to H_2O_2 oxidation (shown in **Figure 4.13.**, panel **C**) was used as an indicator of oxidation which was specifically induced by endogenous ROS. Note that again when the oxidation in the H_2O_2 treated samples was zero, a minimum value of 0.04 was assigned to

Table 4.8.: The percentage of alkylation by NEM and oxidation of the cysteines in different conditions

Domain	Cysteine / Position	NEM (%)[1]	Native Oxidation (%)	H_2O_2 Oxidation (%)[2]	Phenanthridine Oxidation (%)[3]
FeS Domain	44, FeSII	32.26 ± 14.17	0	0	0
	49, FeSII	54.31 ± 30.41	0	0.10	0
	52, FeSII	37.78 ± 23.07	0	0	0
	74, FeSII	39.5 ± 0.15	0	0	1.04 ± 0.05
	79	28.71 ± 4.90	0.02	0.60	0.14
	109	79.67 ± 31.75	0	0	0
	149, FeSI	92.21 ± 11.02	0	0	0
	114, FeSI	86.14 ± 19.60	0	0	0
	117, FeSI	35.20 ± 27.92	1.58 ± 1.36	15.46 ± 6.03	1.64 ± 0.81
	151, FeSI	23.19 ± 11.21	0.44 ± 0.06	3.84 ± 1.79	8.36 ± 7.90
	161, Linker I	23.15 ± 11.15	0.04	0.10	0.47
	165, Linker I	93.07	0	0	0
	170, Linker I	43.56	0	0	0
	171, Linker I	4.00	0	0	0
	179, Linker I	28.86 ± 33.3	0	5.73 ± 5.64	0
	180, Linker I	4.75	0	9.30 ± 5.51	0.10
FAD Domain	377	12.23 ± 9.34	1.76 ± 0.49	4.50 ± 4.41	1.74 ± 1.21
	400	31.05 ± 17.26	3.05 ± 1.90	60.36 ± 34.16	34.23 ± 20.57
	460	30.50 ± 9.62	0.41	17.42 ± 2.59	8.59 ± 0.43
	472	16.48 ± 15.18	0.38	14.83 ± 20.92	0.08 ± 0.03
	477	100	0	0	0
	494	54.69 ± 35.12	0.85 ± 1.16	1.13 ± 0.59	3.02 ± 1.54
Moco Domain	600	64.47 ± 13.02	0	0	73.02
	654, Substrate Gate I	59.75 ± 26.33	0	94.02 ± 4.47	4.70 ± 4.63
	670	86.92 ± 0.26	0	0.82 ± 0.42	0
	676	90.89 ± 12.88	0	0	0
	798	97.22 ± 2.38	0	9.03	4.75
	834	73.52 ± 39.81	0.12	2.15 ± 2.12	8.28
	905	100	0	0	0
	910	32.95 ± 2.03	0	17.06 ± 14.45	0
	935	19.86 ± 16.11	0.62 ± 0.76	2.41 ± 2.03	2.07
	943	99.31 ± 0.88	0	1.25 ± 0.65	0
	976	31.52 ± 13.05	1.99	1.35 ± 0.25	0.32
	980	20.11 ± 9.23	8.49 ± 11.33	0.18 ± 0.06	4.22 ± 3.94
	1103	23.11 ± 18.54	0.42 ± 0.17	0.06	0.74 ± 0.85
	1168	91.09 ± 12.60	0	0	0
	1175	95.52 ± 6.33	0	0	0
	1242	13.68 ± 3.38	0	24.57 ± 15.24	0.32 ± 0.04
	1277	53.75 ± 7.16	0	1.04 ± 0.03	0
	1315	23.55 ± 13.95	3.02 ± 2.75	1.30 ± 0.58	4.11 ± 4.51

1: Samples in the native condition or treated with H_2O_2 or phenanthridine were incubated with 10x molar ratio of NEM for 30 min at room temperature.

2 and **3**: Samples of 150 nM hAOX1 in 50 mM TrisHCl, 200 mM NaCl, 1 mM EDTA, pH 8.0 were incubated with 10 mM H_2O_2 or 160 µM phenanthridine for 30 min at room temperature.

calculate the ratio. It was observed that 3 cysteines, i.e. Cys600, 74 and 1103, were specifically more oxidized with endogenous ROS. Cys74 and 1103 were about 20-30 fold more oxidized, while Cys600 was more than 1800 fold more oxidized in the sample treated with phenanthridine.

A correlation graph of H_2O_2 oxidation (%) against phenanthridine oxidation (%) (**Figure 4.13.**, panel **D**) was plotted to investigate whether a linear behaviour between the cysteines oxidized with the endogenous and exogenous ROS existed. Each spot in the graph represents one cysteine. The graph showed a scattered pattern with no overall linear correlation between oxidation by H_2O_2 and by phenanthridine.

4.2.2.3. Methionine Oxidation

Methionine is one of the most vulnerable amino acids to oxidation (Liang, et al. 2012). The amount of methionine oxidation was measured similarly as for cysteines to investigate whether the specific oxidation behaviour distinguished for cysteines would be consistently observed.

The overall oxidation of methionines was about 20%, 60% and 30%, respectively, in the native condition, and in the H_2O_2 and phenanthridine treated enzymes. The overall oxidation of methionines was significantly higher than that of cysteines, but no significant difference was observed in the oxidation of each domain (**Figure 4.14.**, panel **A**).

The phenanthridine to H_2O_2 oxidation ratio (**Figure 4.14.**, panel **B**) showed the values less than 1, except for Met55, suggesting that exogenous ROS induced more oxidation than endogenous ROS. Met55 was an exception with about 2.5 fold more oxidation when treated with phenanthridine, however, this residue showed more oxidation in the native condition than in the ROS exposed samples. This may be due to the loss of the peptide and hence, the 2.5 fold difference between the oxidation in samples treated with exogenous or endogenous ROS must be carefully interpreted (see **Table A4** in the Appendix of this thesis for the details of methionines oxidation).

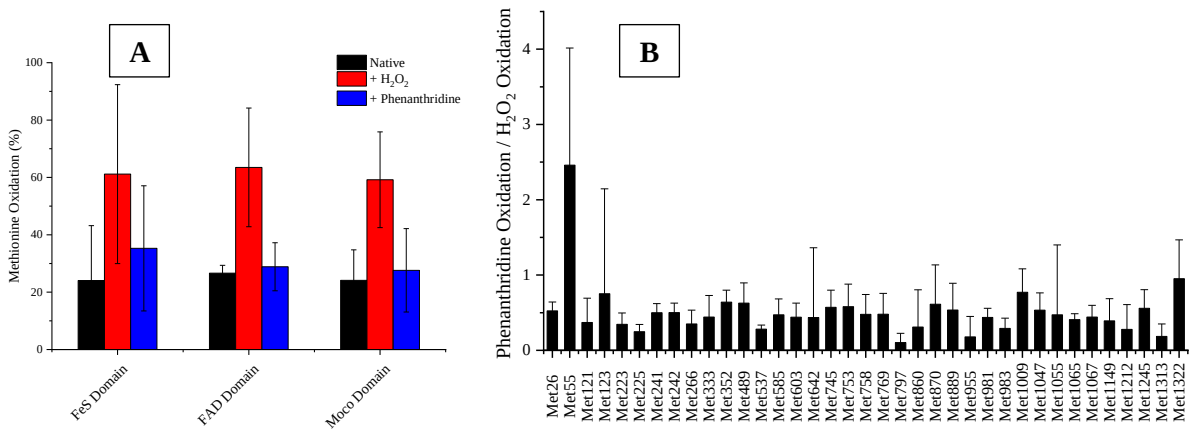

Figure 4.14.: The domain oxidation (A) and specific oxidation (B) of methionines in different conditions: A: The overall percentage of oxidation for each domain was obtained from the sum of the oxidation of methionines in the native condition and in samples treated with 10 mM H_2O_2 or with 160 µM phenanthridine. **B:** The ratio of oxidation in the phenanthridine to the H_2O_2 treated samples was used as an indicator of specific oxidation induced by endogenous ROS.

4.3. The FAD Variable Loop and ROS Production in hAOX1

4.3.1. Production of the Variants with Altered Amino Acid Composition in the FAD Variable Loop

hAOX1 oxidizes aldehydes and N-heterocyclic compounds at the Moco site and internally transfers the electrons to the site where the second substrate binds, accepts the electrons and gets reduced (Hille, et al. 2014). Molecular oxygen is known from early studies to be the endogenous electron acceptor of aldehyde oxidases and FAD is the site where it is widely believed that the electron acceptor binds. Upon reduction, oxygen forms reactive oxygen species (ROS) including hydrogen peroxide (H_2O_2) and superoxide ($O_2^{\cdot-}$). hAOX1-WT predominantly generates hydrogen peroxide over superoxide, however, recently a natural variant of hAOX1 with a leucine residue at the position 438 replaced with a valine has been identified that produces more than 70 percent of the total ROS in the form of superoxide (Foti, et al. 2017). Leu438 locates in proximity to the FAD site on a loop known as the FAD variable loop 1 which consists of 10 amino acids (^{430}AQRQENALAI^{440}) (Coelho, et al. 2015). Leu438 was exchanged to the residues hydrophobic and less bulky i.e. alanine, aromatic bulkier, i.e. phenylalanine and positively charged, i.e. lysine to further examine the role of this position in superoxide production. In addition, the entire FAD variable loop 1, i.e. ^{430}AQRQENALAI^{440}, in hAOX1 was replaced with its counterpart, i.e. ^{423}QASRREDDIA^{433}, from bovine XO (bXO). Two more variants with altered residues to the corresponding bXO amino acids at positions 436 and 437 were also constructed (see **Table 3.2.** in

the Materials and Methods for the list of the plasmids generated in this study). The majority of these plasmids were prepared by Dr. Alessandro Foti who first reported the hAOX1-L438V natural variant (Foti, et al. 2017). The construction of the chimeric variant with the bXO loop was completed in this work.

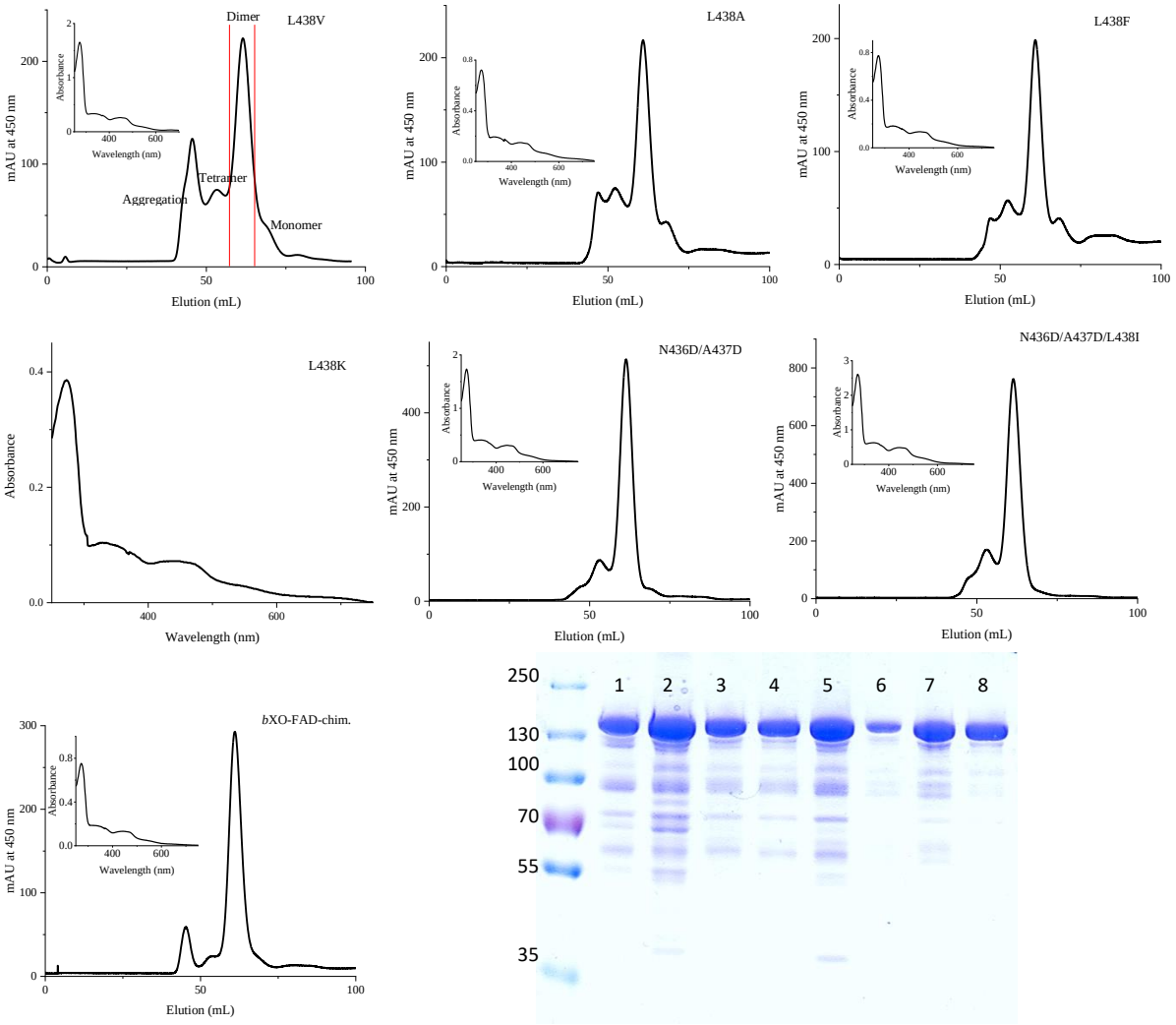

Figure 4.15.: SEC elution profiles, UV-Vis spectra (insets) and Coomassie stained reducing SDS-PAGE of the FAD and chimeric variants: Using a Superdex 200 16/600 pg column and 50 mM TrisHCl, 200 mM NaCl, 1 mM EDTA, pH 8.0 as elution buffer the SEC profiles show consistently aggregation, tetramer, dimer and monomer elution peaks, respectively for the enzymes, around 48, 55, 62 and 70 mL. The UV-Vis absorption of the variants over the range of 250 to 800 nm (insets) present peak maxima at 280, 450 and 550 nm corresponding to the protein backbone, FAD and Fe-S clusters absorption, respectively. The original SEC data of L438K was lost due to some technical problems, hence, only the UV-Vis spectrum is shown for this variant. Coomassie stained reducing SDS-PAGE 10% gel of the variants produced for this work with the lanes labelled from 1 to 8, respectively, related to WT, L438V, L438A, L438F, L438K, N436D/A437D, N436D/A437D/L438I and bXO-FAD-chimera features similar degradation pattern for WT and the variants.

The expression vectors were overexpressed in the *E. coli* TP1000 cells (*ΔmobAB*) (Palmer, et al. 1996) and proteins were purified as described in the previous works (Foti, et al. 2016) following a similar procedure explained in sections 3.2.2. and 4.1.2.1. of this thesis. The SEC elution profiles of

the variants summarized in **Figure 4.15.** presented the eluted peaks corresponding to the tetramer, dimer, and monomer, respectively, at about 55, 62 and 70 mL. The overall elution patterns of the FAD variants were similar to that of WT with about 1.0 mg/L average yield (see **Table 4.9.**). L438K was produced with the lowest yield of 0.3 mg/L together with L438F and the chimeric variant bXO-FAD-chim. with only 0.5 mg/L yield. N436D/A437D and N436D/A437D/L438I gave the highest yields of 1.2 and 1.8 mg/L, respectively. The peak fractions were resolved on reducing Coomassie stained 10 percent SDS-PAGE and the active fractions of the dimer peak were combined for further analysis. For better comparison, the protein samples were run in parallel on a reducing SDS-PAGE presented in **Figure 4.15.** It was observed that the variants behaved similarly on the gel as WT and showed consistent degradation bands similar to what has been reported previously for WT (Hartmann, et al. 2012).

4.3.2. Characterization of the FAD Loop Variants

4.3.2.1. UV-Vis Absorption and Metal Content

The UV-Vis absorption of the variants produced for this work was recorded over the range of 800 to 250 nm (inset graphs in the SEC elution profiles shown in **Figure 4.15.**). The UV-Vis spectra for the variants similar to WT presented three typical maxima for the FeS clusters at 550 nm, FAD at 450 and the polypeptide at 280 nm. The purification index ratios A_{280}/A_{450} and A_{450}/A_{550} were obtained from the UV-Vis spectra (see **Table 4.9.** for the detailed values). A_{280}/A_{450} values for the variants varied narrowly close to 5 with the lowest and highest values of 4.6 and 5.4, respectively, for N436D/A437D/L438I and L438F. A_{450}/A_{550} remained slightly under 3 for the FAD and chimeric variants with a minimum and maximum of 2.4 and 2.8, respectively, corresponding to N436D/A437D/L438I and L438F. WT showed A_{280}/A_{450} of 5.5 and A_{450}/A_{550} of 3.1 which were comparable to the ratios observed for the FAD and chimeric variants and indicated acceptable purification quality.

The molybdenum and iron content of the variants were determined using inductively coupled plasma - optical emission spectrometry (ICP-OES) and 5-10 µM wet-ashed (65% HNO_3, 100 ^{o}C, O/N) protein samples. The calculated percentages of saturation for Mo and Fe represent Moco and two [2Fe-2S] clusters content, respectively, related to the maximum number of one Mo and 4 Fe per monomer of the enzyme. The variants produced for this study were loaded with 40-50 percent molybdenum and 50-60 percent iron which were close to the values of 57 percent Mo and 60 percent Fe obtained for WT (see **Figure 4.16.** and **Table 4.9.** for the details of the values and

comparisons with WT). The amount of molybdenum was used to calculate the amount of active portion of each enzyme in the further steps of characterization of the variants.

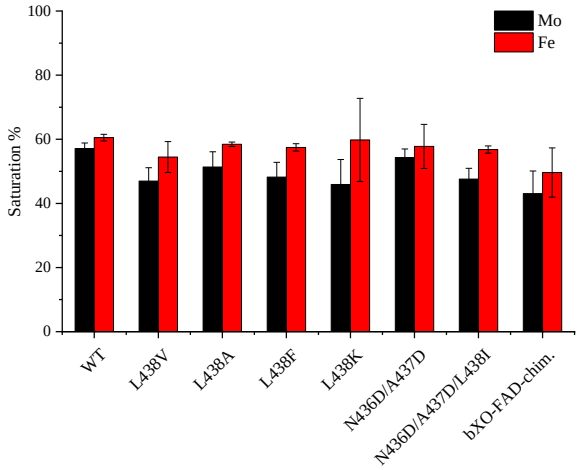

Figure 4.16.: Metal saturation of WT and the FAD and chimeric variants determined by ICP-OES: The Mo and Fe contents, which were determined using 5-10 µM wet-ashed protein samples, vary narrowly around 40-50 percent and 50-60 percent, respectively, for the variants produced in this work. The Mo and Fe loads are comparable with those of WT. For the details of the values see **Table 4.9.**

Table 4.9.: Metal saturation, purification index ratios and yield of the FAD and chimeric variants

Enzyme		**Mo (%)[1]**	**Fe (%)[1]**	**A_{280}/A_{450}[2]**	**A_{450}/A_{550}[2]**	**Yield (mg/L)**
WT		57.1 ± 1.7	60.5 ± 1.0	5.5	3.1	0.8
FAD Variants	L438V	47.0 ± 4.2	54.5 ± 4.8	5.3	2.6	1.0
	L438A	51.3 ± 4.8	58.4 ± 0.7	4.7	2.4	0.6
	L438F	48.2 ± 4.6	57.5 ± 1.2	5.4	2.8	0.5
	L438K	45.9 ± 7.8	59.8 ± 13.0	5.1	2.6	0.3
	N436D/A437D	54.3 ± 53.8	57.8 ± 6.9	4.8	2.6	1.2
	N436D/A437D/L438I	47.6 ± 3.4	56.8 ± 1.3	4.6	2.4	1.8
Chimeric Variant	bXO-FAD-Chim.	43.0 ± 7.1	49.6 ± 7.7	4.9	2.5	0.5

1: Metal saturations were determined by ICP-OES in 5-10 µM wet-ashed samples of enzyme and related to the maximum number of one Mo and 4 Fe per monomer of the enzyme.
2: A_{280}/A_{450} and A_{450}/A_{550} were calculated from the UV-Vis absorption spectra.

4.3.2.2. Steady State Kinetics

The steady state kinetics of the FAD variants were studied using a phenanthridine/oxygen system in which oxygen provided in air-saturated buffer (50 mM TrisHCl, 200 mM NaCl, 1 mM EDTA, pH 8.0) acted as the oxidizing electron acceptor. 2 to 80 µM phenanthridine was used as the substrate for WT, L438V, L438A, L438F and L438K, while for N436D/A437D, N436D/A437D/L438I and bXO-FAD-Chim. due to their lower K_m, the concentration of phenanthridine was changed over 1 to 40 µM. Enzyme concentration was kept 150-200 nM and the reaction was followed at 321 nm for 30 seconds. The absorbance linearly increased over the first 30 seconds of the reaction which was then used to calculate the rate of product formation at each concentration of phenanthridine. Rate against substrate concentration progress curves showed a Michaelis-Menten behaviour from which the V_{max} and K_m for each variant were obtained. The data was in parallel fitted in Hill equation to ensure the Hill coefficient remained around 1.0 ± 0.2 (see **Figure A2** in the Appendix of this thesis for the details of the Hill versus MM fits). The k_{cat} values calculated from V_{max} were normalized to the molybdenum content for each enzyme to obtain comparable values summarized in **Table 4.10.** and presented in **Figure 4.17.**

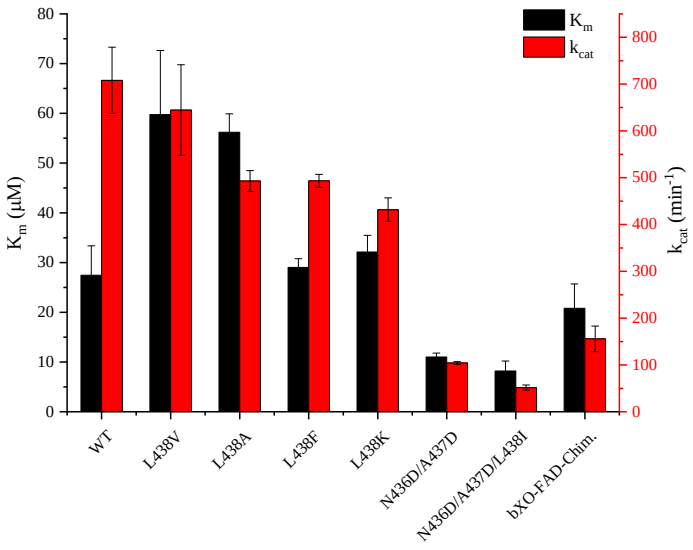

Figure 4.17.: Steady state kinetics parameters of the FAD variants: K_m and k_{cat} were obtained by following the formation of product at 321 nm using 2-80 µM phenanthridine for WT and single amino acid exchanged variants, and 1-40 µM phenanthridine for N436D/A437D, N436D/A437D/L438I and bXO-FAD-chimeric variants. Enzyme concentration was kept at 150-200 nM and the assay was performed in air-saturated buffer (50 mM TrisHCl, 200 mM NaCl, 1 mM EDTA, pH 8.0). To obtain comparable values turnover numbers were normalized to 100 percent molybdenum saturation for each variant.

The steady state kinetic parameters determined for WT were about 700 min^{-1} k_{cat} and 27 µM K_m that resulted in the catalytic efficiency, k_{cat}/K_m, of about 25 $\mu M^{-1}.min^{-1}$. Note that the different value for k_{cat} obtained here than in section 4.1.2.3. is due to normalization to the Mo content. The natural variant L438V represented a k_{cat} of 640 min^{-1} close to that of WT, but with higher K_m of 59 µM that lowered the catalytic efficiency to about 10 $\mu M^{-1}.min^{-1}$. L438A, L438F and L438K showed lowered k_{cat} from 493 min^{-1} for L43A to 431 min^{-1} for L438K. The K_m of L438A was about 56 µM, while L438F and L438K showed K_m values closer to that of WT with 29 µM and 32 µM, respectively. Consequently, the catalytic efficiency for these variants was decreased to lower values than that of WT, i.e. 17, 13.5 and 8.8 $\mu M^{-1}.min^{-1}$, respectively, for L438K, L438F and L438A.

Table 4.10.: The steady state kinetic parameters of WT in comparison with the variants generated to investigate the FAD variable loop

Enzyme		k_{cat} (min^{-1})[1]	K_m (µM)[1]	k_{cat}/K_m ($min^{-1}.\mu M^{-1}$)
WT		708.1 ± 70.7	27.5 ± 5.9	25.8 ± 6.1
FAD Variants	L438V	644.6 ± 96.8	59.7 ± 12.9	10.8 ± 2.8
	L438A	493.0 ± 22.3	56.2 ± 3.7	8.8 ± 0.4
	L438F	493.4 ± 13.7	29.0 ± 1.8	17.0 ± 1.2
	L438K	431.7 ± 25.2	32.1 ± 3.3	13.5 ± 1.6
	N436D/A437D	104.2 ± 2.8	11.0 ± 0.8	9.5 ± 0.7
	N436D/A437D/L438I	51.6 ± 5.5	8.2 ± 2.0	6.3 ± 1.7
	bXO-FAD-Chim.	155.8 ± 27.3	20.8 ± 4.9	7.5 ± 2.2

1: The kinetic measurements were performed in air-saturated buffer (50 mM TrisHCl, 200 mM NaCl, 1 mM EDTA, pH 8.0) in the range of 2 to 80 µM of phenanthridine for WT and single amino acid exchanged variants, and 1-40 µM phenanthridine for N436D/A437D, N436D/A437D/L438I and bXO-FAD-chimeric variants. The enzyme concentration was kept at 150-200 nM depending on the variant. k_{cat} values were normalized to 100 percent Mo content as a full complement of Moco.

The multiple amino acid exchanged variants, N436D/A437D and N436D/A437D/L438I together with bXO-FAD-chimera where the entire ^{430}AQRQENALAI^{440} loop was exchanged to the ^{423}QASRREDDIA^{433} loop present in bovine XO, showed even lower k_{cat} with 155 min^{-1} for bXO-FAD-chimera to 104 and 51 min^{-1} for N436D/A437D and N436D/A437D/L438I, respectively. The K_m values presented higher affinity for phenanthridine with 11 and 8 µM for N436D/A437D and N436D/A437D/L438I, respectively, while the K_m of bXO-FAD-chimera remained close to that of WT at about 20 µM. The K_m/k_{cat} values of these variants were much lower than WT with 9.5, 7.5 and 6.3 $\mu M^{-1}.min^{-1}$, respectively, for N436D/A437D, bXO-FAD-chimera and

N436D/A437D/L438I. Overall, the steady state kinetic parameters of the FAD variants produced in this study were close to those of WT and the natural variant L438V except for the multiple amino-acid exchanged variants which showed lowered turnovers.

4.3.2.3. Reactive Oxygen Species (ROS) Production

hAOX1 generates reactive oxygen species (ROS) in the form of hydrogen peroxide and superoxide when oxygen is reduced as the terminal electron acceptor. hAOX1-L438V is a natural variant that predominantly produces more than 70 percent superoxide (Foti, et al. 2017), while hAOX1-WT generates only about 20 percent of superoxide. The amount of superoxide can be obtained using a cytochrome C assay in which superoxide reduces Fe^{3+} to Fe^{2+} in cytochrome C with an increase in the absorption at 550 nm. The total ROS (H_2O_2 and $O_2^{-}\cdot$) is determined from the oxidation of phenanthridine followed at 321 nm. The ratio of superoxide to total ROS represents the percentage of superoxide generated in the reaction. A positive control reaction in the presence of catalase converting H_2O_2 to H_2O was used to ensure that H_2O_2 is not involved in the reduction of cytochrome C. Superoxide dismutase (SOD) that converts superoxide to peroxide was used as the negative control to confirm that exclusively the superoxide generated over the course of the reaction is responsible for the reduction of cytochrome C. This assay was applied to determine whether the type of ROS was affected by altering the amino acids at the position 438 and the surrounding residues (see **Figure 4.18.,** panel **A** and **Table 4.11.**).

hAOX1-WT produced about 20 percent superoxide which was similar to the percentage of superoxide obtained for N436D/A437D/L438I and bXO-FAD-chimera, while N436D/A437D generated only 4 percent superoxide (see **Figure 4.18.** and **Table 4.11.** for the comparison of the values). Despite the comparable level of superoxide percentage obtained for WT and N436D/A437D, N436D/A437D/L438I and bXO-FAD-chimera, the amount of cytochrome C reduction induced by N436D/A437D, N436D/A437D/L438I and bXO-FAD-chimera was significantly lower and about 74, 73 and 28 nmol/min.mg, respectively, for bXO-FAD-chimera, N436D/A437D/L438I and N436D/A437D; while WT was able to reduce cytochrome C to about 400 nmol/min.mg.

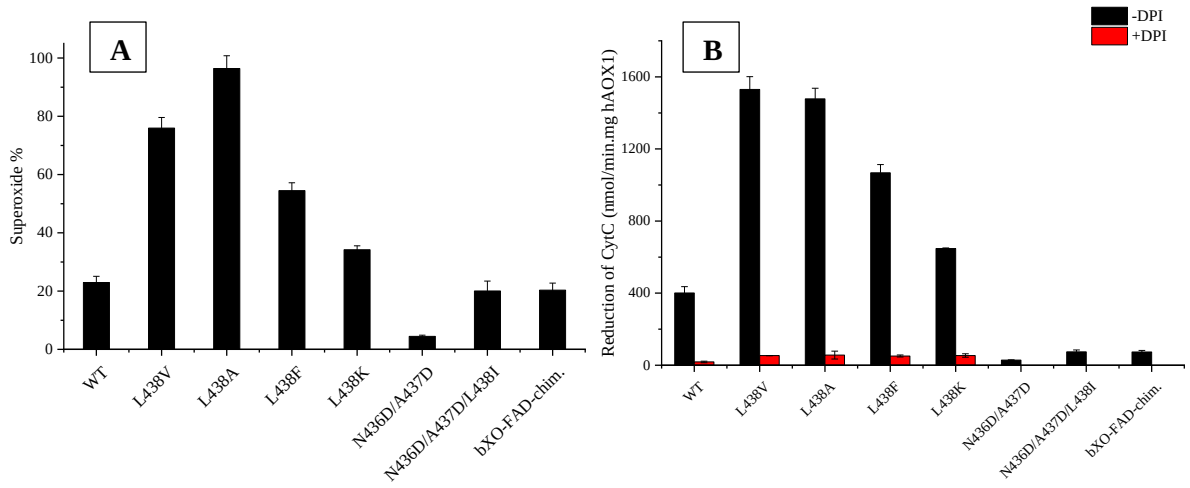

Figure 4.18.: A: The superoxide to peroxide ratio of WT in comparison with the FAD variants: Superoxide production was obtained from the reduction of 40 µM of cytochrome C followed at 550 nm in the presence of 40 µM phenanthridine and 150-200 nM of hAOX1 in air-saturated buffer (50 mM TrisHCl, 200 mM NaCl, 1 mM EDTA). Total ROS was obtained from the oxidation of 40 µM phenanthridine followed at 321 nm in a reaction containing 150-200 nM of hAOX1 in air-saturated buffer. **B: The reduction of cytochrome C in the absence or presence of DPI:** 5 µM of DPI was used to inhibit the FAD site in a reaction described in **A**. The reduction of cytochrome C represents the amount of superoxide produced during the catalytic cycle and is significantly decreased when the FAD site is inhibited by DPI.

The variants with altered amino acid at the position 438, i.e. L438K, L438F and L438A, showed significantly increased percentage of superoxide with 34, 54 and 90 percent, respectively. L438A was able to produce even more superoxide than the natural variant L438V which generated 75 percent superoxide. The amount of cytochrome C reduction carried out by L438V and L438A were similarly close and about 1530 and 1478 nmol/min.mg, respectively, while L438F and L438K were able to reduce less cytochrome C to about 1067 and 647 nmol/min.mg, respectively. Cytochrome C reductions induced by the variants with altered amino acid at the position 438 were all higher than that of WT with about 400 nmol/min.mg. These results suggest that changing the amino acid at position 438 affects the type of the ROS generated by the enzyme.

Diphenyleneiodonium (DPI) is a specific inhibitor of flavoenzymes (Reis, et al. 2020) which is believed to covalently bind at the FAD and inhibits the enzyme. The FAD variants of hAOX1 were incubated with 5 µM of DPI and the reduction of cytochrome C was consequently measured. It was observed that the ability of the variants to reduce cytochrome C was dropped to about 8 to 3 percent of their initial values. Given the specificity of DPI in binding FAD, these results imply that the superoxide is predominantly produced at the FAD site of hAOX1.

Table 4.11.: The effect of the FAD specific inhibitor on the reduction of cytochrome C

Enzyme		Total ROS -DPI[1]	CytC Reduction -DPI[1]	Superoxide (%)[2]	Total ROS +DPI[1]	CytC Reduction +DPI[1]
WT		1748.4 ± 53.6	400.9 ± 35.2	22.9 ± 2.1	45.7 ± 35.7	18.3 ± 4.3
FAD Variants	L438V	2015.2 ± 28.9	1530.4 ± 70.6	75.9 ± 3.7	40.0 ± 21.5	53.3 ± 0.6
	L438A	1637.2 ± 115.1	1478.1 ± 58.7	90.3 ± 7.3	221.5 ± 6.7	56.5 ± 21.8
	L438F	1959.9 ± 49.8	1067.4 ± 46.0	54.5 ± 2.7	58.1 ± 7.4	51.3 ± 5.4
	L438K	1893.8 ± 75.6	647.3 ± 3.2	34.2 ± 1.4	121.2 ± 55.8	53.9 ± 9.6
	N436D/A437D	636.9 ± 51.4	28.5 ± 1.3	4.4 ± 0.4	nd[3]	nd
	N436D/A437D/L438I	370.4 ± 43.4	74.3 ± 10.9	20.0 ± 3.4	nd	nd
	bXO-FAD-chim.	362.7 ± 10.6	73.8 ± 8.4	20.3 ± 2.4	nd	nd

1: The unit is nmol/min.mg hAOX1

2: Superoxide measurements were performed in air-saturated buffer (50 mM TrisHCl, 200 mM NaCl, 1 mM EDTA, pH 8.0) in the presence of 150-200 nM of enzyme and 40 µM phenanthridine with addition of 40 µM of Cytochrome C in the main reaction, supplemented with 100 U/mL of catalase or 20 µM superoxide dismutase in the control reactions. DPI was at 5 µM when present.

3: nd: not detectable.

4.3.3. X-ray Crystal Structure of hAOX1-L438V

As mentioned before, the hAOX1-L438V variant has been previously reported as a superoxide producing natural variant (Foti, et al. 2017). Leu438 locates on the FAD variable loop 1 in close proximity of the N5 position of the FAD isoalloxazine ring. To understand the possible effects of replacing Leu438 with a valine, the hAOX1-L438V variant was crystallized and the diffraction data was collected up to 2.6 Å in collaboration with the lab of Prof Maria Joao Romao by Dr. Cristiano Mota in the Universidade Nova de Lisboa. The structure was determined by Dr. Mota using molecular replacement and the substrate-free structure of hAOX1-WT (PDB code: 4UHW, (Coelho, et al. 2015)) as the search model. The overall structure of L438V is very similar to WT with an RMSD of 0.200 for 1117 C-alphas, suggesting a minimal difference between the two structures. The Moco, FeS clusters and FAD domains did not show any significant global or local conformational changes. The only difference observed was the size of the cavity around the position 438 (see **Figure 4.19.** panels **B** and **C**). The distance from the leucine side chain to the N5 position of the isoalloxazine ring was 3.5 Å, while the side chain of valine in the L348V variant is 1 Å further away, at about 4.6 Å distance from N5 positon of FAD. This subtle change provides a

slightly larger cavity for the reaction of oxygen at FAD which seems to be a crucial factor for determining the type of ROS produced by the enzyme (see section 5.3.2. for discussion).

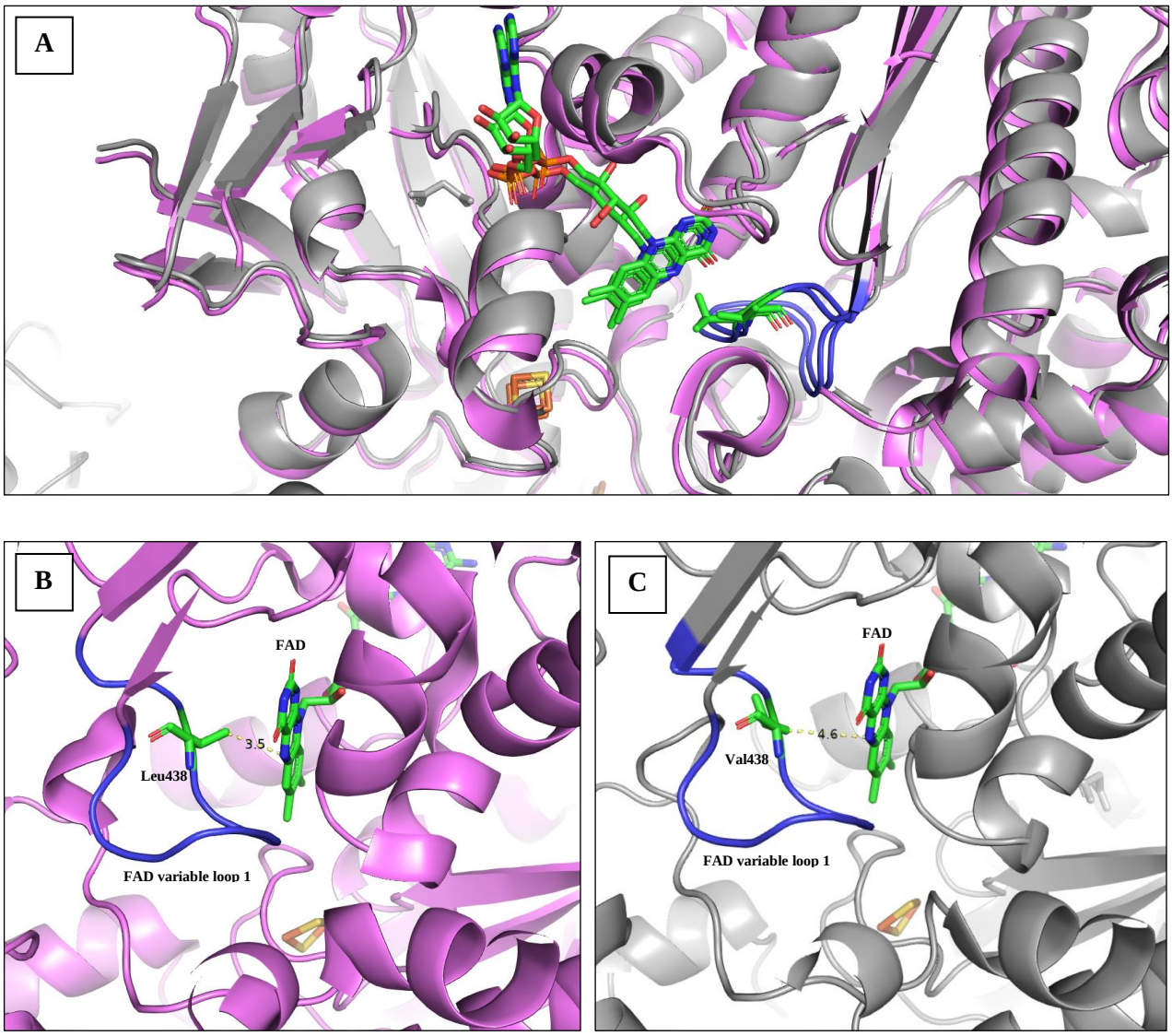

Figure 4.19.: Selected ribbon representation of L438V structure in comparison with WT: A: Superimposition of hAOX1-L438V crystal structure (grey) with hAOX1-WT (PDB code: 4UHW) (violet) around the 438 position located on the FAD variable loop 1 (shown in blue). **B** and **C**: The position 438 shown for WT (**B**) with the leucine residue at 3.5 Å and for L438V (**C**) with the valine residue at 4.6 Å distance from the N5 position of FAD. Representatives are generated using PyMol version 2.4.1. (Schrödinger, LLC).

4.4. Unexpected Effect of Dithiothreitol on hAOX1

4.4.1. The Effect of DTT on Protein Aggregation and Enzyme Activity

Dithiothreitol (DTT) is commonly used as a reducing agent to prevent aggregation in protein production (Cleland 1964). To investigate whether DTT was able to improve the yield of hAOX1

production, one expression batch was split in two and the samples were purified in parallel in the absence and presence of DTT. A Superose 6 column was used for the SEC step while the buffer (50 mM Tris, 200 mM NaCl, 1mM EDTA, pH 8.0) was supplemented with 2.5 mM DTT when present. The SEC trace showed slightly sharper dimer and smaller aggregation peaks in the presence of DTT (**Figure 4.20., A**). The UV-visible absorption of the proteins under both conditions was similar with a slightly higher absorption around 300 nm for the sample purified in the absence of DTT. This indicated slightly lower levels of aggregation in the presence of DTT (**Figure 4.20.**, **A** inset). However, the specific activities measured using 40 μM phenanthridine and oxygen as electron acceptor showed complete loss of activity in the samples treated with DTT (**Figure 4.20., B**). The measurements were repeated by incubating active samples with 1 mM DTT (a 100x molar ratio of the concentration of the enzyme) for 30 minutes at room temperature and the loss of activity was consistently observed. Removal of DTT did not recover the activity of hAOX1, which suggested an irreversible inactivation of the enzyme.

4.4.2. The Nature of hAOX1 Inactivation by DTT

DTT contains two sulfhydryl groups. To examine whether the effect of DTT was due to the presence of reactive sulfhydryl groups, hAOX1 was incubated with 100x molar ratio of 2-mercaptoethanol (2-ME) with a structure similar to DTT but with shorter carbon backbone and only one sulfhydryl group, dithioerythritol (DTE), a slightly less reactive epimer of DTT, the oxidized form of DTT (DTT_{ox}) in which the reactive sulfhydryl groups have formed a disulfide bridge, the reduced form of glutathione (GSH) that contains a sulfhydryl on a tri-peptide backbone, and erythritol, a structural homologue of DTE that carries two hydroxyl groups instead of the sulfhydryl groups on a similar backbone. In addition, the effect of three commonly used thiol alkylating agents, i.e. N-ethylmaleimide (NEM), 4-vinylprydine (4-VP) and iodoacetamide (IAM) on the activity of hAOX1 were investigated. **Table 4.12.** presents the structure of the chemicals used in this study. In each condition the enzyme was recovered after 30 minutes incubation with the chemicals and its activity was measured in parallel with a control sample incubated at room temperature to track any potential decrease in the activity (see **Figure 4.20.**, panel **B**).

It was observed that 2-ME abolished the activity of hAOX1 similar to DTT, but GSH had only a slight negative effect (**Figure 4.20.**). DTE, the epimer of DTT, resulted in more than 90 percent inactivation of hAOX1, while the oxidized form of DTT, DTT_{ox}, lowered the activity to about 50 percent of its initial value. Erythritol, the structural homologue of DTE which does not contain any reactive sulfhydryl groups, did not alter the activity of hAOX1. NEM and 4-VP among the cysteine alkylating agents abolished the hAOX1 activity, but pre-incubation with IAM had only a slight

effect on enzyme activity. The IAM treated sample was consequently incubated with DTT which

Table 4.12.: Chemicals used to investigate the effects on the activity of aldehyde oxidases

	Common Name	Short Name	Structure
Thiol reducing agents	Dithiothreitol	DTT	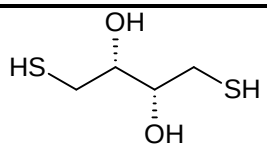
	Dithioerythritol	DTE	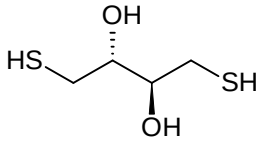
	2-mercaptoethanol	2-ME	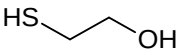
	Glutathione	GSH	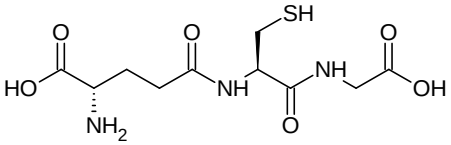
Thiol alkylating agents	Iodoacetamide	IAM	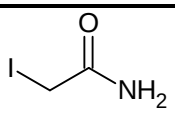
	N-ethylmaleimide	NEM	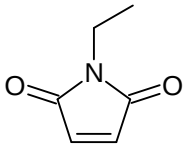
	4-vinylpyridine	4-VP	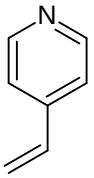
DTT structural homologues	Oxidized DTT	DTT_{ox}	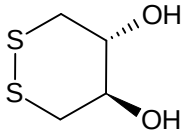
	Erythritol	Erythritol	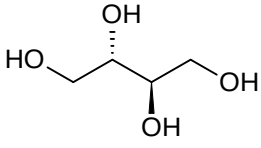

resulted in complete inactivation. These observations suggested that reactions with sulfhydryl groups were involved in the inactivation of hAOX1. However, the site of the sulfhydryl action needed to be further investigated.

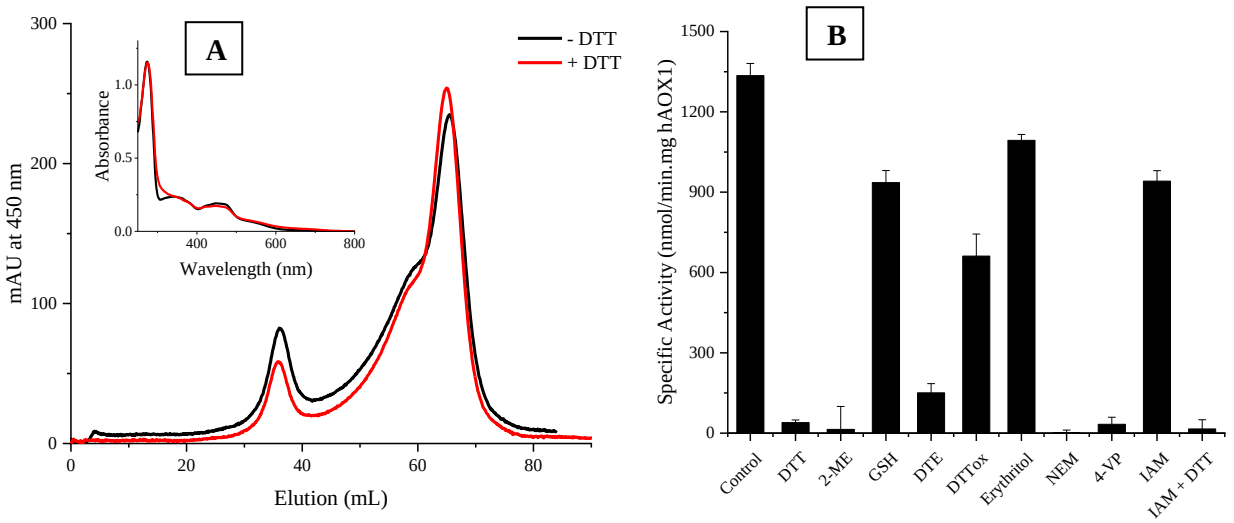

Figure 4.20.: A: The effect of DTT on hAOX1 production: Size exclusion chromatography (SEC) profile of hAOX1 in the absence and presence of DTT: Purification was performed using a Superose 6 column and SEC buffer (50 mM TrisHCl, 200 mM NaCl, 1 mM EDTA, pH 8.0) supplemented with 2.5 mM DTT when DTT was present. Slightly sharper dimer peak around 70 mL and lower aggregation peak around 35 mL is observed when DTT is present. **Inset:** UV-visible spectra of hAOX1 in the absence and presence of DTT in the range of 250 nm to 800 nm: Slightly higher absorption around 300 nm in the untreated sample indicates the presence of soluble aggregations. **B: Nature of the inactivation of hAOX1 by DTT:** hAOX1 (stored in 50 mM Tris, 200 mM NaCl, 1 mM EDTA, pH 8.0) was treated with 100x molar ratio of DTT, DTE, 2-ME, reduced glutathione (GSH), oxidized DTT (DTT_{ox}) and with cysteine alkylating agents including NEM, IAM and 4-VP for 30 min at RT. Erythritol, which does not contain sulfhydryl groups or react with them, was used as a structural homologue of DTT. Chemicals were removed after incubation and the specific activity of hAOX1 was measured using 40 µM phenanthridine in an air-saturated buffer (50 mM Tris, 200 mM NaCl, 1 mM EDTA, pH 8.0) at 321nm. The loss of activity of hAOX1 when incubated at room temperature is not significant (control bar).

4.4.3. The Potential Vulnerable Sites of hAOX1 to Reactive Sulfhydryl

The sulfhydryl group on DTT can potentially react with three main sites on hAOX1: **a)** solvent accessible disulfide bonds, if any, **b)** sulfur ligands bound to the FeS clusters and **c)** sulfido ligand coordinated to molybdenum at Moco. hAOX1 is localized in the reducing environment of cytoplasm where structural disulfide bonds are not favoured to be formed (Hwang, et al. 1992). In accordance to that, no structural disulfide bond has been reported in the structure of hAOX1 or any other XO family members. Moreover, there has not been any report of the formation of a transient disulfide bond to be involved in the catalytic cycle of AOXs. Hence, it seems that it is unlikely that

upon treatment with DTT a disulfide bond, which is structurally or functionally essential for the activity of the enzyme, is disturbed.

The effect of DTT was separately investigated for the sulfur ligands bound to the FeS clusters and the sulfido group coordinated at Moco. In addition, the effect of NEM and IAM modification was studied using ESI-MS.

4.4.3.1. NEM versus IAM Modification of Cysteines

The specific activity of hAOX1 was measured after incubation with cysteine alkylating as well as reducing agents (**Figure 4.20.**). Among the reducing agents reduced glutathione (GSH) that carries bulky groups near the reactive sulfhydryl site showed slight effect on the activity, while small reducing agents, i.e. 2-ME, DTT and DTE, decreased the activity to 90-99 percent of the initial values. The alkylating agents, N-ethylmaleimide (NEM) and 4-vinylpridyne (4-VP) completely abolished the activity, while iodoacetamide (IAM) left the activity only about 25 percent decreased. Interestingly, the activity of an IAM treated sample incubated with DTT was completely lost. These common reagents have specific applications with their preferences in studying solvent accessible cysteines; however, a general pattern that alluded on cysteine involvement in the loss of activity observed with DTT could not be drawn. To further investigate whether there was a different pattern of cysteine accessibility by IAM and NEM that could potentially affect the activity, the samples treated with IAM and NEM were analyzed with ESI-MS in the collaboration with the lab of Prof. Dr. Lothar Jänsch in Helmholtz Centre for Infection Research by Dr. Manfred Nimtz. The IAM and NEM treated samples were resolved on a reducing 10 percent SDS-PAGE. Protein bands were cut and prior to the digestion with trypsin were treated with a second label, i.e. with methyl methanethiosulfate (MMTS) and IAM, respectively, for the IAM and NEM treated samples, to ensure that the exposed free thiols were fully protected. Peptides were subsequently digested and extracted from the gel and injected to an ESI-TIMSTOF mass spectrometer. The identified peptides were analyzed in a semi-quantitative method based on the intensity of the IAM or NEM modified peptides against all the peptides containing each specific cysteine and the level of modification was reported as percentage (see **Table 4.13.** for the percentage of IAM and NEM modification on each cysteine).

It was observed that the overall pattern of the cysteines accessibility for IAM and NEM were comparable and 32 out of 42 cysteines present in hAOX1 were alkylated by both NEM and IAM including the cysteines involved in the FeS clusters binding (**Table 4.13.**). Peptides that contain 7 cysteines, i.e. cysteines 109, 114, 117, 165, 179, 180 and 562 were not detected in any of the

measurements performed on the IAM treated samples. Peptides containing Cys562 were detected in the NEM treated samples, but none of the peptides were modified by NEM. Cys1192 was not found in any of the peptides detected. Overall, 40 out of 42 cysteines present in hAOX1 were accessible by NEM. The average level of modification induced by IAM was about 67 percent which was higher than that of NEM with about 49 percent alkylation. The percentage of NEM against IAM modification was plotted and presented in a correlation graph in which each spot represented one cysteine (**Figure 4.21.**).

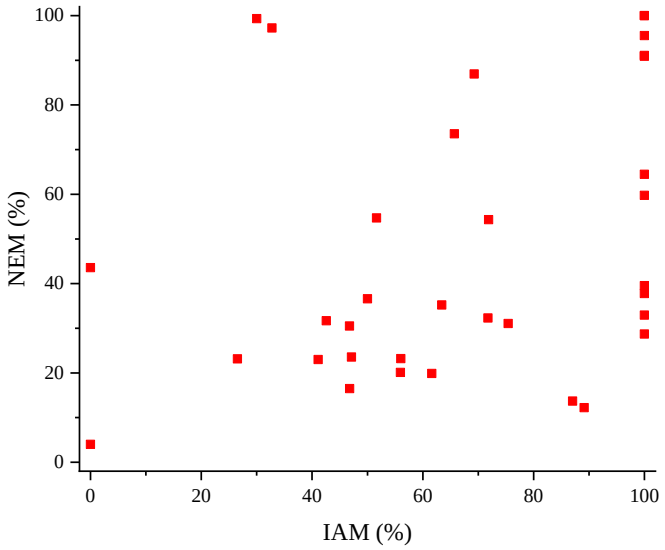

Figure 4.21.: The percentage of NEM against IAM modification: Each spot represents one cysteine and shows the percentage of modification by NEM against IAM (values summarized in **Table 4.13.**). Cysteine 170 located along the NEM axis shows zero percent of IAM and about 40 percent of NEM accessibility. Cysteines 798 and 943 show more than 90 percent NEM modification with only about 40 percent of alkylation by IAM. Cysteines which were not detected in any peptides in the presence of IAM are excluded from the graph.

It was observed that 11 cysteines were accumulated on the IAM 100 percent axis and 2 cysteines showed about 90 percent IAM and less than 15 percent NEM modification. There is only one cysteine, i.e. Cys170, with about 40 percent NEM alkylation that showed no IAM modification. In addition, cysteines 798 and 943 were more than 97 percent reactive towards NEM with about only 30 percent reactivity towards IAM. The higher reactivity of these cysteines with NEM could potentially be linked to the higher loss of activity observed upon treatment with NEM compared with treatment with IAM. Interestingly, the FeS cluster binding sites i.e. Cys44, 49, 52 and 74 bound to FeSII and, to lesser extent, Cys149 and 151 bound to FeSI, were equally accessible by

Table 4.13.: The cysteines reacted with IAM and NEM identified by ESI-MS

Domain	Cysteine / Position	IAM (%)[1, 2]	NEM (%)[1]
FeS Domain	44, FeSII	71.7 ± 39.9	32.3 ± 14.2
	49, FeSII	71.9 ± 39.7	54.3 ± 30.4
	52, FeSII	100	37.8 ± 23.1
	74, FeSII	100	39.5 ± 0.1
	79	100	28.7 ± 4.9
	109	nd[2]	79.7 ± 31.7
	114, FeSI	nd	62.7 ± 51.7
	117, FeSI	nd	86.1 ± 19.6
	149, FeSI	63.4 ± 4.5	35.2 ± 27.9
	151, FeSI	56.0 ± 0.3	23.2 ± 11.2
	161, Linker I	26.5 ± 8.8	23.1 ± 11.1
	165, Linker I	nd	93.1
	170, Linker I	0	43.6
	171, Linker I	0	4.0
	179, Linker I	nd	28.8 ± 33.4
	180, Linker I	nd	4.7
FAD Domain	377	89.1 ± 0.8	12.2 ± 9.3
	400	75.4 ± 34.7	31.1 ± 17.3
	460	46.7 ± 23.9	30.5 ± 9.6
	472	46.8 ± 24.2	16.5 ± 15.2
	477	100	100
	494	51.6 ± 0.4	54.7 ± 35.1
Moco Domain	600	100	64.5 ± 13.0
	654, Substrate Gate I	100	59.7 ± 26.3
	670	69.3 ± 5.0	86.9 ± 0.3
	676	100	90.9 ± 12.9
	798	32.8 ± 12.0	97.2 ± 2.4
	834	65.7 ± 0.1	73.5 ± 39.8
	905	100	100
	910	100	33.0 ± 2.0
	935	61.6 ± 4.4	19.9 ± 16.1
	943	30.0 ± 10.1	99.3 ± 0.9
	976	42.6 ± 0.5	31.7 ± 13.3
	980	55.9 ± 6.6	20.1 ± 9.2
	1103	41.1 ± 5.8	23.0 ± 18.5
	1168	100	91.1 ± 12.6
	1175	100	95.5 ± 6.3
	1242	87.0 ± 18.3	13.7 ± 3.4
	1277	100	36.6 ± 30.1
	1315	47.1 ± 7.1	23.5 ± 13.9

1: The values without standard deviation are result of the identified peptides only found in one sample.

2: Cysteines which were not detected in any peptides are marked as nd.

both NEM and IAM and it seemed that the effect of NEM on FeS clusters was not the reason for the inactivation of the enzyme. However, complementary experiments were performed to further investigate the possibility of the FeS clusters being disturbed in the presence of a reactive sulfhydryl group.

4.4.3.2. Sulfur Ligands Bound to Iron-Sulfur Clusters

The sulfur ligands bound to the FeS clusters are potentially possible sites for the act of DTT and small sulfhydryl containing agents. The NEM vs IAM mapped peptides showed that the eight cysteine residues bound to the FeS clusters were alkylated, and suggested that FeS clusters might potentially be disturbed upon treatment with DTT. The possible effect of DTT on the FeS clusters were studied by circular dichroism (CD), a method that has been successfully applied to distinguish the two FeS clusters in *Rc* XDH (Schumann, et al. 2008). The CD traces of about 5 µM hAOX1 treated and untreated with DTT were recorded in the near UV region from 300 to 600 nm to follow any changes in the FeSI and FeSII with maximum CD signal at 475 nm and 430 nm, respectively (see **Figure 4.22., A** and **Table 4.14.**). Each trace was the average of three accumulations. The buffer (Tris 50 mM, NaCl 200 mM, 1 mM EDTA, pH 8.0) signal was subtracted and the ellipticity over the range of 300 to 600 nm was normalized to the protein concentration based on the absorption of the FAD cofactor at 450 nm. It was observed that the CD signal for FeSI at 475 nm was 33580 and 41662, and for FeSII at 430 nm was 50847 and 65593, respectively, for the enzyme untreated and treated with DTT. The maximum peak ratios for FeSI to FeSII in the absence and presence of DTT were 0.66 and 0.63, respectively, which were not significantly different. This suggested that the iron-sulfur clusters were not the site of DTT inactivation of the enzyme.

In addition to the FeS clusters, the CD trace over the range of 300 to 600 nm exhibited the peaks related to the FAD signals (Kelly and Price 2000) with a positive peak at 342 nm and a negative peak at 377 nm and peaks corresponding to the pterin ligand of Moco in the region between 550 to 580 nm (Ryan, et al. 1995) (see **Figure 4.22., A** and **Table 4.14.** for the values). In the CD trace the sample treated with DTT (red curves in **Figure 4.22.**) showed a slightly higher signal than the sample untreated with DTT (black curve in **Figure 4.22**.), likely due to a slightly higher concentration. Interestingly, while the red curve stayed at about 1.2 to 1.5 times higher values in the region from 300 to 500 nm, the trace got divergent in the region corresponding to the Moco signal at about 500 to 600 nm. The CD trace in the presence of DTT (red curves in **Figure 4.22.**) in the range from 500 to 600 nm did not change to the positive values, but the peak at 580 nm for the

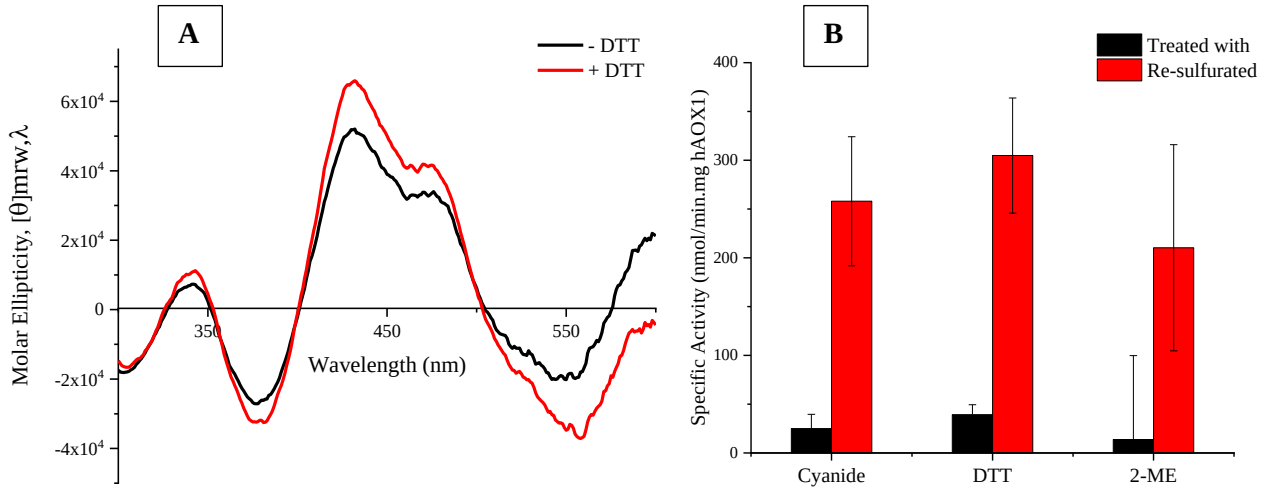

Figure 4.22.: Potential influence of DTT on FeS clusters and Moco in hAOX1. A: Near UV CD of hAOX1 of about 5 µM native and DTT treated samples in the range of 300 to 600 nm in 50 mM Tris, 200 mM NaCl, 1 mM EDTA, pH 8.0: FeS clusters show two distinct peaks at around 475 and 430 nm, respectively, for FeSI and FeSII clusters. The ratio of 475 to 430 nm peaks does not show a significant change in the DTT treated protein. **B:** Re-sulfuration of about 10 µM protein samples treated with 1 mM cyanide, DTT or 2-ME was performed under anaerobic condition (98% N_2, 2% H_2) using 500 µM of sodium dithionite, 2 mM sodium sulfide and 25 µM methylviologen in the sulfuration buffer (50 mM KH_2PO_4, 0.1 mM EDTA, pH 7.4) recovers the activity up to 30 percent of the initial activity. Note that the initial activity was about 1300 nmol/min.mg as shown in **Figure 4.20.**, control bar.

Table 4.14.: The CD signal peaks of hAOX1 cofactor in the samples treated and untreated with DTT

Cofactor	Wavelength (nm)	CD signal (molar ellipticity) - DTT	CD signal (molar ellipticity) +DTT	Ratio (-DTT/+DTT)
FeSI	475	33580	41662	1.2
FeSII	430	50847	65593	1.3
FAD	342	7334	10968	1.5
	377	-27120	-32405	1.2
Moco	555 [1]	-19849	-37108	1.9
	580	7132	-13412	1.9

enzyme in the absence of DTT (black curve in **Figure 4.22**.) exhibited positive values. Similarly, the ratio of the peak CD signals related to the FeS clusters and FAD were about 1.2 to 1.5 higher in the sample treated with DTT than the untreated sample, while the ratio for the Moco related peaks showed 1.9 times higher signals in the hAOX1 treated with DTT than the untreated enzyme. It seems that while the iron-sulfur clusters were not affected, Moco might get disturbed upon treatment with DTT.

4.4.3.3. Sulfido Ligand Coordinated at Moco

The last site of hAOX1 that can potentially be vulnerable to the presence of a reactive sulfhydryl is the sulfido ligand coordinated to molybdenum. This ligand is usually not efficiently inserted during the heterologous expression and should be constructed via a chemical sulfuration step (Foti, et al. 2016). If the sulfhydryl group of DTT removes this ligand, then re-sulfuration should at least partially recover the activity. The samples treated with DTT, 2-ME and cyanide, a suicide inhibitor known to act by removing the sulfido ligand from Moco (Massey and Edmondson 1970) were subjected to the reconstitution of the sulfido ligand in the presence of 500 µM sodium dithionite, 20 mM sodium sulfide and 25 µM methylviologen in the sulfuration buffer (50 mM KH_2PO_4, 0.1 mM EDTA, pH 7.4) under anaerobic conditions (98 percent N_2, 2 percent H_2) at room temperature. The re-sulfurated samples showed regain of the activity up to about 20 to 30 percent for 2-ME, and DTT, respectively, which was comparable to that of the cyanide treated sample (**Figure 4.22.,** panel **B**). This suggests that the Moco site and the sulfido ligand coordinated to Mo center is likely the site of the DTT inactivation.

4.4.4. The effect of DTT on Other Members of the Xanthine Oxidase (XO) Family

To investigate whether DTT has a common effect on other aldehyde oxidases, the specific activity of the four mouse aldehyde oxidase isoenzymes (mAOX1, mAOX2, mAOX3 and mAOX4) and *E. coli* aldehyde oxidase PaoABC were measured and compared with *R. capsulatus* xanthine dehydrogenase (*Rc* XDH) and bovine xanthine oxidase (bXO) (see **Table A3** and **Figure A3** in the Appendix of this thesis for the details of these enzymes). The samples were treated with 100x molar ratio of DTT to enzyme to ensure that all possible sites in the enzyme including solvent accessible cysteines have been exposed to DTT. DTT was subsequently removed and specific activities were measured using 40 µM phenanthridine for mAOX1, mAOX2, mAOX3 and mAOX4, 500 µM benzaldehyde for PaoABC, 1 mM xanthine for bXO and 1 mM xanthine and 1 mM NAD^+ for *Rc* XDH. Oxygen was the electron acceptor provided by air-saturated buffer (50 mM Tris, 200 mM NaCl, 1mM EDTA, pH 8.0) except for *Rc* XDH where NAD^+ was used as the second substrate. In alternative measurements, 100 µM 2,6-dichlorophenol-indophenol (DCPIP) was used as electron acceptor to follow the enzyme reaction for hAOX1, mAOX1, mAOX2, mAOX3 and mAOX4. The loss of activity was observed for hAOX1, mAOX1, mAOX2, mAOX3, but only a slight decrease was distinguishable for mAOX4 (**Figure 4.23.,** panel **A**). *E. coli* PaoABC and bXO did not present a significant negative effect of DTT on their activities, while *Rc* XDH showed slightly improved activity in the presence of DTT consistent with former studies (Leimkuhler, et al. 2003) (**Figure**

4.23., panel **B**). In the presence of DCPIP as electron acceptor the specific activity was lowered about 10 times for mAOX1, 5 times for hAOX1 and mAOX2, and 2 times for mAOX3 compared to when the physiological electron acceptor oxygen was used, a behaviour which was reported previously for hAOX1 (Foti, et al. 2016). However, a pattern of loss of activity when these samples were pre-incubated with DTT was consistently observed, i.e. hAOX1, mAOX1, mAOX2 and mAOX3 showed a significant loss of activity, while mAOX4 was not affected.

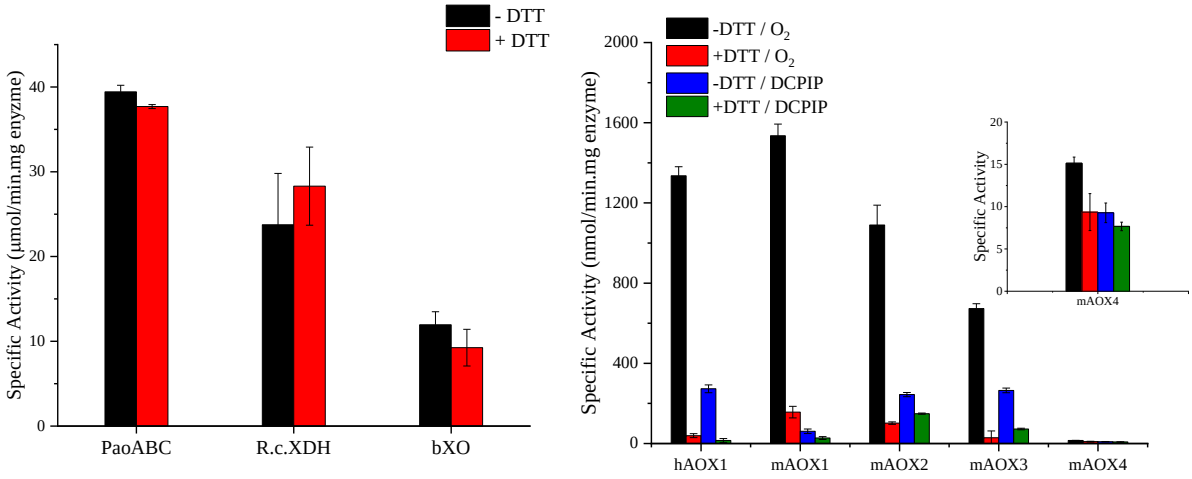

Figure 4.23.: The effect of DTT on hAOX1 in comparison with other members of the XO family: A: Specific activity of *E. coli* aldehyde oxidase PaoABC, bovine xanthine oxidase (bXO) and *R. capsulatus* xanthine dehydrogenase (*Rc* XDH) for the samples pre-incubated with 100x molar ratio of DTT to enzyme did not show a loss of activity. 500 µM benzaldehyde, 1 mM xanthine and 1 mM NAD^+ were used to measure the activities of *E. coli* PaoABC, bXO and *Rc* XDH, respectively, by following the reaction at 295, 295 and 340 nm, respectively. **B:** Specific activity of hAOX1 and four mouse isoenzymes, native condition compared with incubated samples with 100x molar ratio of DTT to enzyme using two different electron acceptors: Specific activities were measured in the activity buffer (50 mM TrisHCl, 200 mM NaCl, 1 mM EDTA, pH 8.0) using 40 µM of phenanthridine and molecular oxygen in air-saturated buffer (black and red bars) and 100 µM DCPIP (blue and green bars) as electron acceptors. **Inset:** Zoom-out mAOX4 specific activity for better visualization. DTT treated hAOX1, mAOX1, mAOX2 and mAOX3 show loss of activity to about 90-99 percent of their initial activities. mAOX4 shows only a slight loss of activity upon treatment with DTT.

5. Discussion

5.1. Mysteries of a Flexible Region Containing Conserved Cysteines

5.1.1. A flexible Region Locating at the FeS Domain Carries Conserved Cysteines in Higher Organisms

In the primary structure of most XO family enzymes in higher eukaryotes a flexible region consisting of 40-70 amino acid residues has evolved at the C-terminus of the FeS domain which carries 4 to 6 highly conserved cysteines (see **Figure 4.1**. in section 4.1.1.). The conserved cysteines are organized in a $C(X)_3C$ motif exclusively found in AOXs and in a $CC(X)_{7-8}CC$ motif present in both AOXs and XDHs. The motifs do not exist in the prokaryotic and plant AOXs or XDHs sequenced so far. The region, particularly in vicinity of the cysteines, is poorly visualized in the X-ray crystal structures available due to its high flexibility. The amino acid composition includes glycine, serine, lysine, glutamate and glutamine (see **Figure 4.1**.) which are the residues found in intrinsically disordered proteins (IDP) that confer flexibility and consequent accessibility and adaptability to the region (Uversky 2013).

Cysteines are potentially reactive amino acid residues. Their high reactivity arises due to the relatively low dissociation energy of the S-H bond of the thiol side chain (Pace and Weerapana 2013). Depending on the microenvironment, the pK_a of cysteines thiol side chain vary significantly from about 10 or 11 in the active site of protein disulfide isomerase (PDI) (Karala, et al. 2010) to as low as 2.5 in the catalytic sites of proteases. Due to the high reactivity, cysteines together with isoleucines, valines and alanines are among the least exposed residues and together with tryptophans are among the least abundant residues in proteins (Miseta and Csutora 2000; Pe'er, et al. 2004). The cysteine content increases with increasing the complexity of organisms. The average cysteine content in *E. coli* is about 1.1 percent, while it increases to as high as 2.3 percent in mammals. The trend of gain and loss of amino acids throughout the evolution shows that cysteines are either highly conserved or completely degenerated (Jordan, et al. 2005; Marino and Gladyshev 2010). Furthermore, the conservation of cysteines clustered in motifs, e.g. CXXC motifs of thioredoxins, is more probable than isolated residues. Cysteine motifs also appear more on the surface to get involve in functional roles which is required in more complex organisms.

Cysteines adopt diverse roles in proteins. Depending on the protein microenvironment cysteines may stabilize protein structure by forming disulfide bonds (mainly in secreted proteins), provide metal binding sites, function as nucleophiles or redox-active sites, or serve as regulatory switches

(Pace and Weerapana 2013). The $C(X)_3C$ and $CC(X)_{7-8}CC$ motifs in AOXs and XDHs contain clustered and conserved cysteines that have appeared in higher eukaryotes and locate on an intrinsically disordered region with high flexibility. The conservation, clusterization, and at least partial surface exposure of these cysteines suggest that they might be involved in playing a role shared within the family.

No potential roles for these cysteines have been mentioned in the literature to date. In all of the X-ray structures available for eukaryotic XOs and AOXs the $CC(X)_{7-8}CC$ motif is missing, probably due to the high flexibility and consequent low electron density of the region. This flexibility together with the sublocalization of the eukaryotic AOXs and XOs in the reducing environment of cytoplasm suggests that the cysteines are unlikely to form structural disulfide bonds. However, they may still provide an interacting interface via mixed disulfides, they may bind to metal ions to stabilize the structure or they may play role in the regulation of the enzyme activity in an oxidative / reductive manner.

5.1.2. Altering the Composition of the Flexible Region Does Not Significantly Affect the Kinetic Parameters

The cysteines in the $C(X)_3C$ and $CC(X)_7CC$ motifs of hAOX1 were exchanged to alanines and the enzyme expression, cofactor load and kinetic parameters were compared to those of WT (see section 4.1.2.). A variant with all the 6 cysteines in the motifs exchanged with aspartates, abbreviated as 6D, was also produced to mimic the effects of potentially oxidized cysteines ($-SO_2^-$ and $-SO_3^-$ species) on the enzyme. Three natural variants have been reported as result of single nucleotide polymorphisms (SNP) in the region (Sherry, et al. 2001). The natural variants, N176Y, G177E and V178F, locate on the IDP region adjacent to the second pair of the vicinal cysteines in the ^{170}**CC**QSKENGV**CC**^{180} motif. These variants may differ from WT due to a potentially altered charge or flexibility of the motif. In addition, the entire region, i.e. K162-V235 in hAOX1 was exchanged with the counterpart region in *Rc* XDH (E147-G172), which is only 26 amino acid long and does not contain any of the cysteines, in *D. melanogaster* AOX1 (dAOX1) (K161-Q206) which is 46 amino acids long and contains only 2 single cysteines, and in *G. gallus* XDH (gXDH) (R164-C254) which carries 4 pairs of vicinal cysteines on an extended (89 amino acid-long) region.

The cysteine and natural variants were expressed similar to the WT enzyme, suggesting that their folding was not impaired with these alterations in this flexible region. The chimeric enzymes were expressed in significantly lower amounts with slightly higher A_{280}/A_{450} ratio implying less efficient

production of the fully active enzyme. The UV-Vis absorption and iron saturation of the obtained enzymes were similar to those of WT, but the molybdenum saturation was exceptionally high (more than 100 percent) in the variants where 2 cysteines or more were replaced. The examination of Moco content of selected variants, i.e. 6A, 6D and 3A in comparison with WT, showed slightly increased amount of Moco, a pattern consistent with the slightly higher iron saturation of these variants. This suggests that alterations around the vicinal cysteine pairs might have affected the region characteristics in a way that have resulted in unspecific binding of molybdenum.

The steady state kinetic parameters of the variants showed slightly less catalytic efficiency in comparison with WT, except for the natural variant G177E that behaved similarly to WT. The lowered catalytic efficiency, accompanied by decreased k_{cat} and/or increased K_m, was more remarkable for 6D, 4A, 3A, 2A-2 and hAOX1-dAOX1-chimera. The cysteines on $C(X)_3C$ and $CC(X)_7CC$ motifs are not directly part of the two active sites of the enzymes, however, they locate on a highly flexible region that may confer them accessibility to the proximity of the active sites which in return, affects the kinetic parameters. Interestingly, changing the first pair of the vicinal cysteines in the $CC(X)_7CC$ motif, as in 2A-1 variant, did not affect the molybdenum content and only slightly lowered the catalytic efficiency. This may imply that Cys170 and Cys171 are not as equivalently important as Cys179 and Cys180. Altogether, the differences observed in the steady state kinetic parameters and cofactor loads between the cysteine variants and the WT enzyme cannot be explained through direct effects on any of the active sites or cofactors involved in the catalytic cycle. These differences also do not suggest a potential role for the cysteines in the flexible region.

5.1.3. Cysteines in the Flexible Region Are Unlikely to Play Structural Roles

hAOX1 localizes in the reducing environment of the cytoplasm where the formation of structural disulfides is not favoured. The cysteines in the $C(X)_3C$ and $CC(X)_7CC$ motifs, however, can provide sites for binding metals that may structurally stabilize the enzyme. A [4Fe-4S] cluster that is thought to play a role in stabilizing the structure has been identified to bind a $C(X)_9C(X)_8C(X)_{18}C$ motif in the B subdomain of *E.coli* aldehyde oxidase, PaoABC (Otrelo-Cardoso, et al. 2014) and in aldehyde oxidase from methylobacillus sp. KY4400 (Uchida, et al. 2018). In addition, in methanogenic archaea heterodisulfide reductase (HdrABC-MvhAGD) two noncubane [4Fe-4S] clusters bind a duplicated CCG motif on a $C(X)_{31-39}CC(X)_{35-36}CXXC$ sequence that contributes in the catalytic reaction (Wagner, et al. 2017). Bacterial aldehyde oxidases are evolutionary divergent enzymes with distinct domain architecture (Garattini, et al. 2003), however,

the possibility of loss of a potentially structural stabilizing FeS cluster or metal ion was considered for hAOX1. hAOX1-WT and selected cysteine variants were examined for the iron content when they were in parallel aerobically and anaerobically produced (see **Table 4.4.** in section 4.1.3.). The amount of iron measured in the presence or absence of oxygen and in the WT or the variants did not differ. WT and 3A were in addition tested for their zinc content since zinc is the most abundant metal ion bound to cysteines (Pace and Weerapana 2014). Again, no zinc was found in the WT or the variant. Furthermore, WT and the cysteine variants 6A, 6D, 3A and 2A-1 were taken forward for native crystallization, co-crystallization and soaking experiments with various metal ions including iron, zinc and arsenite. This was to investigate whether binding of a metal ion which is lost during the purification would stabilize the flexible loop and would result in a more structured region around the cysteines. However, the outcome of none of these experiments alluded to the involvement of cysteines in the $C(X)_3C$ and $CC(X)_7CC$ motifs in metal binding.

5.1.4. Cysteines in the Flexible Region Do Not Affect the Thermal Stability

The cysteines in the $C(X)_3C$ and $CC(X)_7CC$ motifs are part of the linker I that connects the FeS and FAD domains (Coelho, et al. 2015), therefore, the thermal stability of the enzyme may be affected if the cysteines are involved in stabilizing the local structure of the FeS or FAD domains. The thermoFAD analyses (see section 4.1.4., **Figure 4.6.** and **Table 4.5.**) showed that when the cysteines were replaced with aspartates in the 6D variant, the unfolding transition melting temperatures (T_m) decreased about 8 ^oC below the T_m obtained for WT. This effect seemed to be due to introducing 6 negatively charged amino acid residues to the region that might have affected the local structure, specifically around C161 which is part of a short α-helix. In the hAOX1-dAOX1-chimeric variant the destabilizing effect was more enhanced and changed the pattern of the unfolding where only one transition occurred. The flexible region in dAOX1 is 46 amino acid-long which is 28 residues shorter than the original region in hAOX1. Introducing a shorter region could have interfered with the native flexibility of the FeS and FAD domains and disrupted the maintenance of the structure in higher temperatures. The thermal stability of the natural variants and other cysteine, in which 1 to 6 cysteines were replaced with alanines, did not significantly differ from that of WT. The hAOX1-gXDH chimeric variant with a 15 amino-acid-longer flexible region was thermally similarly stable as WT, implying that the flexibility of the region was not disturbed.

5.1.5. Cysteines Seem to be Involved in the ROS Response

In each catalytic cycle hAOX1 reduces oxygen to produce reactive oxygen species (ROS) including hydrogen peroxide (H_2O_2) and superoxide ($O_2^{-\cdot}$). ROS can cause oxidative damage by oxidizing nucleic acids, lipids and proteins (Davies 2016), but, ROS can also play role as cellular messengers and trigger signaling cascades (Forman, et al. 2017). The central feature of the redox-dependent signaling is the reversible oxidation of specific cysteines which can be part of the active site or locate on other positions of the protein. For instance, in PTP1B, a member of the protein tyrosine phosphatase super family, a cysteine residue present in the active site is reversibly oxidized. In Src family of tyrosine protein kinases oxidation of a cysteine which is not part of the active site inactivates the enzyme. Despite the involvement of ROS in cell signalling, when ROS are pathologically or physiologically produced, protective mechanisms are required to ensure minimizing their potential damage. The ubiquitous and best known ROS protecting mechanisms are provided by the enzymatic action of superoxide dismutase (SOD), converting superoxide ($O_2^{-\cdot}$) to hydrogen peroxide (H_2O_2) (Klug, et al. 1972), and catalase (cat), transforming hydrogen peroxide (H_2O_2) to water (Claiborne and Fridovich 1979). In addition to global ROS protecting mechanisms, it has been shown that the enzymes that generate ROS or other reactive oxidizing species such as iron-oxo species as part of their catalytic cycle are equipped with internal protecting mechanisms. Among the best studied of such enzymes are cytochromes P450 (Gray and Winkler 2018). In cytochromes P450 a chain of tyrosine and tryptophan residues are extended from the active site heme to the surface of the enzyme providing a route for hole (electron deficient center) tunnelling to the outside of the bulk of the enzyme. Due to their high potential redox activities cysteines together with tyrosines, tryptophans and possibly methionines can contribute to such protecting mechanisms. Both redox signaling and protective mechanisms require careful regulation, e.g. a feedback relay which is triggered to adjust the enzyme activity and eventually decrease the production of damaging ROS species.

hAOX1 as a ROS generating enzyme that carries two motifs of conserved cysteines seems to be a suitable candidate for studying these roles.

5.1.6. At Least One Cysteine in the Flexible Region Protects the Enzyme During Turnover

The inactivation of hAOX1 was studied in an elongated enzyme reaction. The progress curve (i.e. the plot of absorbance against time) over 1800 seconds and in the presence of 160 µM (about 5 K_m) phenanthridine and 170 nM of the enzyme showed a declining trend after an initial linear and faster

phase (see section 4.1.5. and **Figure 4.7.**, panel **A**). The declining behaviour could occur due to multiple reasons including **a)** substrate depletion, **b)** product inhibition or **c)** enzyme inactivation. The initial linear phase of the enzyme reaction started to decline after about 200-300 seconds when about 50 µM of the substrate was consumed. This leaves 110 µM of phenanthridine still available in the solution, meaning that the depletion of the reducing substrate did not occur. Given the oxygen saturation in the aqueous solutions is about 200 µM (Clegg and Brimblecombe 1990; Lange, et al. 1972) and the reaction stoichiometry is 1 to 1, the depletion of the oxidizing substrate did not seem to occur either. To further confirm that substrate depletion was not the reason for the declining behaviour of the progress curve, another 160 µM of phenanthridine was added to the same reaction mix (see section 4.1.5. and **Figure 4.7.** panel **B**). If the substrate depletion was the reason for the behaviour, an increase in the rate of change of absorbance would be expected in the second reaction, while a similar near plateau behaviour was observed. Consequently, a new batch of 170 nM of enzyme was added to the same reaction mix and a nearly identical progress curve as in the first reaction was recorded. Since in the first reaction 50 µM of phenanthridine was produced, a similar amount of phenanthridinone, the oxidized product of phenanthridine, was present when the third reaction was progressing. This implied that the declining behaviour was not due to the product inhibition either.

The first derivative of the absorbance versus time shows the change in the activity of the enzyme over 1800 seconds (see section 4.1.5. and **Figure 4.7.** panel **C**). An exponential decay fit to this plot gives the half-life of enzyme. The number of turnovers until half of the enzyme was inactivated, i.e. $Turnover * t_{1/2}$, was obtained as an index to compare the half-lives of the enzymes with different turnover numbers.

Since the motifs containing the conserved cysteines could act as potential ROS responding elements, the inactivation of 6A, the variant in which all the 6 cysteines are replaced with alanines, was compared to that of WT. If the presence of the cysteines in the flexible region is to switch off the activity of the enzyme, we would expect to observe higher number of turnovers during the half-life of enzyme for 6A than for WT. On the other hand, if the difference between the number of turnovers during the half-life for WT and 6A was not significant, we would conclude that the cysteines have no effect on the half-life of the enzyme while in turnover. The number of turnovers that WT was able to perform by the time it reached to its 58 seconds half-life was 310, while 6A performed only 105 turnovers during its 65 seconds half-life. This implies that when the cysteine residues are absent, the enzyme is more vulnerable during the turnover, and hence, it seems that at

least one cysteine in the region protect the enzyme from a damage that occurs during the catalytic cycle.

5.1.7. Glutathione and ROS Scavengers Do Not Prevent the Inactivation of hAOX1 while Exogenous ROS Accelerate the Inactivation

Since the cysteines appear to exert a protecting role to hAOX1 during its turnover, it might possible that the addition of a reducing agent play a similar role. Glutathione is the most abundant physiological redox buffer maintaining the reducing environment of cytoplasm through an equilibrium between its reduced (GSH) and oxidized (GSSG) forms (Hwang, et al. 1992). However, the addition of 10 mM glutathione to the reaction of hAOX1 with phenanthridine did not recover the activity of WT or 6A (see **Figure 4.8.** in section 4.1.5.2.). This means that the role of cysteines cannot be replaced by external thiol containing reducing agents.

The addition of the classical ROS scavengers, i.e. catalase (cat) that converts H_2O_2 to H_2O and superoxide dismutase (SOD) that catalyses the conversion of superoxide ($O_2^{-\cdot}$) to H_2O_2, did not delay the inactivation of hAOX1-WT or 6A during the turnover. A similar non-linear activity behaviour with several substrates, which was not recovered upon addition of ROS scavengers (cat and SOD), has been reported for hAOX1 before (Abbasi, et al. 2019). To explain the non-linearity of hAOX1 reaction Abbasi and colleagues suggest that the electron transfer to oxygen is rate limiting and hence, there is an accumulation of the partially reduced form of the enzyme which is unable to initiate another catalytic cycle. This model implies that the declining activity of hAOX1 could be recovered if the rate of electron production at Moco is close to the rate of electron transfer to oxygen. In the first glance it seems that the loss activity of the enzyme over time is not due to the endogenous ROS production. However, other studies have proposed that the inactivation of bovine milk XO (Lynch and Fridovich 1979) and chicken liver XDH (Betcher-Lange, et al. 1979) is irreversible and facilitated by the production of ROS during turnover. The inability of the ROS scavengers cat and SOD in recovering or delaying hAOX1 inactivation can be due to a local effect of the endogenous ROS. This means that endogenous ROS locally damages the enzyme at sites where the large ROS scavenger enzymes cannot access. Moreover, it is possible that in a secondary reaction other types of ROS such as hydroxyl radicals are produced which cannot be detoxified by catalase or superoxide dismutase. The production of hydroxyl radicals has been shown during the inactivation of xanthine oxidase (Terada, et al. 1991), an effect which is kinetically controlled by the rate of ROS production at the FAD site. It is also possible that the rate of inactivation of hAOX1 is higher than the rate of scavenging the generated ROS by the cat/SOD system. This implies that in

the reaction of hAOX1 with slow substrates, in which the rate of ROS production is slow, the ROS scavenging system might be able to delay the inactivation. This trend has been observed in the comparison of a range of substrates oxidized by hAOX1 (Garrido and Leimkeuhler, manuscript under publication). It was reported that the addition of catalase delayed the loss of activity over time for zoniporide and benzaldehyde as slow substrates, while the inactivation of hAOX1 was not prevented when phthalazine as fast substrate was used.

The potential effect of ROS on inactivation of hAOX1 was further investigated in samples of hAOX1-WT and 6A treated with H_2O_2 where H_2O_2 was removed prior to the enzyme reaction. The number of turnovers that H_2O_2 treated WT was able to perform was significantly decreased to about 60 percent of its native condition, suggesting that ROS has a damaging effect on the enzyme (see **Figure 4.8.** in section 4.1.5.3.). Interestingly, the 6A H_2O_2 treated sample did not show a difference in the numbers of turnover during its half-life in comparison with its native sample. This implies that, when pre-incubated with H_2O_2, WT gets damaged and loses its inner protective mechanism, while in 6A where the protective cysteines have been already removed, the exogenous ROS cannot induce damages beyond the damage that the endogenously produced ROS did.

The comparison of the inactivation of WT with the hAOX1-L438V variant, in which the entire flexible region containing cysteines is intact, shows that the L438V variant is more vulnerable during turnover than WT (see section 4.1.5.4., **Table 4.6.** and **Figure 4.10.**). Unlike WT, hAOX1-L438V predominantly produces superoxide over hydrogen peroxide. These results suggest that the production of different type of ROS affects the inactivation behaviour of the enzyme.

5.1.8. The Flexible Region Carrying Conserved Cysteine Has Specifically Evolved for the Protective Role

The comparison of the inactivation of WT and 6A, a variant in which the 6 cysteines present in the $C(X)_3C$ and $CC(X)_7CC$ motifs on a flexible loop are replaced with alanines, suggested that at least one cysteine in the region is involved in protecting the enzyme during turnover. In a similar procedure, the numbers of turnover during the half-life of the enzyme was obtained for the variants with altered composition of the flexible region, either in the cysteine motifs, i.e. the cysteine variants, or in the residues around the cysteines, i.e. the natural variants, or in the entire region, i.e. the chimeric variants (see **Table 4.6.** and **Figure 4.10.** in section 4.1.5.4.).

The inactivation of the cysteine variants show that the single cysteines in the $C(X)_3C$ motif, i.e. Cys161 and Cys165, and the second pair of the vicinal cysteines in the $CC(X)_7CC$ motif, i.e.

Cys179 and Cys180, are the crucial cysteines for the protection of hAOX1 during its turnover. Cys170 and Cys171, i.e. the first pair of the vicinal cysteines in the $CC(X)_7CC$ motif, seem to have no effect for the protection of hAOX1. However, it is possible that Cys170 and Cys171 are involved in interacting with the machinery that enzymatically removes the oxidative modification that is introduced to Cys161, 165, 179 and 180 (see below and **Figure 5.1.** for the model). Given that the exchange of cysteines with alanines did not affect the global thermostability of the enzyme (see **Figure 4.6.** and **Table 4.5.** in section 4.1.4.), it seems that the difference observed in the inactivation is solely related to the lower capacity of the cysteine variants to cope with the ROS produced during turnover. The exchange of cysteines with aspartates influenced the global stability of the enzyme by introducing 6 negatively charged residues in the flexible region, and therefore, the significantly lower numbers of the turnover during the half-life of 6D is the result of combined effects of the lower global stability and the long-term ROS damage.

Among the natural variants, the inactivation of G177E was similar to that of WT, while N176Y and V178F showed decreased numbers of turnover during their half-lives. The region around $CC(X)_7CC$ motif, i.e. ^{170}**CC**QSKENGV**CC**^{180}, where single nucleotide polymorphisms (SNPs) resulted in the occurrence of the natural variants N176Y, G177E and V178F, is composed of residues often forming intrinsically disordered proteins (IDPs). IDP regions are found in sites where flexibility or adaptability is required for maintaining the structure or function of the protein (Uversky 2013). In N176Y or V178F there is an amino acid exchange to more bulky and aromatic residues. It seems that tyrosine and phenylalanine in comparison with asparagine and valine may hinder the accessibility of ROS to Cys179 and Cys180, the two cysteines which play the protecting role during the enzyme turnover. N176Y and V178F show about 175 turnovers per second during their half-lives, which is similar to the number of turnovers during the half-life that the variants with Cys179 and Cys180 exchanged with alanines, i.e. 2A-2, 3A and 4A, are able to perform.

The importance of the exact composition of the flexible region is further reflected in the inactivation of the chimeric variants. In the hAOX1-dAOX1-chimeric variant the region is 28 amino-acid-residue shorter and less negatively charged with only 2 single cysteines in a $C(X)_{10}C$ motif. The hAOX1-dAOX1-chimeric variant presented significantly impaired thermostability (see **Figure 4.6.** and **Table 4.5.** in section 4.1.4.). This suggests that the lowered number of turnovers during its half-life compared to WT is the result of decreased structural stability, possibly combined with the damage induced during the turnover. The hAOX1-gXDH- chimeric variant, on the other hand, seem to be similarly stable as WT, and hence, the decreased performance during its half-life is due to the altered flexible region carrying the protective cysteines. The flexible region in this

variant is 15 amino-acid longer than its counterpart in hAOX1, the $C(X)_3C$ motif is not present and the region carries 4 pairs of vicinal cysteines locating on a sequence with an overall amino acid composition suggesting an IDP region. The region seems to confer a similar stability as observed for WT, but the amino acid composition around the protecting cysteines differ and the $C(X)_3C$ is completely missing. This suggests that the net increase in the number of the vicinal cysteine pairs does not necessarily improve the protection and the exact amino acid composition including both $C(X)_3C$ and $CC(X)_7CC$ motifs are required for the protection during turnover in hAOX1.

Our results suggest that Cys161, 165, 179 and 180 are involved in protecting hAOX1 from the damaging effects of ROS and this protection seems to rely on the reactivity of the cysteine thiol side chains towards ROS (see **Figure 5.1.** for the possible reactions that a cysteine thiol can undergo). In the presence of ROS, short-range disulfide bonds with the adjacent cysteines could be formed. ROS could also reversibly oxidize thiols to sulfenic acids (-SOH) or irreversibly further oxidize them to sulfinic ($-SO_2H$) and sulfonic ($-SO_3H$) acids. Such oxidation processes internally scavenge ROS and delay the damage that they may cause in the enzyme. Formation of short-range intramolecular disulfides, mixed (intermolecular) disulfides or sulfenic acids can be tracked by mass spectroscopic methods specifically designed to detect such species (Alcock, et al. 2018). An initial attempt was made to detect the overoxidation products of Cys-SOH, i.e. Cys-SO_2H and Cys-SO_3H by ESI-MS, but the amount of these species was not significant (data not shown). It seems that the inactivation of hAOX1 occurs prior to the overoxidation of the cysteines in the $C(X)_3C$ and $CC(X)_7CC$ motifs, in case the protecting state of the cysteines were sulfenic acids.

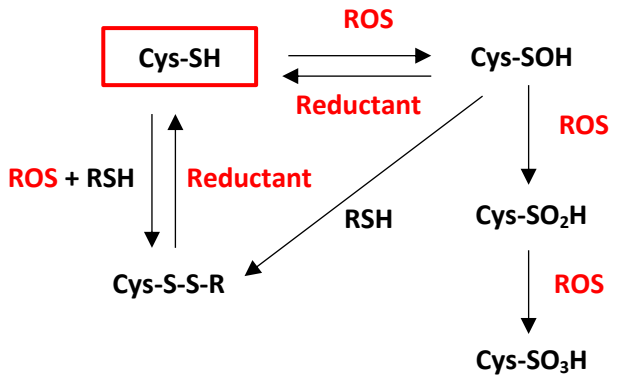

Figure 5.1.: Reactions of thiol side chains of cysteines: A susceptible thiol side chain can reversibly get oxidized in the presence of ROS to sulfenic acid and irreversibly further oxidized to sulfinic and sulfonic acids. The thiol side chain can also reversibly form an intramolecular disulfide or mixed disulfide when another thiol containing species is available.

Disulfide formation and sulfenic acid oxidation of cysteines are reversible processes. The thiol state of cysteines can be physiologically recovered by the GSH/GSSG redox system coupled with

thioredoxins (Trx), glutaredoxins (Grx) or other enzymatic machineries (Berndt, et al. 2007; Claiborne, et al. 1999). It is possible that Cys170 and Cys171 are involved in interacting with the machinery that enzymatically removes the oxidative modification that is introduced to Cys161, 165, 179 and 180 such that they have *in vivo* importance not seen in our *in vitro* assays.

Overall, it seems that the cysteines in the $C(X)_3C$ and $CC(X)_7CC$ motifs in hAOX1 provide an internal ROS protecting system for the enzyme during its turnover. In addition, due to the necessity of removal of the oxidation modifications, they also may provide an interacting interface for the enzymatic machinery regenerating the thiol states of the cysteines. However, the mechanism through which the cysteines in the $C(X)_3C$ and $CC(X)_7CC$ motifs protect hAOX1 during turnover requires further investigation. Furthermore, since the $C(X)_3C$ and $CC(X)_{7-8}CC$ motifs are conserved in the other members of the XO family, a similar approach to study their inactivation may give insight to the generic protecting role of the cysteines in the region.

5.2. The Nature of the Damage to hAOX1 During the Course of Reaction

5.2.1. Loss of the Sulfido Ligand is the Major Damage to hAOX1 During Turnover

The auto-inactivation of XO has been investigated in several studies (Betcher-Lange, et al. 1979; Lynch and Fridovich 1979; Terada, et al. 1991). It has been proposed that the formation of the de-sulfo form of the enzyme during the course of the reaction is the cause of the loss of activity. Our results showed that when hAOX1 was incubated with the substrate phenanthridine, the activity was lost (see **Figure 4.11.** and **Table 4.7.** in section 4.2.1.), and that the re-constitution of the sulfido ligand recovered about 50 percent of the activity. This suggests that the damage during turnover is at least partially due to the loss of the sulfido ligand at Moco. If the production of ROS is involved in the loss of activity, it is expected that exogenous hydrogen peroxide (H_2O_2) would similarly affect the enzyme. Interestingly, incubation of hAOX1 with exogenous H_2O_2 under aerobic condition only slightly decreased the activity, while, H_2O_2 treatment under anaerobic condition resulted in the total loss of activity similar to the behaviour observed for phenanthridine. The chemical reconstitution of the sulfido ligand in the sample treated with H_2O_2 under anaerobic condition resulted in the regain of the activity to about 30 percent of its initial activity.

The anaerobic condition used (98% N_2, 2% H_2) provides a reducing environment. This means that the re-oxidation of the enzyme does not occur and hence, the enzyme is trapped in its reduced form, similar to what is generated during the course of the reaction with a substrate (see **Figure 1.6.** in the Introduction section 1.8. and **Figure 5.2.** below). The vulnerability of the reduced form of hAOX1

during a longer reaction course has been suggested by other studies (Abbasi, et al. 2019), however, the involvement of ROS has not been ruled out. Our studies propose that the reduced state of hAOX1 is vulnerable to the presence of ROS, produced either endogenously or added exogenously, and that this leads to the total inactivation of the enzyme. The removal of the sulfido ligand seems to follow the reverse of the mechanism in which the sulfido ligand is chemically constituted in the first place (see **Figure 5.2.**). pH is the factor determining the abundance of the species present in the solution, and hence, the process is pH dependent. In the absence of a sulfur source under mild basic conditions (pH 8.0) hydroxyl anion (OH^-) is able to substitute the thiol group which is coordinated to Mo(IV) in the reduced state of enzyme (shown in the forward reactions in **Figure 5.2.**). The sulfido ligand, on the other hand, is constituted in the presence of sodium sulfide that at pH 7.4 generates SH^- (Myers 1986). SH^- is a potent nucleophile that substitutes the hydroxyl (-OH) ligand coordinated at Mo(IV) in the inactive reduced form of the enzyme (shown in the reverse reactions in **Figure 5.2.**).

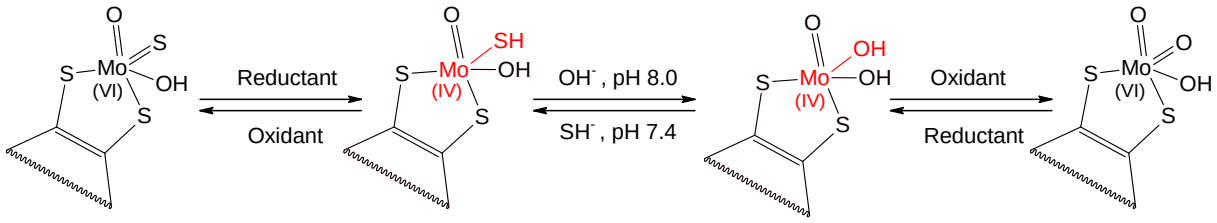

Figure 5.2.: Loss (forward reactions) and gain (back reactions) of the sulfido ligand at Moco: In the absence of oxygen and presence of a reductant the enzyme is trapped in its reduced form in which the substitution events occur more easily at Moco. H_2O_2 during the loss of sulfido and sodium dithionite during the reconstitution are the reductants. The pH of the solution is crucial for both loss and gain of the sulfido ligand.

It seems that H_2O_2, either endogenously produced or exogenously added, keeps the enzyme in the vulnerable reduced form in which the substitution events at Moco are facilitated. However, after reconstitution of the sulfido at Moco, the activity is not fully regained. This implies that the damage to hAOX1 during the course of the reaction is not limited to the loss of the sulfido ligand and some global damages due to the oxidizing effects of ROS also occur.

5.2.2. ROS Induce Oxidation on Particular Amino Acid Residues

5.2.2.1. Domain Oxidation Pattern Differs for the Cysteines and Methionines

The oxidizing effects of ROS on the most susceptible amino acid residues, i.e. methionines and cysteines, can impair the structure or function of proteins (Davies 2016). Cysteine and methionine

each consist about 2.3% of an average human protein (Pe'er, et al. 2004). In the hAOX1 domains the methionine content is slightly more than the average from about 2.5% in the FAD domain to 3.0% and 3.6%, respectively, in the FeS and Moco domains. The cysteine content varies more over the domains, from 1.9%, a slightly below the average value, in the FAD domain to 2.6% in the Moco domain which is slightly above the average. The amount of cysteines in the FeS domain, however, is the highest, about 6.9%, due to the presence of the cysteines providing binding sites for the FeS clusters.

The oxidation state of cysteines and methionines in the native condition compared with samples treated with 10 mM H_2O_2 or 160 µM phenanthridine were analysed by ESI-MS. The overall oxidation of methionines was similar in the 3 domains and about 20%, 60% and 40%, respectively, in the native condition and in samples treated with H_2O_2 and phenanthridine (see **Figure 4.14.** in section 4.2.2.3.). The cysteine oxidation was significantly lower than methionine oxidation. In the native condition, and in the H_2O_2 and phenanthridine treated samples the levels were 0.5%, 5% and 2% in the FeS domain; 1%, 23% and 9% in the FAD domain; and 2%, 25% and 10% in the Moco domain (see **Figure 4.12.**, panel **A** in section 4.2.2.1.). Despite the fact that the cysteine content in the Moco and FAD domains are lower than in the FeS domain, the total cysteine oxidation is higher for the Moco and FAD domains. This suggests that the Moco and FAD domains are potentially more vulnerable to oxidation. Also, the oxidation induced by endogenous ROS, i.e. in the samples treated with phenanthridine, is only about 2.5 fold lower than the oxidation caused by exogenous ROS despite the exogenous ROS concentration (10 mM) being at least 60 folds more than the endogenous ROS concentration (maximally 160 µM). This suggests that the oxidation caused during the turnover is more damaging than that caused by exogenous ROS.

5.2.2.2. Cysteines Are Specifically Oxidized in the Presence of Endogenous ROS

The comparison of the cysteines exposure, determined by the NEM reactivity, with their oxidation did not follow a linear behaviour (see **Figure 4.12.**, panels **B**, **C** and **D** in section 4.2.2.1.), meaning that the majority of the cysteines with high reactivity towards NEM were not oxidized at all. Moreover, endogenous and exogenous ROS showed different patterns of cysteine oxidation (see **Figure 4.13.**, panels **A** and **B** in section 4.2.2.2.). In the sample treated with 10 mM H_2O_2 , Cys654, 1242, 910 were from 2400 to 600 fold and Cys798, 180 and 179 were about 200 fold more oxidized in comparison with the native condition. In the sample incubated with 160 µM of phenanthridine Cys600 was about 1800 fold and Cys654, 798 and 834 were about 100 fold more oxidized than in the native condition. The 1 to 1 stoichiometry of the enzyme reaction suggests that the maximum

concentration of the endogenous ROS would be 160 µM, while the exogenous ROS concentration was at least 60 times higher. This means that the cysteines which were oxidized in the presence of both exogenous and endogenous ROS, i.e. Cys654 and Cys798, would get to much higher levels of oxidation in the presence of endogenous ROS at a similar concentration. Cys654 locates on a loop on the surface of the enzyme as part of the substrate gate 1, ^{652}SFCFFTEAEK^{662}, through which the substrate is oriented to Moco (Coelho, et al. 2015). Oxidation of Cys654 to sulfinate and sulfonate adducts introduces negative charge at the entrance of the substrate gate 1 that can potentially disturb the access of the substrate to the active site.

The ratio of oxidation in the sample treated with phenanthridine to the one incubated with H_2O_2 yields the specific oxidation induced by endogenous ROS (see **Figure 4.13.**, panels **C** and **D** in section 4.2.2.2.). Cys600 was identified to be oxidized as high as 73 percent in the sample treated with phenanthridine, which is about 1800 folds more than the oxidation of this cysteine in the native or H_2O_2 treated samples. Cys600 locates at the N-terminus of a short α-helix in the Moco domain at about 20 Å distance from Moco, 16 Å from FeSI and 18 Å from FeSII (see **Figure 5.3.**). α-helices exhibit a dipole moment with the positive charge at their N-termini. The cysteine residues locating in these regions show lowered pK_a of their thiol side chain that confers them relatively high reactivity (Poole 2015). Oxidation of Cys600 to sulfonate ($-SO_3^-$) introduces charge repulsion that may eventually lead to a local disruption of the structure. These events in a 16-20 Å distance from the FeS clusters and Moco may potentially contribute in an irreversible inactivation of hAOX1 during turnover.

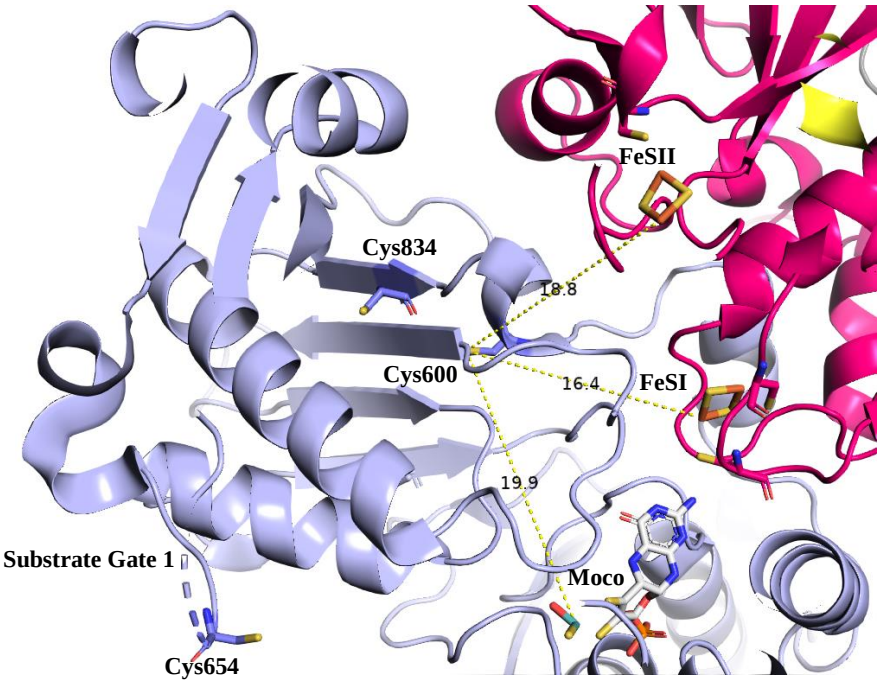

Figure 5.3.: Position of the cysteines highly oxidized in samples treated with hydrogen peroxide or phenanthridine: Cys654 locates at the substrate gate 1 on a loop on the surface of hAOX1 and is accessible for the ROS present in the solution. Cys600 locates at the N-terminal of a short α-helix at 20 Å distance from Mo center, 16 Å from FeSI and 18 Å from FeSII. Cys834 is at about 10 Å distance from Cys600. In the ribbon representative, generated using PyMol version 2.4.1. (Schrödinger, LLC), Moco domain is shown in light blue, and FeS domain in pink.

The sulfonate ($-SO_3^-$) adduct of cysteine is not known to be enzymatically reversible, and hence, the oxidation damge detected *in vitro* might not be physiologically relevent. However, the sulfonate adduct of Cys600 might be an overoxidation artefact of an original sulfenate ($-SO^-$) modification as a result of the ROS effects on Cys600. The relatively close distances of Cys600 to the FeS clusters, i.e. 16 Å from FeSI and 18 Å from FeSII (see **Figure 5.3.**), suggest that electron transfer from the FeS clusters, especially from FeSI to Cys600 is not unlikely. Since Cys600 is solvent accessible, oxygen can easily access the thiol group and the reduction of oxygen as the physiological electron acceptor of hAOX1 can take place at this cysteine. The Moco-FeSI-Cys600 system can provide an alternative internal electron path, especially when the main electron transfer path is overloaded in turnover with fast substrates such as phenanthridine.

Cys834, the other cysteine with 8 percent oxidation in the presence of phenanthridine locates about 10 Å from Cys600. Interestingly, the pair of Cys600-Cys834 is partially conserved in higher eukaryotes (see **Figure 5.4.** for the partial alignment around Cys600 and Cys834). Given the high reactivity of Cys600 owing to its position at the N-terminus of a short α-helix, oxidation of Cys600 seems to be facilitated upon the exposure with ROS. The enzymatic machinery for removal of sulfenic acid (-SOH) modification from cysteines require another adjacent cysteine together with a reducing agent, e.g. glutathione as the most abundant physiological redox buffer (Berndt, et al. 2007). It seems plausible that the Cys600-Cys834 pair provides a candidate for such reversible processes for hAOX1 in turnover *in vivo*.

A similar analysis for methionine showed that despite the overall oxidation of methionines being 3 to 10 fold higher than cysteine oxidation in different domains, none of the methionines appeared to be specifically oxidized as was observed for cysteines (see **Figure 4.14.** in section 4.2.2.3.).

Taken together, the major damage caused by ROS, endogenously generated or exogenously added, is the detachment of the sulfido ligand from Moco in the vulnerable reduced state of the enzyme. In addition, the specific oxidation of cysteines, i.e.Cys654 which is in particular crucial for the substrate orientation and Cys600 which locates in close distance from the cofactors Moco and FeS clusters, eventually impair the enzyme function or local structure. It seems that the irreversible oxidation of specific cysteines in our *in vitro* studies together with high level of methionine oxidation is the reason why the reconstitution of the sulfido ligand only recovers up to 50 percent of the activity of hAOX1.

```
H.sapiensAOX1          MHLSGVKHATGEAIYCDDMPLVDQELFLTF 614 ..... HGRAV-RC-VLERGEDMLITGGRHPYLGKY 850
B.taurusAOX1           MHLSGIKHATGEAIYCDDMPVVDRELFLTF 614 ..... HGRPV-RC-ILERGEDILITGGRHPYLGKY 851
M.musculusAOX1         MHLSGIKHATGEAIYCDDMPAVDRELFLTF 613 ..... HGRPV-RC-ILERGEDILITGGRHPYLGKY 845
M.musculusAOX2         MHLSGLKHATGEAVFCDDIPRVDKELFMAL 624 ..... TGHPI-RL-VLDREDDMLITGGRHPLFAKY 856
M.musculusAOX3         MHQSGIKHATGEAVFCDDMSVLPGELFLAV 614 ..... TGRPI-RF-ILERRDDMLITGGRHPLLGKY 846
M.musculusAOX4         MHQSGIKHATGEAIFIDDMPPIDQELCLAV 616 ..... TGRPI-RF-ILERSDDMLITAGRHPLLGKY 848
R.norvegicusAOX1       MHLSGIKHATGEAIYCDDMPAVDRELFLTF 613 ..... HGRAV-RC-TLERGEDMLITGGRHPYLGKY 845
R.norvegicusAOX2       MHLSGLKHATGEAVFCDDIPRVDKELFMAL 624 ..... TGRPI-RL-VLDREDDMLITGGRHPLFAKY 856
R.norvegicusAOX4       MHQSGIKHATGEAKFVDDMPRINQELCLTV 614 ..... TGRPI-RF-ILDRSNDMLITAGRHPLLGKY 846
C.porcellusAOX1        MHLSGIKHTTGEAIYCDDMPLVDRELSLAF 612 ..... HCRAV-RC-ILERGEDMLITGGRHPYLGKY 844
C.porcellusAOX4        MHQAGLKHATGEAAFVDDLPLVSQELFLAV 617 ..... TGRPI-RF-VLERGDDMLITAGRHPLLGRY 849
O.cuniculusAOX1        MHLSGVKHATGEAIYLDDMPAVDQELFMAF 614 ..... HGRAV-RC-ILERGEDMLITGGRHPYLGKY 846
O.cuniculusAOX4        MHQSAIKHATGEAVFIDDMPAVDQELYLAV 615 ..... TGRPI-RF-ILERGDDMLITAGRHPLFAKY 847
E.cabullusAOX1         MHLSGIKHTTGEAIYCDDMPVLDGELFLAF 614 ..... HGRPV-RC-ILERGEDMLITGGRHPYLGKY 850
E.cabullusAOX4         MHQSAIKHATGEAVFVDDMPPIAQELFLAV 615 ..... TGRPI-RF-VLERGDDMLITAGRHPLLARY 847
C.l.familiarisAOX2     MHQSAIKHATGEAVFSDDTPPIARELFLAV 615 ..... TGRPI-RF-ILERGDDMLITGGRHPLLGKY 847
C.l.familiarisAOX3     VHLSGLKHATGEAIFCDDIPTMDRELFMVL 622 ..... TGRPI-RL-VLDREDDMLITGGRHPLFGKY 854
C.l.familiarisAOX4     MHQSAIKHATGEAVFSDDTPPIARELFLAV 607 ..... TGRPI-RF-ILERGDDMLITGGRHPLLGKY 839
P.capensisAOX1         MHLSGIKHATGEAIYCDDMPVVDQELFLTF 618 ..... LGRAV-RC-ILERGEDMLITGGRHPYLGKY 854
E.europaesAOX          MHLSGIKHATGEAIYCDDMPKLDQELFLTF 627 ..... HGRPV-RC-ILERGEDMLITGGRHPYFAKY 863
N.visonAOX             MHLSGIKHATGEAIYCDDMPTVDQELFLSF 614 ..... HGRAV-RC-VLERGEDMLITGGRHPYLGKY 850
D.ordiiAOX             MHLSGIKHATGEAVYCDDMPAVDQELFLMF 614 ..... HGRAV-RC-ILERGEDMLITGGRHPYLGKF 846
S.scrofaAOX1           MHLSGIKHATGEAVYCDDMPAVDRELFLTF 615 ..... KVTQLYVCVYLSSGEDLA---VRHQXVAXT 851
S.scrofaAOX2           MHLSGLKHATGEAIFCDDIPMVDKELCMAL 623 ..... TGHPI-RL-VLDREDDMLITGGRHPLFGKY 855
B.mutusAOX             MHLSGIKHATGEAIYCDDMPVVDRELFLTF 613 ..... HGRPV-RC-ILERGEDILITGGRHPYLGKY 850
I.tridecemlineatusAOX1 MHLSGIKHATGEAIYCDDMPAVDRELFLTF 614 ..... HGRAV-RC-VLERGEDMLITGGRNPYFAKY 846
T.syrichtaAOX1         MHLSGTKHATGEAIYCDDMPVVDQELFLTF 589 ..... HGRAV-RC-VLERGEDMLITGGRHPYIGKY 825
M.lucifugusAOX1        MHLSGIKHATGEAIYCDDMPAMDGELFLAF 614 ..... HGRAV-RC-ILERGEDMLITAGRHPYLGKY 832
L.africanoAOX1         MHLSGIKHATGEAIYCDDMPAVDQELFLTF 618 ..... QGRAV-RC-ILERGEDMLITAGRHPYLGKY 854
M.fascicularisAOX1     MHLSGVKHATGEAIYCDDMPLVDQELFLTF 614 ..... HGRAV-RC-VLERGEDMLITGGRHPYLGKY 850
M.fascicularisAOX2     MHLSALKHATGEAMFCDDIPVVDKELFMAL 628 ..... TGHPI-RL-VLDREDDMLITGGRHPLFGKY 851
P.paniscusAOX1         MHLSGVKHATGEAIYCDDMPLVDQELFLTF 601 ..... HGRAV-RC-VLERGEDMLITGGRHPYLGKY 837
G.g.gorillaAOX1        MHLSGVKHATGEAIYCDDMPLVDQELFLTF 614 ..... HGRAV-RC-VLERGEDMLITGGRHPYLGKY 850
A.melanoleucaAOX3      MHLSGLKHATGEAIFCDDIPMVDRELFMVL 622 ..... TGHPI-RL-VLDRKDDMLITGGRHPLFGKY 854
H.sapiensXDH           PHLAADMQASGEAVYCDDIPRYENELSLRL 608 ..... TGRPV-RC-MLDRDEDMLITGGRHPFLARY 842
B.taurusXDH            PHLAAAMQASGEAVYCDDIPRYENELFLRL 607 ..... TGHPV-RC-MLDRNEDMLITGGRHPFLARY 841
R.norvegicusXDH        PHLAANMQASGEAVYCDDIPRYENELSLRL 607 ..... TGRPV-RC-MLDRDEDMLITGGRHPFLAKY 841
M.musculusXDH          PHLAADMQASGEAVYCDDIPRYENELSLRL 610 ..... TGRPV-RC-MLDRDEDMLITGGRHPFLAKY 844
F.catusXDH             PHLAAAMQASGEAVYCDDIPRYENELSLRL 606 ..... TGRPV-RC-MLDRDEDMLITGGRHPFLARY 840
M.lucifugusXDH         PHLASAMQASGEAVYCDDIPRYENELSLRL 611 ..... TGRPV-RC-MLDRDEDMLITGGRHPYLGRY 845
M.gallopavoAOX1        MHQSGIKHATGEAVYIDDIPAVDGELFLAV 616 ..... TNRAV-RL-ILSRGDDMLITGGRHPFIGKY 854
S.c.australisAOX       MHQSGIKHATGEAVYIDDLPSVDGELFLAV 615 ..... TSRAV-RL-ILSRGDDMLITGGRHPFIGKY 851
A.platyrhynchosAOX     MHQSGIKHATGEAVYIDDLPSVDGELFLAV 543 ..... TNRAV-RL-ILSRGDDMLITGGRHPFIGKY 779
G.gallusAOX1           MHQSGIKHATGEAVYIDDIPSVDGELFLAV 615 ..... TNRAV-RL-ILSRGDDMLITGGRHPFIGKY 851
G.gallusAOX2           MHQSGIKHATGEAVFIDDIRPVDRELSLAV 617 ..... TGRPV-RF-ALERNMDMLITGGRHPFFGKY 848
G.gallusXDH            VHLSAAKQACGEAVYCDDIPHYENELYLTL 636 ..... TGRPV-RC-MLDRDEDMLISGGRHPFLGRY 870
M.gallopavoXDH         VHVSAAKQACGEAVYCDDIPHYENELYLTL 636 ..... IGRPV-RC-MLDRDEDMLISGGRHPFLGRY 870
A.carolinensisAOX1     MHQAGIKHATGEAVYCDDIRTIDGELFLAL 622 ..... TGQAV-RC-ILDRGTDMLITGGRHPLIGKY 858
A.sinensisXDH          MHLSAMKQATGEAVYCDDVPLYENELYLSL 632 ..... LKRPV-RC-MLDRDEDMLITGGRHPFYGKY 867
A.sinensisAOXlike      MHESAVKHATGEAVYCDDICPMDEELFLAV 622 ..... TGRAV-RC-ILDRSDDMLITGGRHPYLGKY 858
A.sinensisAOX4         MHLAGIKHATGEAIYCDDIRAVEEELFLAV 619 ..... TGRVV-RC-ILDRGDDMLITGGRHPFLGKY 855
P.sinensisXDH          VHLSAAKQACGEAVYCDDIPCYENELYLTL 614 ..... TGRPV-RC-MLDRDEDMLITGGRHPFLGQY 848
P.sinensisAOX2         MHQSGVKHATGEAVYCNDIRAVAEELFLAV 617 ..... TGRPI-RF-ALERDEDMLITGGRHPFFGKY 848
X.laevisAOX1           MHYSGIKHATGEAVYCDDMPCVDGELFLYF 601 ..... TRRAV-RC-VFERGDDMLITGGRHPFLGKY 841
D.rerioAOX6            MHRSALSQATGEAVYCDDLPYTDGELVLAI 609 ..... TGLPV-RC-VLERGEDMLITGGRHPVWGKY 845
X.maculatusAOXbeta     MHRSAISQATGEAVYCDDIPKTDGELVMVL 608 ..... TNRAV-RC-VLERGEDMLITGGAP----SC 844
O.latipesAOXbeta       MHRSAISHATGEAVYCDDIPRTEGELFLVL 609 ..... TNRAV-RC-VLERGEDMLITGGRHPLLAKY 845
L.oculatusAOXbeta      MHRSAISQATGEAVYCDDIPKTEGELFLVL 609 ..... TDRAV-RC-VLERGEDMLITGGRHPVLAKY 862
S.salarAOX1like        MHRSAISQATGEAVYCDDIPKMDGELHIVL 614 ..... TGRAV-RC-VLERGEDMLITGARHPVLGKH 850
D.rerioXDH             MHLSAMKQATGEAVYCDDVPLYENELYLSL 632 ..... LKRPV-RC-MLDRDEDMLITGGRHPFYGKY 867
C.elegansAOXGad3       ANYFNERAITGEAFYVNDIQAYN-AVHLGF 549 ..... LNRPTYGF--LSRADDLAITGKRHEVHAKY 791
C.elegansXDH           KHVSGDKHTTGEAVYCDDINVADCN-HIAF 629 ..... FGRPM-KF-KFERFDDMAITGTRHPFTLQY 868
D.melanogasterXDH      VHAAALKQATGEAIYTDDIPRMDGELYLGL 627 ..... LRRPV-RC-MLDRDEDMLITGTRHPFLFKY 854
D.melanogasterAOX1     EKHEGLIQCSGEATYSNDLPTQHNQLWAAF 575 ..... LNRPI-RF-VQSLESIMTSLGKRWAFHCDY 823
O.sativaAOX1           KKVGAELQASGEAVYVDDIPAPKDCLYGAF 622 ..... LRRPV-RM-YLDRKTDMIMAGGRHPMKAKY 867
A.thalianaAAO3         IKVGAALQASGEAVFVDDIPTLPDCLHGAF 599 ..... LQRPV-KM-FLNRKTDMIMAGGRHPMKINY 843
G.maxAOX2              IKSGAALQASGEAVFVDDIPSPKNCLHGAY 635 ..... LRRPV-RM-YLNRKTDMIMAGGRHPMKITY 879
R.communisAOX          TKSGASLQASGEAIFVDDIPSPSNCLHGAF 491 ..... LQRPV-RI-YLNRKTDMIMAGGRHPMKITY 735
S.lycopersicumABA      KKFGASMQASGEAVYVDDIPSPPNCLYGAF 627 ..... LQCPV-RM-YLNRKTDMIMAGGRHPMKITY 871
R.capsulatusXDH        PHDSARAHVTGQARYLDDLPCPANTLHLAF 499 ..... TGRPC-KM-RYDRDDDMVITGKRHDFRIRY 733
T.vaginalisXDH         HMRSSAQQTTGEAVYTDDLPTFPHGLHAYF 598 ..... LKRPV-RM-VLDRNDDMAIMGGRHPFYATY 832
```

Figure 5.4.: Partial alignment around Cys600 (shown in red highlighted yellow) and Cys834 (shown in black highlighted cyan): The Cys600-Cys834 pair (hAOX1 numbering) is partially conserved in most vertebrates. The organisms are abbreviated as following: *Homo sapiens: H. sapiens, Bos taurus: B. Taurus, Mus musculus: M. musculus,*

Rattus norvegicus: R. norvegicus, Cavia porcellus: C. porcellus, Oryctolagus cuniculus: O. cuniculus, Equus caballus: E. caballus, Canis lupus familiaris: C. l. familiaris, Procavia capensis: P. capensis, Erinaceus europaes: E. europaes, Neovison vison: N. vison, Dipodomys ordii, Sus scrofa: S. scrofa,Bos mutus: B. mutus, Ictidomys tridecemlineatus: I. tridecemlineatus, Tarsius syrichta: T. syrichta, Myotis lucifugus: M. lucifugus, Loxodonta africano: L. africano, Macaca fascicularis: M. fascicularis, Pan paniscus:P. paniscus, Gorilla gorilla gorilla: G. g. gorilla, Ailuropoda melanoleuca: A. melanoleuca, Anolis carolinensis: A. carolinensis, Felis catus: F. catus, Meleagris gallopavo: M. gallopavo, Struthio camelus australis: S. c. australis, Anas platyrhynchos: A. platyrhynchos, Gallus gallus: G. gallus, Taeniopygia guttata: T. guttata, Ficedula albicollis: F. albicollis, Alligator sinensis: A. sinensis, Pelodiscus sinensis: P. sinensis, Xenopus laevis: X. laevis, Danio rerio: D. rerio, Xiphophorus maculatus: X. maculatus, Oryzias latipes: O. latipes, Lepisosteus oculatus: L. oculatus, Salmo salar: S. salar, Caenorhabditis elegans: C. elegans, Drosophila melanogaster: D. melanogaster, Oryza sativa: O. sativa, Arabidopsis thaliana: A. thaliana, Glycine max: G. max, Ricinus communis: R. communis, Solanum lycopersicum: S. lycopersicum, Escherichia coli: E. coli, Rhodobacter capsulatus: R. capsulatus, Trichomonas vaginalis: T. vaginalis.

5.3. The FAD Variable Loop and ROS Production in hAOX1

5.3.1. Altering the Amino Acid Composition of the FAD Variable Loop Affects the Kinetic Parameters

hAOX1 oxidizes aldehydes and N-heterocyclic rings as the reducing substrates at Moco and generates electrons that have to be received by an electron acceptor as the oxidizing substrate (Hille, et al. 2014). Electrons produced at Moco have to be internally transferred through the electron sink FeS clusters to the site where the electron acceptor receives them. In hAOX1 molecular oxygen is the physiological electron acceptor and hence, oxygen is reduced and forms reactive oxygen species (ROS) including hydrogen peroxide and superoxide. hAOX1-WT produces about 20 percent superoxide in each catalytic cycle, while hAOX1-L438V a natural variant of hAOX1 first identified in 2017, generates more than 70 percent superoxide (Foti, et al. 2017).

Leu438 is part of the FAD variable loop 1, ^{430}AQRQENALAI^{440}, in proximity of the N5 position of the FAD isoalloxazine ring, where it is widely believed that ROS are produced (see **Figure 4.19.**, **A** for the position of the FAD loop 1). 6 variants were produced to investigate the effect of the amino acid composition of the FAD variable loop 1 and in particular the position 438 on the type of the ROS generated by hAOX1. In the chimeric variant bXO-FAD-chimera the whole loop, ^{430}AQRQENALAI^{440}, was exchanged to its counterpart, i.e. ^{423}QASRREDDIA^{433}, from bovine XO (bXO). bXO loop is overall negatively charged and an isoleucine has replaced the leucine at position 438. Two more variants with two sequential aspartates at positions 436 and 437 similar to what is found in the bXO corresponding positions were also constructed. In N436D/A437D leucine was kept at position 438, while in N436D/A437D/L438I leucine was exchanged with an isoleucine. 3 more variants with Leu438 exchanged to alanine as a smaller hydrophobic residue, to

phenylalanine as a bulky aromatic residue and to lysine as a positively charged residue were constructed in parallel.

The enzyme expression, cofactor load and kinetic parameters were compared to those of WT and L438V (see section 4.3.2.). The variants showed elution profiles, UV-Vis absorption, and metal content similar to those of WT and the L438V variant, indicating that protein expression and cofactor saturation were not affected by altering the composition of the FAD variable loop 1.

The steady state kinetic parameters of the variants in comparison with those of WT showed lowered catalytic efficiency (see **Figure 4.17.** and **Table 4.10.** in section 4.3.2.2.). The bXO-FAD-chimeric variant, N436D/A437D and N436D/A437D/L438I were significantly slower enzymes than WT such that, despite their lowered K_m, they had about 70 percent less catalytic efficiency. L438K was a faster enzyme than the bXO-FAD-chimeric variant, N436D/A437D and N436D/A437D/L438I, but still slower than WT and L438V with decreased catalytic efficiency. It has been shown that the alteration of the electrostatic environment of the FAD isoalloxazine ring affects the oxygen reactivity of FAD dependent enzymes (Gadda 2012; Mattevi 2006). In bXO-FAD-chimeric variant, N436D/A437D and N436D/A437D/L438I two negatively charged aspartates and in L438K one positively charged lysine change the electrostatic environment of flavin. The negative charge is in particular a negative effector on the reactivity of flavin towards oxygen mainly due to the destabilization effect of the negative charges on the 'caged radical pair' generated as the intermediate (see below and **Figure 5.5.** for more details) (Chaiyen, et al. 2012; Pennati and Gadda 2011). L438A and L438F were both less efficient enzymes than hAOX1-WT despite the fact that in L438A the replaced residue at position 438 is smaller, while in L438F phenylalanine is an amino acid residue with a bulkier aromatic side chain than leucine. Extensive studies on flavoenzymes have demonstrated that the geometry, i.e. size and orientation, of the residue in close contact to the N5-C4a position of the FAD isoalloxazine ring plays crucial role in the reactivity of flavin with oxygen (Hernández-Ortega, et al. 2011; Leferink, et al. 2009). It seems that the environment around the FAD isoalloxazine ring and in particular the position 438 affects either the electron transfer potency of FAD or the electron acceptor binding. These changes eventually result in lowered turnover of the variants with altered amino acid composition of the FAD loop 1.

5.3.2. The FAD Variants Produce Different Amount of Superoxide

The mechanism of the reaction of oxygen with reduced flavin is one of the most widely studied yet enigmatic reactions in biochemistry. The reaction is initiated with the transfer of one electron from

the fully reduced flavin i.e. hydroquinone ($FADH_2$ or $FADH^-$), to oxygen (Chaiyen, et al. 2012) (see **Figure 5.5.**). This forms a caged radical pair intermediate between the flavin semiquinone and superoxide. A second electron transfer accompanied with a proton transfer generates the fully oxidized form of flavin (FAD) and hydrogen peroxide as the end products. The semiquinone/superoxide radical pair is short-lived; however, superoxide can be released from the flavin site of some flavoenzymes such as XOs and AOXs, and leads to the formation of a mixture of superoxide and hydrogen peroxide.

To investigate whether the substitution of the residue at position 438 with amino acids with different characteristics influences the ratio of superoxide to peroxide formation, the amount of superoxide for each variant was measured using a cytochrome C assay (McCord and Fridovich 1969) (see **Figure 4.18.** and **Table 4.11.** in section 4.3.2.3.). It was observed that the superoxide generation differs among the variants with altered amino acid residue(s) at or around position 438. Furthermore, the addition of DPI, a specific inhibitor of FAD (Reis, et al. 2020), to the cytochrome C assay reactions showed that when the FAD site is blocked, the reduction of cytochrome C is largely inhibited. This confirms that the reduction of oxygen and production of superoxide mainly takes place at FAD and other redox active sites of the enzyme are not involved in superoxide formation.

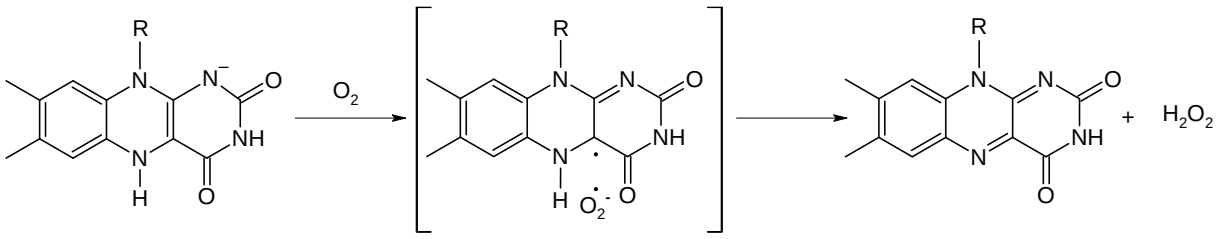

Figure 5.5.: The reaction of reduced flavin with oxygen: When fully reduced, flavin ($FADH^-$) transfers one electron to oxygen to form an unstable 'caged radical pair' of semiquinone/superoxide intermediate. The second electron transfer generates fully oxidized flavin (FAD) and hydrogen peroxide as the end products. The release of superoxide is possible when the semiquinone/superoxide intermediate is thermodynamically stabilized or when the superoxide binding to the cavity is loose and the rate of the release of superoxide is higher than the rate of the second electron transfer.

hAOX1-WT reduces cytochrome C at a rate of about 400 nmol/min.mg, while L438V reduces about 4 times more cytochrome C than WT. Compared to the amount of their total ROS, L438V generates about 75 percent of its total ROS in the form of superoxide, while WT produces only 20 percent superoxide. The difference between WT and L438V is the size of the amino acid residue at

the position 438 in proximity of the N5 position of the FAD isoalloxazine ring (see **Figure 4.19.** for the crystal structures of WT in comparison with L438V in section 4.3.3.). L438A reduces cytochrome C nearly to the same amount as L438V, but with less total ROS, i.e. superoxide and hydrogen peroxide mix. This results in about 90 percent superoxide formation. It seems that there exists a correlation between the size of the residue at position 438 and the amount of the superoxide produced, i.e. the smaller the amino acid residue the more the amount of superoxide. The amount of superoxide generated by L438F and L438K is, respectively, about 50 and 30 percent. Both phenylalanine and lysine that have replaced the leucine at position 438 affect the volume of the cavity in proximity of the isoalloxazine ring, but both, in addition, either by a positive charge or π-electron interaction, alter the electrostatic environment around FAD. It seems that the higher superoxide produced by L438F and L438K is the result of the combined effects of the size and charge changes at the position 438. A similar trend to that observed between WT, L438V and L438A is distinguished when N436D/A437D and N436D/A437D/L438I are compared. Despite the rate of cytochrome C reduction by N436D/A437D/L438I being much less than that of WT and about 70 nmol/min.mg, the percentage of the superoxide that this variant produces, remains similar to that of WT. N436D/A437D is even slower at reducing cytochrome C, about 30 nmol/min.mg, however, the ratio of superoxide is about 10 percent, which is half the amount of the superoxide produced by WT. N436D/A437D and N436D/A437D/L438I differ in the amino acid at position 438 as a leucine is replaced with an isoleucine, a substitution that again changes the size of the cavity near the N5 position of the isoalloxazine ring. Note that in N436D/A437D and N436D/A437D/L438I the negatively charged residues at positions 436 and 437 affect the electrostatic field around FAD, which consequently affects the enzyme efficiency (see **Figure 4.17.** and **Table 4.10.** in section 4.3.2.2. for the comparison of the kinetic parameters). Again a similar trend is observed and the size of the residue at position 438 determines the type of ROS produced at FAD.

Oxygen can only accept one electron at a time (see **Figure 5.5.**). This means that superoxide can be generated when the release of superoxide from the FAD site is faster than the second electron transfer to oxygen. The amount of superoxide can increase if the rate of the electron transfer from FeSII to FAD is slow, i.e. when there are not enough electrons for two consequent electron transfers to oxygen (see **Figure 5.6.** for electron transfer paths compared in XO and AOXs). This would happen if the rate of the electron transfer from FeSII to FAD is slow, and as a result, the formation of semiquinone state of FAD ($FADH^{\cdot}$) is expected. This is the mechanism proposed to explain how semiquinone and superoxide are formed in fumarate reductase (Frd) (Messner and Imlay 2002) and

in partially reduced XO (Hille and Massey 1981; Porras, et al. 1981). The electron transfer rate from the FeS clusters to FAD and hence, the formation of the partially reduced enzyme depends on the redox potentials of the redox active centers of the enzyme. In XO the redox potentials pattern provides the possibility for the formation of the partially reduced enzyme (see **Figure 5.6.** for a comparison of the redox potentials of the cofactors in XO and AOX). The redox potentials of FAD/FADH$^{\cdot}$ or FADH$^{\cdot}$/FADH$_2$ couples have not been reported for hAOX1 to date, but the redox potential of all redox active centers are reported for mAOX3 (Mahro, et al. 2013) and for rabbit liver AOX (Barber, et al. 1982a). As a general trend in both mAOX3 and rabbit liver AOX the redox

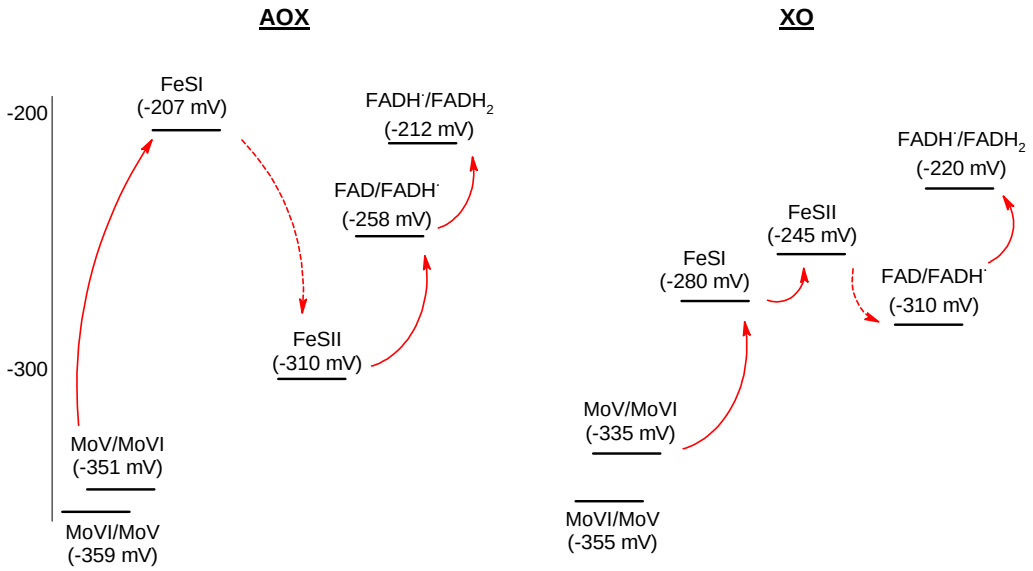

Figure 5.6.: The redox potentials of redox active centers in AOXs and XOs based on the work by Barber and colleagues (Barber, et al. 1982b): Unlike XO, the FeSII in AOX presents a more negative redox potential than FeSI and hence there is an electron accumulation on FeSI in AOX. Once the electrons are received by FeSII, their transfer to FAD is fast. Note that in this schematic FAD in XO shows the FADH$^{\cdot}$/FADH$_2$ couple, while in AOX it represents the redox potential of the FAD/FADH$_2$ couple.

potential of FeSI is more positive than that of FeSII. A similar pattern has also been observed for the redox potentials of FeSI and FeSII for hAOX1 (FeSI: -279 mV, FeSII: -329 mV, Dr. Martin Mahro PhD thesis, 2013). Given the most negative redox potential of Moco, the more positive redox potential of FeSI than FeSII in AOXs implies that the electron transfer from FeSI to FeSII is slow and there will be an electron accumulation on FeSI. However, once electrons reach FeSII, their transfer to FAD can be fast. This also implies that the formation of hydroquinone from semiquinone in AOXs can be fast. In other words, the semiquinone intermediate is not likely to be detected in AOXs. Interestingly, in the redox titration experiments performed using sodium dithionite or

substrate under anaerobic condition, semiquinone was not detected for hAOX1-WT or L438V variant (Dr. Alessandro Foti PhD thesis, 2017). Moreover, there was no significant difference between the redox titration behaviour of hAOX1-WT and L438V variant. The lack of semiquinone detection suggests that the electron transfer to FAD from FeSII is not rate limiting, and overall, it seems that the increased amount of superoxide in L438V is not due to electron deficiency on FAD.

The increase in the amount of superoxide can also be due to the loose oxygen binding in the site. A larger cavity where oxygen is bound results in slightly different positioning of oxygen further away from FAD. Hence, when superoxide is produced, it starts to drift away from the FAD site before the second electron is transferred. In this scenario the starting state of FAD is the hydroquinone and semiquinone would not be detected in the process. The geometry of the cavity and positioning of oxygen has been shown in various flavoenzymes to be determining the reactivity of oxygen with flavin. In choline oxidase a Val-to-Ala (Finnegan, et al. 2010) and in aryl-alcohol oxidase a Phe-to-Ala (Hernández-Ortega, et al. 2011) i.e. a smaller amino acid substitution decreased the rate of the reaction with oxygen. In *p*-hydroxyphenylacetate hydroxylase a Phe-to-Trp (Baron, et al. 2009) and in *D*-amino acid oxidase a Gly-to-Val (Saam, et al. 2010) i.e. a larger amino acid exchange decreased the rate. It seems that on one side, the oxygen accessibility to flavin should not be hampered by the residues in close contact to the flavin, while on the other side, higher physical confinement of oxygen near the flavin facilitates its reaction at the site. These studies have focused on the overall reactivity of oxygen towards flavin; however, they emphasize the importance of the local environment and geometry of flavin near the N5 position.

In hAOX1-WT in comparison with the variants there appear to be a good correlation between the size of the side chain residue at position 438 and the amount of the superoxide produced. Since no semiquinone has been detected in the WT or L438V variant redox titrations, and since there is virtually no difference between the crystal structures of hAOX1-WT and L438V, it seems that the reaction is affected by the geometry and size of the cavity near N5 position of FAD.

5.4. Unexpected Effect of Dithiothreitol on hAOX1

5.4.1. DTT Slightly Lowers the Protein Aggregation, But Abolishes the Activity

Dithiothreitol (DTT) is a common reducing agent used for studying proteins (Cleland 1964). It provides two thiol groups to reduce a disulfide bond (**Figure 5.7.**) and forms an oxidized state (DTT_{ox}) containing an intramolecular disulfide. In return, the protein substrate is reduced to the dithiol state. The reaction goes through two steps where a mixed disulfide intermediate is formed.

Despite the fact that cysteines can adopt different redox potentials depending on their microenvironment and different values have been reported (e.g. -221 mV for L-cysteine at pH 7.0 (Cleland 1964; Jocelyn 1967)), the significantly more negative redox potential of DTT (-330 mV at pH 7.0 and -366 mV at pH 8.0) ensures a favourable equilibrium towards the formation of protein cysteine thiols.

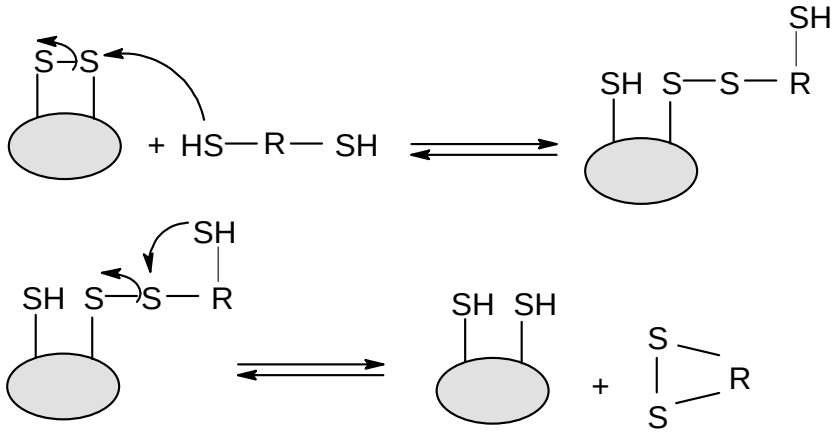

Figure 5.7.: The mechanism of reduction of disulfide bonds by dithiol containing reducing agents: In the first step the first electron transfer occurs: The nucleophilic attack of one the thiols on the reducing agent breaks the disulfide bond that generates a reduced thiol and a mixed disulfide. In the second step, the mixed disulfide species is resolved by the second electron transfer: The internal nucleophilic attack of the other thiol on the reducing agent forms fully reduced thiols on the proteins and produces the cyclic oxidized form of the dithiol reducing agent. R represents the carbon backbone including the hydroxyl groups of DTT, DTE or 2-ME (see **Table 4.12.** for the structures of DTT, DTE and 2-ME).

The disulfide forms of cysteines are essential for the structure of disulfide bond containing proteins (Anfinsen, et al. 1961). In addition, the reduced or disulfide forms of cysteines can have an impact on the physiological function of proteins. For instance, mammalian xanthine oxidoreductase (XOR) enzymes can switch between the xanthine dehydrogenase (XDH) and xanthine oxidase (XO) forms. In the dehydrogenase form two cysteines (Cys535 and Cys992 in bovine XDH) are in their reduced thiol state while they form a disulfide in the oxidase form (Nishino, et al. 2008; Stirpe and Della Corte 1969). The formation of this particular disulfide bond leads to a conformational change that eventually determines the native electron acceptor of the enzyme. In *in vitro* studies of XOR enzymes DTT has been used to keep the enzyme in the XDH state and there has been no report of the negative effect of DTT on its activity (Leimkuhler, et al. 2003). Unlike XOR enzymes, aldehyde oxidases are not able to interconvert between dehydrogenase and oxidase states, therefore the use of DTT in studying AOXs seems irrelevant.

In our studies on hAOX1, the initial aim was to improve the yield of production; however, an entirely unexpected effect of DTT broadened the investigation. It was observed that the aggregation

peak was slightly lowered when the enzyme was purified in the presence of 2.5 mM DTT, but the activity of the enzyme was completely abolished (see **Figure 4.20.,** panel **A** in section 4.4.2.). The activity was not regained when DTT was removed or when the enzyme was air re-oxidized. Such unusual impact of a reducing agent on AOXs has not been reported previously. There has been only one report that briefly mentioned 0.1 mM DTT among the negative effectors on the amount of active enzyme obtained in a purification trial of hAOX1 (Rodrigues, et al. 2014).

5.4.2. Small Reducing Agents Containing Sulfhydryl Group Negatively Affect hAOX1 Activity

The irreversible inhibitory effect of DTT could potentially be due the presence of the reactive sulfhydryl groups on DTT. Therefore, the effect of a series of chemicals (listed in **Table 4.12.**) with or without a reactive sulfhydryl group on the activity of hAOX1 was examined.

Erythritol structurally resembles DTT, except that the sulfhydryl groups on C1 and C4 on DTT are replaced with hydroxyl groups in erythritol. It was observed that when hAOX1 was incubated with erythritol, there was no significant effect on the activity (see **Figure 4.20.**, panel **B** in section 4.4.2.). The effect was persistent even over an elongated incubation time, implying that the presence of a reactive sulfhydryl was crucial for the irreversible inhibitory effect of DTT.

Dithioerythritol (DTE), 2-mercaptoethanol (2-ME), and glutathione (GSH) contain sulfhydryl groups on different carbon backbones than DTT. DTE is an epimer of DTT. It can be a potentially slower reducing agent than DTT due to the stereo chemistry of the hydroxyl groups that might hinder the formation of the disulfide in the oxidized cyclic product (Cleland 1964). In our experiments DTE lowered the activity of hAOX1 to about 90 percent of its initial value, comparable to the effect of DTT. 2-ME similarly abolished the hAOX1 activity, while GSH only had a slight effect. DTT, DTE and 2-ME contain sulfhydryl on two- to four-carbon backbone while GSH is a 307 Da tripeptide that carries one thiol group on a cysteine residue. It seems that the significantly larger size of GSH and/or the three charged groups on the tripeptide, prevents its -SH group to reach and react on the same site where the -SH group of DTT, DTE and 2-ME do, thus the activity of hAOX1 remains nearly unaffected. Interestingly, the oxidized form of DTT (DTT_{ox}), which initially lacks the reactive sulfhydryl, was able to lower the activity of hAOX1 to about 60 percent of its initial value. Apart from the potential for small amounts of contaminating reduced forms of DTT that could be present in the sample, the reactivity of DTT_{ox} suggested that its site of reaction is different from that of DTT, a possibility that needs further investigation to understand.

5.4.3. The Vulnerable Sites of hAOX1 to a Reactive Sulfhydryl Group

The potential vulnerable sites of hAOX1 reacting with sulfhydryl groups such as DTT include **a)** any disulfide bond which is structurally or functionally essential for the activity of the enzyme, **b)** sulfur ligands bound to the iron-sulfur clusters and **c)** the sulfido ligand bound at Moco. While the disturbance of any of the cofactors can potentially impair the activity of a cofactor dependent enzyme, the reaction with a disulfide bond may exert a local or global effect depending on the position of the cysteines forming the disulfide.

5.4.3.1. Cysteines in hAOX1 Are Unlikely to Form a Disulfide Bond Essential for the Activity

hAOX1 contains 42 cysteine residues. The FeS cluster domain carries 16 cysteines, 8 of which provide binding sites for the two [2Fe-2S] clusters, i.e. the thiol side chains of Cys44, 49, 52 and 74 binding to FeSII, and Cys114, 117, 149 and 152 binding to FeSI. They coordinate to the iron centers and are therefore buried. 6 other cysteines locate on the linker I that connects the FeS domain to the FAD domain, 5 of which, i.e. Cys165, 170, 171, 179 and 180, are in a region with poor electron density in hAOX1 X-ray crystal structure and are not visualized. The FAD domain contains only 6 cysteines, while the Moco domain carries 20 cysteine residues. The structure of hAOX1 indicates that the majority of the thiol side chains of cysteine residues, except for those binding the FeS sites, are fully or partially solvent accessible. Our experiments showed that small reducing agents, i.e. DTT, DTE and 2-ME, abolished the activity of hAOX1, while GSH only slightly reduced the activity. This suggests that if the cysteines in a disulfide bond were responsible for the loss of activity, they would be only accessible by small uncharged reducing agents and hence not on the surface of the protein.

hAOX1 is localized in the reducing environment of cytoplasm where the formation of disulfide bond is not facilitated (Hwang, et al. 1992). In accordance to that, there has been no report of a structural disulfide bond for hAOX1 (Coelho, et al. 2015) or for any other members of the XO family (e.g. bXO with PDB code 1FO4 or human XO with PDB code 3E1Q). Moreover, and unlike the XO state of the mammalian XOR enzymes, there has been no report of formation of a transient disulfide bond, which is involved in the catalytic cycle or is essential for the activity of AOXs. Despite these basic facts, the cysteines in hAOX1 were mapped using ESI-MS and NEM and IAM as alkylating agents of cysteine. NEM and IAM were chosen for the MS studies as they have contrasting effect on the activity of the enzyme. Similar to the reducing agents, NEM, which is a small uncharged alkylating agent, completely abolished the activity of hAOX1, while IAM, which

contains a large iodine center as the reacting site, only slightly reduced the hAOX1 activity. It seems that, similar to the reducing agents, size is a determining factor for the alkylating agents too.

The ESI-MS studies showed that 40 out of 42 cysteines present in AOX1 were fully or partially alkylated by NEM, indicating that 40 cysteines in hAOX1 are not in a disulfide bond. Out of the two remaining cysteines, Cys562 was not modified by NEM in any of the peptides detected, while Cys1192 did not appear in any of the peptides. The thiol side chain of Cys562 and Cys1192 are 28 Å apart in the crystal structure of hAOX1. Since disulfide bonds are typically 2-3 Å long (Wiedemann, et al. 2020), the 28 Å distance between Cys562 and Cys1192 is impossible to be favourable for the formation of a disulfide bond.

Comparing NEM and IAM showed that 32 out of 42 cysteines present in hAOX1 were alkylated by both NEM and IAM, while 3 cysteine residues i.e. Cys170 located on the linker I and Cys798 and 943 in the Moco domain were exclusively or predominantly reactive towards NEM (see **Table 4.13.** and **Figure 4.21.** in section 4.4.3.1.).

Cysteines 798 and 943 were about 30 percent reactive towards IAM, but nearly fully accessible for NEM. These residues have not been reported to play roles in the cofactor or substrate binding or orienting, however, reaction of an alkylating agent with either could potentially disturb Moco. The near fully modified Cys798 and 943 by NEM along with the total abolishment of the activity and the 30 percent modification of these cysteines by IAM while the activity was reduced about 25 percent, hint on the potential importance of these cysteines in the catalytic behaviour of hAOX1. Interestingly, these cysteines are conserved in higher organisms i.e. vertebrate AOXs, which suggests similar potential roles for them in other family members. However, the mechanism through which alkylation of Cys798 and 943 inactivated hAOX1 could be essentially different from the effect of small sulfhydryl containing agents such as DTT.

Cys170 locates on linker I at the C-terminus of the FeS domain and gets 40 percent modified by NEM, but not modified by IAM. Specific NEM modification of this residue could potentially disturb the FeS clusters. Moreover, the FeS clusters binding sites, i.e. Cys49, 51, 74, 79 and Cys149, 151, respectively, bound to FeSII and FeSI, were similarly accessible by both NEM and IAM, which suggested that both FeSI and FeSII would potentially be disturbed by NEM and IAM. Since IAM treatment did not significantly affect the activity of hAOX1, it could be concluded that the alkylation of the cysteines at the FeS binding sites did not impair the electron transfer through the FeS clusters. It has to be noted that the alkylation at the FeS binding sites might have occurred on the apo-enzyme and devoid-of-FeS species where the cysteines had become exposed.

Overall, the pattern of cysteine exposure mapped by IAM and NEM suggests that the FeS clusters or Moco are vulnerable to the disturbance caused by particular alkylating agents of cysteines. A behaviour that could be essentially different from the effect of the sulfhydryl containing reducing agents and needs to be further investigated. In addition, the alkylating pattern of cysteines by NEM showed that only two cysteines, i.e. Cys562 and Cys1193, are not modified by NEM, however, the 28 Å distance between these two cysteines and considering the fact that hAOX1 is a cytosolic enzyme suggests that it is very unlikely that the disturbance of a disulfide bond in the protein upon treatment with DTT would result in the inactivation of the enzyme.

5.4.3.2. FeS Clusters Are Unlikely Affected by Reactive Sulfhydryl

The FeSII in AOXs, coordinated to Cys44, 49, 52 and 74, is known to be unusually solvent accessible (Hartmann, et al. 2012). ESI-MS experiments suggested that the both FeS binding sites might be partially solvent exposed and hence might get disturbed upon treatment with small sulfhydryl containing agents. Circular dichroism (CD) has been successfully used to distinguish the two FeS clusters in *Rc* XDH (Schumann, et al. 2008) where it was reported that the FeSI and FeSII showed maximum CD signals at 470 and 434 nm, respectively. A similar approach was applied for hAOX1 native and treated with DTT, and it was observed that the ratio of the two FeS clusters CD signals did not show a significant difference in the two conditions (see **Figure 4.22.**, panel **A** in section 4.4.3.2.). This suggests that the FeS clusters are unlikely to be disturbed upon treatment with DTT and the alkylation at the FeS binding sites might have only occurred on the apo-enzyme and the iron-devoid species.

The comparison of the CD traces of the DTT treated hAOX1 with the untreated enzyme, presented a divergent feature around 500 to 600 nm. The CD studies on molybdoenzymes is limited, but it seems that this region with the peaks around 550 nm and 580 nm is contributing to the CD signal of Moco (Ryan, et al. 1995). This implies that, unlike FeS clusters, the Moco site of hAOX1 might be significantly affected by DTT.

5.4.3.3. Sulfido Ligand at Moco Is the Most Vulnerable Site to Reactive Sulfhydryl

It has been known since 70s that AOXs get inactivated by a class of agents, including cyanide, known as sulfhydryl inhibitors (Massey and Edmondson 1970). The nomenclature refers to the sulfido ligand coordinated to the Mo center which is disturbed in the presence of this class of inhibitors and the enzyme activity is fully abolished. Previous studies have shown that cyanide is able to remove the sulfido ligand and replace it with an oxo group (Branzoli and Massey 1974;

Massey and Edmondson 1970). Since the sulfido ligand can be chemically removed, it can also be chemically reconstituted, a method used to obtain active mammalian AOXs when expressed heterologously (Foti, et al. 2016; Kucukgoze, et al. 2017). As a sulfhydryl and similarly to cyanide, the sulfido ligand can react with another sulfhydryl group, a reaction through which the treatment with the small sulfhydryl containing agents might have affected the activity of the enzyme. Interestingly, it was observed that the reconstitution of the sulfido ligand in samples treated with 2-ME and DTT recovered the activity of the enzyme up to 20-30 percent similar to the sample treated with cyanide (see **Figure 4.22.**, panel **B** in section 4.4.3.2.). It seems that the inactivation of hAOX1 by small sulfhydryl containing agents involves the sulfido ligand bound to Mo center through a similar mechanism that DTT reduces disulfide bonds to free thiols (see **Figure 5.7.** and **5.8.** for comparison). Moreover, when DCPIP was used as an alternative electron acceptor, the total abolishment of the activity for the sample treated with DTT was consistently observed (see **Figure 4.23.**, panel **B** in section 4.4.4.). DCPIP directly binds at Moco and receives the electron from the sites where they are generated (Hartmann, et al. 2012; VanderJagt, et al. 1986). The similar loss of activity to the reactions where oxygen was used as the electron acceptor further confirmed the involvement of Moco upon inactivation by small sulfhydryl containing agents.

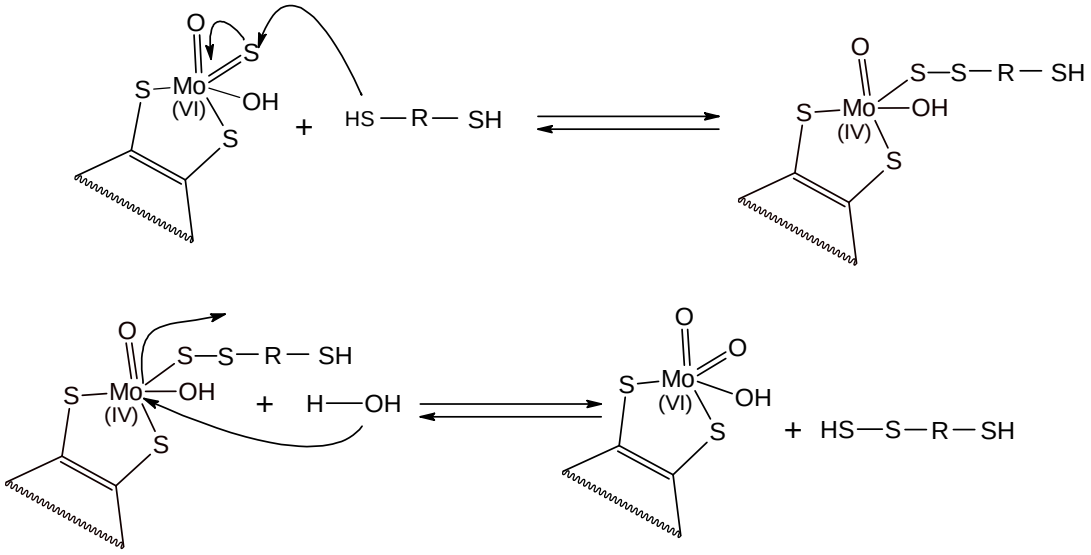

Figure 5.8.: The mechanism of inactivation of Moco in the reaction with small sulfhydryl containing agents: In the first step, the nucleophilic attack of a thiol group on the reducing agent to the sulfido ligand bound at Moco forms a mixed disulfide species. In the second step, the mixed disulfide species is resolved by an electron transfer from a water molecule that forms an inactive oxo-Moco and a persulfide on the reducing agent. R represents the carbon backbone including the hydroxyl groups of DTT, DTE or 2-ME (see **Table 4.12.** for the structures of DTT, DTE and 2-ME).

It is possible that the thiol group of DTT nucleophilically attacks the sulfido ligand bound to Mo and forms a mixed disulfide intermediate (**Figure 5.8.**, first step). This reaction can go further and with the involvement of a water molecule an oxo group replaces the sulfido ligand on Moco, while the mixed disulfide species breaks down to a persulfide-DTT species (**Figure 5.8.**, second step).

Formation of the mixed disulfide-Moco, oxo-Moco and the persulfide-DTT species depends on the redox potential of the species present in the equilibrium. Since the incubation with DTT was an essential step to obtain the crystals of hAOX1 for the structural studies (Coelho, et al. 2015), the presence or absence of the mixed disulfide or oxo-Moco species could be observed in the structure. Unfortunately, the resolutions of the structures available for hAOX1 are not enough to directly visualize the sulfido ligand and hence, the existence of the mixed disulfide-Moco or oxo-Moco species cannot be investigated with the available structural evidences.

5.4.4. DTT Specifically Affects Some of the Members of the Xanthine Oxidase Family

Unlike hAOX1, rabbit liver aldehyde oxidase has been intensively investigated for a potential interconversion between the dehydrogenase and oxidase forms *in vitro* (Turner, et al. 1995). In this study DTT was used as the reducing agent, but no loss of activity has been observed upon treatment with DTT. To further investigate whether the DTT effect was specific to hAOX1, aldehyde oxidases from other species, including the four mouse isoenzymes, mAOX1, mAOX2, mAOX3 and mAOX4, and *E. coli* PaoABC, in parallel with *Rc* XDH and bXO were subjected to DTT treatment. As expected, and consistent with the previous works, DTT did not significantly influence the activity of *Rc* XDH (Leimkuhler, et al. 2003) and bXO (Nishino, et al. 2008), however, different behaviour was observed among AOXs. For hAOX1, mAOX1, mAOX2 and mAOX3 the loss of activity was significant, while mAOX4 seemed only to be slightly affected (see **Figure 4.23.** in section 4.4.4.).

For tracking the change of activity of mAOXs and hAOX1 upon treatment with DTT two electron acceptors, i.e. DCPIP and molecular oxygen, were used (see **Figure 4.23.**, panel **B** in section 4.4.4.). Oxygen is the physiological oxidizing substrate that receives electrons from the FAD site, while DCPIP, a redox dye which is widely used as electron acceptor in biochemical assays (VanderJagt, et al. 1986), is thought to take electrons directly from the Moco site (Hartmann, et al. 2012). In our experiments the specific activities measured with molecular oxygen were 2 to 10 times higher than when DCPIP was used. This implies that the inhibitory effect of DCPIP previously explained for hAOX1 (Foti, et al. 2016) is common among mouse isoenzymes too. Regardless the type of the electron acceptor, a similar pattern for the activity was obtained in the

absence or presence of DTT, i.e. mAOX4 did not show a significant loss of activity upon treatment with DTT, while hAOX1, mAOX1, mAOX2 and mAOX3 were up to 90 to 99 percent inactivated. Given DCPIP receives electrons directly from the Moco site, and the activity is not regained after subsequent removal of DTT from solution, these observations suggest that for hAOX1, mAOX1, mAOX2 and mAOX3, but not for mAOX4, DTT might act as an irreversible or suicide inhibitor by bonding likely at the sites around Moco.

The difeerent behaviour of the rabbit liver AOX reported before (Turner, et al. 1995), mAOX4, PaoABC, bXO and *Rc* XDH in comparison with hAOX1, mAOX1, mAOX2 and mAOX3 upon treatment with DTT can be due to the diverse shape and size of their substrate funnels. It has been shown in the X-ray crystal or modelled structures of bXO (Cao, et al. 2011), *Rc* XDH (Truglio, et al. 2002), and mAOX4 (Terao, et al. 2020) that their substrate funnel is narrow, while hAOX1, mAOX1, mAOX2 and mAOX3 show wider substrate funnel which confers them a broad substrate specificity (Terao, et al. 2020). The wide substrate binding funnel in hAOX1, mAOX1, mAOX2 and mAOX3 can allow sulfhydryl containing agents such as DTT to access the sulfido ligand and provide space for the formation of the mixed disulfide intermediate. PaoABC (Otrelo-Cardoso, et al. 2014) is an exception to this trend by presenting a very wide substrate funnel. It is possible in the case of PaoABC that the accessibility of substrate to Moco is facilitated by the wide funnel so that the mixed disulfide adduct is removed by the substrate. In other words, in PaoABC the substrate and DTT compete for biding at Moco. Another explanation for the different behaviour of XO family members in reaction with DTT can be the different redox potential of their Moco site. DTT exhibits a redox potential in the range of the redox potentials reported for Moco in the XO family members (e.g. compare DTT: -366 mV at pH 8.0 (Cleland 1964) with bXO Mo(IV/V): -355 mV (Barber, et al. 1982b) and with mAOX3 Mo(IV/V): -468 mV (Mahro, et al. 2013) and hAOX1: -476 mV (Dr. Martin Mahro PhD thesis, 2013)). It seems that when the redox potential of the Moco redox active center is significantly more negative than the redox potential of DTT, the enzyme is prone to get inactivated by DTT. Hence, it is likely that the differences between Moco redox potential in different members of the XO family determine the reactivity of the sulfido ligand towards sulfhydryl.

The precise mechanism of the act of DTT on hAOX1 or any other members of the XO family can only be fully elucidated with high resolution crystallographic studies. Overall, it seems that the sulfido ligand at Moco is vulnerable to reactive sulfhydryl groups in AOXs and the level of its vulnerability depends on the accessibility and reactivity determined by the size and shape of the substrate binding funnel and the redox potential of Moco.

6. Conclusion

Previous studies on hAOX1 reported that while the hAOX1-WT enzyme produces 20 percent superoxide, a Leu-to-Val substitution at position 438 results in 75 percent superoxide production (Foti, et al. 2017). Our studies showed that a Leu-to-Ala replacement at this position increased the amount of superoxide to more than 90 percent. Furthermore, the redox titration of the WT enzyme and the L438V variant did not differ in the overall pattern and a semiquinone ($FADH^{\cdot}$) intermediate was not detected for either enzymes (Dr. Alessandro Foti PhD thesis, 2017). This implies that the stabilization of semiquinone is unlikely to be the driving force for generation of superoxide. The crystal structure of the L438V variant in comparison with the WT enzyme showed a slightly wider cavity near the N5 position of FAD (see **Figure 4.19.** in section 4.3.3.), while the other redox centers remained unchanged. Substitution of Leu with Val results in slight alterations of the hydrophobic interactions around the FAD isoalloxazine ring, and hence, it seems unlikely that the redox potential of the $FAD/FADH^{\cdot}$ or $FADH^{\cdot}/FADH_2$ couples to be affected. However, determination of the redox potentials of these species for hAOX1-WT and hAOX1-L438V can allow to further confirm whether the effect of the hydrophobic interaction is indeed minor. The redox potentials can be measured using redox titration methods or EPR measurements. Overall, our results suggest that the type of ROS generated by hAOX1 seems to be determined by the size of the residue at position 438 in proximity to the isoalloxazine N5 position of FAD.

In addition, our studies show that the endogenous ROS produced by hAOX1 inactivate the enzyme. One major effect of ROS is removal of the sulfido ligand from Moco, as has been recently reported (Garrido and Leimkeuhler, manuscript under publication). Here, we demonstrated that the sulfido ligand at Moco is vulnerable under conditions when the enzyme is turning over or when it is anaerobically treated with hydrogen peroxide. Detachment of the sulfido ligand leads to total loss of the activity; however, this is not the only modification that ROS produced by hOAX1 induce in the enzyme. ESI-MS experiments showed that two cysteines, Cys600 and Cys654, were highly and specifically oxidized when exposed to endogenous ROS. Oxidation of these cysteines seems to irreversibly inactivate hAOX1 *in vitro*. Site directed mutagenesis and production of the variants with Cys600 and Cys654 exchanged with alanines may provide evidences to rule out the effects of these cysteines on the activity or stability of hAOX1. Substitution of these cysteines with methionine, a residue highly susceptible to oxidation, and exposing the enzyme to endogenous ROS may further confirm the specific oxidation of the residues in positions 600 and 654. However, the effect of methionine sulfoxide as a neutral species on the enzyme activity might not be similar to

those of cysteine sulfonate ($-SO^-$), sulfinate ($-SO_2^-$) or sulfonate ($-SO_3^-$) as negatively charged modifications.

A similar loss of activity was observed when hAOX1 was incubated with small and uncharged sulfhydryl containing agents such as DTT (see **Figure 4.20.** in section 4.4.2.). When treated with DTT, hAOX1 completely lost its activity. Furthermore, the activity was not recovered after removing DTT. CD and resulfuration experiments suggested that the loss of the activity was due to loss of the sulfido ligand (see **Figure 4.22.** in section 4.4.3.3.). This effect seems to be specific to some AOXs including hAOX1, mAOX1, mAOX2 and mAOX3, but not to mAOX4 or *E. coli* PaoABC (see **Figure 4.23.** in section 4.4.4.). Also, the activity of bXO and *Rc* XDH was not affected in the presence of small uncharged sulfhydryl containing agents. The redox potential of the Moco redox center differs among the members of the XO family. This may lead to different reactivity of the sulfido ligand towards a sulfhydryl group, and hence, determination of the redox potentials of Moco may explain the behaviour of PaoABC, mAOX4, bXO and *Rc* XDH in comparison with hAOX1, mAOX1, mAOX2 and mAOX3 when treated with DTT. In those enzymes which are vulnerable to DTT, it is possible that the sulfhydryl group of DTT reacts with the sulfido ligand and forms a mixed disulfide attached to the Mo center. It is also possible that the sulfido ligand is substituted with an oxo ligand. Either of the mechanisms leads to the total inactivation of the enzyme, however, the precise mechanism cannot be elucidated from the data obtained so far. A high resolution crystal structure with sufficient quality of the electron densities around the sulfido ligand may allow to better explain the mechanism.

As they are ROS producing enzymes, it is not unexpected that AOXs may have evolved an intramolecular ROS responding mechanism. Cysteine residues have been reported to be reversibly modified under physiological or pathological conditions in response to ROS (Claiborne, et al. 1999; Forman, et al. 2017). A cluster of conserved cysteines that locate on a flexible region at the C-terminus of the FeS cluster domain has evolved in some of the eukaryotic AOXs and XDHs (see **Figure 4.1.** in section 4.1.1.). This flexible region carries a highly conserved $CC(X)_{7\text{-}8}CC$ motif in AOXs and XDHs together with a less conserved $C(X)_3C$ motif exclusively found in AOXs. We hypothesized that these cysteine residues might **a)** form a metal binding site and be involved in stabilizing the structure, **b)** provide an interface for interacting with other protein partners or **c)** function as ROS responding elements. Our results show that the cysteines are unlikely to form a metal binding site or to stabilize the structure (see sections 4.1.3. and 4.1.4.). Also, since hAOX1 is localized in the reducing environment of the cytoplasm, it is unlikely for them to form a structural disulfide bond. However, the inactivation of the WT enzyme in comparison with a variant in which

all the cysteines in the region were substituted with alanines (the 6A variant) suggest that at least one cysteine in the region play role in protecting the enzyme during turnover (see section 4.1.5.2.). Similar studies on the variants with different combination of cysteines in the region being exchanged with alanines demonstrated that 4 cysteines, i.e. the single cysteines in the $C(X)_3C$ motif and the second pair of the vicinal cysteines in the $CC(X)_7CC$ motif, exert the protecting role during the enzyme turnover. However, deciphering the mechanism through which the cysteines delay ROS damage to the enzyme requires further investigation. Cysteines are able to get oxidized and form intramolecular short-range disulfides, intermolecular mixed disulfides or short-lived sulfenic acids (-SOH) (see **Figure 5.1.** in section 5.1.8.). Formation of such species can be tracked using mass spectroscopic methods and specific labels such as modified biotin or 1,3-diketon chemical tags that allow detecting of sulfenic acid modifications (Alcock, et al. 2018). Sulfenic acid and disulfide modifications of cysteines are enzymatically reversible processes *in vivo* (Claiborne, et al. 1999; Forman, et al. 2017). This implies that the cellular machinery such as glutaredoxins or thioredoxins which are able to remove these oxidation modifications (Berndt, et al. 2007) could be the potential partners interacting with hAOX1 through the cysteines present in the $C(X)_3C$ and $CC(X)_7CC$ motifs. Furthermore, the $C(X)_3C$ and $CC(X)_{8\text{-}7}CC$ motifs are conserved among the members of the XO family, and hence, similar studies on mouse AOXs or bXO that contain the motifs and on *E. coli* PaoABC and *Rc* XDH that do not contain the motifs may hint on generic roles that the cysteines may play.

Altogether, our studies emphasize the importance of ROS production by hAOX1. ROS not only affect hAOX1 itself, but they may bring a link for understanding the physio-pathological impact of this enzyme on other cellular pathways.

References

Abbasi, Armina, et al.

2019 Time Course of Aldehyde Oxidase and Why It Is Nonlinear. Drug Metabolism and Disposition 47(5):473-483.

Afonine, P. V., et al.

2012 Towards automated crystallographic structure refinement with phenix.refine. Acta Crystallogr D Biol Crystallogr 68(Pt 4):352-67.

Akaba, S., et al.

1999 Production of homo- and hetero-dimeric isozymes from two aldehyde oxidase genes of Arabidopsis thaliana. J Biochem 126(2):395-401.

Alcock, Lisa J., Michael V. Perkins, and Justin M. Chalker

2018 Chemical methods for mapping cysteine oxidation. Chemical Society reviews 47(1):231-268.

Alfaro, Joshua F., and Jeffrey P. Jones

2008 Studies on the Mechanism of Aldehyde Oxidase and Xanthine Oxidase. The Journal of Organic Chemistry 73(23):9469-9472.

Anfinsen, C. B., et al.

1961 The kinetics of formation of native ribonuclease during oxidation of the reduced polypeptide chain. Proceedings of the National Academy of Sciences of the United States of America 47(9):1309-1314.

Barber, M. J., et al.

1980 Electron paramagnetic resonance properties and oxidation-reduction potentials of the molybdenum, flavin, and iron-sulfur centers of chicken liver xanthine dehydrogenase. Arch Biochem Biophys 201(2):468-75.

Barber, M. J., et al.

1982a Properties of the prosthetic groups of rabbit liver aldehyde oxidase: a comparison of molybdenum hydroxylase enzymes. Biochemistry 21(15):3561-8.

Barber, Michael J., et al.

1982b Properties of the prosthetic groups of rabbit liver aldehyde oxidase: a comparison of molybdenum hydroxylase enzymes. Biochemistry 21(15):3561-3568.

Barber, Michael J., and Lewis M. Siegel

1982 Oxidation-reduction potentials of molybdenum, flavin, and iron-sulfur centers in milk xanthine oxidase: variation with pH. Biochemistry 21(7):1638-1647.

Baron, Riccardo, et al.

2009 Multiple pathways guide oxygen diffusion into flavoenzyme active sites. Proceedings of the National Academy of Sciences 106(26):10603-10608.

Bendotti, Caterina, et al.

1997 Selective localization of mouse aldehyde oxidase mRNA in the choroid plexus and motor neurons. NeuroReport 8(9):2343-2349.

Berndt, C., C. H. Lillig, and A. Holmgren

2007 Thiol-based mechanisms of the thioredoxin and glutaredoxin systems: implications for diseases in the cardiovascular system. Am J Physiol Heart Circ Physiol 292(3):H1227-36.
Bertani, G.

1951 Studies on lysogenesis. I. The mode of phage liberation by lysogenic Escherichia coli. Journal of bacteriology 62(3):293-300.
Betcher-Lange, S. L., M. P. Coughlan, and K. V. Rajagopalan

1979 Syncatalytic modification of chicken liver xanthine dehydrogenase by hydrogen peroxide. The nature of the reaction. J Biol Chem 254(18):8825-9.
Branzoli, U., and V. Massey

1974 Evidence for an active site persulfide residue in rabbit liver aldehyde oxidase. The Journal of biological chemistry 249(14):4346-4349.
Burén, Stefan, et al.

2020 Biosynthesis of Nitrogenase Cofactors. Chemical Reviews 120(12):4921-4968.
Cao, H., J. Hall, and R. Hille

2011 X-ray crystal structure of arsenite-inhibited xanthine oxidase: μ-sulfido,μ-oxo double bridge between molybdenum and arsenic in the active site. J Am Chem Soc 133(32):12414-7.
Chaiyen, P., M. W. Fraaije, and A. Mattevi

2012 The enigmatic reaction of flavins with oxygen. Trends Biochem Sci 37(9):373-80.
Claiborne, A., and I. Fridovich

1979 Purification of the o-dianisidine peroxidase from Escherichia coli B. Physicochemical characterization and analysis of its dual catalatic and peroxidatic activities. J Biol Chem 254(10):4245-52.
Claiborne, A., et al.

1999 Protein-sulfenic acids: diverse roles for an unlikely player in enzyme catalysis and redox regulation. Biochemistry 38(47):15407-16.
Clegg, Simon L., and Peter Brimblecombe

1990 The solubility and activity coefficient of oxygen in salt solutions and brines. Geochimica et Cosmochimica Acta 54(12):3315-3328.
Cleland, W. W.

1964 Dithiothreitol, a New Protective Reagent for SH Groups*. Biochemistry 3(4):480-482.
Coelho, C., et al.

2015 Structural insights into xenobiotic and inhibitor binding to human aldehyde oxidase. Nat Chem Biol 11(10):779-83.
Coelho, Catarina, et al.

2012 The first mammalian aldehyde oxidase crystal structure: insights into substrate specificity. The Journal of biological chemistry 287(48):40690-40702.
Corran, H. S., et al.

1939 Xanthine oxidase and milk flavoprotein: With an Addendum by J. St L. Philpot. Biochem J 33(10):1694-708.
Davies, Michael J.

2016 Protein oxidation and peroxidation. The Biochemical journal 473(7):805-825.

Davis, I. W., et al.

2007 MolProbity: all-atom contacts and structure validation for proteins and nucleic acids. Nucleic Acids Res 35(Web Server issue):W375-83.

Ellis, John E.

2003 Metal Carbonyl Anions: from [Fe(CO)4]2- to [Hf(CO)6]2- and Beyond. Organometallics 22(17):3322-3338.

Emsley, P., et al.

2010 Features and development of Coot. Acta Crystallogr D Biol Crystallogr 66(Pt 4):486-501.

Evans, P. R., and G. N. Murshudov

2013 How good are my data and what is the resolution? Acta Crystallogr D Biol Crystallogr 69(Pt 7):1204-14.

Finnegan, S., et al.

2010 Role of valine 464 in the flavin oxidation reaction catalyzed by choline oxidase. Biochemistry 49(13):2952-61.

Forman, H. J., et al.

2017 Protein cysteine oxidation in redox signaling: Caveats on sulfenic acid detection and quantification. Arch Biochem Biophys 617:26-37.

Forneris, Federico, et al.

2009 ThermoFAD, a Thermofluor®-adapted flavin ad hoc detection system for protein folding and ligand binding. The FEBS Journal 276(10):2833-2840.

Foti, A., F. Dorendorf, and S. Leimkühler

2017 A single nucleotide polymorphism causes enhanced radical oxygen species production by human aldehyde oxidase. PLoS One 12(7):e0182061.

Foti, A., et al.

2016 Optimization of the Expression of Human Aldehyde Oxidase for Investigations of Single-Nucleotide Polymorphisms. Drug Metab Dispos 44(8):1277-85.

Gadda, Giovanni

2012 Oxygen Activation in Flavoprotein Oxidases: The Importance of Being Positive. Biochemistry 51(13):2662-2669.

Garattini, E., et al.

2003 Mammalian molybdo-flavoenzymes, an expanding family of proteins: structure, genetics, regulation, function and pathophysiology. Biochem J 372(Pt 1):15-32.

Gordon, A. H., D. E. Green, and V. Subrahmanyan

1940 Liver aldehyde oxidase. Biochem J 34(5):764-74.

Graessler, J., and S. Fischer

2007 The dual substrate specificity of aldehyde oxidase 1 for retinal and acetaldehyde and its role in ABCA1 mediated efflux. Horm Metab Res 39(11):775-6.

Gray, Harry B., and Jay R. Winkler

2018 Living with Oxygen. Accounts of chemical research 51(8):1850-1857.

Hanahan, Douglas

1983 Studies on transformation of Escherichia coli with plasmids. Journal of Molecular Biology 166(4):557-580.
Harding, Marjorie M., Matthew W. Nowicki, and Malcolm D. Walkinshaw

2010 Metals in protein structures: a review of their principal features. Crystallography Reviews 16(4):247-302.
Hartmann, Tobias, et al.

2012 The Impact of SNPs on Human Aldehyde Oxidase. Drug Metabolism and Disposition:dmd.111.043828.
Hernández-Ortega, A., et al.

2011 Modulating O2 reactivity in a fungal flavoenzyme: involvement of aryl-alcohol oxidase Phe-501 contiguous to catalytic histidine. J Biol Chem 286(47):41105-14.
Hille, R., and V. Massey

1981 Studies on the oxidative half-reaction of xanthine oxidase. J Biol Chem 256(17):9090-5.
—

1986 The equilibration of reducing equivalents within milk xanthine oxidase. J Biol Chem 261(3):1241-7.
Hille, Russ

1996 The Mononuclear Molybdenum Enzymes. Chemical Reviews 96(7):2757-2816.
—

2002 Molybdenum and tungsten in biology. Trends in Biochemical Sciences 27(7):360-367.
Hille, Russ, James Hall, and Partha Basu

2014 The Mononuclear Molybdenum Enzymes. Chemical Reviews 114(7):3963-4038.
Householder, Alston S., and George Gomori

1943 The kinetics of enzyme inactivation. The bulletin of mathematical biophysics 5(3):83-90.
Huang, D. Y., A. Furukawa, and Y. Ichikawa

1999 Molecular cloning of retinal oxidase/aldehyde oxidase cDNAs from rabbit and mouse livers and functional expression of recombinant mouse retinal oxidase cDNA in Escherichia coli. Arch Biochem Biophys 364(2):264-72.
Hwang, Christopher, Anthony J. Sinskey, and Harvey F. Lodish

1992 Oxidized Redox State of Glutathione in the Endoplasmic Reticulum. Science 257(5076):1496-1502.
Ichida, K., et al.

2001 Mutation of human molybdenum cofactor sulfurase gene is responsible for classical xanthinuria type II. Biochem Biophys Res Commun 282(5):1194-200.
Igo, Robert P., and Bruce Mackler

1960 Liver aldehyde oxidase: A form of xanthine oxidase. Biochimica et Biophysica Acta 44:310-314.
Jocelyn, P. C.

1967 The Standard Redox Potential of Cysteine-Cystine from the Thiol-Disulphide Exchange Reaction with Glutathione and Lipoic Acid. European Journal of Biochemistry 2(3):327-331.
Johnson, J. L., B. E. Hainline, and K. V. Rajagopalan

1980 Characterization of the molybdenum cofactor of sulfite oxidase, xanthine, oxidase, and nitrate reductase. Identification of a pteridine as a structural component. J Biol Chem 255(5):1783-6.
Johnson, J. L., et al.

1984 The pterin component of the molybdenum cofactor. Structural characterization of two fluorescent derivatives. J Biol Chem 259(9):5414-22.
Jordan, I. King, et al.

2005 A universal trend of amino acid gain and loss in protein evolution. Nature 433(7026):633-638.
Kabsch, W.

2010 XDS. Acta Crystallogr D Biol Crystallogr 66(Pt 2):125-32.
Karala, A. R., A. K. Lappi, and L. W. Ruddock

2010 Modulation of an active-site cysteine pKa allows PDI to act as a catalyst of both disulfide bond formation and isomerization. J Mol Biol 396(4):883-92.
Kelly, S. M., T. J. Jess, and N. C. Price

2005 How to study proteins by circular dichroism. Biochim Biophys Acta 1751(2):119-39.
Kelly, S. M., and N. C. Price

2000 The use of circular dichroism in the investigation of protein structure and function. Curr Protein Pept Sci 1(4):349-84.
Klug, Dina, Joseph Rabani, and Irwin Fridovich

1972 A Direct Demonstration of the Catalytic Action of Superoxide Dismutase through the Use of Pulse Radiolysis. Journal of Biological Chemistry 247(15):4839-4842.
Knox, W. Eugene, and William I. Grossman

1948 The Location of the Reactive Carbon in N1-Methylnicotinamide. Journal of the American Chemical Society 70(6):2172-2172.
Koiwai, H., et al.

2004 Tissue-specific localization of an abscisic acid biosynthetic enzyme, AAO3, in Arabidopsis. Plant Physiol 134(4):1697-707.
Kramer, S. P., et al.

1987 The structure of the molybdenum cofactor. Characterization of di-(carboxamidomethyl)molybdopterin from sulfite oxidase and xanthine oxidase. J Biol Chem 262(34):16357-63.
Kucukgoze, G., et al.

2017 Direct Comparison of the Enzymatic Characteristics and Superoxide Production of the Four Aldehyde Oxidase Enzymes Present in Mouse. Drug Metab Dispos 45(8):947-955.
Kurosaki, Mami, et al.

2013 Structure and evolution of vertebrate aldehyde oxidases: from gene duplication to gene suppression. Cellular and Molecular Life Sciences 70(10):1807-1830.
Laemmli, U. K.

1970 Cleavage of structural proteins during the assembly of the head of bacteriophage T4. Nature 227(5259):680-5.
Lancaster, Kyle M., et al.

2011 X-ray emission spectroscopy evidences a central carbon in the nitrogenase iron-molybdenum cofactor. Science (New York, N.Y.) 334(6058):974-977.
Lange, Rolf, Hans Staaland, and Arvid Mostad

1972 The effect of salinity and temperature on solubility of oxygen and respiratory rate in oxygen-dependent marine invertebrates. Journal of Experimental Marine Biology and Ecology 9(3):217-229.
Leferink, Nicole G. H., et al.

2009 Identification of a Gatekeeper Residue That Prevents Dehydrogenases from Acting as Oxidases*♦. Journal of Biological Chemistry 284(7):4392-4397.
Leimkuhler, S., et al.

2003 Recombinant Rhodobacter capsulatus xanthine dehydrogenase, a useful model system for the characterization of protein variants leading to xanthinuria I in humans. J Biol Chem 278(23):20802-11.
Liang, Xinwen, et al.

2012 Characterization of methionine oxidation and methionine sulfoxide reduction using methionine-rich cysteine-free proteins. BMC Biochemistry 13(1):21.
Lynch, R. E., and I. Fridovich

1979 Autoinactivation of xanthine oxidase: the role of superoxide radical and hydrogen peroxide. Biochim Biophys Acta 571(2):195-200.
Mackler, B., H. R. Mahler, and D. E. Green

1954 Studies on metalloflavoproteins. I. Xanthine oxidase, a molybdoflavoprotein. J Biol Chem 210(1):149-64.
Mackler, Bruce, Marilyn L. Cowger, and Robert P. Igo

1961 Liver aldehyde oxidase: Relation to the electron transport systems. Biochimica et Biophysica Acta 52(1):203-205.
Mahler, H. R., B. Mackler, and D. E. Green

1954 Studies on metalloflavoproteins. III. Aldehyde oxidase: a molybdoflavoprotein. J Biol Chem 210(1):465-80.
Mahro, Martin, et al.

2013 Identification of Crucial Amino Acids in Mouse Aldehyde Oxidase 3 That Determine Substrate Specificity. PLOS ONE 8(12):e82285.
Mahro, Martin, et al.

2011 Characterization and crystallization of mouse Aldehyde Oxidase 3 (mAOX3): from mouse liver to E. coli heterologous protein expression. Drug Metabolism and Disposition:dmd.111.040873.
Marino, S. M., and V. N. Gladyshev

2010 Cysteine function governs its conservation and degeneration and restricts its utilization on protein surfaces. J Mol Biol 404(5):902-16.
Massey, V., and D. Edmondson

1970 On the mechanism of inactivation of xanthine oxidase by cyanide. J Biol Chem 245(24):6595-8.
Mattevi, A.

2006 To be or not to be an oxidase: challenging the oxygen reactivity of flavoenzymes. Trends Biochem Sci 31(5):276-83.
McCord, J. M., and I. Fridovich

1969 Superoxide dismutase. An enzymic function for erythrocuprein (hemocuprein). J Biol Chem 244(22):6049-55.
McCoy, A. J., et al.

2007 Phaser crystallographic software. J Appl Crystallogr 40(Pt 4):658-674.
Messner, Kevin R., and James A. Imlay

2002 Mechanism of Superoxide and Hydrogen Peroxide Formation by Fumarate Reductase, Succinate Dehydrogenase, and Aspartate Oxidase*. Journal of Biological Chemistry 277(45):42563-42571.
Min, X., et al.

2000 Molecular cloning and expression patterns of three putative functional aldehyde oxidase genes and isolation of two aldehyde oxidase pseudogenes in tomato. Biochim Biophys Acta 1493(3):337-41.
Miseta, Attila, and Peter Csutora

2000 Relationship Between the Occurrence of Cysteine in Proteins and the Complexity of Organisms. Molecular Biology and Evolution 17(8):1232-1239.
Mota, Cristiano, et al.

2018 Critical overview on the structure and metabolism of human aldehyde oxidase and its role in pharmacokinetics. Coordination Chemistry Reviews 368:35-59.
Mota, Cristiano, et al.

2019 Human aldehyde oxidase (hAOX1): structure determination of the Moco-free form of the natural variant G1269R and biophysical studies of single nucleotide polymorphisms. FEBS open bio 9(5):925-934.
Myers, Rollie J.

1986 The new low value for the second dissociation constant for H2S: Its history, its best value, and its impact on the teaching of sulfide equilibria. Journal of Chemical Education 63(8):687.
Neumann, Meina, and Silke Leimkühler

2008 Heavy metal ions inhibit molybdoenzyme activity by binding to the dithiolene moiety of molybdopterin in Escherichia coli. The FEBS Journal 275(22):5678-5689.
Nishino, T., et al.

2008 Mammalian xanthine oxidoreductase - mechanism of transition from xanthine dehydrogenase to xanthine oxidase. Febs j 275(13):3278-89.
Nishino, Takeshi, and Ken Okamoto

2000 The role of the [2Fe–2S] cluster centers in xanthine oxidoreductase. Journal of Inorganic Biochemistry 82(1):43-49.
Omarov, Rustem T., et al.

1999 Aldehyde oxidase in roots, leaves and seeds of barley (Hordeum vulgare L.). Journal of Experimental Botany 50(330):63-69.
Otrelo-Cardoso, Ana Rita, et al.

2014 Structural data on the periplasmic aldehyde oxidoreductase PaoABC from Escherichia coli: SAXS and preliminary X-ray crystallography analysis. International journal of molecular sciences 15(2):2223-2236.

Pace, Nicholas J., and Eranthie Weerapana

2013 Diverse Functional Roles of Reactive Cysteines. ACS Chemical Biology 8(2):283-296.

—

2014 Zinc-binding cysteines: diverse functions and structural motifs. Biomolecules 4(2):419-434.

Palmer, Tracy, et al.

1996 Involvement of the narJ and mob gene products in distinct steps in the biosynthesis of the molybdoenzyme nitrate reductase in Escherichia coli. Molecular Microbiology 20(4):875-884.

Pateman, J. A., et al.

1964 A Common Co-Factor for Nitrate Reductase and Xanthine Dehydrogenase which also Regulates the Synthesis of Nitrate Reductase. Nature 201(4914):58-60.

Pe'er, I., et al.

2004 Proteomic signatures: amino acid and oligopeptide compositions differentiate among phyla. Proteins 54(1):20-40.

Pennati, Andrea, and Giovanni Gadda

2011 Stabilization of an Intermediate in the Oxidative Half-Reaction of Human Liver Glycolate Oxidase. Biochemistry 50(1):1-3.

Poole, Leslie B.

2015 The basics of thiols and cysteines in redox biology and chemistry. Free Radical Biology and Medicine 80:148-157.

Porras, A. G., J. S. Olson, and G. Palmer

1981 The reaction of reduced xanthine oxidase with oxygen. Kinetics of peroxide and superoxide formation. Journal of Biological Chemistry 256(17):9096-9103.

Rajagopalan, K. V., I. Fridovich, and P. Handler

1962 Hepatic aldehyde oxidase. I. Purification and properties. J Biol Chem 237:922-8.

Rajagopalan, K. V., et al.

1968 Studies of aldehyde oxidase by electron paramagnetic resonance spectroscopy. I. Spectra at equilibrium states. J Biol Chem 243(14):3784-96.

Reis, Joana, et al.

2020 A closer look into NADPH oxidase inhibitors: Validation and insight into their mechanism of action. Redox Biology 32:101466.

Rodrigues, Diogo, et al.

2014 Production of Recombinant Human Aldehyde Oxidase in Escherichia coli and Optimization of Its Application for the Preparative Synthesis of Oxidized Drug Metabolites. ChemCatChem 6(4):1028-1042.

Rodriguez-Trelles, F., R. Tarrio, and F. J. Ayala

2003 Convergent neofunctionalization by positive Darwinian selection after ancient recurrent duplications of the xanthine dehydrogenase gene. Proc Natl Acad Sci U S A 100(23):13413-7.

Romão, M. J., et al.

1995 Crystal structure of the xanthine oxidase-related aldehyde oxido-reductase from D. gigas. Science 270(5239):1170-6.
Ryan, M. G., K. Ratnam, and R. Hille

1995 The molybdenum centers of xanthine oxidase and xanthine dehydrogenase. Determination of the spectral change associated with reduction from the Mo(VI) to the Mo(IV) state. J Biol Chem 270(33):19209-12.
Rychlik, W., W. J. Spencer, and R. E. Rhoads

1990 Optimization of the annealing temperature for DNA amplification in vitro. Nucleic Acids Res 18(21):6409-12.
Saam, J., et al.

2010 O2 reactivity of flavoproteins: dynamic access of dioxygen to the active site and role of a H+ relay system in D-amino acid oxidase. J Biol Chem 285(32):24439-46.
Schumann, S., et al.

2008 The mechanism of assembly and cofactor insertion into Rhodobacter capsulatus xanthine dehydrogenase. J Biol Chem 283(24):16602-11.
Schumann, Silvia, et al.

2009 Site Directed Mutagenesis of Amino Acid Residues at the Active Site of Mouse Aldehyde Oxidase AOX1. PLOS ONE 4(4):e5348.
Schwarz, Günter, Ralf R. Mendel, and Markus W. Ribbe

2009 Molybdenum cofactors, enzymes and pathways. Nature 460(7257):839-847.
Seo, M., et al.

2000a The Arabidopsis aldehyde oxidase 3 (AAO3) gene product catalyzes the final step in abscisic acid biosynthesis in leaves. Proc Natl Acad Sci U S A 97(23):12908-13.
Seo, Mitsunori, et al.

2000b Abscisic aldehyde oxidase in leaves of Arabidopsis thaliana. The Plant Journal 23(4):481-488.
Sherry, S. T., et al.

2001 dbSNP: the NCBI database of genetic variation. Nucleic Acids Res 29(1):308-11.
Shetty, V., D. S. Spellman, and T. A. Neubert

2007 Characterization by tandem mass spectrometry of stable cysteine sulfenic acid in a cysteine switch peptide of matrix metalloproteinases. J Am Soc Mass Spectrom 18(8):1544-51.
Sigruener, A., et al.

2007 Human aldehyde oxidase 1 interacts with ATP-binding cassette transporter-1 and modulates its activity in hepatocytes. Horm Metab Res 39(11):781-9.
Spatzal, T., et al.

2011 Evidence for interstitial carbon in nitrogenase FeMo cofactor. Science 334(6058):940.
Srivastava, Sudhakar, et al.

2017 Aldehyde Oxidase 4 Plays a Critical Role in Delaying Silique Senescence by Catalyzing Aldehyde Detoxification. Plant Physiology 173(4):1977.
Stirpe, F., and E. Della Corte

1969 The regulation of rat liver xanthine oxidase. Conversion in vitro of the enzyme activity from dehydrogenase (type D) to oxidase (type O). J Biol Chem 244(14):3855-63.
Terada, L. S., et al.

1991 Inactivation of xanthine oxidase by hydrogen peroxide involves site-directed hydroxyl radical formation. Free Radic Biol Med 10(1):61-8.
Terao, M., et al.

2020 Evolution, expression, and substrate specificities of aldehyde oxidase enzymes in eukaryotes. J Biol Chem 295(16):5377-5389.
Terao, Mineko, et al.

2009 Role of the Molybdoflavoenzyme Aldehyde Oxidase Homolog 2 in the Biosynthesis of Retinoic Acid: Generation and Characterization of a Knockout Mouse. Molecular and Cellular Biology 29(2):357.
TERAO, Mineko, et al.

1998 Isolation and characterization of the human aldehyde oxidase gene: conservation of intron/exon boundaries with the xanthine oxidoreductase gene indicates a common origin. Biochemical Journal 332(2):383-393.
Terao, Mineko, et al.

2016 Structure and function of mammalian aldehyde oxidases. Archives of Toxicology 90(4):753-780.
Truglio, J. J., et al.

2002 Crystal structures of the active and alloxanthine-inhibited forms of xanthine dehydrogenase from Rhodobacter capsulatus. Structure 10(1):115-25.
Turner, N. A., et al.

1995 Properties of rabbit liver aldehyde oxidase and the relationship of the enzyme to xanthine oxidase and dehydrogenase. Eur J Biochem 232(2):646-57.
Uchida, H., et al.

2018 Crystal structure of an aldehyde oxidase from Methylobacillus sp. KY4400. J Biochem 163(4):321-328.
Uversky, Vladimir N.

2013 The alphabet of intrinsic disorder: II. Various roles of glutamic acid in ordered and intrinsically disordered proteins. Intrinsically disordered proteins 1(1):e24684-e24684.
VanderJagt, D. J., P. J. Garry, and W. C. Hunt

1986 Ascorbate in plasma as measured by liquid chromatography and by dichlorophenolindophenol colorimetry. Clin Chem 32(6):1004-6.
Wagner, T., et al.

2017 Methanogenic heterodisulfide reductase (HdrABC-MvhAGD) uses two noncubane [4Fe-4S] clusters for reduction. Science 357(6352):699-703.
Wahl, R. C., et al.

1982 Drosophila melanogaster ma-l mutants are defective in the sulfuration of desulfo Mo hydroxylases. J Biol Chem 257(7):3958-62.
Waldron, Kevin J., et al.

2009 Metalloproteins and metal sensing. Nature 460(7257):823-830.

Wiedemann, Christoph, et al.

2020 Cysteines and Disulfide Bonds as Structure-Forming Units: Insights From Different Domains of Life and the Potential for Characterization by NMR. Frontiers in Chemistry 8(280).

Xia, M., R. Dempski, and R. Hille

1999 The reductive half-reaction of xanthine oxidase. Reaction with aldehyde substrates and identification of the catalytically labile oxygen. J Biol Chem 274(6):3323-30.

Yamamoto, T., et al.

2003 Identification of a new point mutation in the human molybdenum cofactor sulferase gene that is responsible for xanthinuria type II. Metabolism 52(11):1501-4.

Yergaliyev, Timur M., et al.

2016 The involvement of ROS producing aldehyde oxidase in plant response to Tombusvirus infection. Plant physiology and biochemistry : PPB 109:36-44.

Zheng, Lei, Ulrich Baumann, and Jean-Louis Reymond

2004 An efficient one-step site-directed and site-saturation mutagenesis protocol. Nucleic acids research 32(14):e115-e115.

Appendix

Figure A1: Hill versus Michaelis Menten fit for the variants generated to study the flexible region containing cysteines (see **Table A5** for the details of the fitting values)

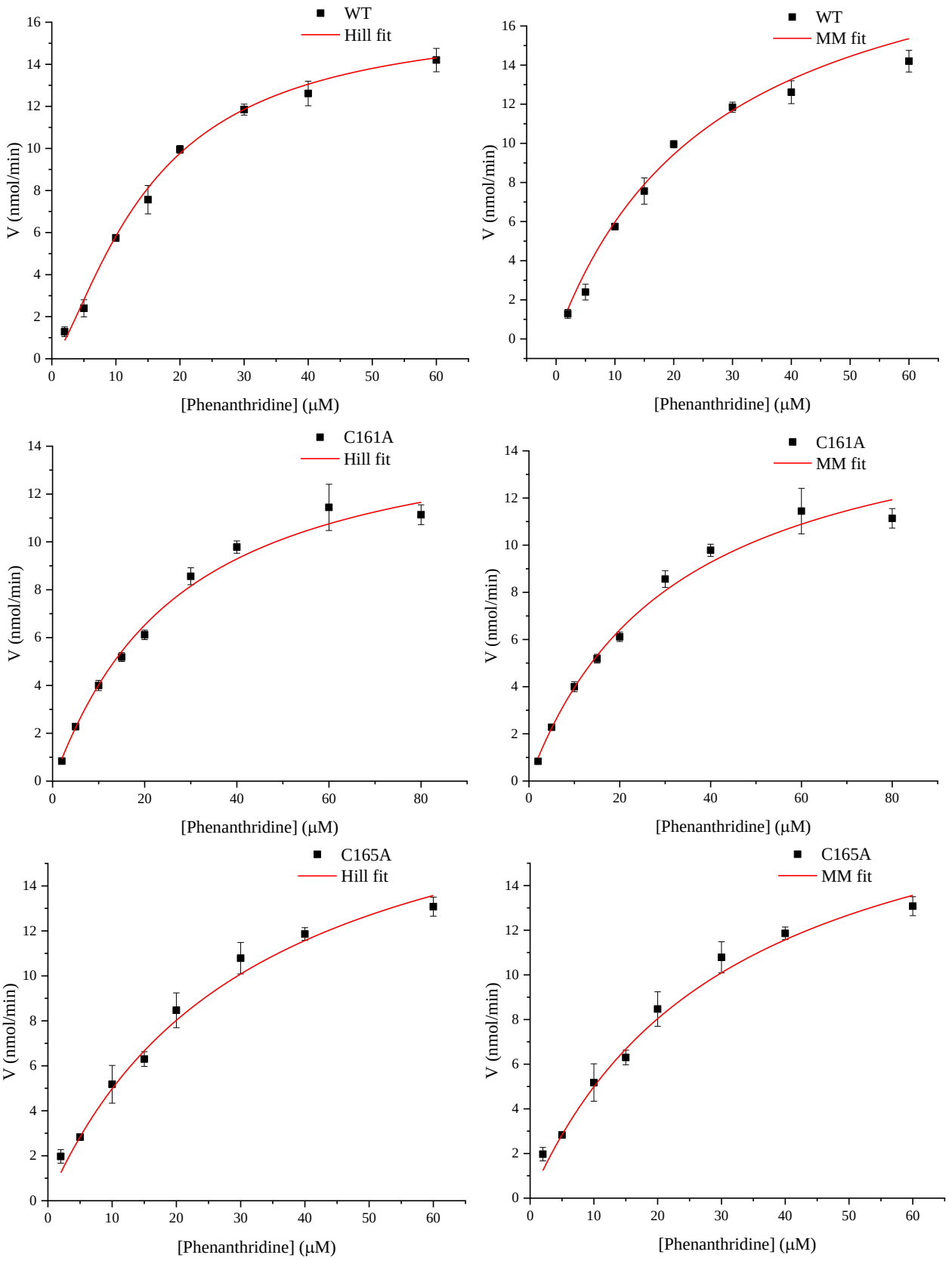

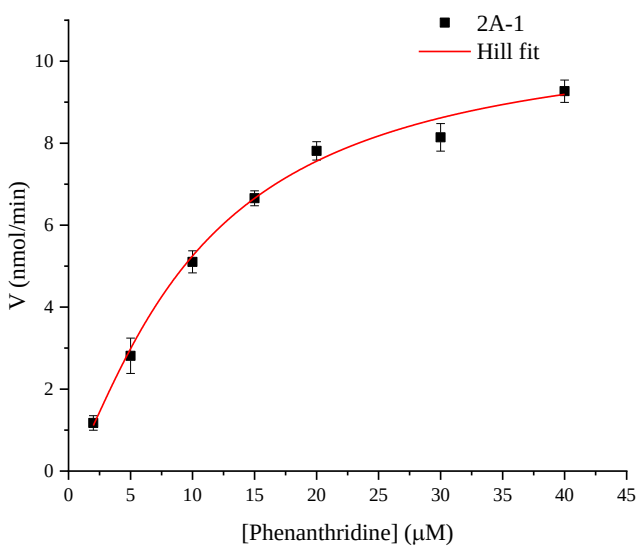
2A-1
Hill fit
V (nmol/min)
[Phenanthridine] (μM)

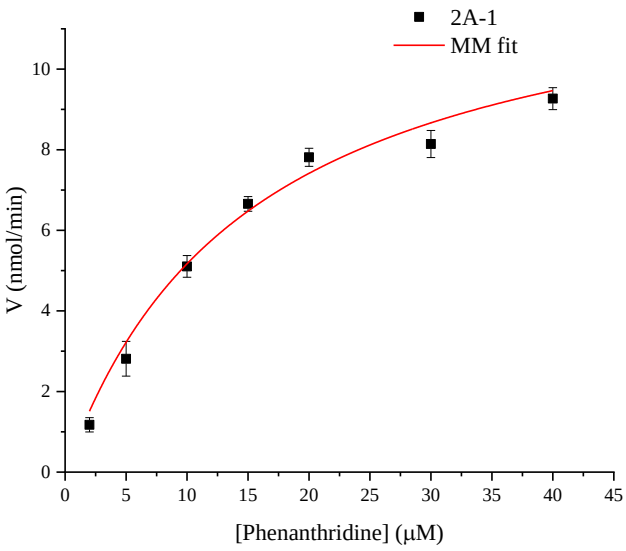
2A-1
MM fit
V (nmol/min)
[Phenanthridine] (μM)

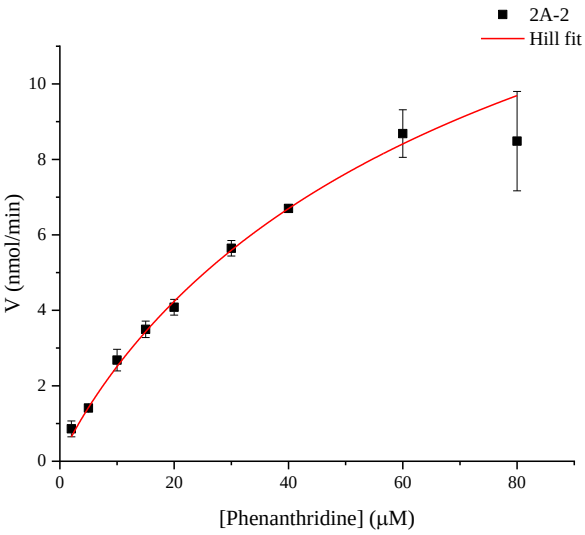
2A-2
Hill fit
V (nmol/min)
[Phenanthridine] (μM)

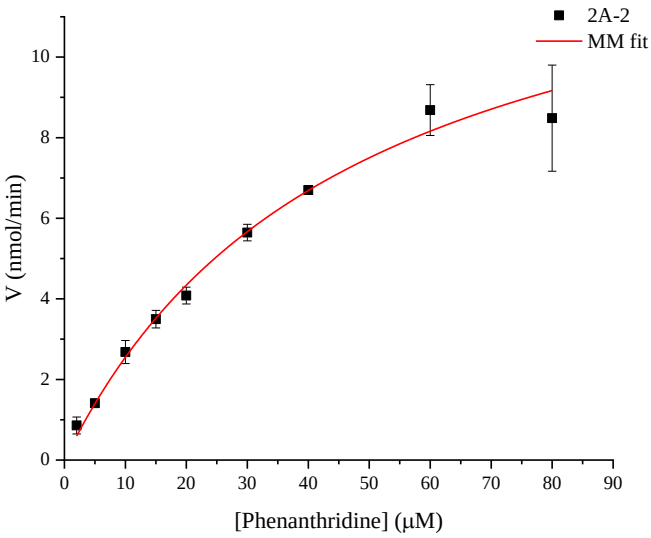
2A-2
MM fit
V (nmol/min)
[Phenanthridine] (μM)

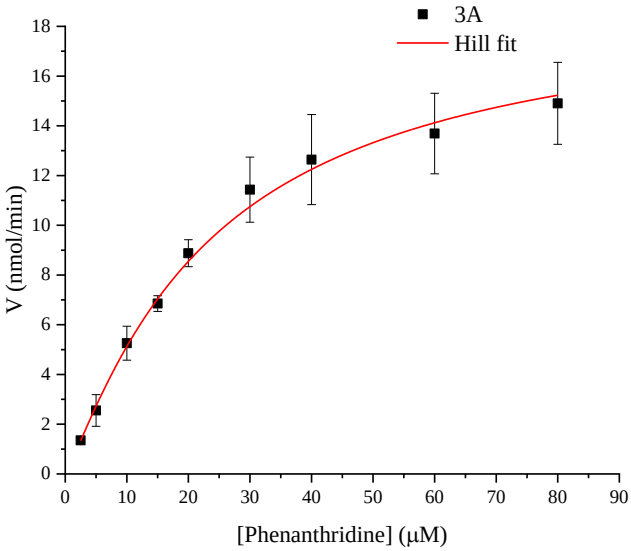
3A
Hill fit
V (nmol/min)
[Phenanthridine] (μM)

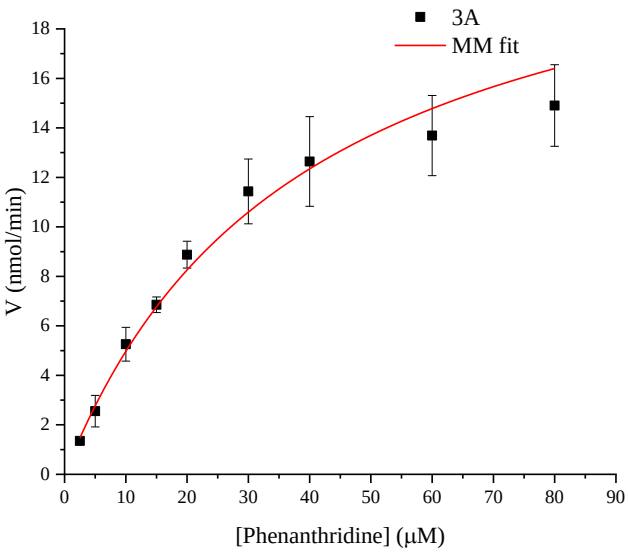
3A
MM fit
V (nmol/min)
[Phenanthridine] (μM)

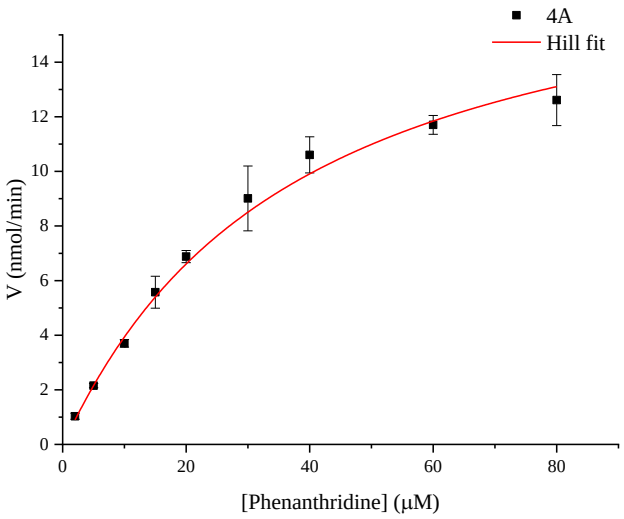
4A
Hill fit
V (nmol/min)
[Phenanthridine] (μM)

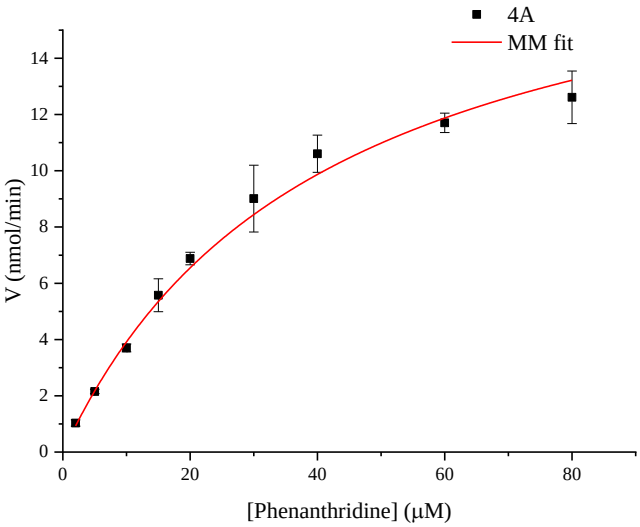
4A
MM fit
V (nmol/min)
[Phenanthridine] (μM)

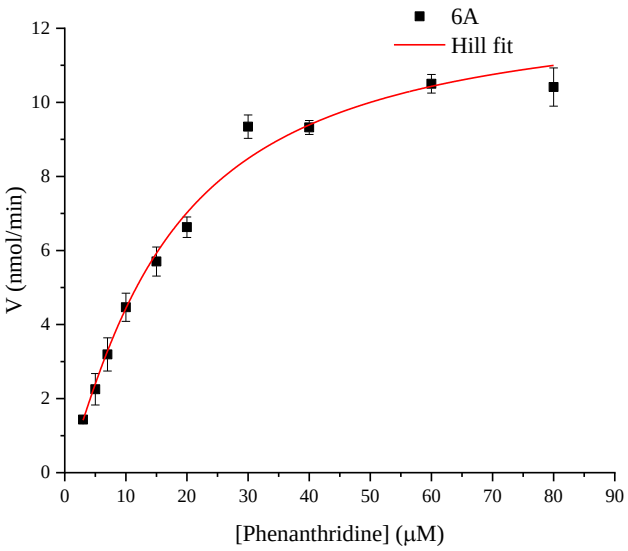
6A
Hill fit
V (nmol/min)
[Phenanthridine] (μM)

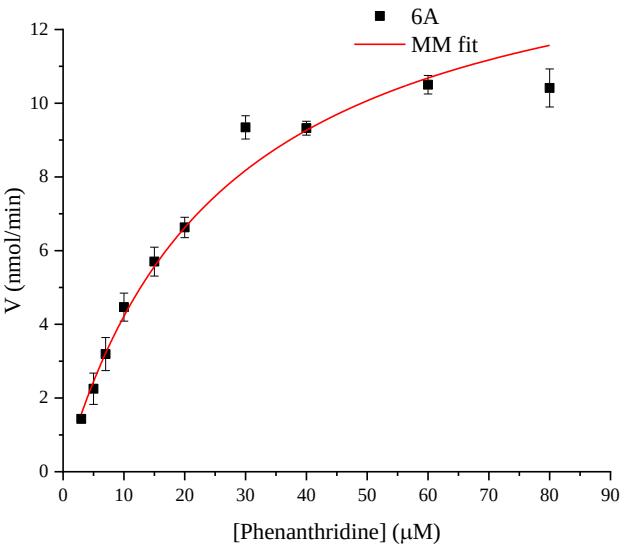
6A
MM fit
V (nmol/min)
[Phenanthridine] (μM)

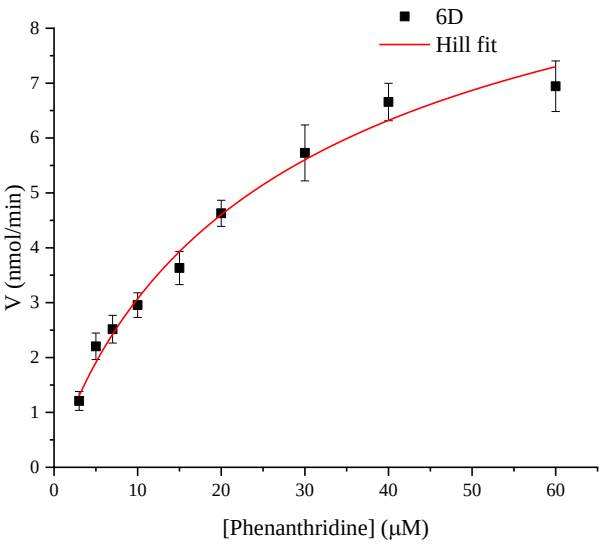
6D
Hill fit
V (nmol/min)
[Phenanthridine] (μM)

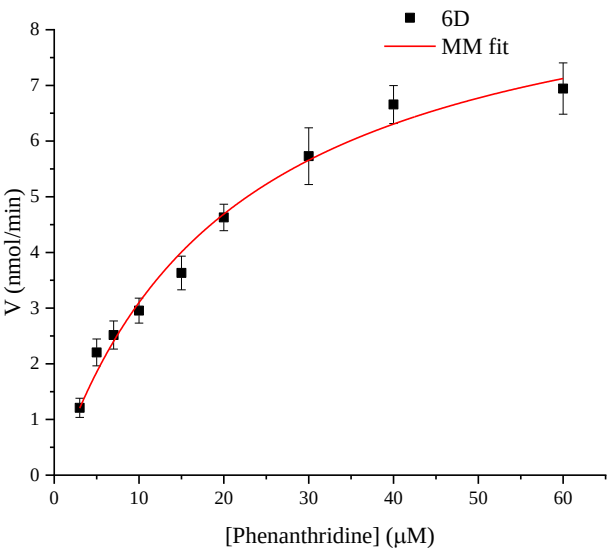
6D
MM fit
V (nmol/min)
[Phenanthridine] (μM)

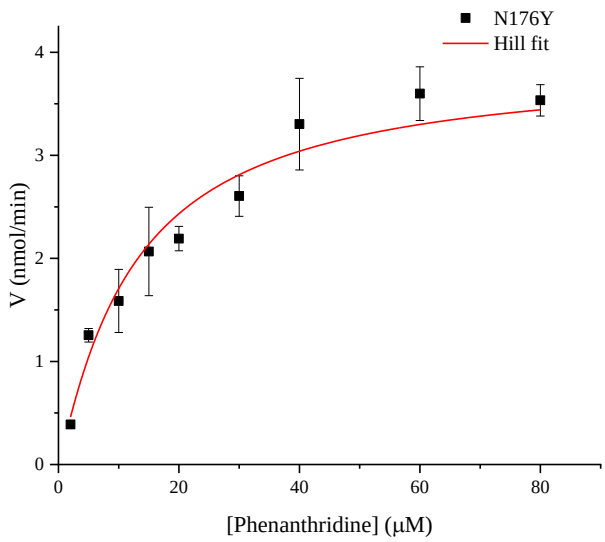
N176Y
Hill fit
V (nmol/min)
[Phenanthridine] (μM)

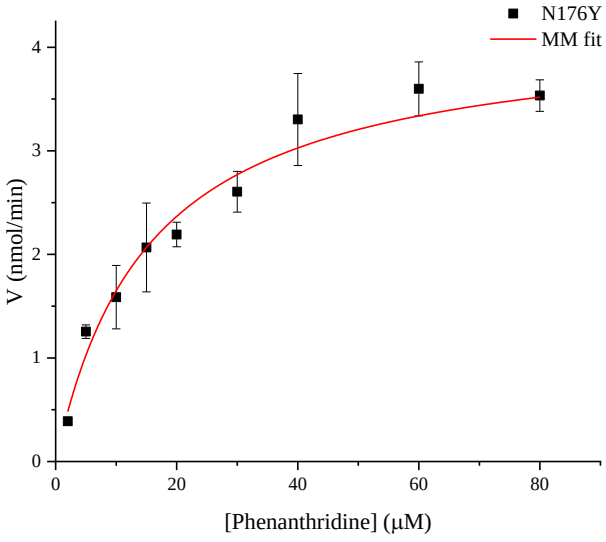
N176Y
MM fit
V (nmol/min)
[Phenanthridine] (μM)

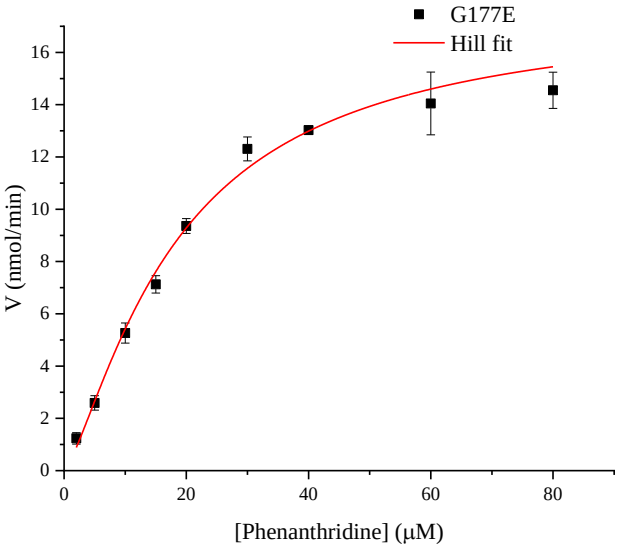
G177E
Hill fit
V (nmol/min)
[Phenanthridine] (μM)

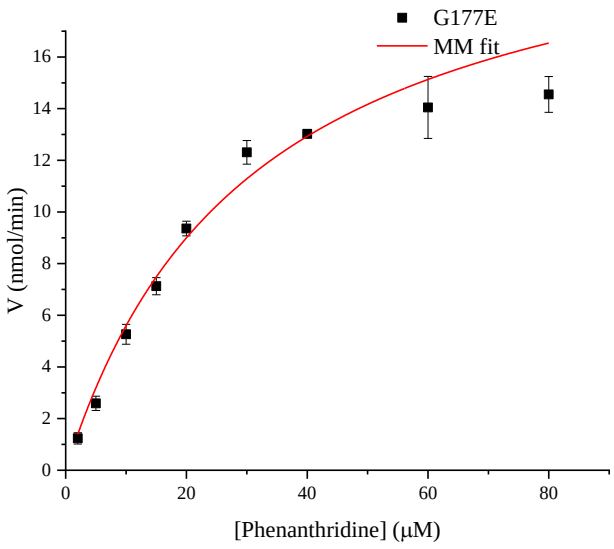
G177E
MM fit
V (nmol/min)
[Phenanthridine] (μM)

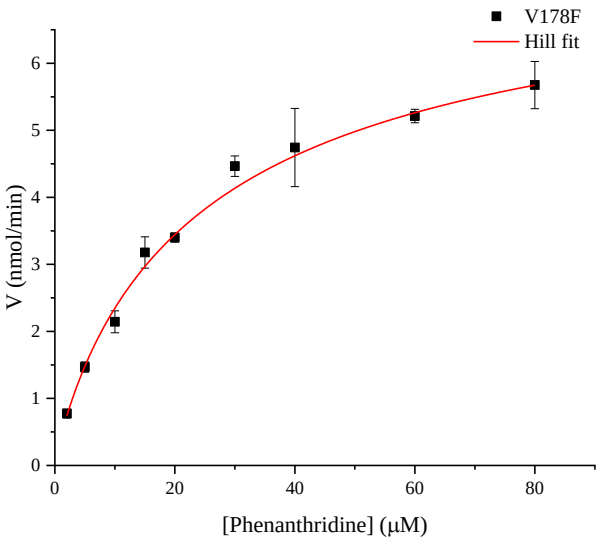
V178F
Hill fit
V (nmol/min)
[Phenanthridine] (μM)

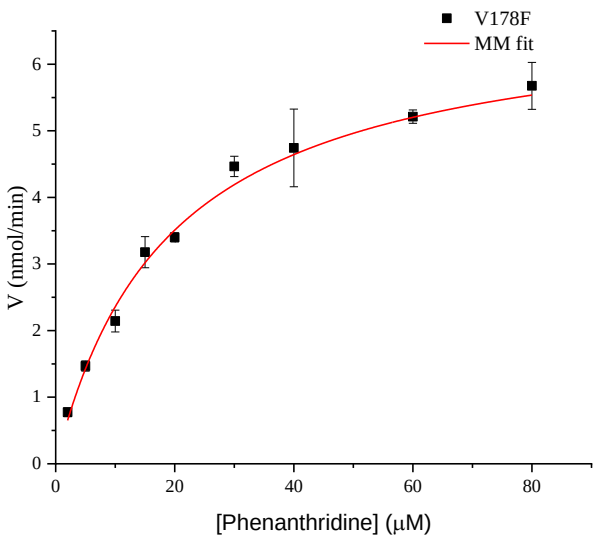
V178F
MM fit
V (nmol/min)
[Phenanthridine] (μM)

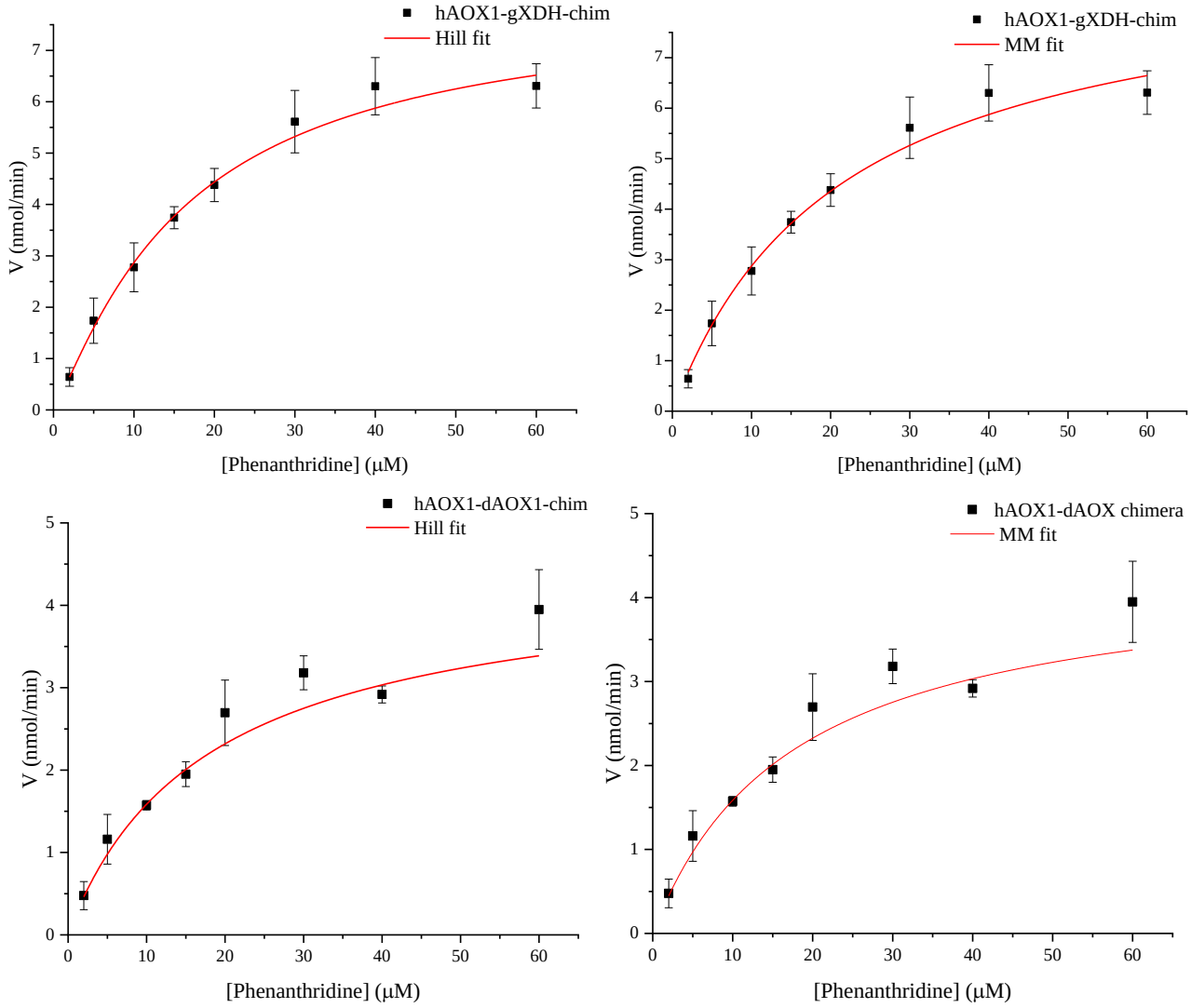

Table A.1.: Inactivation studies: Details of the measurements and steps of calculations

	V_{max} (Abs/s)	SD	µmol enzyme	Fe%	Turnover (s^{-1})	Exponential fit value	SD	k inactivation (s^{-1})	$t_{1/2}$	turnover x $t_{1/2}$
WT native 1	0.00257	2.20E-05	8.60E-05	47	4.96737	84.38	2.35	0.01185	58.47534	290.46887
WT native 2	0.00334	5.60E-05	8.60E-05	47	6.45565	76.14	1.79	0.01313	52.76502	340.63267
WT native 3	0.0029	3.09E-05	8.60E-05	47	5.60521	79.47	1.88	0.01258	55.07271	308.69398
WT native 2	0.00255	3.10E-05	8.60E-05	47	4.92872	90.78	2.5	0.01102	62.91054	310.06826
WT native 1	0.00258	3.10E-05	8.60E-05	47	4.9867	87.56	2.4	0.01142	60.67908	302.5885
WT GSH 1	0.00251	3.60E-05	8.60E-05	47	4.8514	86.96	2.6	0.0115	60.26328	292.36152
WT GSH 2	0.00273	3.90E-05	8.60E-05	47	5.27663	94.27	2.5	0.01061	65.32911	344.71732
WT GSH 3	0.00278	3.40E-05	8.60E-05	47	5.37327	92.89	2.4	0.01077	64.37277	345.89216
WT cat/sod 1	0.00269	3.10E-05	8.60E-05	47	5.19931	86.3	2.2	0.01159	59.8059	310.94962
WT cat/sod 2	0.00265	2.90E-05	8.60E-05	47	5.122	85.4	2.2	0.01171	59.1822	303.13124
WT cat/sod 3	0.00274	3.10E-05	8.60E-05	47	5.29595	88	2.3	0.01136	60.984	322.96852

WT H_2O_2 2	0.00141	1.40E-05	8.20E-05	47	2.85823	99.4	4.5	0.01006	68.8842	196.887
WT H_2O_2 3	0.00148	1.68E-05	8.20E-05	47	3.00013	83.4	3.2	0.01199	57.7962	173.3961
WT H_2O_2 1	0.0015	1.60E-05	8.20E-05	47	3.04067	85.5	3.5	0.0117	59.2515	180.16438
6A native 1	7.62E-04	8.06E-06	6.20E-05	68	1.41203	116.4	9.1	0.00859	80.6652	113.90181
6A native 2	8.95E-04	9.50E-06	6.20E-05	68	1.65849	84.6	6.3	0.01182	58.6278	97.23353
6A native 3	8.48E-04	1.01E-05	6.20E-05	68	1.57139	108.05	9.4	0.00925	74.87865	117.66391
6A native 1	9.25E-04	8.04E-06	6.20E-05	68	1.71408	88.11	5.6	0.01135	61.06023	104.66214
6A native 2	9.32E-04	1.03E-05	6.20E-05	68	1.72705	87.33	5.5	0.01145	60.51969	104.52063
6A native 3	8.87E-04	6.10E-06	6.20E-05	68	1.64366	84.15	6	0.01188	58.31595	95.85183
6A GSH 1	8.90E-04	1.00E-05	6.20E-05	68	1.64922	96.17	6.05	0.0104	66.64581	109.91382
6A GSH 2	9.03E-04	1.10E-05	6.20E-05	68	1.67331	83.25	5.7	0.01201	57.69225	96.53719
6A GSH 3	9.10E-04	1.20E-05	6.20E-05	68	1.68628	102.09	6.21	0.0098	70.74837	119.30187
6A GSH 4	9.54E-04	1.50E-06	6.20E-05	68	1.76782	111.37	7.3	0.00898	77.17941	136.43923
6A cat sod 1	8.10E-04	6.80E-06	6.20E-05	68	1.50098	101.3	7.1	0.00987	70.2009	105.37004
6A cat sod 2	8.50E-04	1.50E-05	6.20E-05	68	1.5751	94.7	6.2	0.01056	65.6271	103.3693
6A cat sod 3	6.80E-04	8.50E-06	6.20E-05	68	1.26008	99.2	8.5	0.01008	68.7456	86.625
6A + cat sod	0.00116	1.11E-05	6.21E-05	68	2.14609	79.13	4.56	0.01264	54.83709	117.68522
6A cat sod 2	9.99E-04	8.70E-06	6.20E-05	68	1.85121	82.41	4.97	0.01213	57.11013	105.72266
6A H_2O_2 4	8.40E-04	8.80E-06	6.20E-05	68	1.55657	105.4	6.9	0.00949	73.0422	113.69531
6A H_2O_2 3	8.80E-04	8.90E-06	6.20E-05	68	1.63069	93.2	6.5	0.01073	64.5876	105.32252
6A H_2O_2 2	7.90E-04	9.40E-06	6.20E-05	68	1.46392	95.2	6.5	0.0105	65.9736	96.57989
6A H_2O_2 1	8.50E-04	1.00E-05	6.20E-05	68	1.5751	84.3	5.5	0.01186	58.4199	92.01723
6D native 1	0.00103	1.40E-05	9.00E-05	72	1.2418	61.38	4.3	0.01629	42.53634	52.8217
6D old	0.00118	2.30E-05	9.00E-05	72	1.42265	46.53	2.5	0.02149	32.24529	45.87365
6D native 2	8.86E-04	1.20E-05	9.00E-05	72	1.06819	65.11	5.18	0.01536	45.12123	48.19807
4A native 1	0.00252	3.90E-05	8.88E-05	64	3.46416	70.71	1.9	0.01414	49.00203	169.75075
4A native 2	0.00254	2.70E-05	8.88E-05	64	3.49165	71.43	1.98	0.014	49.50099	172.84017
4A native 3	0.0024	2.40E-05	8.88E-05	64	3.2992	70.05	1.98	0.01428	48.54465	160.15839
3A native 1	0.00244	4.30E-05	8.75E-05	80	2.72321	84.09	2.44	0.01189	58.27437	158.6936
3A native 2	0.0026	3.70E-05	8.75E-05	80	2.90179	90.79	2.4	0.01101	62.91747	182.57302
3A native 3	0.0025	3.30E-05	8.75E-05	80	2.79018	91.97	2.4	0.01087	63.73521	177.83262
2A-2 native 1	0.00198	2.90E-05	6.35E-05	58	4.20004	64.74	2.1	0.01545	44.86482	188.43407
2A-2 native 2	0.00208	2.80E-05	6.35E-05	58	4.41216	62.49	2.1	0.016	43.30557	191.07128
2A-2 native 3	0.00178	2.40E-05	6.35E-05	80	2.73745	72.26	2.66	0.01384	50.07618	137.08108
2A-1 native 1	0.00263	1.20E-05	8.60E-05	44	5.42994	109.62	2.9	0.00912	75.96666	412.49405
2A-1 native 2	0.00261	1.16E-05	8.60E-05	44	5.38864	112.5	3.4	0.00889	77.9625	420.11208
2A native 1	0.00265	4.10E-05	8.60E-05	44	5.47123	84.65	2.35	0.01181	58.66245	320.95561

2A native 2	0.0023	2.80E-05	8.60E-05	44	4.74861	100.16	2.93	0.00998	69.41088	329.60538
2A native 3	0.00246	3.30E-05	8.60E-05	44	5.07895	89.1	2.5	0.01122	61.7463	313.60642
C161A native 1	0.0019	2.40E-05	6.75E-05	67	3.28E+00	73.3	2.3	0.01364	50.7969	166.72559
C161A native 2	0.00179	1.60E-05	6.75E-05	67	3.09E+00	84.95	3.04	0.01177	58.87035	182.0376
C161A native 3	0.00176	1.50E-05	6.75E-05	67	3.04E+00	82.95	3	0.01206	57.48435	174.77276
C165A native 2	0.0025	2.90E-05	8.50E-05	77	2.98E+00	89.57	2.4	0.01116	62.07201	185.23208
C165A native 3	0.00282	3.00E-05	8.50E-05	77	3.37E+00	86.29	2.2	0.01159	59.79897	201.29046
C165A native 4	0.00228	2.30E-05	8.50E-05	77	2.72E+00	94.6	2.7	0.01057	65.5578	178.41838
N176Y native 1	9.70E-04	1.10E-05	7.00E-05	48	2.25539	115.65	6.4	0.00865	80.14545	180.75959
N176Y native 2	8.91E-04	6.50E-05	7.00E-05	48	2.07171	120.12	7.5	0.00833	83.24316	172.45549
N176Y native 3	0.00109	1.06E-05	7.00E-05	48	2.53441	105.53	6	0.00948	73.13229	185.34737
G177E native 1	0.00262	4.30E-05	8.60E-05	47	5.06402	75.45	2.1	0.01325	52.28685	264.78141
G177E native 2	0.00232	3.30E-05	8.60E-05	47	4.48417	88.49	2.6	0.0113	61.32357	274.98508
G177E native 3	0.00253	3.40E-05	8.60E-05	47	4.89006	82.55	2.3	0.01211	57.20715	279.74643
V178F native 1	8.80E-04	1.10E-05	5.26E-05	49	2.66742	87.33	5.6	0.01145	60.51969	161.43124
V178F native 2	0.00105	6.10E-06	5.26E-05	49	3.18271	77.03	4.5	0.01298	53.38179	169.89893
V178F native 3	0.00105	9.20E-06	5.26E-05	49	3.18271	88.65	5.1	0.01128	61.43445	195.52823
L438V native 1	0.00192	1.80E-05	1.26E-04	54.5	2.18436	114.4	3.8	0.00874	79.2792	173.17431
L438V native 2	0.00201	1.80E-05	1.26E-04	54.5	2.28675	104.2	3.2	0.0096	72.2106	165.12772
L438V native 3	0.00209	1.30E-05	1.26E-04	54.5	2.37777	113.7	3.6	0.0088	78.7941	187.354
L438V native 4	0.00221	1.40E-05	1.26E-04	54.5	2.51429	102.2	3.1	0.00978	70.8246	178.07354
gXDH chim native 1	0.00161	2.30E-05	6.96E-05	66	2.73818	81.07	3.1	0.01234	56.18151	153.83535
gXDH chim native 2	0.002	4.40E-05	6.96E-05	66	3.40147	77.59	5	0.01289	53.76987	182.89669
gXDH chim native 3	0.00281	9.70E-05	6.96E-05	66	4.77907	36.96	1.3	0.02706	25.61328	122.4076
dAOX chim native 1	6.75E-04	9.50E-06	6.60E-05	63	1.26826	98.6	9.1	0.01014	68.3298	86.66016
dAOX chim native 2	8.00E-04	7.40E-06	6.60E-05	63	1.50313	80.7	5.8	0.01239	55.9251	84.0625
dAOX chim native 3	7.70E-04	8.20E-06	6.60E-05	63	1.44676	80.51	6.3	0.01242	55.79343	80.71966

Table A.2.: Inactivation studies: Average values and T-test results

Enzyme	Average values						T-test vs WT native			T-test native vs other conditions		
	turnover	SD	$t_{1/2}$	SD	turnover x $t_{1/2}$	stdev	vs turnover	vs $t_{1/2}$	vs turnover x $t_{1/2}$	vs turnover	vs $t_{1/2}$	vs turnover x $t_{1/2}$
WT native	5.39	0.66	57.98	4.11	310.49	18.54						
WT GSH	5.16	0.28	63.32	2.69	327.66	30.57				0.5344	0.0696	0.4454
WT cat/sod	5.21	0.09	59.99	0.91	312.35	9.99				0.5718	0.3448	0.8600
WT H_2O_2	2.97	0.10	61.98	6.026	183.48	12.09				0.0010	0.3813	2.9E-05
6A native	1.62	0.12	65.68	9.60	105.64	8.73	0.0002	0.118	1.3E-06			

6A GSH	1.69	0.05	68.07	8.16	115.55	16.77				0.2173	0.6851	0.3365
6A cat/sod	1.67	0.34	63.30	6.94	103.75	11.11				0.7873	0.6464	0.7663
6A H_2O_2	1.56	0.07	65.51	6.00	101.90	9.61				0.3050	1.4E-05	0.5550
6D	1.24	0.18	39.97	6.81	48.96	3.54	5.1E-05	0.0272	2.3E-06			
4A	3.42	0.10	49.02	0.48	167.58	6.61	0.0021	0.0076	1.1E-05			
3A	2.80	0.09	61.64	2.94	173.03	12.64	0.0008	0.1974	2.3E-05			
2A-2	3.78	0.91	46.08	3.54	172.19	30.44	0.0692	0.0078	0.0063			
2A-1	5.22	0.31	68.75	8.49	359.35	52.36	0.6304	0.0448	0.1065			
C161A	3.14	0.13	55.72	4.32	174.51	7.66	0.0011	0.5039	1.1E-05			
C165A	3.02	0.32	62.48	2.90	188.32	11.74	0.0005	0.1237	3.1E-05			
N176Y	2.29	0.23	78.84	5.18	179.52	6.53	0.0001	0.0059	1.7E-05			
G177E	4.81	0.30	56.94	4.52	273.17	7.65	0.1436	0.7608	0.0082			
V178F	3.01	0.30	58.44	4.41	175.62	17.75	0.0005	0.8893	0.0003			
L438V	2.28	0.10	76.76	3.95	175.22	11.25	0.0003	0.0007	6.7E-06			
gXDH chim	3.64	1.04	45.19	16.99	153.05	30.25	0.0797	0.3212	0.0042			
dAOX chim	1.41	0.12	60.02	7.20	83.81	2.98	9.9E-05	0.6865	5.5E-06			

Figure A2: Hill versus Michaelis Menten fit for the variants generated to study the FAD loop (see **Table A5** for the details of the fitting values)

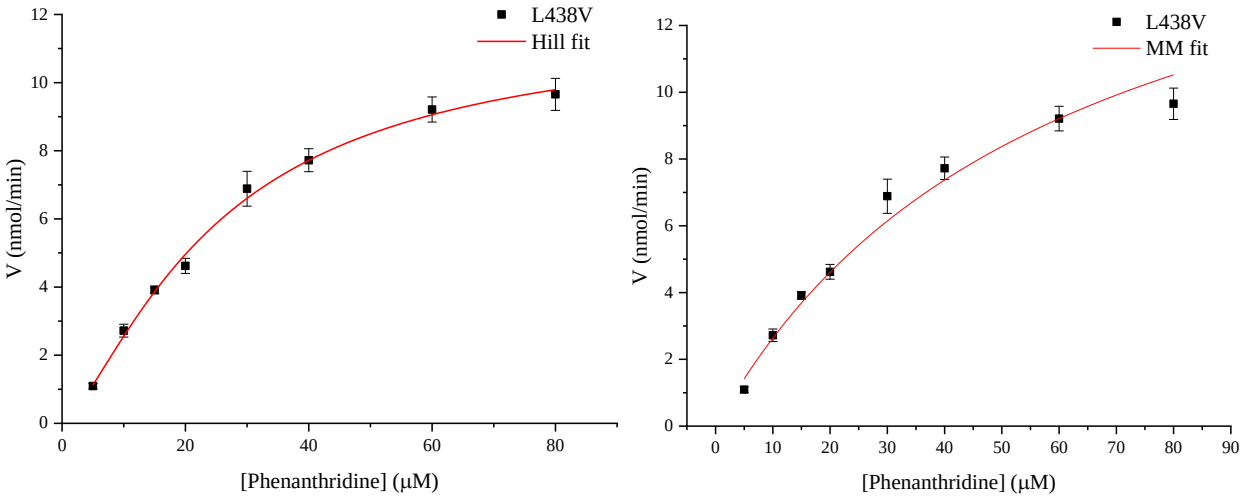

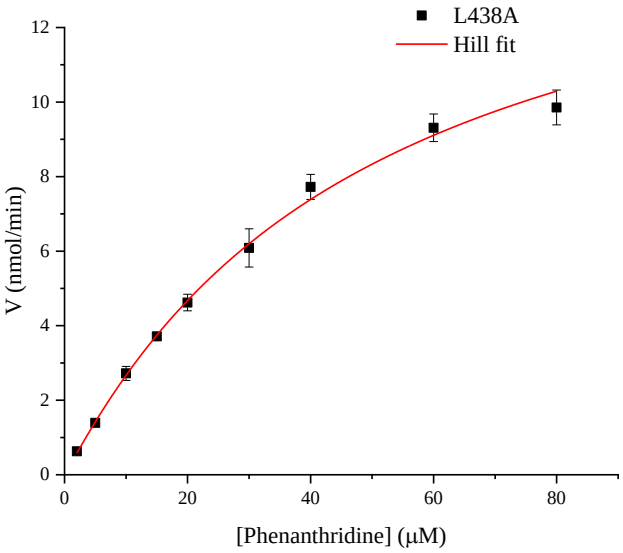
L438A
Hill fit
V (nmol/min)
[Phenanthridine] (μM)

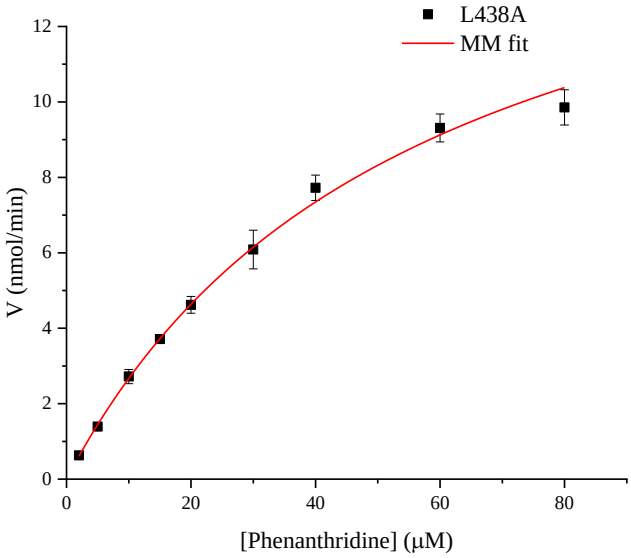
L438A
MM fit
V (nmol/min)
[Phenanthridine] (μM)

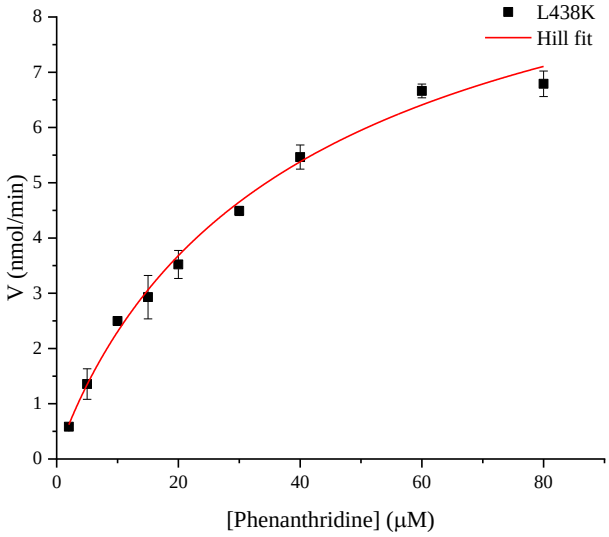
L438K
Hill fit
V (nmol/min)
[Phenanthridine] (μM)

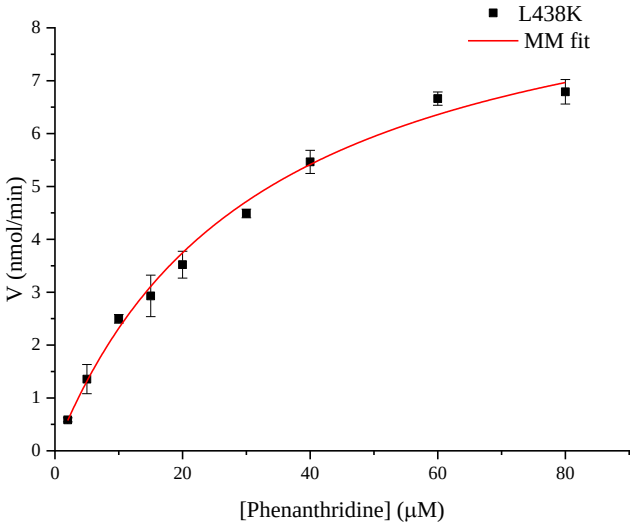
L438K
MM fit
V (nmol/min)
[Phenanthridine] (μM)

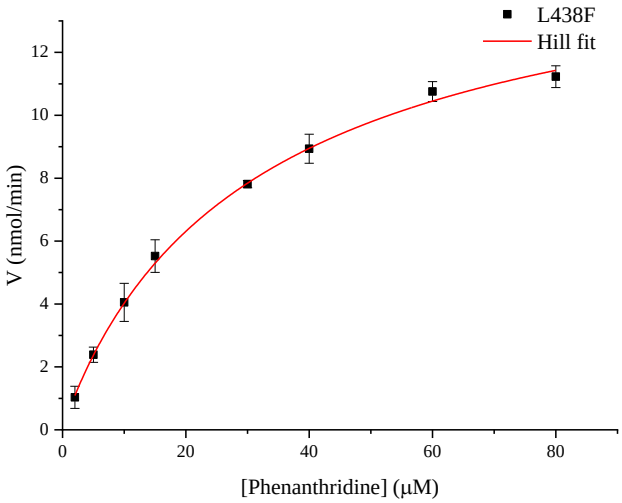
L438F
Hill fit
V (nmol/min)
[Phenanthridine] (μM)

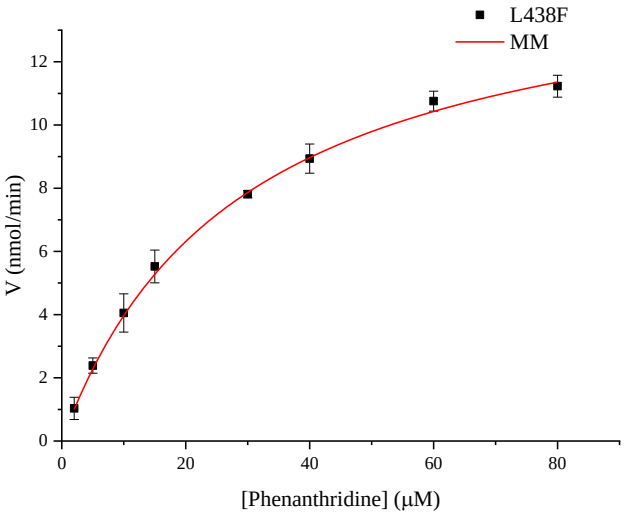
L438F
MM
V (nmol/min)
[Phenanthridine] (μM)

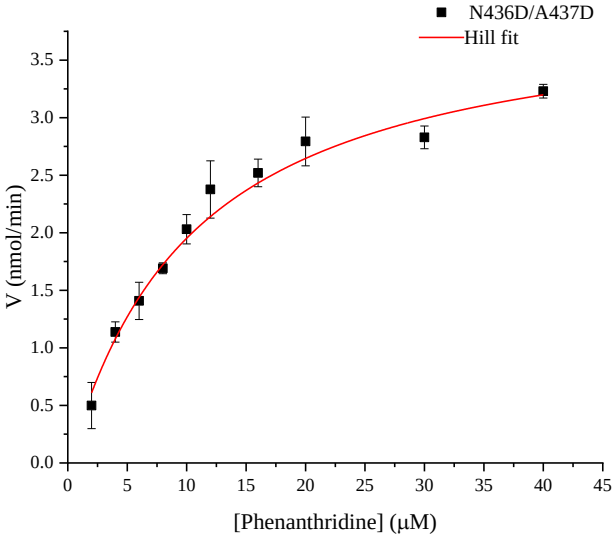
N436D/A437D
Hill fit
V (nmol/min)
[Phenanthridine] (μM)

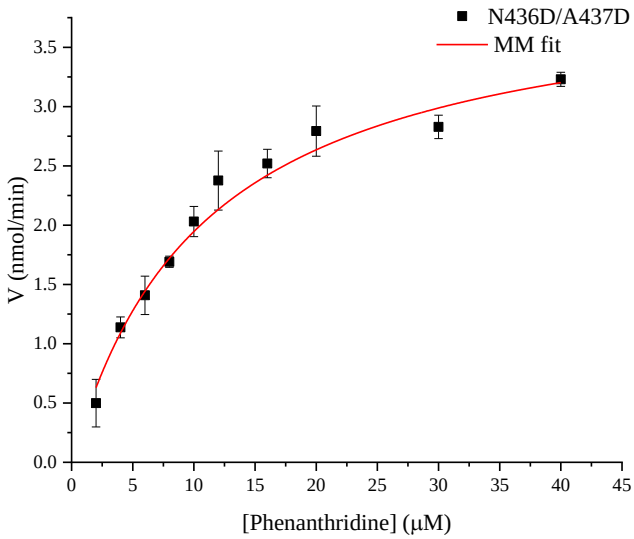
N436D/A437D
MM fit
V (nmol/min)
[Phenanthridine] (μM)

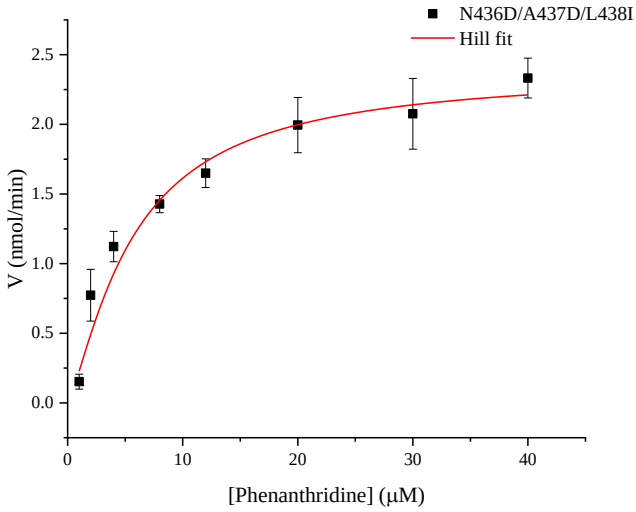
N436D/A437D/L438I
Hill fit
V (nmol/min)
[Phenanthridine] (μM)

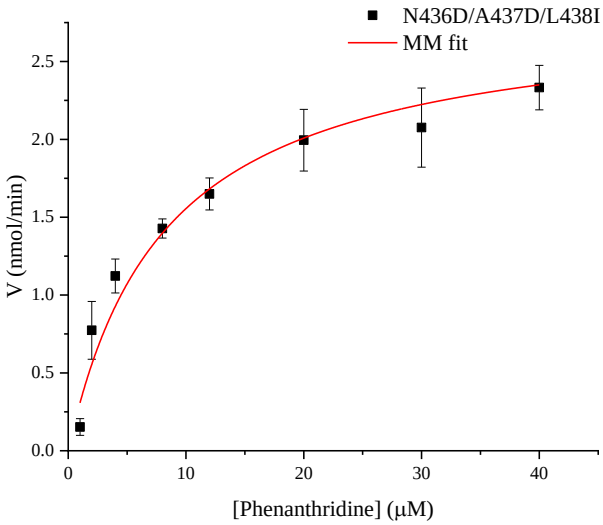
N436D/A437D/L438I
MM fit
V (nmol/min)
[Phenanthridine] (μM)

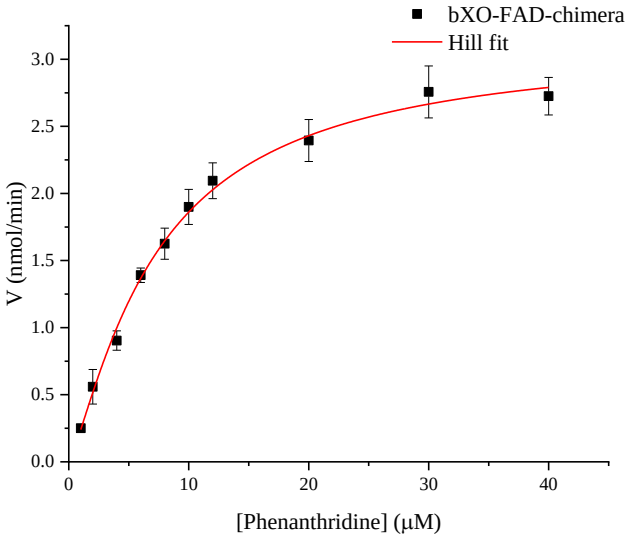
bXO-FAD-chimera
Hill fit
V (nmol/min)
[Phenanthridine] (μM)

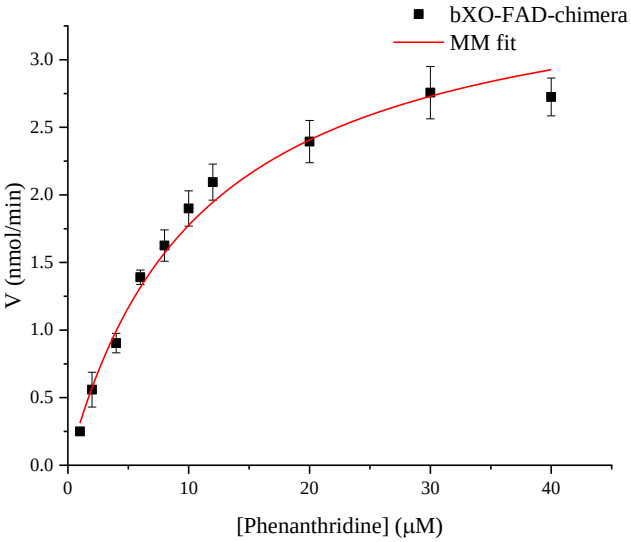
bXO-FAD-chimera
MM fit
V (nmol/min)
[Phenanthridine] (μM)

Table A3: Metal saturation, purification index ratios and yield of the enzymes used to study the effect of DTT

Enzyme	Mo (%)[1]	Fe (%)[1]	A_{280}/A_{450}[2]	A_{450}/A_{550}[2]	Yield (mg/L)
mAOX1	55.56 ± 3.80	57.59 ± 6.78	4.71	3.02	2.7
mAOX2	73.73 ± 2.75	67.82 ± 0.98	4.51	3.20	1.5
mAOX3	43.96 ± 4.49	41.45 ± 0.96	4.97	3.10	1.4
mAOX4	66.23 ± 2.53	52.09 ± 1.22	4.68	2.88	2.3
PaoABC	21.06 ± 4.14	55.18 ± 2.73	-	-	-
Rc XDH	100	100	-	-	-

1: Obtained from the ICP-EOS measurements of 8-10 µM wet-ashed protein samples and related to the maximum number of one Mo and 4 Fe per monomer of the enzyme.
2: Obtained from the UV-Vis absorbance at 280, 450, and 550 nm.

Figure A3: Size exclusion chromatography traces, UV-Vis spectra (insets) and Coomassie stained reducing SDS-PAGE (10%) of the mouse aldehyde oxidases used to study the effect of DTT: Using a Superdex 200 16/600 pg column and 50 mM TrisHCl, 200 mM NaCl, 1 mM EDTA, pH 8.0 as elution buffer the SEC profiles show consistently aggregation, tetramer, dimer and monomer elution peaks, respectively for the enzymes, around 48, 55, 62 and 70 mL. The UV-Vis absorption of the variants over the range of 250 to 800 nm (insets) present peak maxima at 280, 450 and 550 nm corresponding to the protein backbone, FAD and Fe-S clusters absorption, respectively.

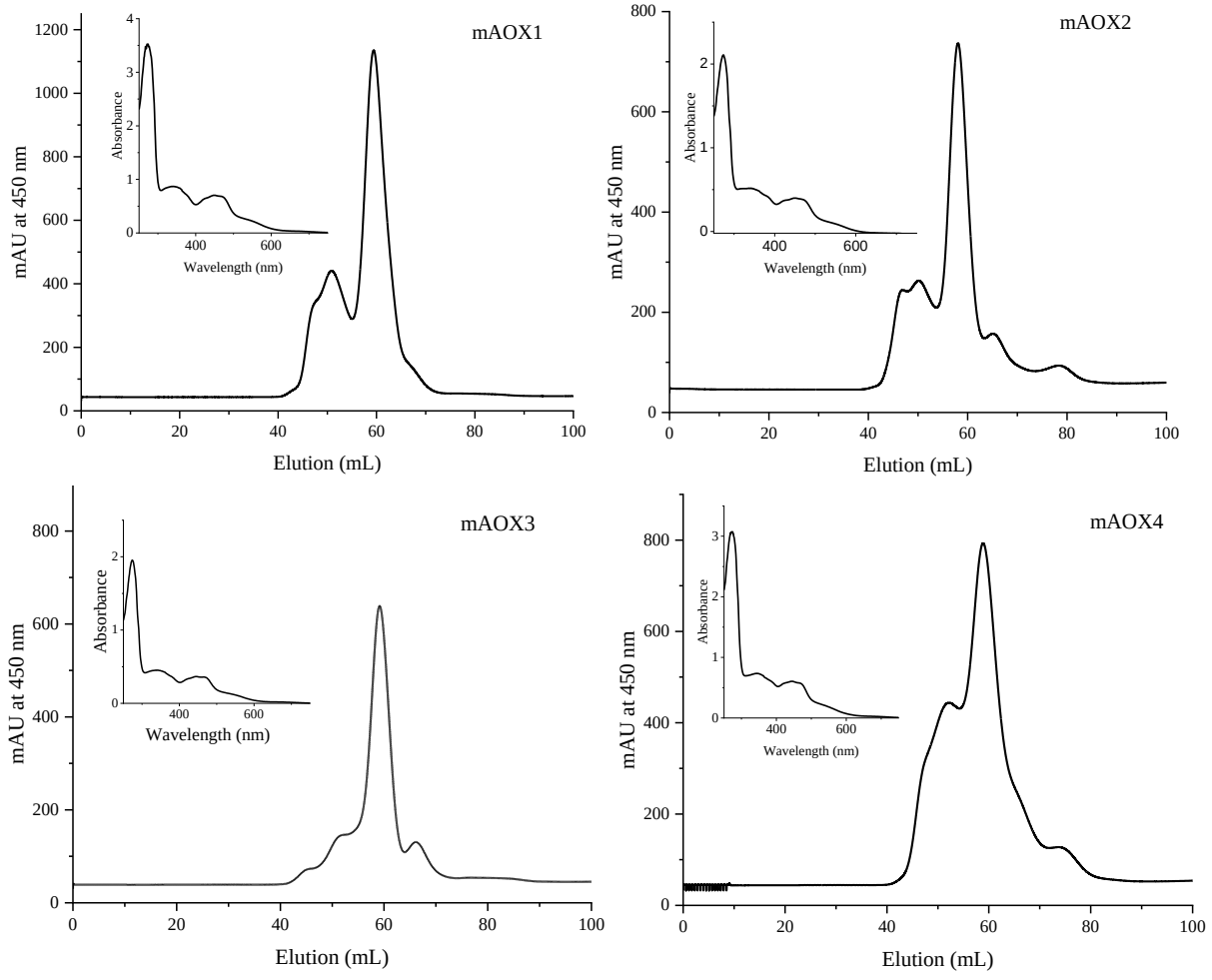

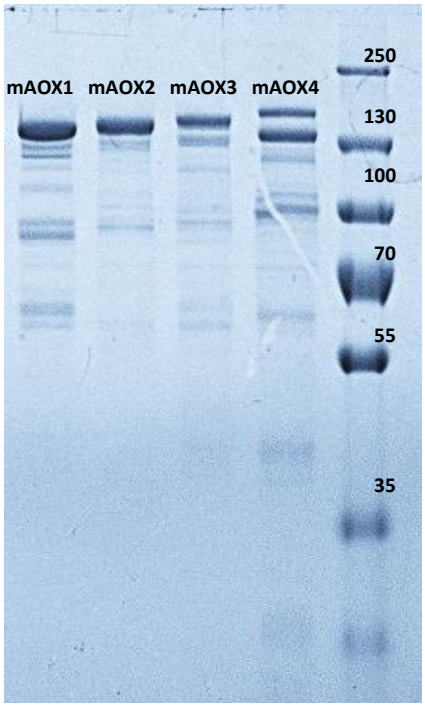

Table A4: Methionine oxidation in the native condition and in samples treated with H_2O_2 and phenanthridine

		Native	stdev	H_2O_2	stdev	Substrate	stdev
FeS Domain	Met26	30.56107	17.48064	93.6618	3.00031	49.1263	9.47459
	Met55	52.03711	21.66048	29.46258	13.19837	72.46742	13.3485
	Met121	2.16131	1.87646	35.90094	22.85083	13.29361	3.0844
	Met123	2.56133	2.44816	33.04911	28.95462	24.82884	24.29152
	Met223	31.92498	11.54203	88.35695	12.22415	30.52587	9.05969
	Met225	25.07718	16.12493	86.47866	12.21399	21.45306	5.19805
FAD Domain	Met241	30.24814	21.05216	79.75094	6.04515	39.84866	6.58883
	Met242	29.28265	8.1222	79.55049	6.81468	39.85278	6.59072
	Met266	27.30968	8.16252	68.07579	13.04977	23.80839	7.9326
	Met333	24.48127	11.22641	39.95994	11.005	17.65272	6.57748
	Met352	27.19419	4.51934	47.22665	6.82157	30.22496	3.15356
	Met489	22.50203	9.67797	40.44154	6.80545	25.35246	6.60803
	Met537	25.50614	11.72418	89.50063	3.61875	25.2506	3.75649
Moco Domain	Met585	25.41092	9.31748	55.18791	10.97454	26.0412	6.43451
	Met603	25.82537	12.23326	97.93805	1.80806	43.15696	17.43816
	Met642	10.45526	15.48692	74.18361	49.47969	32.36041	47.1806
	Met745	27.41133	4.04284	63.56606	18.56915	36.34731	3.81606
	Met753	20.81481	3.97363	51.13547	20.97526	29.64261	3.16017
	Met758	24.8327	8.58474	59.83456	19.24036	28.63265	6.52756
	Met769	39.62081	18.84186	63.3909	21.11079	30.43488	7.40859
	Met797	43.19861	50.55524	49.41881	12.32939	5.13611	4.73471
	Met860	20.20665	22.2439	29.1943	10.99996	9.0232	11.06588
	Met870	36.57506	15.9356	48.30933	18.88973	29.60972	13.60923
	Met889	28.99282	8.59078	64.82055	15.55278	34.71149	14.75277
	Met955	12.85512	10.04976	56.52643	20.30526	10.13349	11.70406
	Met981	21.41939	4.86998	91.2477	14.05547	39.88068	4.95299

Met983	15.90772	7.40222	74.8009	14.31638	21.85362	5.96338
Met1009	29.31205	13.95911	61.45751	13.92562	47.35814	8.39513
Met1047	26.8369	3.85409	52.89459	14.82503	28.20738	4.23913
Met1055	12.32433	12.16594	26.72573	21.19887	12.60955	14.82543
Met1065	27.77701	11.75122	55.21257	8.82272	22.48458	0.74763
Met1067	22.8322	12.45689	46.10402	9.65139	20.35495	2.92082
Met1149	24.67002	26.04491	59.98522	23.9594	23.4674	8.29607
Met1212	0	0	60.99725	23.2264	16.97275	13.59919
Met1245	34.03281	17.40216	69.5576	17.31483	38.79518	7.64414
Met1313	7.58953	8.87977	35.46768	9.65637	6.55379	4.10409
Met1322	39.75544	12.88595	72.55825	16.45874	69.0491	21.80311

Table A5: The MM versus Hill fit values for the representative graphs shown in **Figure A1** and **Figure A2**

	Hill fit			MM fit	
	V	k	n	Vmax	Km
WT	16.32 ± 1.16	15.10 ± 1.76	1.42 ± 0.13	22.37 ± 2.24	27.45 ± 4.89
L438V	11.72 ± 0.71	25.00 ± 2.54	1.39 ± 0.07	18.37 ± 2.76	59.73 ± 12.91
L438A	16.44 ± 1.48	48.69 ± 8.17	1.03 ± 0.04	17.67 ± 0.81	56.20 ± 3.71
L438F	16.31 ± 1.01	32.54 ± 4.50	0.94 ± 0.05	15.47 ± 0.42	29.01 ± 1.76
L438K	11.06 ± 1.72	42.43 ± 14.50	0.92 ± 0.07	9.76 ± 0.57	32.12 ± 3.77
N436D/A437D	3.99 ± 0.36	10.42 ± 2.18	1.03 ± 0.16	4.07 ± 0.10	10.96 ± 0.76
N436D/A437D/L438I	2.38 ± 0.26	5.67 ± 1.26	1.29 ± 0.2	2.83 ± 0.30	8.20 ± 1.98
bXO-FAD-Chim.	3.12 ± 0.12	7.34 ± 0.58	1.24 ± 0.05	3.73 ± 0.25	11.01 ± 1.38
6A	12.65 ± 0.84	16.66 ± 2.59	1.20 ± 0.08	15.40 ± 0.88	26.52 ± 3.25
6D	11.48 ± 2.75	31.69 ± 17.68	0.87 ± 0.12	9.61 ± 0.64	21.02 ± 2.71
4A	18.95 ± 2.38	36.62 ± 9.28	1.03 ± 0.07	20.01 ± 1.09	41.11 ± 3.34
3A	19.07 ± 1.30	23.99 ± 2.87	1.14 ± 0.03	24.42 ± 2.29	39.15 ± 5.22
2A-2	19.81 ± 5.35	83.89 ± 41.59	0.90 ± 0.06	14.56 ± 0.65	47.11 ± 3.46
2A-1	10.75 ± 0.66	10.37 ± 1.24	1.31 ± 0.11	13.09 ± 1.03	15.32 ± 2.73
C161A	15.24 ± 1.81	26.30 ± 6.32	1.06 ± 0.07	16.74 ± 0.99	32.24 ± 2.71
C165A	20.85 ± 4.86	32.06 ± 16.26	32.06 ± 16.26	20.65 ± 1.07	31.39 ± 2.37
N176Y	3.89 ± 0.54	12.55 ± 4.56	1.09 ± 0.18	4.19 ± 0.34	15.47 ± 2.65
G177E	17.68 ± 1.35	18.53 ± 2.66	1.32 ± 0.12	22.95 ± 1.86	31.00 ± 5.17
V178F	7.79 ± 0.78	26.08 ± 6.53	0.87 ± 0.06	6.85 ± 0.27	19.08 ± 1.78
dAOX1-chim.	4.46 ± 1.51	18.45 ± 14.22	0.97 ± 0.35	4.35 ± 0.34	17.48 ± 2.87
gXDH-chim.	7.96 ± 0.56	16.42 ± 2.31	1.16 ± 0.09	9.01 ± 0.54	21.38 ± 2.61